Generation-recombination measurements in silicon M.O.S. capacitors

Zainol Abidin Ibrahim

GENERATION-RECOMBINATION MEASUREMENTS IN SILICON M.O.S. CAPACITORS

by

Zainol Abidin Ibrahim, B.Sc.

A thesis submitted in according with the regulations for the degree of Doctor of Philosophy at the University of Durham, Department of Applied Physics and Electronics.

1983

To my beloved

father, Ibrahim Daud,

mother, Asma Kassim,

and brother, Aziz.

ABSTRACT

This thesis is concerned with the change in charge on a silicon MOS capacitor (MOS-C) subjected to a voltage step. The transient charge (Q-t) is controlled by the generation and recombination processes in the silicon. A review of these processes in the MOS-C, and of Q-t and other methods of measuring generation lifetime (τ_g) is given. A thorough experimental investigation of Q-t transients is given including the effects of the guard ring voltage, applied bias, voltage step magnitude, and voltage step polarity. The measurements were performed with an automated apparatus, using a micro-computer controlled measuring system developed for the purpose.

An improved theory for the Q-t transient has been developed for determining the lifetime. This is midway between the simple theory of Hofstein and the more elaborate computer method of Collins and Churchill. Both the generation and recombination cases of the Q-t transient are covered for the first time and the theoretical results compare well with the experiments. The present Q-t method of determining lifetime is also compared to other Q-t analyses and with the C-t, C-V, and fast ramp methods. Good agreement is obtained with other Q-t and C-t methods, but not with the C-V and fast ramp methods.

More than one hundred samples were used in this work but detailed results are presented for typical ones only. This investigation gives confidence in the use of the Q-t method for measuring the minority carrier lifetime easily and accurately.

ACKNOWLEDGEMENTS

I would like to express my gratitude to my supervisor, Dr. M.J.Morant, for his constant guidance and supervision and also for his valuable advice in the preparation of this thesis, without whom this work would never have been completed. I would also like to thank Professor G.G. Roberts for making available the facilities in the Department of Applied Physics and Electronics, University of Durham.

I am also grateful to Dr. P.G.C.Allman for his valuable discussions and also to Dr.R.N.Campbell of ITT for providing the samples.

I am also thankful to the Department's technicians for their technical help and particularly to Mr.J.E.Gibson for his constant assistance in the preparation of samples.

I would also like to thank Mrs.S.Mellanby for her typing of this thesis.

I greatly acknowledge the Malaysian Government for providing the financial assistance and the University of Malaya for awarding the fellowship.

Finally I would like to thank Siti Meriam Abdul Gani for her help and encouragement throughout my stay in Durham.

MEMORANDUM

I declare that the work has not been submitted for any other degree. This thesis is my original work, except where indicated by reference to other work.

CONTENTS

CHAPTER 1

INTRODUCTION

1.1 Background and Objectives

The metal-oxide-semiconductor (MOS) device structure has become very important in modern electronics for high performance silicon integrated circuits particularly in very large scale integration (VLSI) design. In the study of the MOS device characteristics, two of the most important parameters are the doping concentration N of the semiconductor and the minority carrier lifetime τ_g (also known as the generation lifetime). The doping density is one of the parameters that determine the value of the threshold voltage of MOS transistors while the lifetime is responsible for the dynamics of charge storage devices such as charge-coupled-devices (CCD's) and dynamic memory cells.

In CCD's the minimum frequency of operation is determined by the carrier generation rate or the generation lifetime τ_g. A high generation rate, or low τ_g, would mean that the minimum frequency of operation of CCD's has to be high. For the dynamic RAM, as the number of cells gets larger, the storage time becomes more critical. This is because the memory cells are not available for reading or writing while being refreshed, therefore giving rise to delay in the system if it has to wait for the refresh cycle to be completed. The value of τ_g determines the time interval between refresh signals that are used to restore the information which is held in the form of charge in MOS capacitors before it decays away through recombination and leakage processes.

Due to the importance of these applications, generation-recombination processes in MOS devices have been extensively studied. This thesis is concerned with the study of the measurement of τ_g itself and particularly with measurements based on the transient response of MOS capacitors, which have not yet been fully explored.

In the past decade or so, many papers have been written on methods of measuring τ_g. Many of them are concerned with the capacitance transient analysis that is based on the method of Zerbst (1) and several authors have suggested improvements and refinements to this technique. The capacitance transient (C-t) method, the fast-ramp method, and the capacitance-voltage (C-V) method form the background for the thesis. These methods will be critically discussed and some comparative results using them will be presented. However, the main parts of the thesis are concerned with the charge transient (Q-t) method of determining τ_g which has been comparatively little used.

The objectives of the work presented were to carry out a thorough experimental investigation of the Q-t method of measurement and to compare it with the alternative methods mentioned above from the point of view of accuracy, ease of measurement, etc. The work showed that, although there are several papers on the theory of the Q-t method, very few experimental results have been published previously. The thesis contains the first thorough investigation of the experimental variables affecting the form of the Q-t transient and hence the lifetime values determined from it. It was only possible to make the large number of measurements required by automating the method with microcomputer control which was successfully done.

All the methods of measuring τ_g can, in principle, be used in conditions of carrier generation or carrier recombination. With large deviations from equilibrium, it is not possible to define a single lifetime τ_g for both because the details of the generation and recombination processes are different. The published analyses of all the methods of measurement have applied almost entirely to the experimental conditions in which generation predominates because it is the simplest. In the Q-t measurements made here, equal emphasis is given to conditions for generation and recombination and an attempt is made to analyse results for both of them in terms of fundamental transitions. This is aided by a numerical modelling program which has been written by the author.

The device structures used for the study in this thesis were MOS capacitors of aluminium, silicon oxide, and silicon. A variety of samples were used, some made by the author using standard microelectronic techniques. Basically, the capacitors were prepared by thermally growing the oxide on the surface of the silicon followed by the deposition of aluminium electrodes, the areas of both being determined by standard photolithographic techniques. Details of the fabrication process are given in Chapter 3 of the thesis.

1.2 The Physics of the MOS Capacitor in Equilibrium

Although the physics of the MOS capacitor is now well understood, we will review it briefly here to introduce many terms used throughout the thesis. We will consider the energy band diagrams of the MOS structure under the influence of an external bias, at first under equilibrium conditions, and then in the non-equilibrium case following the application

of a step voltage to the metal electrode (Section 1.3). For the sake of simplicity an ideal MOS capacitor will be considered first. This implies that the charge in the oxide and at the interface are negligible and that the work function of the metal is equal to that of the semiconductor. The effect of these assumptions, which do not hold for real capacitors, will be considered later.

We need to consider four types of conditions for the band structure of the MOS capacitor depending on the applied voltage as shown in Figure 1.1. Considering a p-type semiconductor, a negative voltage applied to the metal relative to the bulk of the semiconductor biases the silicon surface into accumulation, zero voltage corresponds to "flat-band", and positive voltages give depletion or inversion of the surface. Each of these conditions will need to be considered in more detail.

1.2.1 The Accumulation Condition

Fig 1.1(a) shows the band diagram for the capacitor biased negatively into accumulation. The concentrations of electrons and holes in the semiconductor are given by the equations

$$n = n_i \exp \frac{(E_f - E_i)}{kT} \qquad (1.1a)$$

$$p = n_i \exp \frac{(E_i - E_f)}{kT} \qquad (1.1b)$$

where n_i, P and n are the intrinsic, hole and electron concentrations respectively.

E_f is the Fermi energy level

E_i is the intrinsic energy level

k is Boltzman's constant

T is the absolute temperature

When a negative bias is applied to the metal electrode the metal Fermi level is raised and the energy band in the surface of the semiconductor bends slightly upwards creating an electric field which pulls the holes towards the semiconductor-oxide interface. Since the oxide is an insulator, the holes accumulate very close to the surface. From equations(1.1) it is seen that the concentration of the holes increases at the surface of the silicon where (E_i-E_f) is greatest while the electron density is even less than in the bulk. The MOS capacitor is now similar to a parallel plate capacitor with the oxide as the dielectric and the capacitance per unit area is that of the oxide, C_{ox}. A very small amountof band bending can give the positive charge on the capacitor because of the rising exponential in Equation (1.1b).

1.2.2 The Flat Band Condition

Since we have assumed an ideal case, when the applied voltage is zero the energy bands are flat, with no potential gradients anywhere in the sample as shown in Figure 1.1(b). The flat band voltage V_{FB} is said to be zero in the ideal condition. In practice V_{FB} is not zero for reasons that will be given in Section 1.2.5.

1.2.3 The Depletion Condition

When the voltage applied to the metal has a small positive value the energy levels near the semiconductor-oxide interface are pulled downwards reducing the distance between E_i and E_f as shown in Figure 1.1(C). From Equations (1.1) it is seen that the hole density therefore decreases while the electron density increases near the surface. This is due to the holes being repelled by the electric field of the charge on the metal electrode. Thus a layer depleted of majority carriers is formed between the semiconductor surface and the bulk. The negative charge in the semiconductor which balances the positive charge on the electrode is mainly that of the uncompensated ionised doping atoms in the depletion region. The magnitude of this charge per unit area is

$$Q_d = q N_a x_d \qquad (1.2)$$

where N_a is the doping concentration

and x_d is the width of the depletion layer formed

From Poisson's equation and using the depletion approximation which ignores the mobile carriers, the potential ψ at a distance X into the depletion region is

$$\psi = \frac{qN_a}{2\,\epsilon_s} (x_d - x)^2 \qquad (1.3)$$

where ϵ_s is the permittivity of the semiconductor.

At the semiconductor-oxide interface where $x = 0$, the potential relative to the bulk is known as the "surface potential" ψ_s given by :-

$$\psi_s = \frac{qN_a}{2\epsilon_s} x_d^2 \qquad (1.4)$$

The magnitude of the positive charge on the metal is $Q_m (=Q_d)$ so that the electric field in the oxide, F_{ox}, is

$$F_{ox} = \frac{q N_a x_d}{\varepsilon_{ox}} = \frac{V_{ox}}{t_{ox}}$$

where ε_{ox} is the permittivity of the oxide

t_{ox} is the oxide thickness

and V_{ox} is the voltage across the oxide

$$V_{ox} = \frac{q N_a x_d t_{ox}}{\varepsilon_{ox}} = \frac{q N_a x_d}{C_{ox}}$$

The applied voltage, V_a, is therefore

$$V_a = V_{ox} + \psi_s$$

$$V_a = \frac{q N_a x_d}{C_{ox}} + \frac{q N_a x_d^2}{2 \varepsilon_s}$$

This equation enables x_d to be found for a given V_a, and hence ψ_s, and V_{ox} to be evaluated.

1.2.4 The Inversion Condition

As the positive applied voltage is increased the surface potential increases and the energy bands are bent more significantly. The distance between E_i and E_f gets smaller so that the holes are repelled further into the bulk so increasing the depletion layer width. At the same time the electron density must increase at the surface because the p.n product remains constant in the equilibrium condition. When the applied voltage reaches the threshold value for weak inversion the midgap energy E_i crosses the constant Fermi energy level E_f. When this occurs the electron density at the surface is greater than the hole density giving a weak inversion layer.

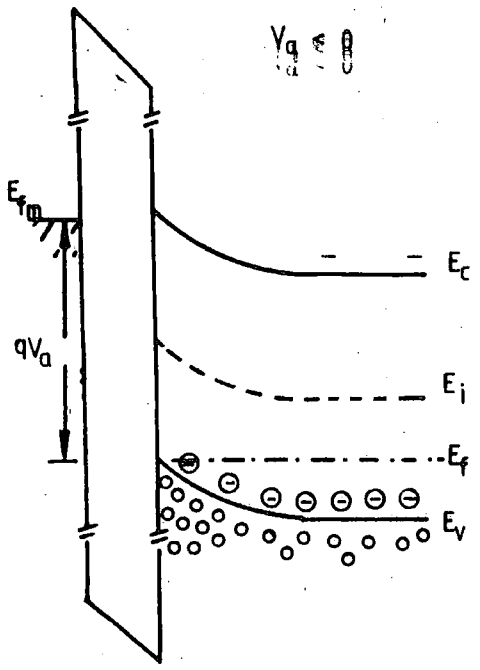

(a) Accumulation

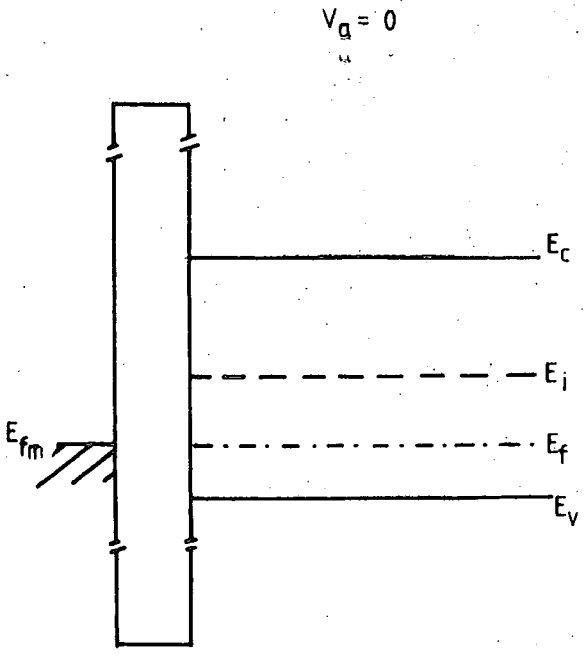

(b) Flat band

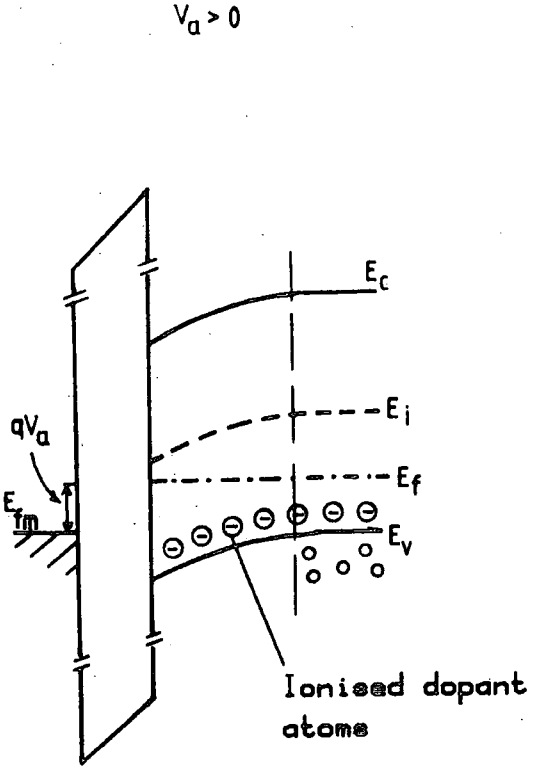

(c) Depletion

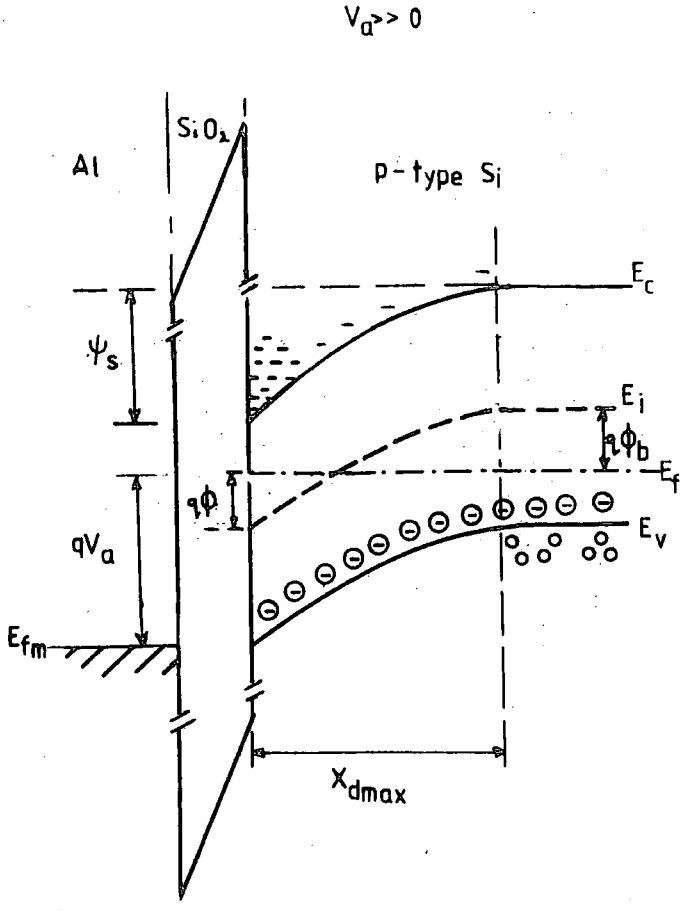

(d) Inversion

($\psi_s = 2\phi_b$)

FIG. 1.1 Energy Band Diagram showing the Effect of Bias on an Ideal MOS Capacitor

With further increase of voltage the electron density in the surface reaches N_a at the onset of strong inversion as shown in Figure 1.1(d), and the difference between E_f and E_i at the surface is

$$E_f - E_i = \phi_b \tag{1.5}$$

where ϕ_b is the energy difference between E_i and E_f in the neutral bulk of the semiconductor. This corresponds to the surface electron concentration, n_s, becoming equal to N_a (= P_p) in the bulk. From the figure it is seen that the surface potential ψ_s at the onset of strong inversion becomes

$$\psi_s = 2\,\phi_b \tag{1.6}$$

Now if the applied voltage is further increased beyond the onset of strong inversion, ψ_s the difference between E_i and E_f will increase only slowly because of the exponential rise in the concentration of electrons in the inversion layer, Equations (1.1). Thus the extra charge beyond inversion is easily provided by an increase in the electron charge in the surface with little change of ψ_s. So, the depletion layer charge, which is due to the uncompensated ionised doping atoms, remains almost constant beyond inversion.

1.2.5 The Non-Ideal MOS Capacitor

In this section we shall be looking briefly at the non-ideal MOS capacitor. In practice a real MOS capacitor contains interface traps and oxide charges. The interface traps are due to the occurrence of energy states resulting from the discontinuity of the silicon bonds at the semiconductor-oxide interface, while the oxide charges are usually

due to the presence of ionised sodium atoms as well as the charge density that remains after the interface trap charge is annealed out. The charges present in the interface traps and in the oxide are both normally positive. In addition, the workfunctions of aluminium and the semiconductor of a real MOS capacitor are not equal. For aluminium the vacuum work function Φ_m is 4.25 volts therefore giving the work function difference Φ_{ms} between aluminium and p-type silicon of 0.90 volt if the doping concentration of the silicon is 10^{15} cm^{-3}.

The effect of these imperfections is that when there is no bias the bands are no longer flat as assumed in the ideal case thus causing the high frequency C-V curve to be shifted by an amount equal to the flat band voltage V_{FB} which is the voltage required to bring about the flat band condition. Figure 1.2 shows the energy band diagram for a non-ideal p-type MOS capacitor with zero bias and positively biased into the inversion mode.

In this work, since the MOS capacitor is initially biased into the inversion mode the problem of charging up of the interface states does not arise and so the effect of the interface states can generally be neglected.

1.3 The MOS Capacitor out of Equilibrium

The preceding discussion holds for the MOS capacitor in the equilibrium condition where the relation $pn = n_i^2$ holds throughout the semiconductor. Since this work is concerned with the response immediately after the application of a voltage step the capacitor is in a non-equilibrium condition during the transient. When the step is first applied equilibrium is disrupted for a while and we have the situation where $np < n_i^2$ or $np > n_i^2$ near the semiconductor-oxide interface.

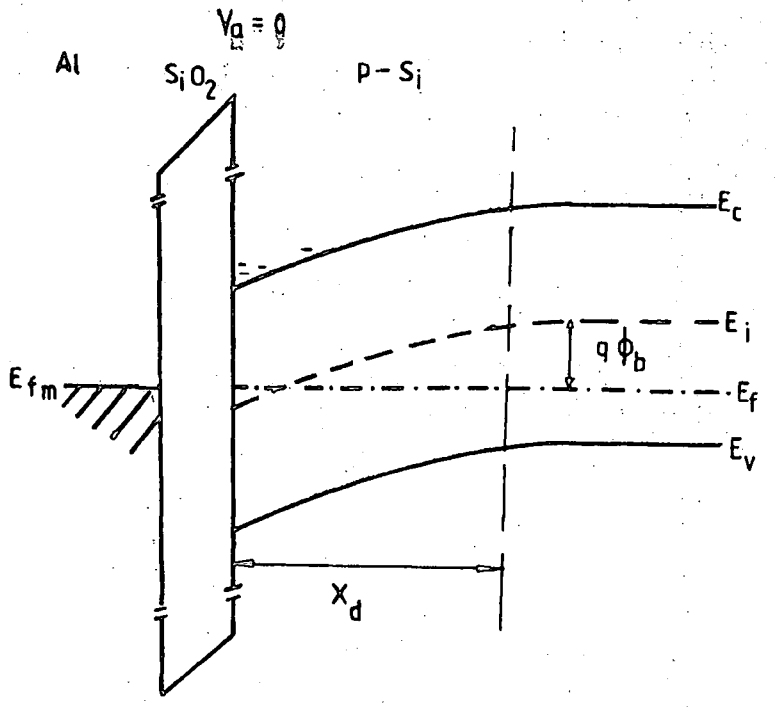

(a)

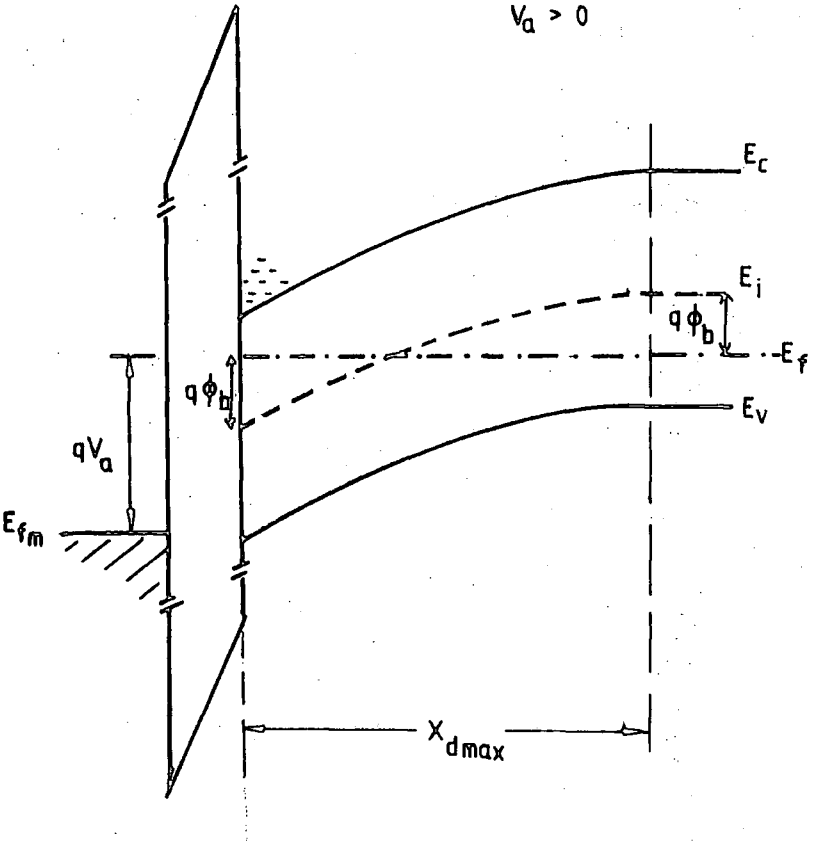

(b)

FIG. 1.2 Energy Band Diagram for a Non-ideal MOS Capacitor
(a) At zero Bias
(b) Biased into Heavy Inversion
indicating Heavy Inversion condition is similar to the Ideal case
(doping ions omitted)

Figure 1.3 shows the effect of band bending immediately after the application of a step voltage where the sample is taken from an equilibrium inversion condition to heavier inversion. Before reaching the final equilibrium condition the sample goes into "deep depletion" where the depletion width extends beyond the maximum equilibrium width, returning to the equilibrium value at a rate determined by the generation of carriers. The surface potential is much greater than $2\phi_b$ in deep depletion. As electrons are generated thermally they flow rapidly to the surface and build up the extra inversion charge required by the increased applied voltage. This causes ψ_s to relax back from the deep depletion value to little more than $2\phi_b$. The relaxation rate is therefore a measure of the minority carrier generation rate if the transient can be correctly analysed. Similarly the relaxation of the surface charge following a step of the opposite polarity is determined by minority carrier recombination although the analysis is more complicated in this situation.

There has been some controversy as to which region in the semiconductor contributes most to the carrier generation. Zerbst (1) suggested that the net generation is in that part of the depletion layer which is in excess of the equilibrium width. This implies that there is no net generation in the region near the surface and this has been disputed by several authors. The work of Simmons and Wei (2) has given a more acceptable model for the analysis of the generation in the depletion layer. Collins et al (3,4) showed by a computer simulation that the generation rate as used by Zerbst is inaccurate and that another alternative suggested by Sah et al

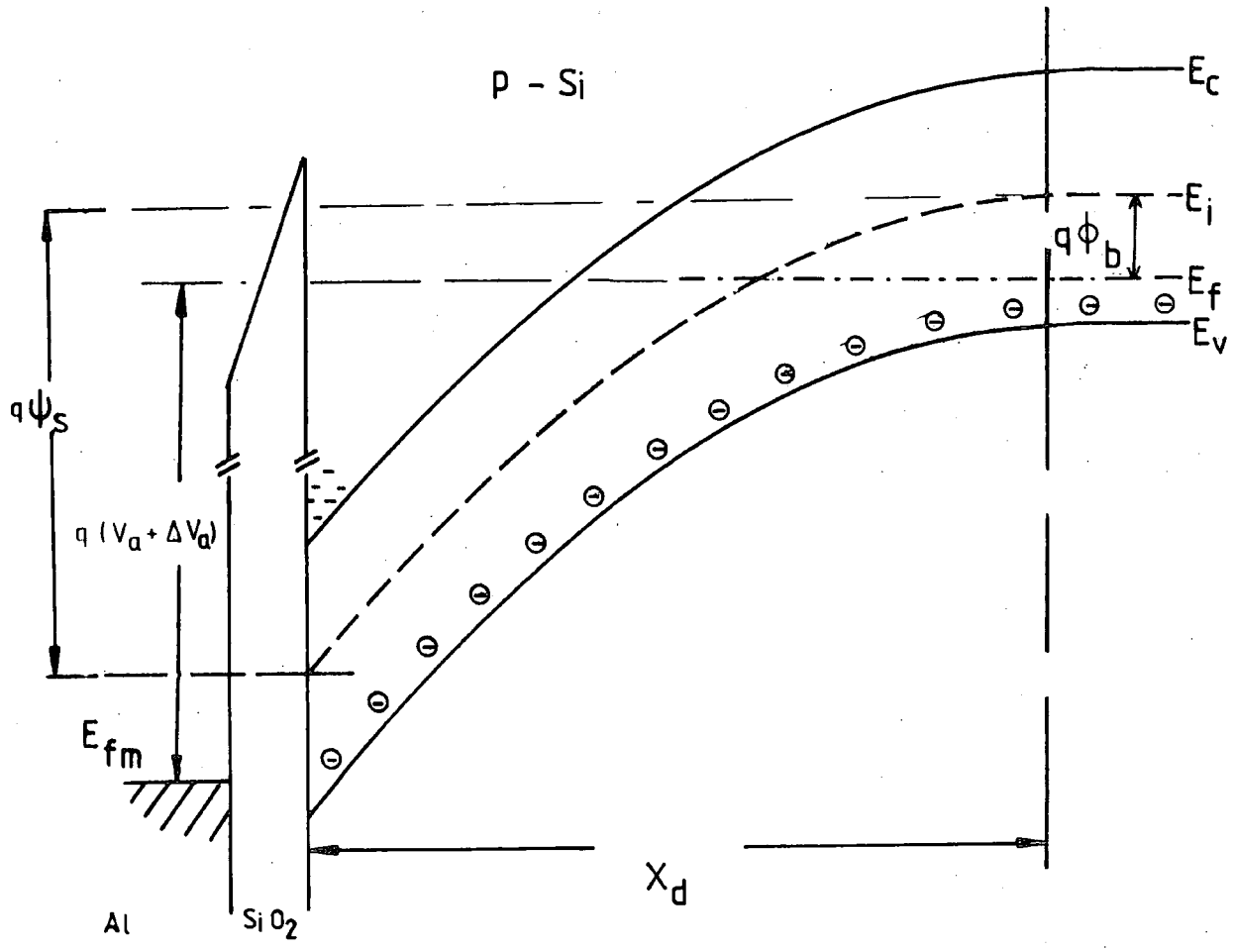

FIG. 1.3 Energy Band Diagram of a p-type MOS Capacitor in Non-equilibrium condition (after voltage application)

(5) gives a better approximation. They also showed good agreement between their computer calculations and the analytical solution of Simmons and Wei. Carrier generation from the bulk appears to have been neglected by these and all other authors although it will later be shown to be important. All these models will be discussed in greater detail in this thesis.

1.4 Methods of Measuring τ_g

Nearly all the methods used to study the MOS capacitor out of equilibrium have been used to find the minority carrier lifetime in charge generation conditions. For this reason the symbol τ_g will generally be used in the thesis except when referring specifically to recombination.

1.4.1 The Capacitance Transient (C-t) Method

The determination of minority carrier lifetime τ_g from a capacitane transient curve is the most widely used of several methods available. A considerable amount of work has been done on the C-t method (6-16) and a number of authors have suggested methods of lifetime determination involving capacitance transients. These are mainly based on the work of Zerbst (1) who was the first to develop an analysis of the C-t transientin terms of charge generation. In this method the MOS capacitor is pulsed into inversion by applying a voltage step to the metal electrode and the small signal a.c. capacitance transient is recorded and analysed. The equation developed by Zerbst is based upon the rate of change of the inversion charge at the semiconductor surface. From the slope and intercept of a particular plot the value of τ_g

as well as the surface recombination velocity S can be extracted. The advantage of this method is that the response time of the sample capacitance is very much greater than the minority carrier lifetime itself thus allowing very short lifetimes to be determined from a comparatively slow experiment. Details of this method are described in Chapter 7.

Other workers have tried to improve on the interpretation of the capacitance transient response given by Zerbst. These include Schroder and Nathanson (17) who included the effect of lateral spreading of the depletion layer. Heiman (6) suggested an analytical rather than graphical solution to the C-t differential equation while Huang (7) proposed a simple method of obtaining τ_g by graphical means. His method uses large voltage steps and requires the condition that the depletion capacitance should be very much greater than the oxide capacitance for his approximation to hold. Tomanek (18) suggested a method where a pulse of opposite polarity is applied to the MOS capacitor in inversion so that the depletion layer collapses. By measuring the capacitance at the end of a pulse of variable duration he was able to calculate τ_g. Muller and Schiek (8) also worked on the pulsed C-t measurement using pulses of opposite polarity. In their method the MOS capacitor is pulsed from inversion to accumulation, where in this case the transient response is very much faster than in Zerbst's method. Consequently a broad band high frequency detecting system was used to allow a good time resolution in the capacitance measurements. The value of τ_g was obtained by choosing a suitable time constant for a close fit between the calculated values and the measured results.

1.4.2 The Charge Transient (Q-t) Method

Instead of measuring the capacitance transient to obtain the value of τ_g it is also possible to measure the charge response (Q-t) of the MOS capacitor subjected to a suitable voltage step. Hofstein (21) was the first to use the Q-t method for the evaluation of the lifetime. His method requires the application of a small voltage step ($\sim$ kT/q) superimposed on a fixed bias which maintains the MOS capacitor in heavy inversion. The voltage step takes the sample into heavier inversion and immediately after its application the depletion layer widens before relaxing back to its equilibrium inversion width. During this return to equilibrium the charge Q on the sample is measured. For a small deviation from equilibrium Hofstein assumed that Q varies exponentially with time and by using an equivalent circuit for the MOS capacitor in inversion he obtained the time constant which is related to the generation lifetime of the sample. This method of analysis is limited to the case of a very small deviation from equilibrium.

Zechnall and Werner (22) tried to improve on Hofstein's method of determining τ_g by using the Shockley-Read-Hall(25,26) expression for the generation of carriers. Although this method is very similar to the Hofstein's it requires rather laborious calculations to obtain the lifetime and has the same disadvantage which is the limitation to very small voltage steps which give only small changes of charge.

Viswanathan and Takino (24) proposed a different approach to the analysis of the Q-t transient. They adopted similar equations to those of Zerbst and obtained an expression

that allows the determination of τ_g and S from Q-t measurements with large voltage steps. The method however requires differentiation of the Q-t trace as in Zerbst's method and this is quite difficult to do accurately in practice.

Apart from these authors the Q-t method appears to have been neglected in spite of some experimental advantages. The main part of the present thesis is concerned with the Q-t method which will be described in more detail in later chapters and compared with alternative methods in Chapter 7.

1.4.3 The Non-Equilibrium Fast Ramp Method

In the preceding methods the MOS capacitor was stimulated with a voltage step. In the fast ramp method a continuously varying voltage in the form of a triangular wave is used. Measurements involving the application of voltage ramps have been used in the characterisation of MOS devices for many years. Usually they are in conjunction with capacitance or conductance measurements which require an a.c. signal superimposed on the d.c. voltage. A slow voltage ramp is used in this way for the purpose of varying the d.c. bias on the sample automatically. The fast ramp method requires no a.c. signal as the sample current due to the changing bias voltage can be measured directly. Charge is moving continuously in the MOS capacitor under the influence of the changing bias voltage.

There are two periods in the voltage sweep that can be considered. The first is where the ramp voltage is tending to bring the sample towards deeper depletion. For a p-type sample this is the period of positive slope. The sample will be taken into accumulation, depletion and inversion modes if the rate of voltage increase is slow enough. However, for the

higher rate used in fast ramp method, the MOS capacitor never reaches the equilibrium inversion mode as the inversion charge cannot be generated fast enough. In the second period, the reverse sweep, the sample is nearer to equilibrium as the depletion edge moves in the same direction as the generation current. A plot of current versus the applied voltage (I-V) forms a closed loop for the complete sweep. The shape has been analysed by Board and Simmons (27) who have shown how the value of τ_g can be determined from it. Details of this techique are presented in Chapter 7.

1.4.4 The C-V Method

The measurement of the small signal high frequency capacitance versus bias voltage (C-V) is the basic tool used for most MOS capacitor characterisation. It is used for the determination of doping profile, extraction of the interface trap level density and the determination of the flatband voltage. A number of authors have also tried to extend the basic C-V measurement technique to give the generation lifetime τ_g.

Pierret (28) suggested one method of using the C-V plot for the determination of τ_g. In this, several C-V plots are required for different sweep rates starting from inversion and moving rapidly into deep depletion. When the sweep voltage becomes sufficiently large the deep depletion capacitance reaches saturation. The saturation capacitance is plotted against the sweep rate and the slope of this plot gives τ_g. The main drawback is that the MOS sample has to be perfectly free of leakage in order to obtain the saturation capacitance.

Taniguchi (30) worked on a similar region of the C-V curve but his method needed only two sweep rates. Instead

of depending on the saturation capacitance he measured the length of the flat inversion portion of the C-V plot with decreasing bias. By plotting a set of complicated theoretical curves for different lifetimes and surface recombination velocities, the actual value of τ_g and S can be obtained by fitting the experimental data to the plot. One advantage claimed for this method is that a single set of curves can be used to cover a wide range of minority carrier lifetime and surface recombination velocities, so simplifying the analysis of experimental measurements.

1.4.5 Other Methods

There are still other methods that can be used for the determination of the minority carrier lifetime in MOS capacitors. To describe all of them is beyond the scope of this thesis, but among the methods that have been used are the current time transient of Trullermans and Van De Weile (34) , the current-capacitance measurements of Calzolari et al (9) ,and the admittance measurement method by Baccarani et al (35) .

1.5 Outline of the Thesis

This thesis is concerned with the measurement of generation and recombination processes in MOS capacitors from the transient response to applied step voltages. Most of it is concerned with the Q-t method of determining the minority carrier lifetime because there are very few publications on the Q-t method as compared to elaborate studies of the C-t case. Very few Q-t results have been published and there is still no completely satisfactory description of the actual charge generation/recombination processes in MOS capacitors.

In Chapter 2 various techniques involving previous Q-t measurements are reviewed. This chapter also covers the work on the improvements of the analysis of the transient response which have been applied to the Q-t method. Typical plots of the methods described are also given. The experimental techniques used in the present work are given in Chapter 3 which also includes details of the MOS sample preparation. In Chapter 4 results are presented to show the effects of various experimental conditions on the measured transient. The theory of the $\hat{Q}$-t method and the analysis of the results is presented in Chapter 5 while Chapters 6, 7 and 8 give a comparison of the Q-t method with some of the others also described in this thesis. Finally, the conclusions from the work are given in Chapter 9.

CHAPTER 2

PREVIOUS WORK ON THE Q-t METHOD

2.1 Introduction

This chapter describes the published work on the Q-t method of measuring the minority carrier lifetime in MOS capacitors. This previous work formed the basis for the present investigation of the Q-t method described in Chapters 4 and 5.

The published papers differ mainly in their methods of analysing the transient conditions in the MOS capacitors and in the presentation of the Q-t data in a form suitable for extracting the carrier generation lifetime, τ_g. All of them make necessary approximations to an exact analysis of the problem.

2.2 Transient Analysis by Hofstein

In Hofstein's method of measuring lifetime (21), a small step of voltage is applied to the MOS capacitor which is initially biased into the inversion mode in equilibrium. The response of the capacitor immediately following the step is monitored. Assuming the MOS capacitor in inversion can be approximated by the equivalent circuit of Figure 2.1 for a small deviation from equilibrium, the transient should follow an exponential law. The time constant of the exponential response τ_R is measured and related to the generation lifetime τ_g by the following equation :-

$$\tau_R = \tau_g \frac{\psi_s}{q\, n_i x_d} (C_d + C_{ox}) \qquad (2.1)$$

where C_d and C_{ox} are the depletion and oxide capacitances respectively.

ψ_s is the surface potential

x_d is the depletion width

n_i is the intrinsic carrier concentration.

By substituting for C_d in terms of the inversion capacitance, C_m, the lifetime τ_g can be obtained from the equation :-

$$\tau_g = \tau_R \quad \frac{q\, n_i \epsilon_s}{\psi_s} \quad \frac{1}{C_{ox}^2} \quad \frac{(1-\alpha)}{\alpha}$$

where $\alpha = C_m/C_{ox}$ (the ratio of the inversion capacitance to that of the oxide). The time constant of the response (τ_R) is obtained by plotting the normalised charge versus time on a log-linear graph. The exponential relationship for the change of charge during the transient is

$$Q = Q_m - B\, e^{-t/\tau_R} \qquad (2.3)$$

where Q is the change of charge at time t

Q_m is the maximum charge increase (as in Figure 2.2a)

$B = Q_m - Q_{o+}$ where Q_{o+} is the change of charge ΔQ at $t = 0+$

Rearranging Equation (2.3) gives

$$\ell n \left(\frac{Q_m - Q}{B} \right) = - \frac{1}{\tau_R} \, t \qquad (2.4)$$

Thus the plot of $\ell n \left(\frac{Q_m - Q}{B} \right)$ against t gives a straight line with a slope equal to $- \frac{1}{\tau_R}$. The lifetime τ_g is then calculated from Equation (2.2).

Hofstein measured the charge with an electrometer connected to a storage oscilloscope to monitor the output signal. The electrometer was an operational amplifier with an external MOSFET to increase the input impedance and it was connected to

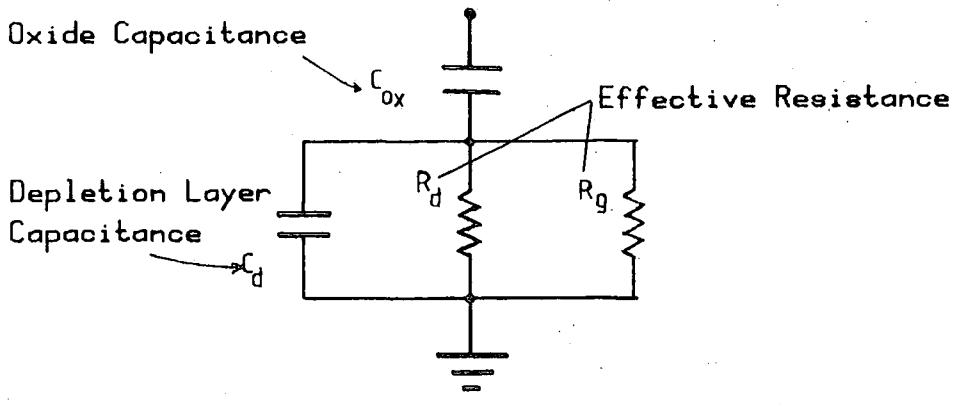

FIG. 2.1 Equivalent Circuit of MOS Capacitor in Inversion for Small Voltage Steps after Hofstein (21)

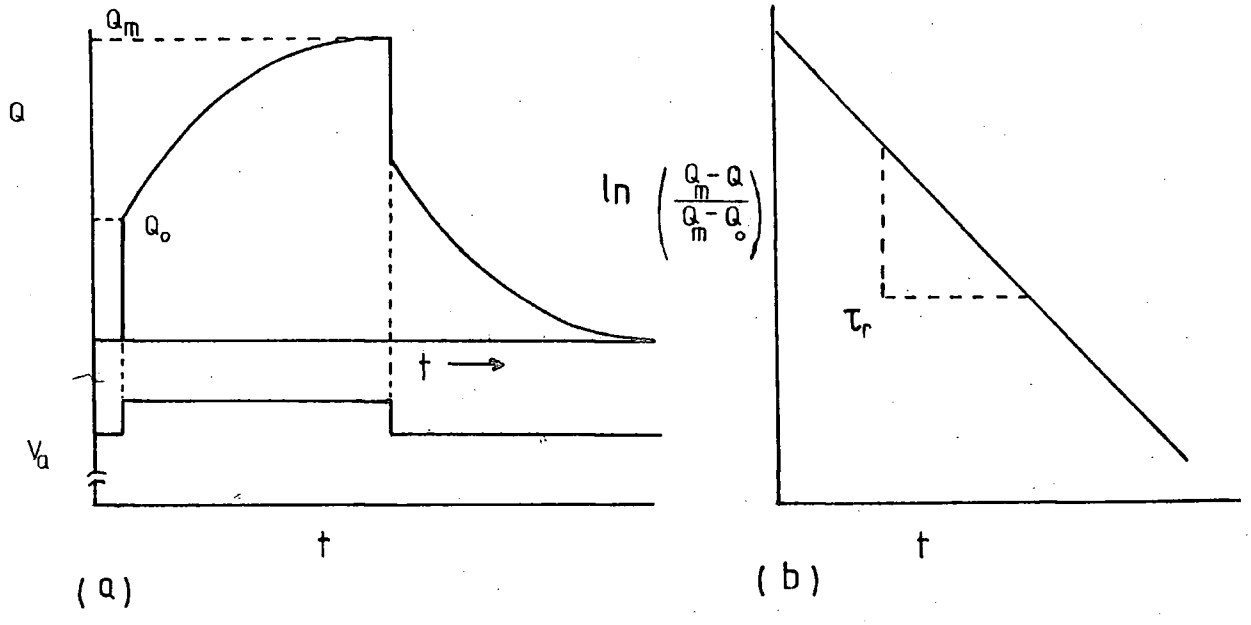

FIG. 2.2 Diagram showing (a) the Q-t Transients for increasing and decreasing Inversions and (b) the Hofstein and Zechnall and Werner Log. Plot for the Transient

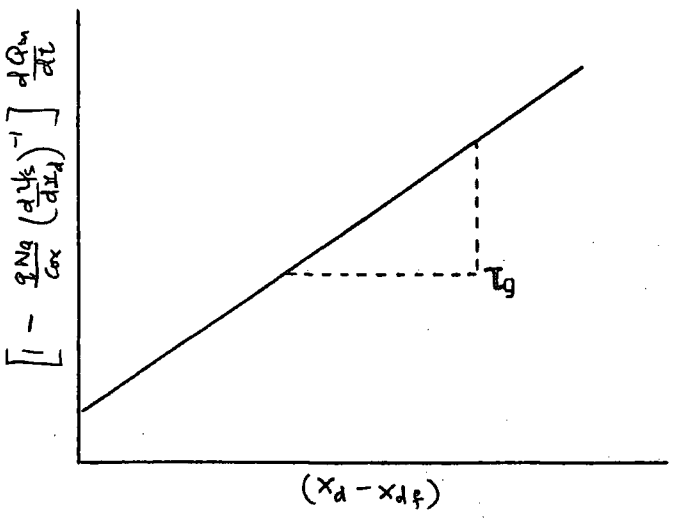

FIG. 2.3 The Plot of Viswanathan and Takino Method

a charge amplifier. The sample was connected with its back contact to the input of the electrometer and the metal electrode to a d.c. supply for biasing. The voltage step was applied on top of the bias by a suitable circuit. The charge generated during the relaxation period was recorded and analysed. A typical plot of the generated charge is shown in Figure 2.2(a) and a log plot of charge against time is given in Figure 2.2(b).

This approximate method of analysis gives a quick and simple means of evaluating the bulk lifetime of minority carriers since the device is in inversion before and after the application of the voltage step, and surface effects can thus be neglected. The drawback is in the approximation made in assuming the exponential behaviour of the response. Also the charge measurement is affected by noise since the voltage step is very small ($\sim$ millivolts) so that it requires careful instrumentation techniques to produce a reasonably clean Q-t trace.

2.3 Transient Analysis by Zechnall and Werner

Although Hofstein's method of analysis has the advantage of simplicity, its major drawback is in over-simplifying the Q-t transient by assuming that the time constant is directly related to the minority carrier lifetime by a simple expression. Zechnall and Werner (22) proposed another method of analysis without taking such an assumption. Their experimental set up was the same as that of Hoftstein's but with improvements in the method of analysing the response. The basic expression for the generation rate as used by Hofstein was

$$U_g = \frac{n_i}{\tau_g} \qquad (2.5)$$

This was replaced by the Schockley, Read, and Hall (12,13) expression.

$$U_g = \frac{pn - n_i^2}{\tau_{no}(p+n_i) + \tau_{po}(n+n_i)} \tag{2.6}$$

where p and n are the hole and electron densities during the transient response.

τ_{no} is the lifetime of electrons

τ_{po} is the lifetime of holes.

The generation current J_{gen} was obtained by integrating the above expression over the width of the space charge region. That is

$$J_{gen} = \frac{d\, Q_{inv}}{dt} = q \int_o^{x_d(t)} U_g\, dx \tag{2.7}$$

By substituting the value of the p n product which was simplified by a Taylor's expansion, and by approximating the integral to that with equilibrium values of carrier densities, they modified the expression for the generation current from Equation (2.7) to

$$\frac{d\, Q_{inv}}{dt} = \frac{q\, n_i}{\tau_g} A\, [x_d(t) - x_{d\infty}] \tag{2.8}$$

where Q_{inv} is the mobile charge in the inversion region

$x_d(t)$ and $x_{d\infty}$ are the depletion widths of time t and $t = \infty$ respectively.

A is a constant which is independent of τ_g provided τ_{no}/τ_{po} is constant.

If the value of A is unity in the above expression then Equation (2.8) becomes the same as used in the large signal C-t analysis by Zerbst. The value of A is very dependent on the dopant concentration however.

To obtain τ_g, Zechnall and Werner combined Equation (2.8)with the expression for the total charge in the MOS capacitor in inversion.

$$Q_{tot} = Q_{inv} + q\ N_a\ x_d(t) \tag{2.9}$$

This is differentiated with respect to time and combined with the relationship between $x_d(t)$ and the applied voltage using a Taylor's expansion and neglecting high order terms. The following expression was finally obtained.

$$\frac{d\Delta}{dt} = - \frac{A\ n_i}{N_a\ \tau_g R}.\Delta \tag{2.10}$$

where R is a constant that depends on the parameters of the sample

$\Delta = Q^{\infty}_{tot} - Q_{tot}$ is the change of charge stored in the MOS capacitor as in Figure 2.2(a). The differential equation above implies an exponential behaviour of Δ with time. The solution of Equation (2.10) is

$$\ell n\ \Delta = - \frac{A\ n_i}{N_a\ \tau_g R}\ .t + K \tag{2.11}$$

where K is a constant of integration.

From Equation (2.11) the lifetime can be obtained from the slope of the plot of $\ell n\ \Delta$ versus t.

Although the analysis of the Q-t trace and the calculation of the lifetime in this method is quite similar to

that of Hofstein's, the constant A which is present in this method has to be evaluated numerically to obtain the result. Also, the ratio τ_{no}/τ_{po} needs to be constant for the assumption that A is independent of τ_g to be valid. A further assumption is made in that the integral that is present in the expression for A is evaluated using equilibrium conditions instead of the real-time dependent ones.

2.4 Transient Analysis by Viswanathan and Takino

In the analyses of Hofstein and Zechnall and Werner, the measured Q-t responses were assumed to be exponentials. An improvement over these methods was proposed by Viswanathan and Takino (23) and by Takino (24) which is supposed to overcome the limitation of the two previous methods to a very small step size. In this method the approximation to an exponential response was also removed.

Viswanathan and Takino started their analysis with the Zerbst expression for the rate of increase of the mobile inversion charge, Q_{inv},

$$-\frac{d\,Q_{inv}}{dt} = \frac{q\,n_i}{2\,\tau_g}\,(x_d - x_{df}) + q\,n_i S \qquad (2.12)$$

S is the surface recombination velocity.

x_d and x_{df} are the depletion widths at times t and ∞ respectively. Equation (2.12) implies that the generation region is assumed to be just that part between x_d and x_{df}. From the basic equations for the MOS capacitor together with Equation (2.12) the following equation was obtained :

$$\left[1 - \frac{q\,N_a}{C_{ox}}\left(\frac{d\psi_s}{dx_d}\right)^{-1}\right]\frac{d\,Q_m}{dt} = \frac{d\,n_i}{2\,\tau_g}\left(x_d - x_{df}\right) + qn_iS \qquad (2.13)$$

In this method, a straight line is obtained by plotting

$$\left[1 - \frac{q\ N_a}{C_{ox}} \left(\frac{d\psi_s}{dx_d} \right)^{-1} \right] \frac{dQ_m}{dt}$$

as a function of $(x_d - x_{df})$. The value of $d\psi_s/dx_d$ is obtained from the relation

$$\psi_s = \frac{q\ N_a}{2\ \varepsilon_s} \cdot x_d^2 \qquad (2.14)$$

so that Equation (2.13) becomes simply

$$\left[1 - \frac{1}{C_{ox}} \sqrt{\frac{q\ N_a \varepsilon_s}{2\ \psi_s}} \right] \frac{d\ Q_m}{dt} = \frac{q\ n_i}{2\ g} (x_d - x_{df}) + qn_i S \qquad (2.15)$$

The value dQ_m/dt is obtained from the Q-t plot. The other unknown is ψ_s which is calculated from the expression

$$\psi_s(t) = \psi_{so} + \Delta V_a - \frac{\Delta Q_m(t)}{C_{ox}} \qquad (2.16)$$

where ψ_{so} is the equilibrium surface potential in inversion.

ΔV_a is the voltage step

$\Delta Q_m(t)$ is the increment of the charge stored in the MOS capacitor after time t.

Taking the slope of the linear portion of the plot of Equation (2.15), the minority carrier lifetime is calculated and the intercept on the vertical axis gives the surface recombination velocity S as shown in Figure 2.3.

The apparatus used by Viswanathan and Takino was similar to Hofstein's. The voltage step was applied in the same way with the sample already in heavy inversion and the

polarity was such as to take the sample into heavier inversion. This eliminates effects due to the charging up of surface states at the oxide-semiconductor interface. The surface potential in equilibrium was assumed to be the same before and after the application of the step even though the voltage increment could be large.

2.5 Surface Correction due to Schröder and Nathanson

An improvement to the analysis of the transient response of the MOS capacitor was suggested by Schröder and Nathanson (17). Although they worked on the C-t transient, their model for separating the bulk and surface components of carrier generation, is applicable to other non-equilibrium MOS processes particularly the Q-t method of Viswanathan and Takino.

Due to the influence of the surface and the edge of the capacitor the lifetime obtained from the measurements of Zerbst or Heiman must be an effective lifetime rather than the true bulk generation lifetime. These authors showed that measurements of lifetime made on different devices from the same wafer were very variable, and that the bulk lifetime and surface generation velocity apparently varied inversely with each other. This should not happen because, although the surface state densities may vary a great deal, the bulk lifetime should be quite constant across the wafer. Thus the observed variation of the bulk lifetime could be a spurious effect due to the surface. In their paper Schröder and Nathanson explained this by the fact that when a depleting voltage is applied, the space charge region spreads laterally around the capacitor electrode as well as into the depth of the semiconductor. This lateral spread is assumed to be of the same dimension as the depletion

layer width. After the application of a step voltage the semiconductor surface beyond the electrode becomes further depleted while the surface beneath it first becomes depleted and then inverted as minority carriers are generated. The surface generation velocity is greatest where there is depletion and beneath the electrode the inversion layer screens off the surface generation from the bulk, lowering the value of S there. It follows that there are two values of surface generation, one beneath the electrode and the other at the laterally depleted surface. Also since the surface beneath the electrode changes from depletion to inversion during the transient, the value of S for this region is time dependent. Taking this into consideration the lifetime value obtained from a Zerbst plot is found to be that for the inverted surface which is now known as the effective lifetime τ_g'. This is related to the actual bulk lifetime τ_g by the equation :-

$$\frac{1}{\tau_g} = \frac{1}{\tau_g'} - \frac{4\,S_o}{d} \qquad (2.17)$$

where S_o is the surface generation velocity at the depleted surface beyond the electrode (as in Figure 2.4)

d is the diameter of the electrode assumed to be circular. From the Zerbst expression for the transient capacitance following the application of a step voltage, which will be described in detail in Chapter 7,

$$-\frac{d}{dt}\left(\frac{C_{ox}}{C_d}\right)^2 = \frac{2\,n_i}{N_a} \cdot \frac{C_{ox}}{C_{df}} \cdot \frac{1}{\tau_g'} + \frac{2\,C_{ox}}{\varepsilon_s} \cdot \frac{n_i}{N_a} \cdot S \qquad (2.18)$$

where C_{df} is the final capacitance at $t = \infty$

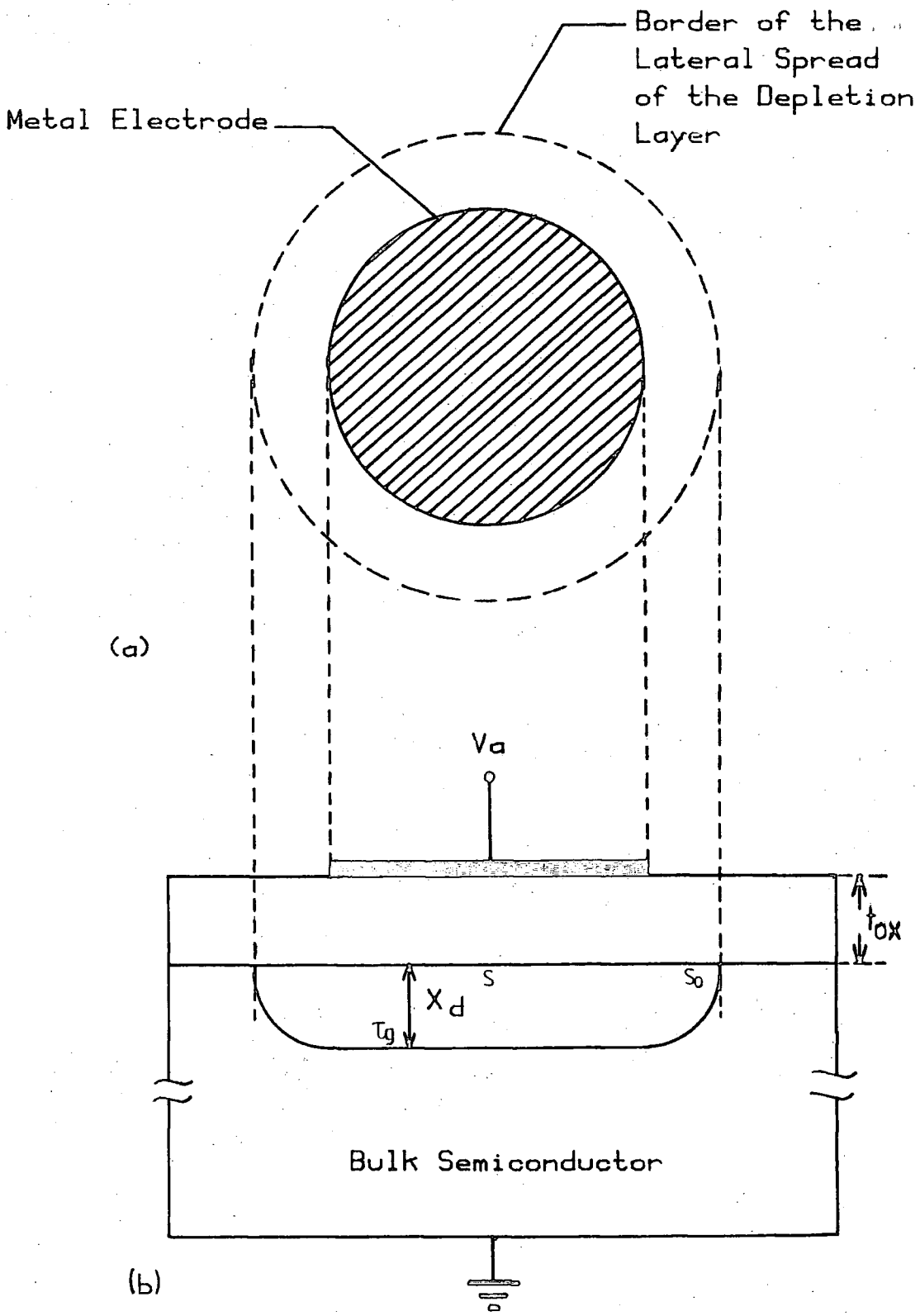

FIG. 2.4 The MOS Capacitor after a Step Voltage at t=0+ Showing the Lateral Spread of the Depletion Layer.

(a) The Plan
(b) The Cross-section

it is possible to obtain the variation of S during the transient. The value of S at the beginning ($t = o$) gives the value S_o for the surface outside the electrode. A further correction was made to τ_g' by Schroder and Nathanson to allow for the variation of S with time. This is given by the relation

$$\tau_{ge} = \tau_g' \left[1 - \left(\frac{1}{n}\right) \frac{2\, n_i\, C_{ox}}{t_{ox} N_a \varepsilon_s} \right]^{-1} \qquad (2.19)$$

where τ_{ge} is the corrected τ_g'

n is the gradient of a plot of s against $- \frac{d}{dt}\left(\frac{C_{ox}}{C}\right)^2$

t_{ox} is the oxide thickness.

The actual lifetime is then obtained from the expression

$$\frac{1}{\tau_{ge}} = \frac{1}{\tau_g} + \frac{4\, S_o}{d} \qquad (2.20)$$

This correction can only be used if the sample is pulsed from flat band to strong inversion,as the value of S_o has to be obtained before the formation of the inversion layer. Once the inversion layer has formed, the surface will be screened off from the depletion region by the width of the inversion layer. Therefore the surface recombination velocity will appear to be small. When the sample is pulsed from inversion into heavier inversion as in the Q-t measurements, a separate experiment is required to obtain the value of S_o, and this has to be done on a MOS capacitor from the same wafer and having the same area electrode but with large perimeter-to-area ratio.

For the Q-t method, this correction can be applied by using Equation (2.20) provided the value of S_o is known. This would require the whole experiment to be done from the initial stage of preparation of samples with different perimeter to area ratios, and hence it is not practical in this work. As long as the perimeter to area ratio is kept low, the influence of the interface generation is very small.

2.6 Published Experimental Results for the Q-t Method

In the Q-t papers by Hofstein, Zechnall and Werner, and Viswanathan and Takino, there are relatively few experimental results compared with many for the C-t method elsewhere. Hofstein published only one Q-t result for an n-type MOS capacitor and the distortion observed to occur between the Q-t traces biased into heavier inversion and for the return to initial state was not explained at all. Zechnall and Werner published results from four n-type samples of varying oxide thicknesses. They too did not investigate the problem of the deviation from an exponential transient for larger voltage steps. In the work of Viswanathan and Takino again only four samples were used, two with a uniform and two with a non-uniform doping concentration, N. These authors used both p- and n-type samples. They also published the plot of the variation of depletion width with surface potential during the Q-t transient. In all the published work on Q-t method, none of the authors included either the recombination or bulk diffusion terms for the carriers in the depletion layer. Also the case of "negative" voltage steps, i.e. voltage steps of polarity such as to bring the MOS capacitor from heavier inversion into less heavy inversion, was not dealt with at all.

Finally, all the above authors compared the lifetime obtained from the Q-t method with that of the Zerbst method of evaluation but none of them made a comparison with any of the other methods of measuring lifetime. The research described in this thesis attempts to overcome some of these deficiencies.

CHAPTER 3

SAMPLE PREPARATION AND Q-t EXPERIMENTAL MEASURING DETAILS

3.1 Introduction

The Q-t measurement method as developed by Hofstein (21) is susceptible to both noise pick-up and drift. Noise can be reduced by careful experimental technique and some of the drift can be eliminated using a suitable electrometer. However, drift can also be due to leakage of charge through the sample oxide. With this in mind the experimental lay-out and the samples were carefully constructed so that the Q-t transient could be accurately traced out for analysis. This called for close attention to the pulsing circuit and the transient recording technique, as well as the sample fabrication.

It is the purpose of this chapter to describe the sample used in the experiment and its preparation as well as to give an account on the construction of the measuring gear. The first half of the chapter deals with the steps taken in the making of the MOS devices in this department while the other half is devoted to the instrumentation involved and its development leading to the full computer-controlled set-up.

3.2 Sample Design

In Figure 3.1, a cross-section of the devices used for measurement is shown. Figure 3.1(a) is the type prepared in the department's own clean room and Figure 3.1(b) is the MOS capacitor sample made by ITT. The structure of the former is advantageous because its gate oxide is grown in

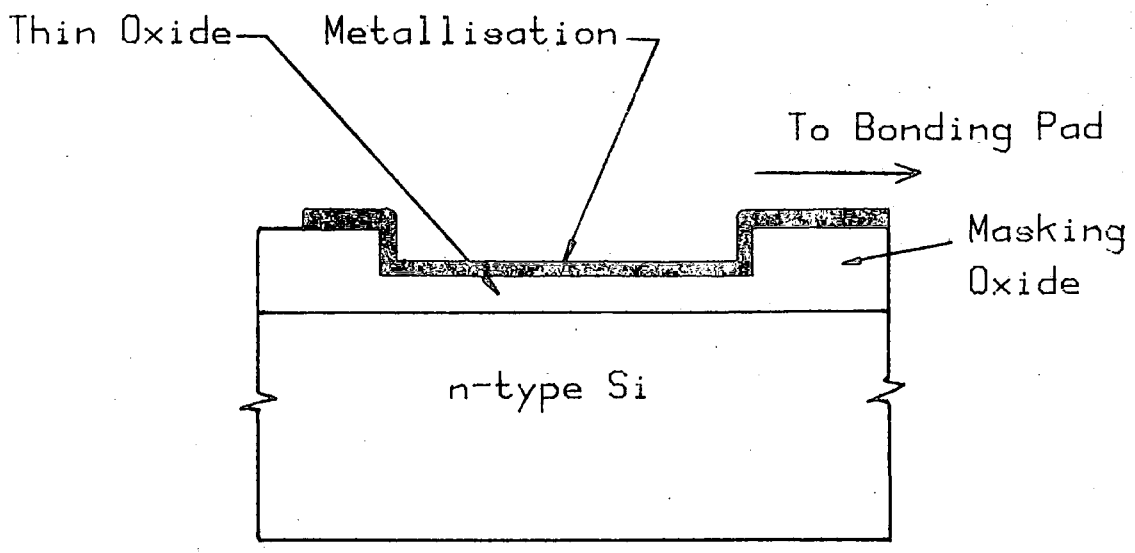

(a) MOS Capacitor as Constructed in this Department

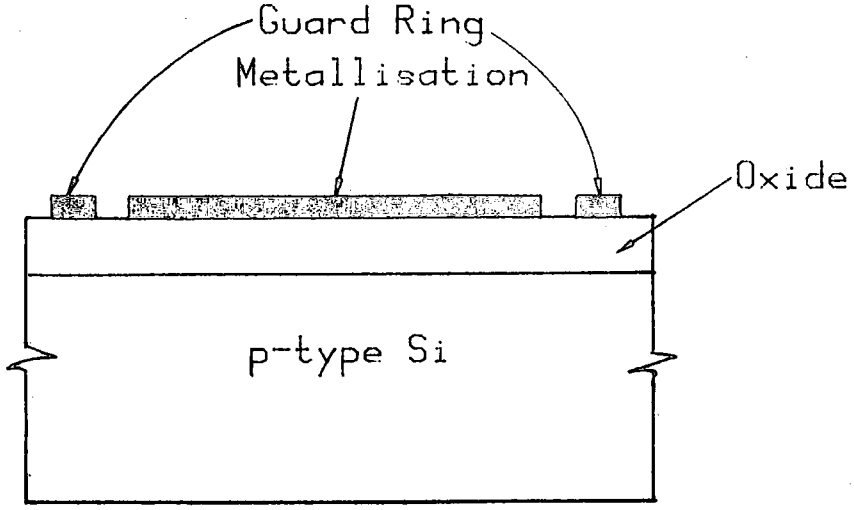

(b) The ITT MOS Capacitor Sample

Fig. 3.1 Cross-sections of the MOS Capacitor Samples used in this Experiment

areas etched away from the masking or field oxide which is about 1.50 μm thick. This reduces the intense edge field effects, as the aluminium metallisation overlaps over the edges of the masking oxide windows resulting in a more uniform electric field at the edges compared to the ordinary dot-evaporated capacitors. Electrical connections were made using microprobes on bonding pads, well away from the capacitors themselves. The pads are 130 μm square and are connected to the gate electrode by 15 μm wide aluminium strips. The capacitance contribution from the pads is very small and about 0.30 pF each as compared to the devices capacitance of about 120 pF for the biggest capacitor (Figure 3.2).

In the process of fabricating the capacitor, two masks were used. Mask 1 was for defining windows through the thick oxide for the growth of the thin oxide of the capacitors. Mask 2 is for removing excess aluminium to define the metal electrodes for the capacitors. Each of the masks is made on a glass plate containing a 5 x 5 array of chips 1.8 mm square using a step-and-repeat camera. A single cell from this array is shown in the diagram of the single chip of Figure 3.2.

The ITT samples were fabricated on p-type silicon substrates of resistivity about 8 Ω cm. The capacitors have a simple cross-sectional structure without the masking oxide. Each circular electrode is about 1.00 mm in diameter with an annular guard-ring around it of 45 μm width. There is a gap between the gate and the guard-ring of 30 μm. The oxide thickness is about 1000 Å.

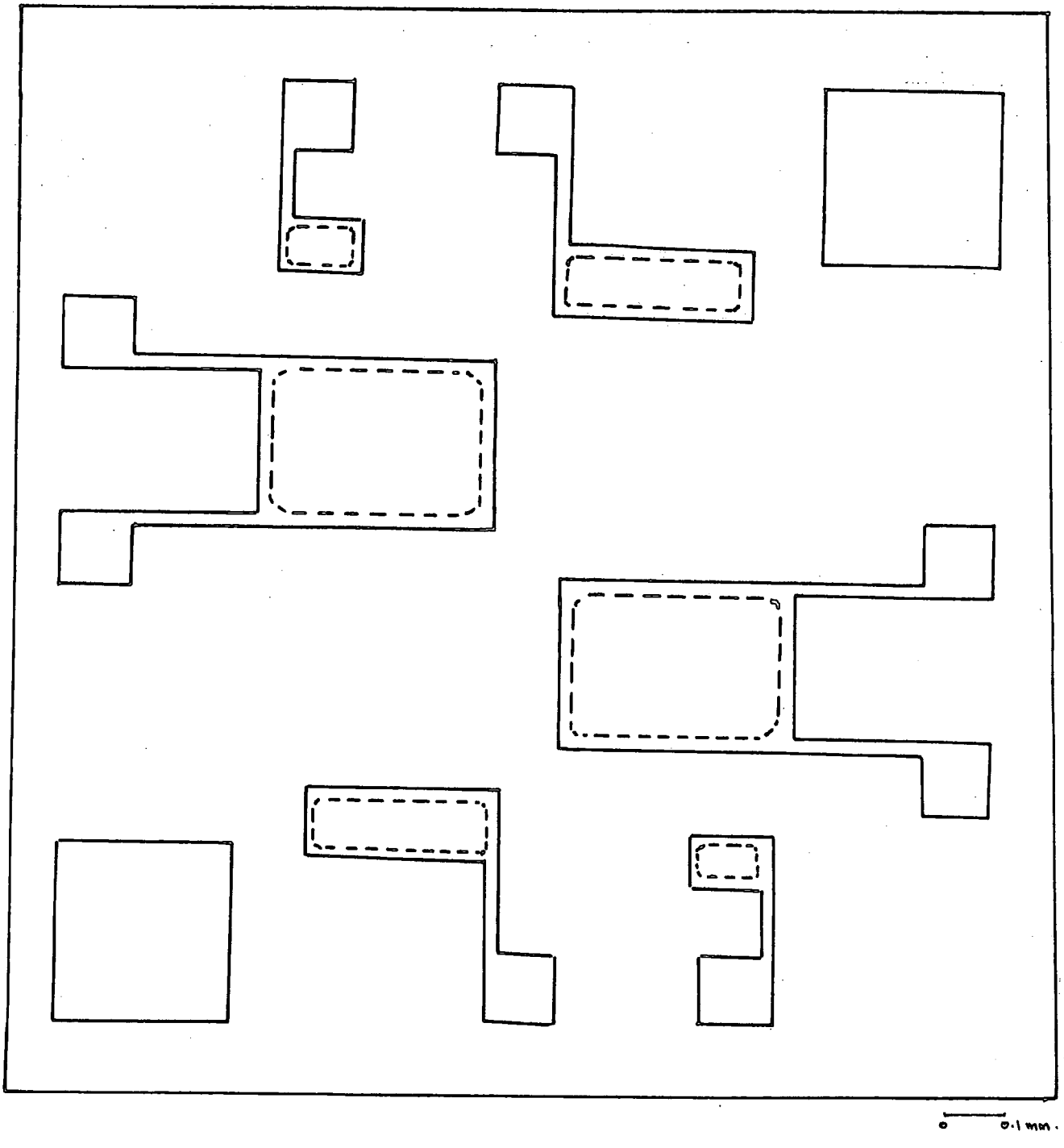

FIG. 3.2 MASK 1 - Dotted line (oxide window)
MASK 2 - Full line (Metal electrode and Connection Pad)

3.3 Sample Preparation

The fabrication process for MOS devices is outlined by Allison (36-39) and the present procedure is similar. Before doing the fabrication, the silicon slice was given a standard chemical cleaning procedure in chemicals of electronic grade (Ultrar and Aristar). The details were as follows:-

(a) Boil the sample in 111-Trichloroethane(TCE) for 5 minutes and follow with an ultrasonic wash in TCE for 1 minute.

(b) Blow dry with a hot air blower.

(c) Boil for 30 minutes in 'bomb' solution (1:1, H_2O_2 : H_2SO_4).

(d) Leave it in recirculating deionised (D.I.) water until the resistivities of the incoming and outgoing water are equal at above 12 Ω cm.

(e) Etch in 10% Hydrofluoric (H.F.) acid for 2 minutes.

(f) Repeat step (d).

(g) Rinse in propan-2-ol (IPA) in an ultrasonic bath.

(h) Blow dry.

The masking oxide was then thermally grown by wet oxidation at 1100°C after checking the furnace temperature profile. The flow of gas through the furnace was turned on two hours prior to loading the tube to allow it to stabilise. The flow rate for dry nitrogen and oxygen for flushing the tube was 500 c.c. per minute, and for oxidation it was 200 c.c. per minute.

The gate oxide was grown after windows had been etched through the masking oxide by standard photolithography. The photoresist used was a Shipley AZ-1350 positive type and was spun on at 4000RPM. The evenness of the photoresist layer

was checked by watching the light reflected from the film surface. The ultraviolet exposure was made on the Kulicke and Soffa mask alignment machine Model 682 A through Mask 1 (refer Fig 3.2). The exposed photoresist was developed away in Shipley MF 312 developer and the remaining photoresist was baked to harden it. This was followed by etching the unprotected oxide in 1:5 HF-NH_4F solution. To find out whether the etching was complete, the sample was occasionally pulled slightly above the surface of the etchant to watch for the onset of the hydrophobic state which, being due to the absence of SiO_2, indicated adequate etching. The sample was then washed in recirculating DI water and the remaining photoresist was removed in photoresist remover (diluted 1:2), followed by another wash in D.I.water. To ensure that no oxide remained behind in the etched areas, the sample was dipped again for 10 seconds in 10% H.F ; followed by a final wash in recirculating D.I.water. After a quick rinse in IPA in an ultrasonic bath the sample was left to dry in the mouth of the furnace tube. It was then oxidised in dry oxygen at $1100^{o}C$ at a flow rate of 200 c.c. per minute, for 30 minutes. Metallisation was done in an ion-pumped electron beam evaporation system. The metal used was 99.99% pure aluminium. The thickness evaporated was checked by observing the aluminium deposition on a glass plate placed in the evaporating chamber with the sample. Following the standard photolithography process using Mask 2 (refer Fig.3.2) the unwanted aluminium was etched away in an orthophosphoric-nitric acid solution of composition 30 parts to 2 parts to 7 parts of water. The hardened photoresist was removed and the sample was washed in D.I.water followed by a wash in IPA in an ultrasonic bath and

blown dry. The sample was then annealed at 490°C for 10 minutes in a nitrogen flow of 400 c.c. per minute.

The electrical connection to the substrate was made through the back contact. This was done by evaporating gold-antimony for the n-type substrate and pure gold for the p-type substrate. Great care was taken in the removal of oxide prior to evaporation so that a good ohmic contact was obtained. The details were as follows:-

(1) Lap off the oxide on the underside of the sample by using 'Hyprez' diamond compound of 3 μm grain size.

(2) Clean off traces of the diamond paste with acetone and blow dry.

(3) Apply a few drops of 10% H.F. onto the lapped back and observe for the hydrophobic condition.

(4) Wash in D.I. water.

(5) Dry in oven.

The gold was evaporated in a conventional diffusion-rotary pump evaporator. The contact was then annealed for 7 minutes at 400°C in nitrogen. Two strips of gold were evaporated and the resistance between them was measured to ensure that proper ohmic contacts had been formed.

3.4 Construction and Development of the Manual Measurement Apparatus

In the following sections the construction and development of the manual version of the measurement apparatus is given. It involves the construction of the probing box, the electrometer and the bias control circuits.

3.4.1 Basic Circuit

As outlined previously the circuit used for the Q-t

experiments was basically a charge amplifier. A schematic diagram is shown in Figure 3.4 which shows that it is a charge-to-voltage converter. The charge on the input capacitor is determined by the voltage across it and also its capacitance. This is given by

$$Q_{in} = C_{in} V_{in}$$

where V_{in} is the voltage across C_{in}.

This charge will also appear on the feedback capacitor C_f as they are in series, and since the input of the op amp is virtually at ground this charge is related to the output voltage V_o of the amplifier by

$$V_o = - \frac{Q_{in}}{C_f}$$

Thus the output voltage is directly proportional to the input charge. This charge amplifier circuit was used as an electrometer to measure the transient charge resulting from the pulsing of the MOS capacitor which was used in place of the input capacitor of the amplifier. In this section we discuss the experimental details and their development.

The construction of the measuring gear started with the building of a box for holding the sample under test, probers for making the electrical connection to the gate electrode and the guard-ring when present, and a conducting platform as a base plate to hold the sample firmly and to provide the electrical connection to the back contact of the sample.

The box was cut out of a cubic block of stainless steel with the top opening slightly recessed to take a glass plate for viewing when setting up. An aluminium plate was used to

slide on top of the glass plate to provide electrical screening. Tubes were built into the box to allow flushing the chamber with nitrogen when required. An opening was provided on one side for the main prober to enter. The latter was clamped to the x-y movement mechanism which also had a lever for the vertical movement. This enabled the prober to be raised or lowered on to the sample. Teflon sleeves were used to provide electrical insulation. Another opening was also provided on the same side, to take a second prober, of simpler construction than the main one. This was used for probing the guard ring. The base plate on which the samples were placed during measurements was built on Teflon pillars to make the leakage path as long as possible. A vacuum chuck was built into it to hold the sample firmly so as to provide a good electrical connection to the back contact of the sample. The electrometer circuit was placed inside an aluminium box screwed to one side of the probe chamber. Its input was connected to the baseplate through a hole at the side of the chamber. On the other side was another box which contained the voltage step generator circuit. A schematic diagram showing the top view of the probe chamber is shown in Figure 3.3. In the following paragraphs the circuits used are described.

The electrometer circuit was based on Hofstein's method and its circuit diagram as shown in Figure 3.5. The operational amplifier used was the Philbrick Nexus SQ-10a and an RCA MOSFET type 3N128 was coupled to the input of the operational amplifier to increase the input impedance of the circuit. The feedback capacitor was a mica type and a reed switch was used for dis-

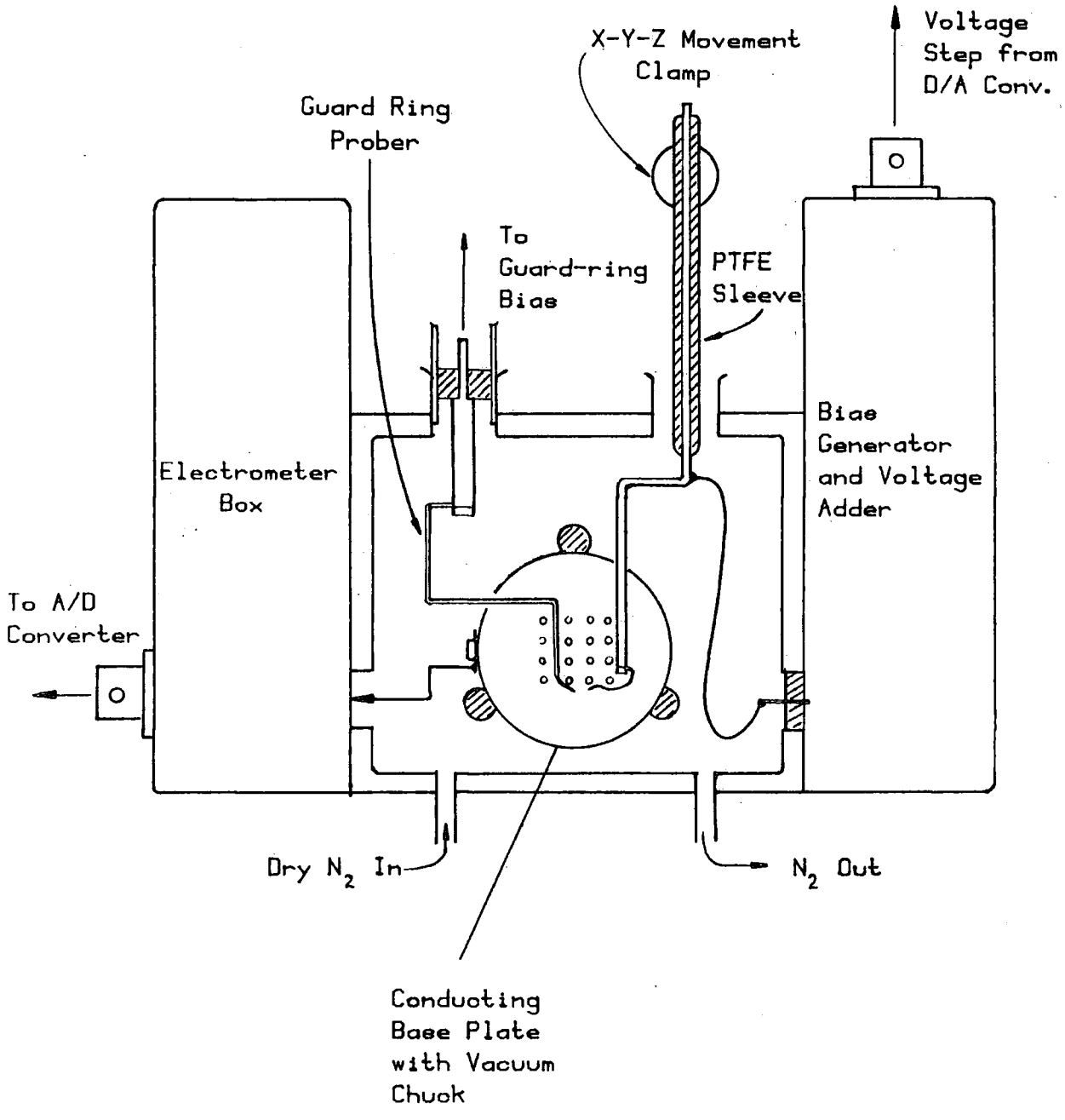

FIG. 3.3 Schematic Diagram of the Probing Box

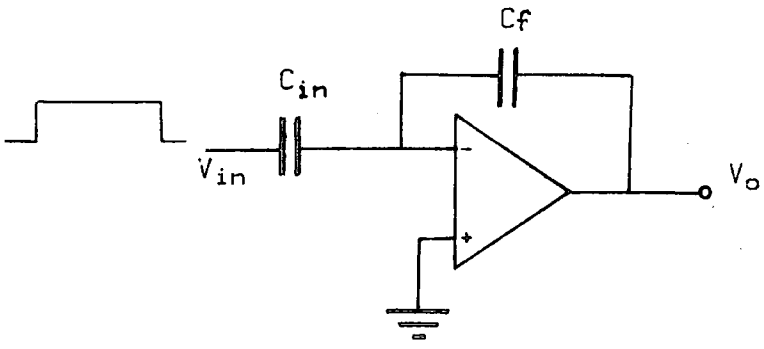

Fig. 3.4 The Charge Amplifier Circuit

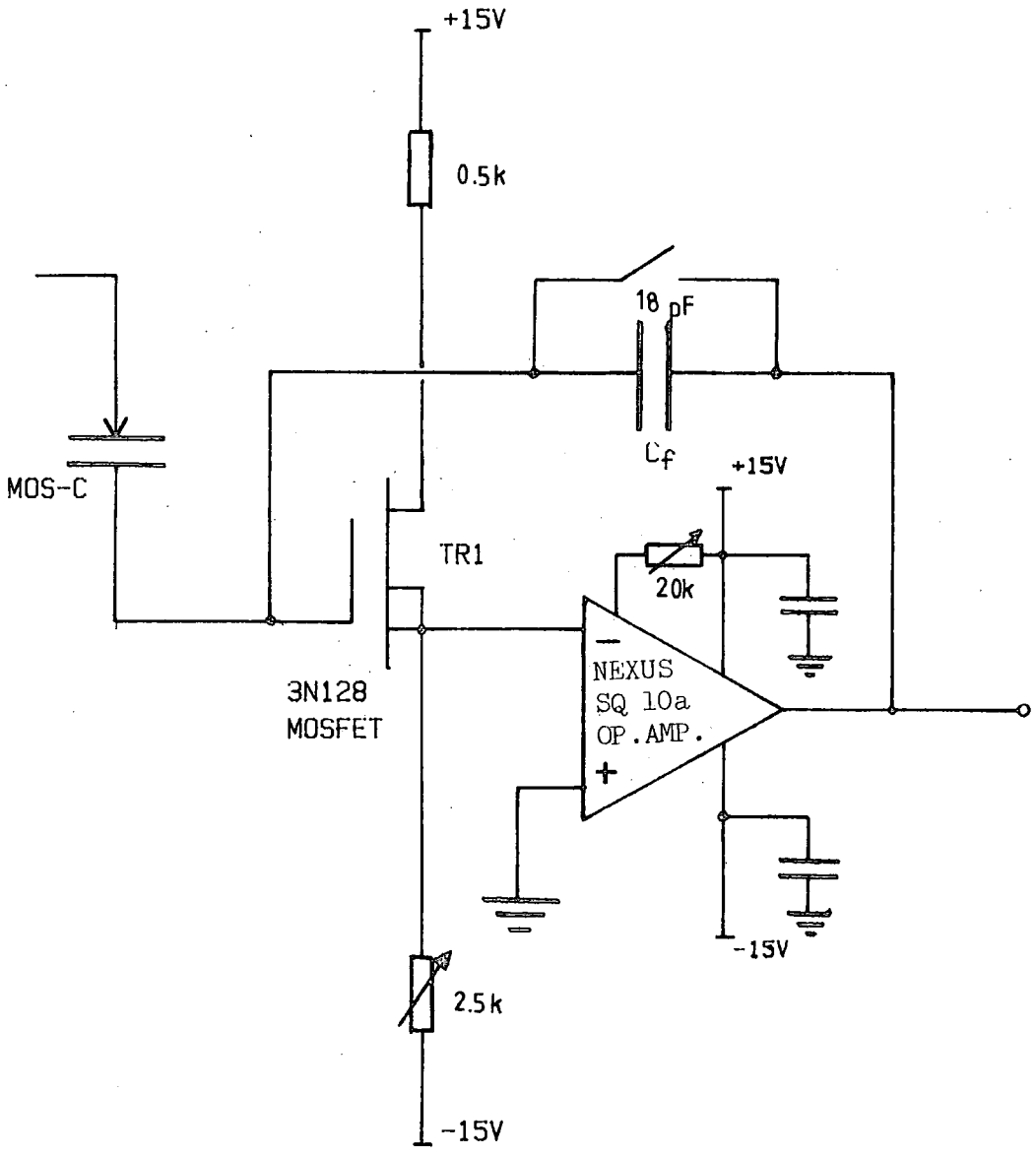

Fig. 3.5 The Electrometer Circuit Diagram

charging it prior to making a measurement. These components were connected to the input of the electrometer which is the gate of the MOSFET. The connection of the baseplate, the feedback capacitor and the reed switch to the input of the electrometer were carefully made to ensure that there was no leakages to the other parts of the circuit, otherwise the output reading of the electrometer would drift excessively.

Due to the sensitivity of the measuring circuit and the low level of charge injection, the millivolt step generator had to be carefully designed. Various methods were tried. At first a reed switch was used to change the applied potential. The circuit diagram for this arrangement is shown in Figure 3.6 where points A and B were set such that their potential difference was controllable to give a few tens of millivolts on top of the fixed bias voltage which was normally needed to bring the device under test into the inversion mode. This fixed voltage was determined by the values of R_1 and R_2. An electronic control circuit, was built to drive the solenoid of the reed switch. This supplied pulses of variable duration to suit the test device characteristic ; and also a controlled pre-pulse output before the main pulse to allow proper triggering of the recording equipment. The problem with this set up was that spikes were seen on the output signal at the beginning and at the end of the trace as shown in Figure 3.7. This was found to be due to contact bounce and noise pickup by the reed switch. In view of this a purely electronic switch was designed.

The circuit used is as shown in Figure 3.8. A 741 operational amplifier was connected up in a non-inverting mode. The transistor TR1 was used to change the potential at point A,

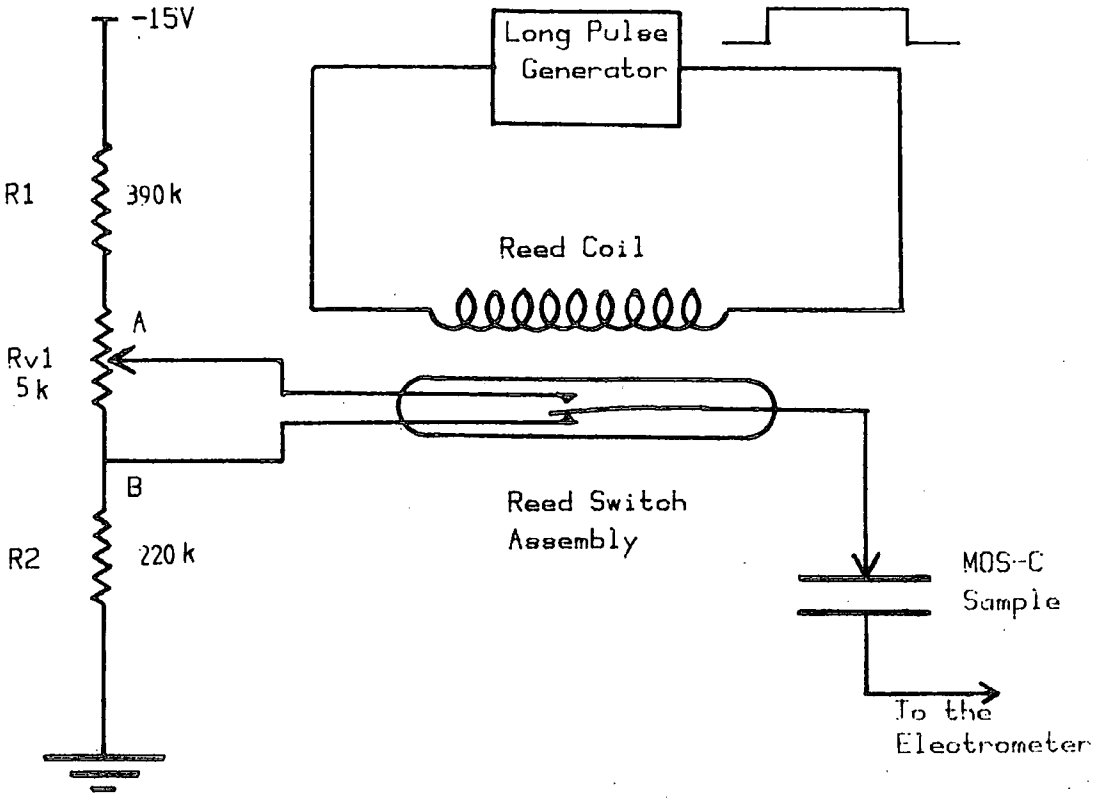

Fig. 3.6 The Reed Switch Voltage-Step Generator

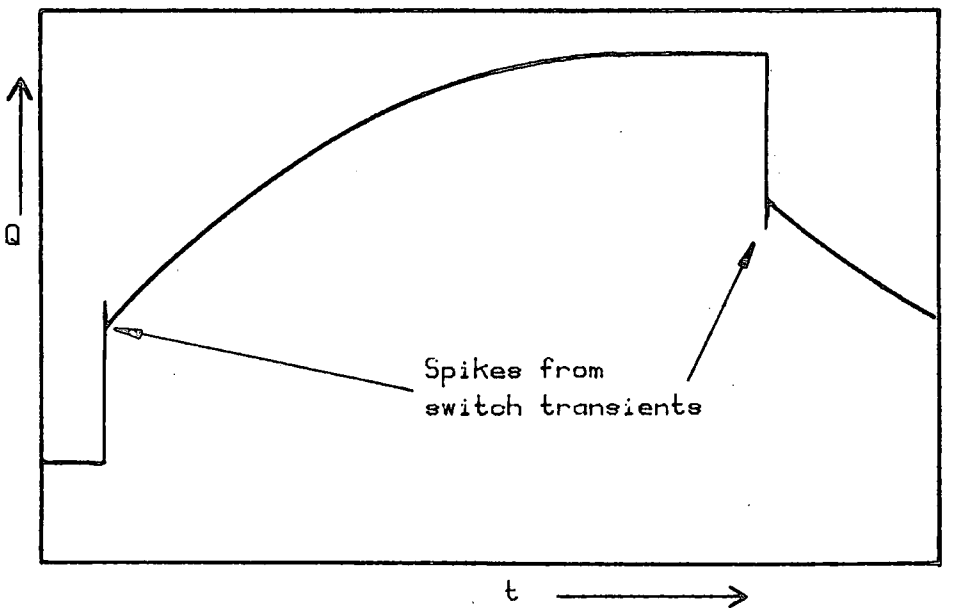

Fig. 3.7 A Typical Q-t Plot

while control and timing was provided by the same box as was used with the reed switch circuit. This simple circuit was adequate for producing the millivolt steps without the spikes that occurred previously. However in doing the experiments it was found that the bias level and the voltage step magnitude needed to be changed to cater for the different devices being tested. To achieve this the resistors in the network had to be changed each time different settings were required. The situation was the same with the pulse generator as it would need further modification to the circuit in order to produce timing pulses to cope up with different samples. Multiple pole switches could have been used for the above purpose but as this became complicated, it was decided to go for a programable voltage-step generator.

3.4.2 Use of KIM Microprocessor Board

The Figure 3.9 shows the set-up which employed the KIM microprocessor board. This board has two input/output (I/O) ports. All the 8 bits of the I/O port A were programmed to be in the output mode. A Ferranti ZN 425 D/A converter was used to convert the digital information into analogue form. By changing the contents of the output register, it was possible to change the voltage step height, with 255 values possible with an 8-bit machine. Finer adjustments could be made on the analogue signal by the use of a 741 operational amplifier to give the exact voltage step required for the device under test. One line from the second I/O port (port B) was used for triggering the oscilloscope. In this arrangement the timing and control of the voltage step and the triggering pulse were all software controlled

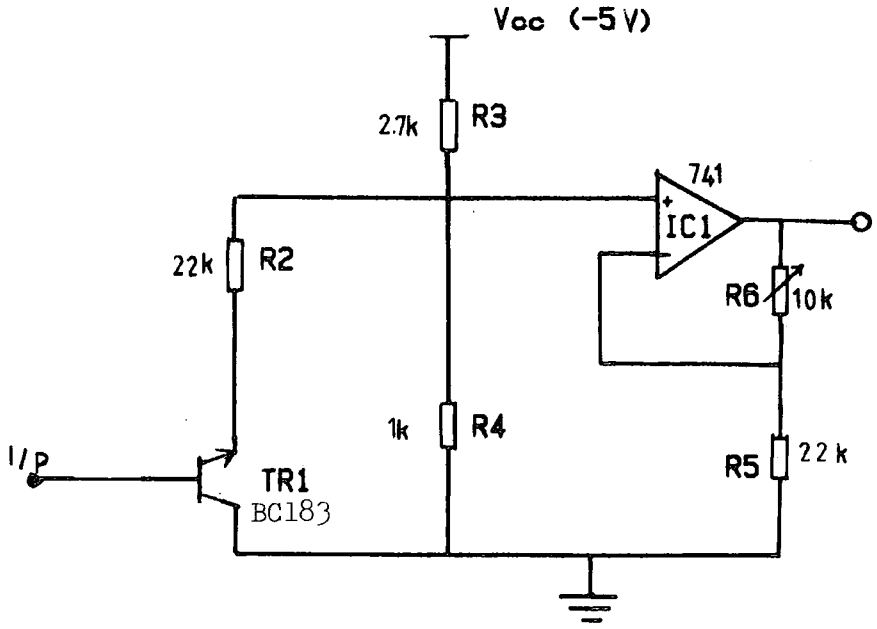

FIG. 3.8 The Electronic Voltage Step Generator

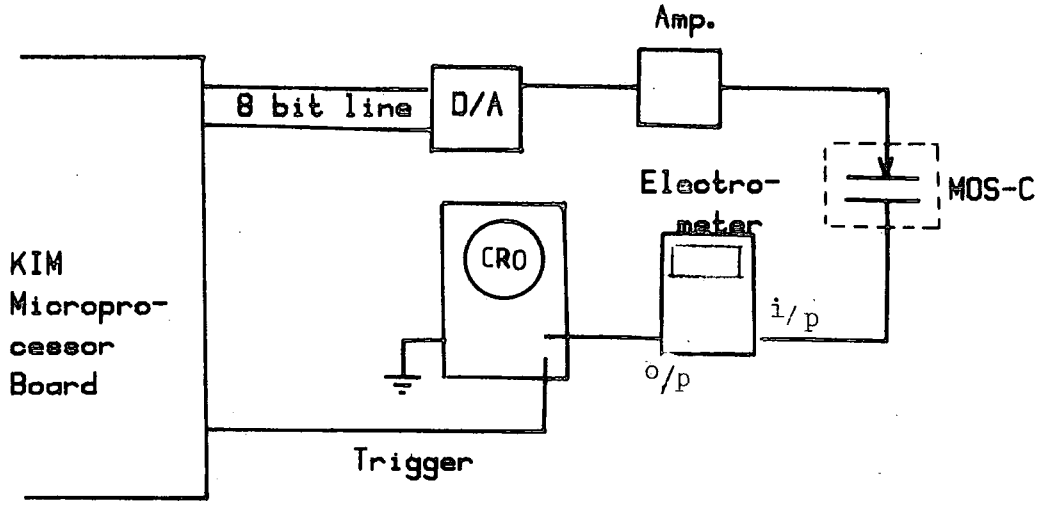

FIG. 3.9 Set-up using KIM Microprocessor board to supply the Voltage Steps

using the internal timer of the microprocessor. The KIM microprocessor was programmed in Machine code and the program is summarized in the flowchart of Figure 3.10.

The voltage output from the electrometer, which is a measure of the input charge from the device after a pulse application, was monitored on the oscilloscope and the trace was first recorded using a Polaroid camera. However, this record was found to be too small for an accurate analysis to be made. The Bryans x-y plotter was too slow for the purpose so an ultraviolet recorder was tried instead. This did not prove to be a very convenient way of doing the experiment. The recording paper did not have proper grid and it was affected by ambient light which caused deterioration to the recorded transient trace which had to be normalised and replotted before it could be analysed. Furthermore the electrometer was very sensitive and as the signal measured was rather small, there were serious noise pick-up problems. A digital recording technique was therefore considered which overcame the above problems. This involved interfacing the experiment to a microcomputer so that the output trace could be recorded and stored at fast speed and then plotted later at the speed of the plotter.

3.5 Construction and Development of the Automated Measurement Apparatus

With the need for digital recording, the opportunity was taken to put the entire experiment under microcomputer control which would also reduce the tedium of doing the measurements and analysing the results. The KIM microprocessor was suitable for controlling voltage steps but it

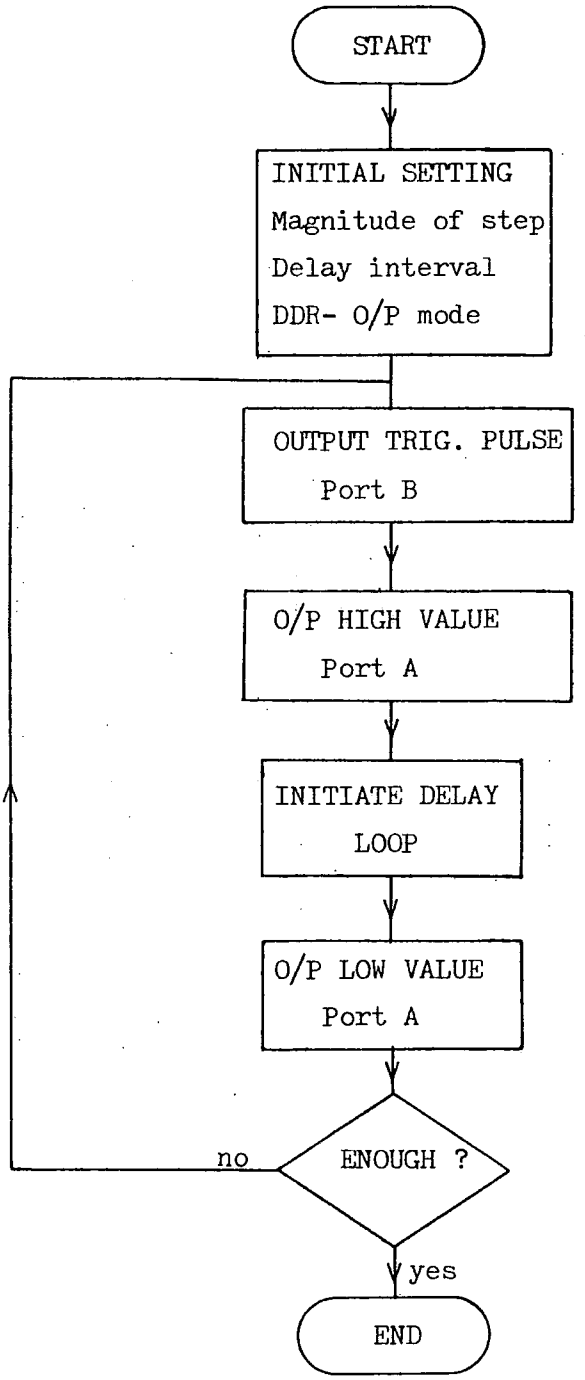

FIG. 3.10 FLOWCHART FOR PRODUCING STEP OUTPUT ON KIM MICROPROCESSOR.

has limited memory size for data storage and requires programs written in Machine Language (41). A microcomputer could therefore do a great deal more. Apart from handling the voltage step control,it can store data from the electrometer output in its memory and on magnetic tape. This can then be plotted out, either as obtained from the electrometer, or as a calculated mathematical function. Most important of all, it can also do averaging on the data over a few measurements and so reduce the effects of noise. In the following sections a detailed account on the use of a microcomputer to control the experiment(42,43) is given. It turned out to be extremely satisfactory and well worth the development effort.

3.5.1 Use of PET Microcomputer to Control the Experiment

The microcomputer used was the CBM microcomputer (better known as PET). To use a PET to control the experiment in machine code required a good understanding of the function of the IEEE-488 and user ports. This knowledge was not widely available when the project started.

Figure 3.11 shows the block diagram of the set-up, where the PET was used to provide the voltage step as well as recording the electrometer output signal. The IEEE port was used to provide the voltage step as controlled by a second 6520 peripheral interface adapter (PIA) chip (40). Table 3.1 outlines the basic functions of this chip. This port works with standard IEEE-488 bus peripherals so a special IEEE D/A converter built in the Department was used. The output is obtained by writing into a file allocated to the device number of the peripheral (in this case the D/A con-

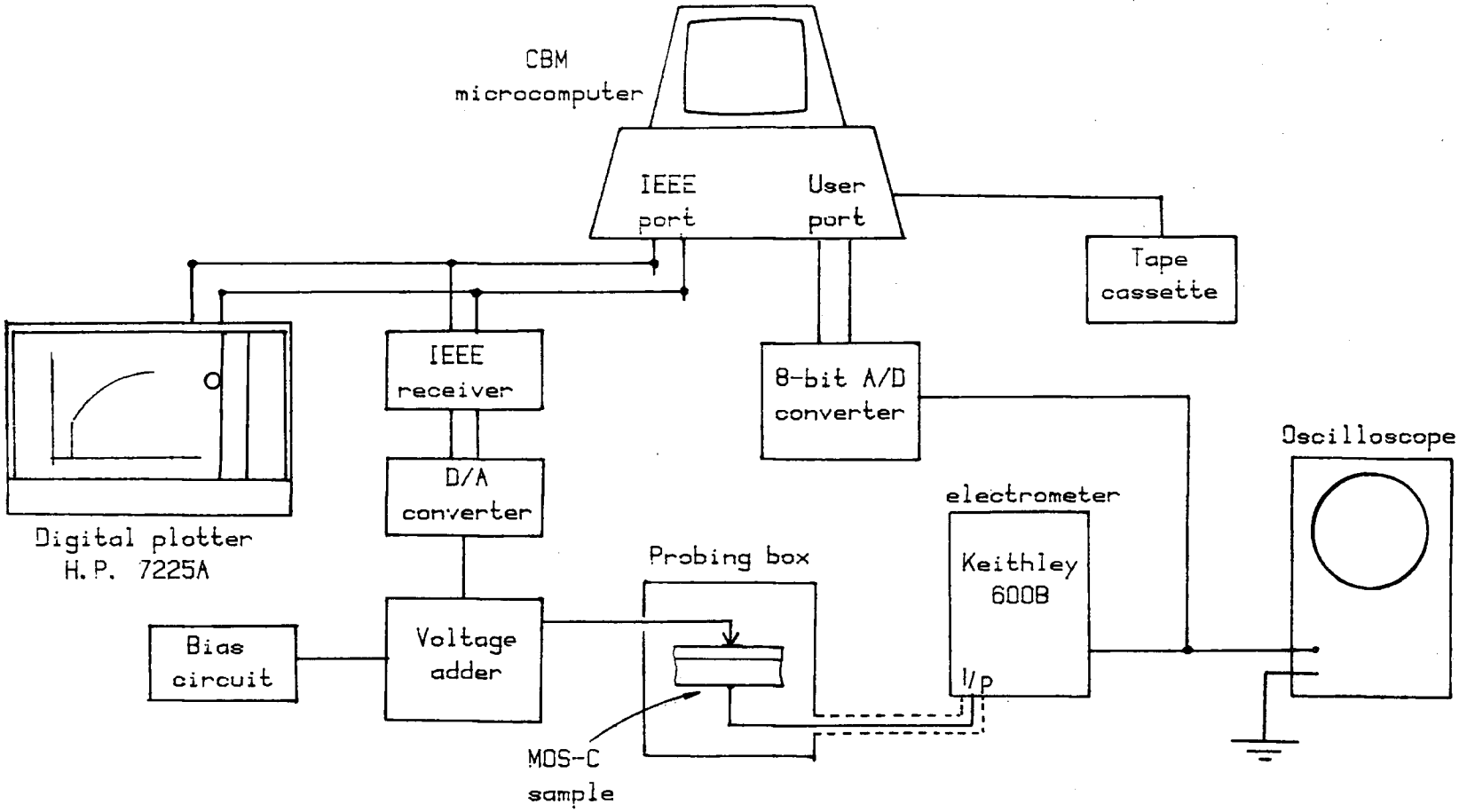

FIG. 3.11 PET Interface

	7	6	5	4	3	2	1	0	
E810	Diagnos. Sense	IEEE EOI in	Cassette Sense #2	#1	Keyboard Row Select			PA	59408
E811	Tape #1 InputFlag	...	Screen Blank Output			CA2	DDRA ACCESS	Cassette #1 Read Control CA1	59409
E812	KEYBOARD ROW INPUT								59410
E813	Retrace I Flag	...	Cassette # Motor Output			CB2	DDRB ACCESS	Retrace Interr. Control CB1	59411

6520 - PIA 1

	7	6	5	4	3	2	1	0	
E820	IEEE INPUT								59424
E821	ATN I Flag	...	IEEE NDAC OUT			CA2	DDRA ACCESS	IEEE ATN in Control CA1	59425
E822	IEEE OUTPUT								59426
E823	SRQ I Flag	...	IEEE DAV OUT			CB2	DDRB ACCESS	IEEE SRQ in Control CB1	59427

6520 - PIA 2

TABLE 3.1 MEMORY MAP OF 6520 IN CBM MICROCOMPUTER (40)

verter, IEEE address 6) with an instruction to send out a binary character. The analogue output from the converter was added to the bias value through a 741 operational amplifier which provided the final setting of the voltage step height.

The prober box used with this arrangement was improved over the previous design by using three Electroglas Microprobers Model 252. One prober was used for the gate connection, one for the guardring bias and one for continuity and contact checks. The general layout was still the same but a Keithley 600B electrometer was used to replace the home-built one. As the output from the electrometer was in analogue form an A/D converter was used to interface it to the PET input. The A/D converter built for this work used a Ferranti ZN 425 D/A converter chip which has a built-in 8-bit binary counter. There is an output terminal that produces a staircase ramp as the counter is fed with clock pulses. A clock inhibiting gate and a comparator were the other main parts used as shown in Figure 3.12. A crystal oscillator circuit was used to provide the 1 MHz clock pulses and a 531 operational amplifier was used as the voltage comparator. This changes its output state whenever the voltage ramp catches up with the input voltage. In this set up the conversion rate was dependent on the magnitude of the input voltage. To overcome this disadvantage, a time delay loop was incorporated into the software control where a delay, which was equal to the maximum time required to convert the highest input voltage capable of being converted, was used. The conversion was arranged to take place during this delay

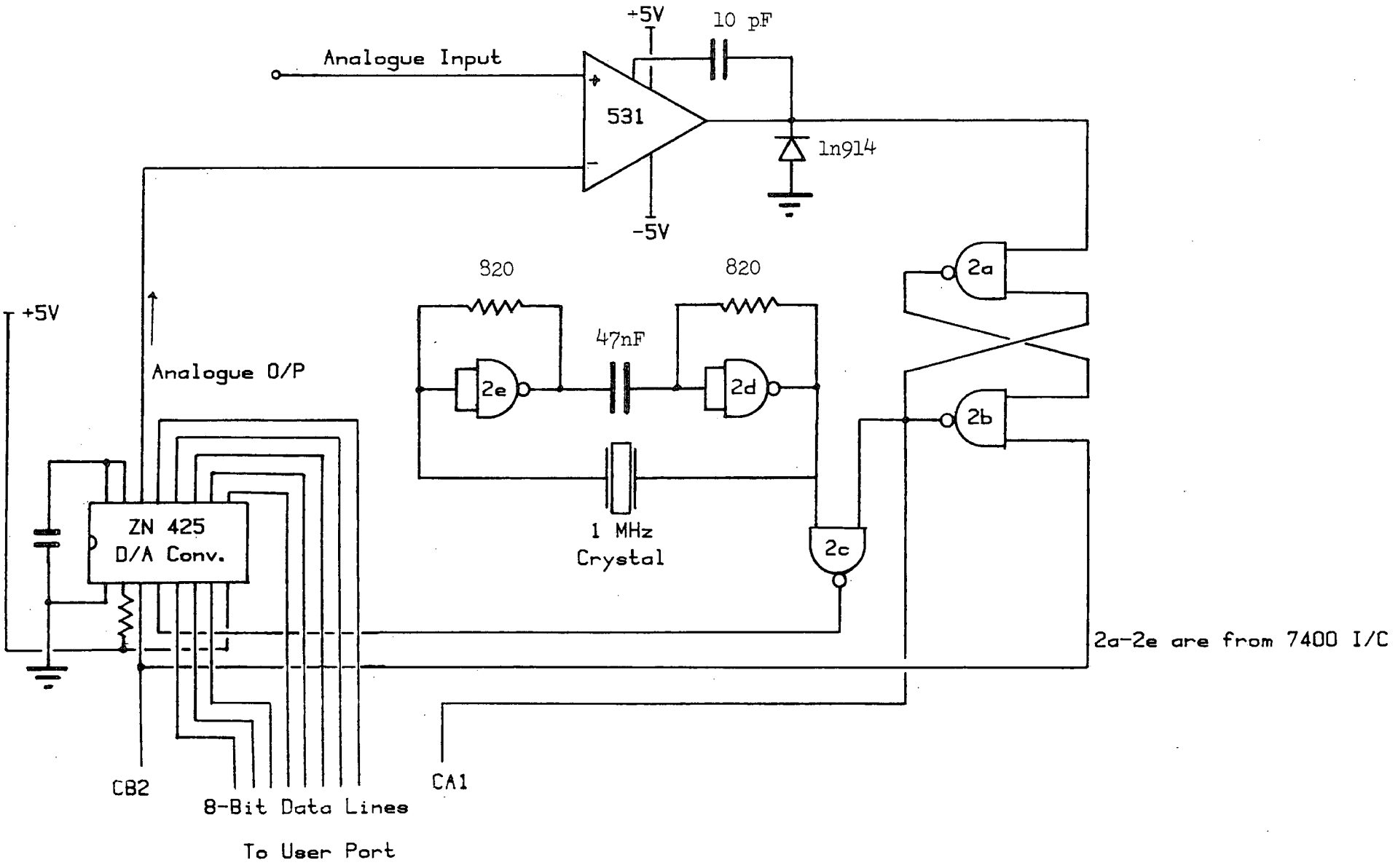

FIG. 3.12 Layout of the 8-Bit A/D Converter used in this Work

period. Thus the conversion time remained dependent only on the clock frequency.

On receiving the "start-convert" signal on the CB 2 line the gate starts to pass clock pulses to the converter where a staircase ramp is produced. This is compared to the input voltage from the electrometer. When the ramp voltage equals the input voltage the comparator changes its output state causing the gate to open and thus stop the conversion. At the same time an "end-of-conversion" signal is sent on the CA 1 line to latch the data on the input line into the PET's input register.

An alternative method to do the analogue-to-digital conversion would now be to use a successive approximation A/D converter. A low cost one chip converter of this type was not available when the project started. It would only have produced a significant difference over the one used if the Q-t transient was very fast. However, the transients measured on the samples used in this work were all slow enough to be accurately stimulated by the step converter described above.

3.5.2 The User Port Interface

The user port was used to record the output Q-t signal from the A/D converter by putting it into the PET memory. The user port provides faster data acquisition when programmed in machine code than the IEEE port which has a timing sequence to be followed. It has a 24-terminal edge connector in 2 groups of 12. The lower 12 were used in the experiment while the rest are for diagnostic purposes. Of the 12 lines 8 are I/O lines, 2 lines (CA1 and CB2) are

for the handshake control and the remaining 2 are ground connections. The I/O lines are individually programable. This port communicates with the microprocessor through the 6522 versatile-interface-adapter (VIA) chip(44). This chip has 6 registers with 16 addresses. Table 3.2 shows the addresses to these registers. The individual bits of the contents of these addresses have their own functions.

In the experiment the 8 data lines of port A were programmed through the data direction register as inputs and the CB2 line, which is controlled by the peripheral control register (PCR), was programmed as an output. The latter line was used for sending the "start-to-convert" signal to the A/D converter. It was normally held high as determined by the software, to inhibit the clock pulses from the converter and prevent the conversion process occurring. The CA1 line was used as an interrupt line and looking at the block diagram of the A/D converter we see that the CA1 line will be normally low. The "start-convert" signal was sent by setting CB2 line low. This allowed the clock signal to pass through to the clock input terminal of the converter chip. The CB2 line should only be momentarily low before returning to its high state again, otherwise the conversion will not end. During this time the programme is halted and waits for an interrupt to occur. When the conversion is complete, the CA1 line goes low again and as the interrupt is programmed to detect a negative transition, the change in the CA1 line logic level (from high to low) sets the interrupt flag and also latches the data on the input line into the input register. When this occurs the input is read and

	7	6	5	4	3	2	1	0	
E840	DAV in	NRFD in	RETRACE in	CASS # 2 MOTOR	CASSETTE OUTPUT	ATN out	NFRD out	NDAC in PB	59456
E841	ORA (CONTROLS HANDSHAKES)								59457
E842	DIRECTION REGISTER B (FOR E840)								59458
E843	DIRECTION REGISTER A (FOR E84F) (P.U.P.)								59459
E844	TIMER 1							L	59460
E845								H	59461
E846	TIMER 1							L	59462
E847	LATCH							H	59463
E848	TIMER 2							L	59464
E849								H	59465
E84A	SHIFT REGISTER								59466
E84B	T1 Control One-Shot PB7 out, Free Run		T2 Contr PB6 Sense	Shift Reg. Control			PB, PA LATCH Control		59467
E84C	CB2 (P.U.P. Pin M) Control IN/OUT			CB1 in cass # 2 polarity	CA2 (graphics, Lower Case) Control IN/OUT			CA1 in polarity	59468
E84D	IRQ STATUS	T1 INT	T2 INT	CB1 Cass # 2 INT	CB2 INT	SR INT	CA1 (PUPB) INT	CA2 INT	59469
E84E	Enable Clear/ Set	T1 INT enab	T2 INT enab	CB1 INT enab	CB2 INT enab	SR INTenab	CA1 INT enab	CA2 INT enab	59470
E84F	PARALLEL USER PORT I/O (PA)							PA	59471

TABLE 3.2 MEMORY MAP OF 6522 IN THE CBM MICROCOMPUTER (40)

stored into the allocated memory location. Another time delay loop was incorporated into the data acquisition program before the start of the next convert command. This determined the sampling rate of the data acquisition.

The programme for the above data acquisition routine is summarised in the flowchart of Figure 3.13. It was written in Machine language. This was done on the PET by loading the machine code instructions into the second cassette buffer using BASIC where the machine code program was treated as a subroutine. The reason for choosing the second cassette buffer was that BASIC program and its variables and strings might corrupt the machine code instructions if the latter was stored elsewhere and unprotected in the user RAM. There are 2 cassette buffers in PET. These are protected from BASIC programs and as only one cassette recorder was used, so the second cassette buffer was available for storing the Machine Code subroutine.

The digitised Q-t transient signal could be read and stored directly from a single measurement if the noise level was not too large. Alternatively, a number of transients could be averaged to remove the random noise pick-up. As with the Machine Code instructions the storage area of the data had to be protected from the BASIC program and as the second cassette buffer was used for storing the machine code program instructions, these were stored in locations reserved aside for them. In PET the BASIC program instructions are stored from the bottom of the RAM upwards while the variables and strings are stored from the top of the user RAM downwards. The size of this user memory is then

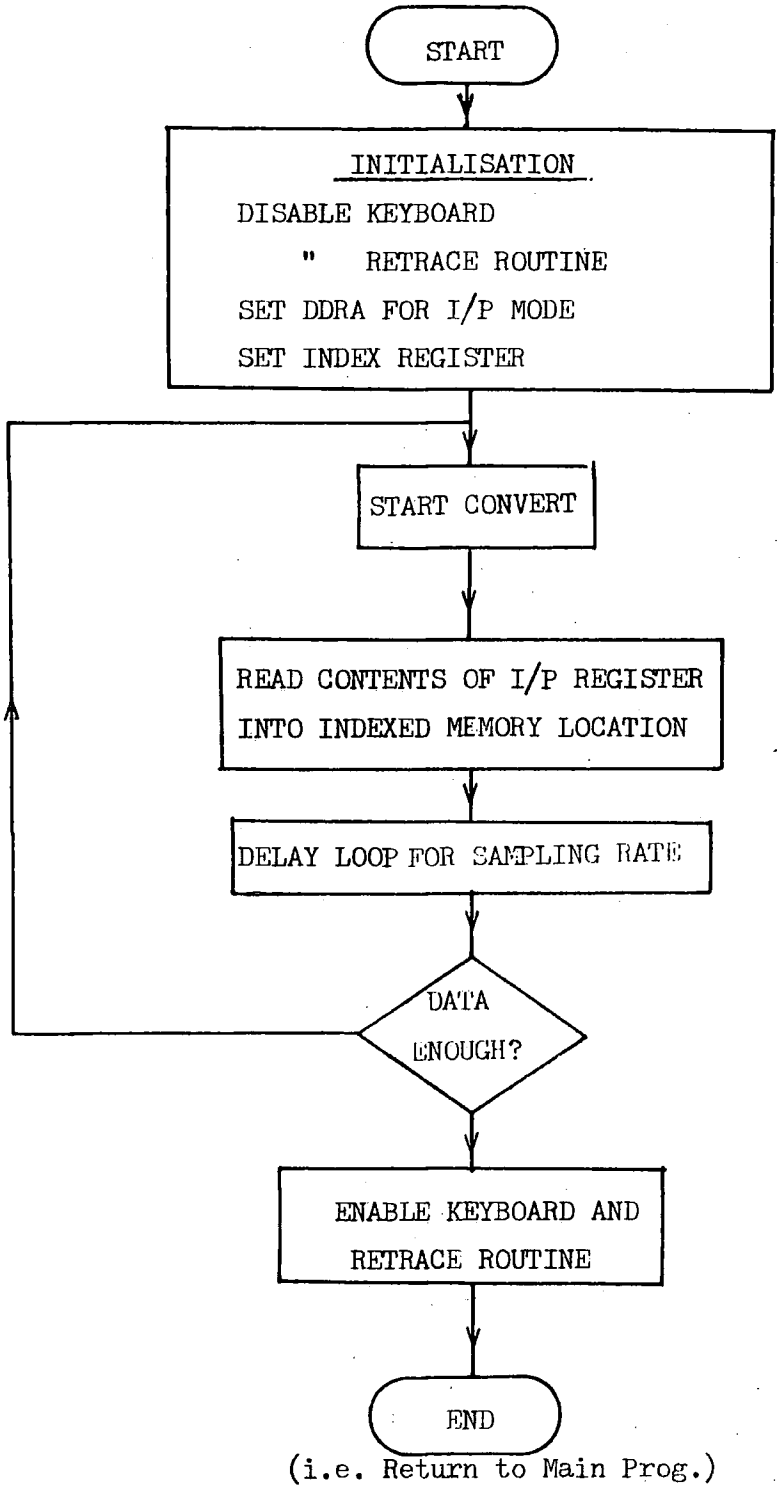

FIG. 3.13 FLOWCHART FOR THE MACHINE-CODE SUB -ROUTINE

reduced by changing the content of the top of the RAM pointer to point to a lower location in the memory. This has the effect of lowering the upper limit of the RAM. Variables and strings will now be stored from this new address location downwards. Thus there will be some area of the memory left above this new limit which can be used to store data. As this area is protected from the BASIC program, the data once stored in it are not lost when the program resets. The above method was adopted for storing the data from the experiment. The data was then transferred into an array for the purpose of doing calculations and for it to be plotted to give the required transient for analysis. Permanent storage was possible by storing this array on magnetic tape.

3.5.3 The BASIC Programs

The main program to control the overall experimental set-up was written in BASIC language. It consisted of several parts. The first being the 'set-up' part to adjust the settings of the equipments. This was to allow direct communication between the experimental set up and PET. A trial run was then performed where the program was made to continuously interrogate the output from the electrometer and display the information on the VDU to enable adjustments for the correct sensitivity and range to be made. Then the program was put into an interactive state where various devices were displayed on the VDU screen awaiting instructions as to which routine to be performed. To start off the experiment, an instruction was sent to output the voltage step through the IEEE port. Both the positive and negative Q-t transients were recorded, i.e. for both directions of the applied voltage step. In this experiment the measured charge was of the order of

10^{-12} Coulomb and this was thus susceptible to noise. The Q-t data was therefore averaged over several readings to reduce the random noise pick-up. On completing this task the program then sent the computer into the interactive state again to enable other parts of the program routine to be chosen. These are (a) the plot routine, (b) the calculation, (c) the data storage routine and (d) the reset routine repeats the whole experiment. A summary of the program steps is given in the flowchart of Fig 3.14 and the full program is in Appendix 1

3.5.4 Performance

The effort made in interfacing the experiment to the microcomputer greatly improved the efficiency of the work. It allowed the magnitude of the voltage step and the bias voltage to be varied by keyboard control, and the Q-t transient results were recorded, averaged and transformed very rapidly. The overall performance was therefore far superior to the earlier methods, particularly in the elimination of noise. As will be shown, smooth and reproducible Q-t curves could easily be obtained for the first time. The microcomputer made the tedious and laborious measurements and analyses easy to perform, and enabled very many more results to be obtained than in any of the published papers on the Q-t method.

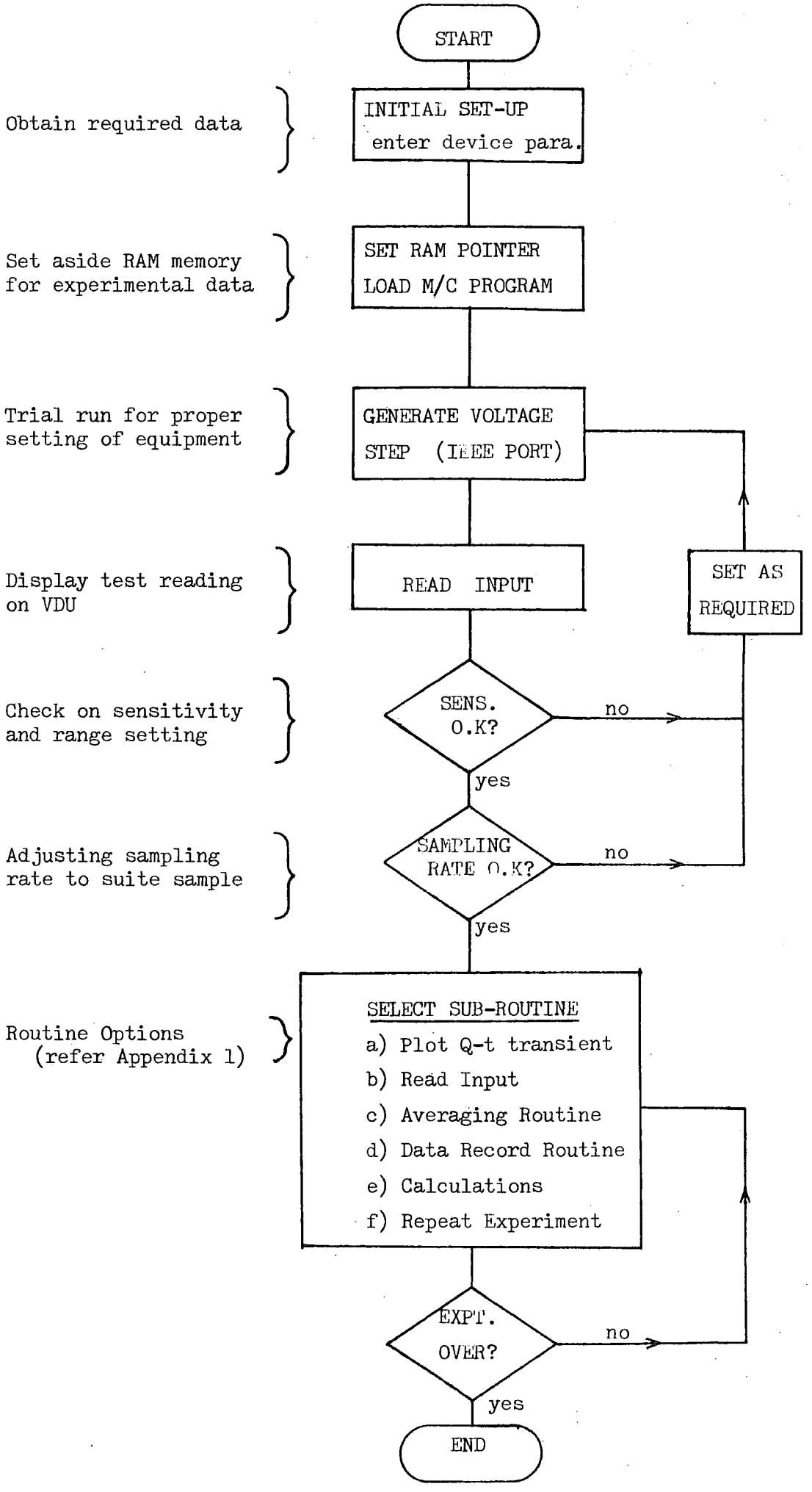

FIG. 3.14 FLOWCHART OF THE MAIN PROGRAM IN BASIC

CHAPTER 4

THE Q-t EXPERIMENTAL RESULTS

In this chapter the principal new results of the Q-t measurements are presented. This will show the main features of the true transient response of the MOS capacitor and the various parameters affecting it before a more detailed analysis is carried out in Chapter 8.

In this work more than five hundred results were obtained on Q-t transients alone and those presented here are just typical ones. More measurements were made on p-type samples than n-type because they were readily available and only the p-type samples had a guard ring around the electrode.

The apparatus and techniques used in obtaining these results have been described in the last chapter together with the experimental precautions for charge measurements with minimum noise and drift.

Section 4.1 is concerned with experiments on the influence of a guard ring and the choice of bias to ensure minimal lateral flow of charge and also a well defined effective electrode area. This is followed by a description of experiments to find the influence of the initial d.c. bias on the Q-t transient. Section 4.3 is on experiments on the effect of the voltage step magnitude which are only partly described here, as they will be dealt with in more detail in the analysis of Chapter 8. Therefore only the preliminary experiments with a limited range of the step magnitudes are described in this section. In Section 4.4, results on the

effect of the polarity of the voltage step are presented. For this experiment the guard ring potential and the voltage step magnitude also influence the results. Measurements were also made on the effect of exposure to U/V light and of the atmospheric conditions but these are not given here as it has not been possible to explain them in detail.

4.1 The Effect of a Guard Ring on the Measured Q-t Transient

In carrying out any electrical measurements on p-type MOS capacitors in inversion, care should always be taken to minimize lateral charge flow. This is especially important when measuring charges as in the Q-t experiment. The silicon dioxide layer in a practical MOS capacitor normally contains charged impurities which are neglected in the ideal case. These impurities are normally positively charged ions of sodium and potassium which enter the oxide during the fabrication processes. At room temperature the oxide charge is generally constant except at very high electric field strengths and it tends to increase towards one of the interfaces. Also there are fixed charges at the interface between oxide and silicon formed after the interface states, due to the "dangling bonds", are annealed (45,46). Consequently the surface beneath the oxide of a p-type sample will often be depleted and with electrons attracted towards the interface, it may even be inverted over the entire surface independently of any voltage applied to an electrode. The situation is the opposite in the case of an n-type sample, where a positive oxide charge will produce an accumulation layer in the surface thus repelling minority carriers (holes) from the interface just below the electrode area when a voltage is applied.

When a voltage step is applied to an MOS capacitor as in a Q-t experiment, a deep potential well is created below the electrode and the depletion width extends beyond its maximum equilibrium value. The return of the depletion width to its equilibrium value is mainly due to the thermal generation of carriers which partly fill the well in the depletion region. In p-type samples, the presence of an inversion layer around the metal electrode, induced by positive oxide charge, will supply electrons which can move laterally into the potential well. This will have the effect of increasing the rate of change of charge after the voltage step and so producing a faster response which is no longer entirely due to thermal generation. Erroneous results for lifetime are therefore obtained for p-type samples.

To overcome this problem, a guard ring around the metal electrode should be used. This is seen in Figure 4.1 which is a cross-section of a p-type MOS sample made by ITT. The idea is to apply a negative voltage bias on the guard ring such that the p-type semiconductor surface beneath it is in accumulation with a high concentration of holes and very few electrons in the surface surrounding the depletion layer laterally. Hence the effective area of the capacitor is confined by the accumulated charges. In this section we shall investigate the effects of the guard ring on the Q-t transients.

The experiment was carried out as in a normal Q-t measurement but with an extra probe to apply different voltages to the guard ring (Figure 4.2). The probing box was flushed with dry nitrogen to prevent surface conduction which may be caused by the presence of water vapour in the atmosphere. The Q-t transient was recorded and analysed for each guard ring voltage.

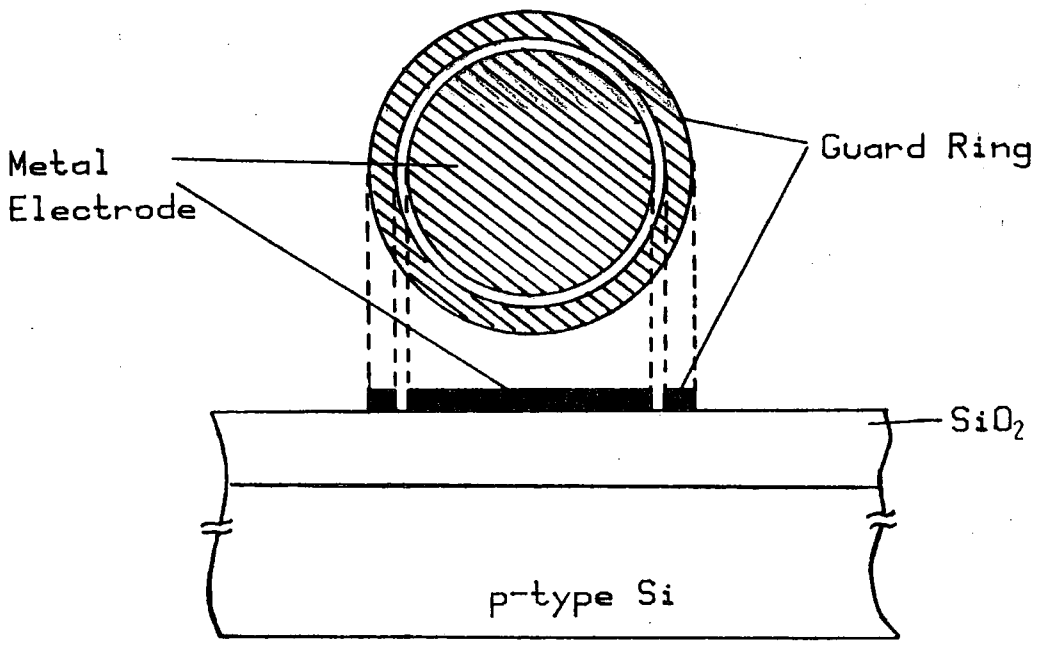

FIG. 4.1 p-MOS Capacitor with Guard Ring as made by ITT

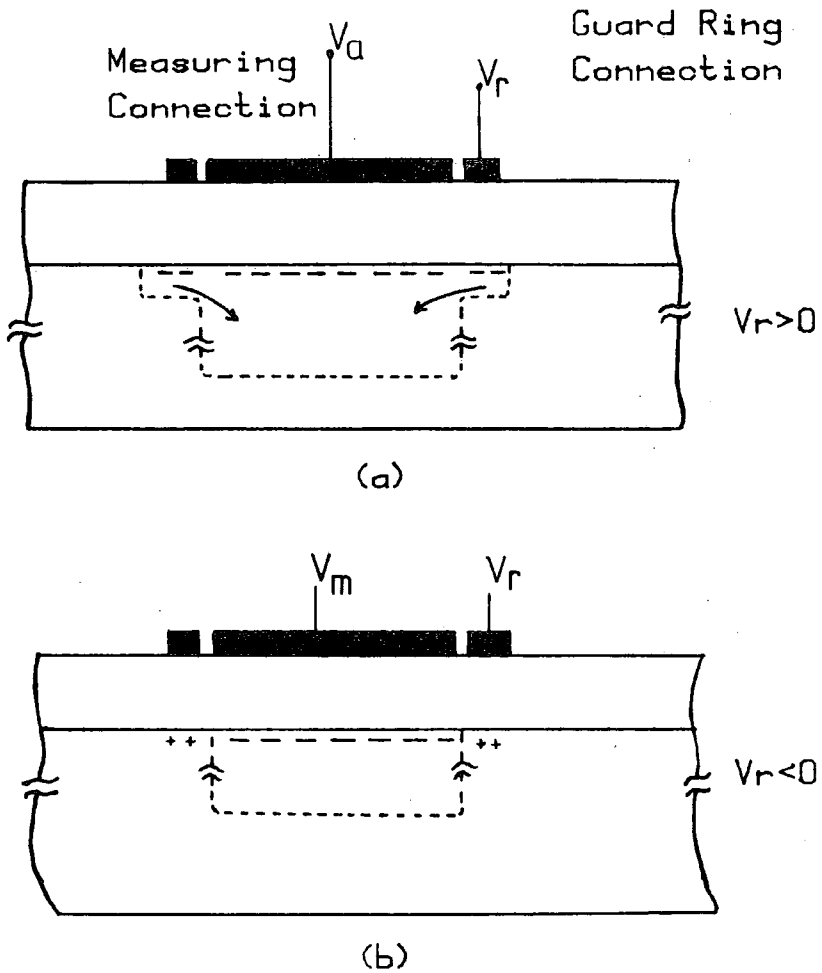

FIG. 4.2 Depletion Layer in p-MOS Capacitor at t=0+

(a) With Vr=0
(b) With Vr Biased to Accumulation

4.1.1 Results

For the investigation on the guard ring effect, the ITT samples were used exclusively as these are the only ones available having guard rings around their electrodes. Since this problem does not arise with n-type MOS capacitors, only p-type samples were measured. In this investigation a voltage step of 25 mV was used for all the samples and the initial fixed bias was + 5 V. For the first sample ITTAU2,2, the guard ring voltages V_r of -1 V, -3 V, and -5 V were used. The transients for positive voltage steps are shown in Figure 4.3. From these curves, the time taken to reach 90% of the maximum charge Q_{max} were 0.87s, 0.88s, and 0.99s for the V_r values of -1 V, -3V, and -5 V respectively. The faster response for the case when V_r = -1V and V_r = -3 V is due to the fact that the surface beneath the guard ring is not fully accumulated by such a low bias so that the remaining electrons from beneath the guard ring can flow into the potential well to cause the faster response. For the case of V_r = -5 V the voltage had come close to producing total accumulation so the response time in this case was longer. Similar results were also found on the sample ITTF4 where the times to reach 90% of Q_{max} was 3.66 s and 5.43s for V_r values of 0 V and -5 V (Figure 4.4).

For the sample ITTF2 the values of V_r were + 8V, +5V, +2V, and -5V. This was done to compare positive and negative guard ring voltages as well to show the effect that an increased positive oxide charges would have. As can be seen from Figure 4.5, when the surface beneath the guard ring is inverted for V_r = +8V, +5V, and +2V, the Q-t transients show evidence of

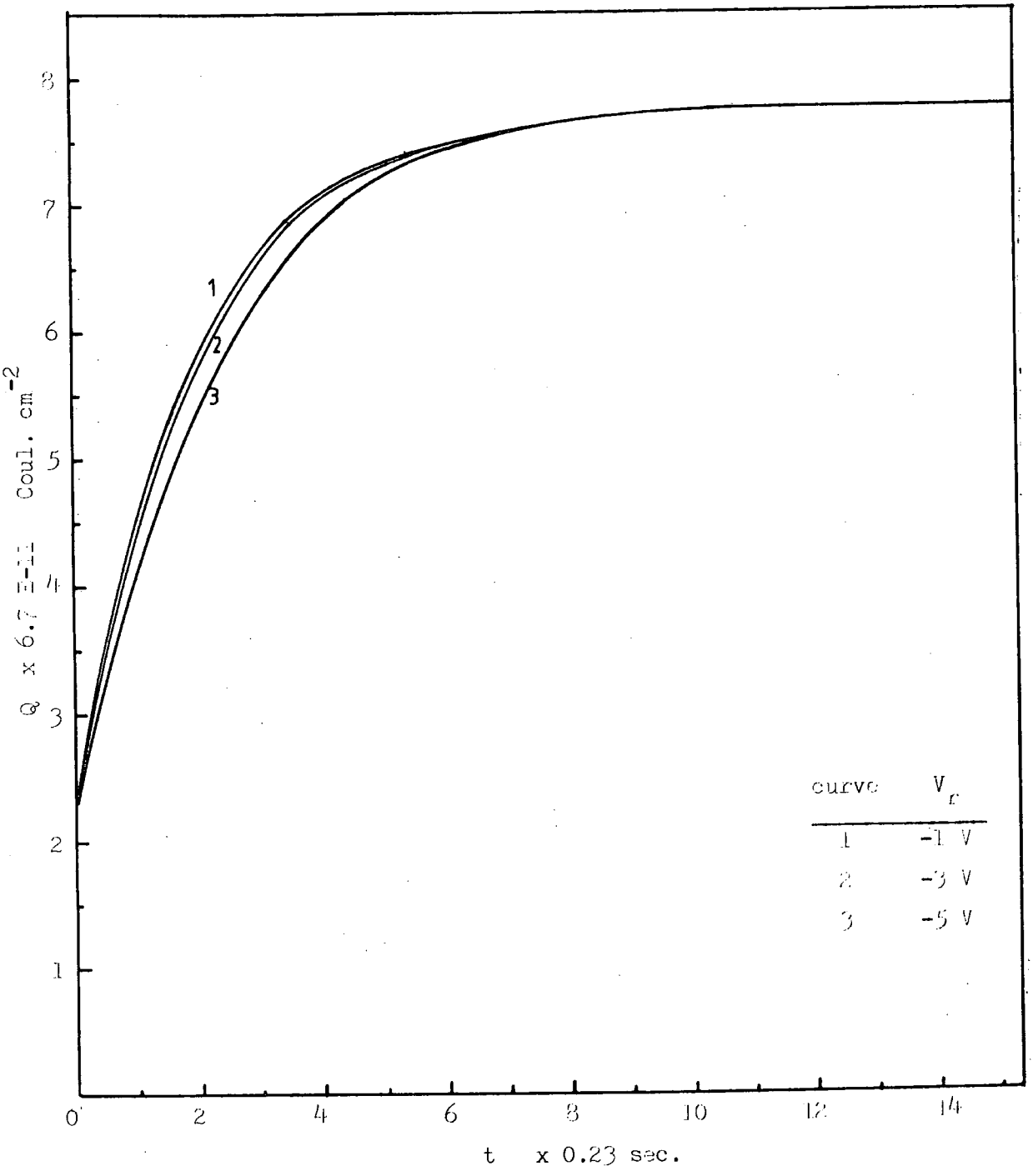

FIG. 4.3 THE Q-t TRANSIENTS FOR ITTAU2,2 WITH DIFFERENT GUARD RING VOLTAGE VALUES, Vr.

(ΔV_a = + 25 mV , V_a = + 5 V)

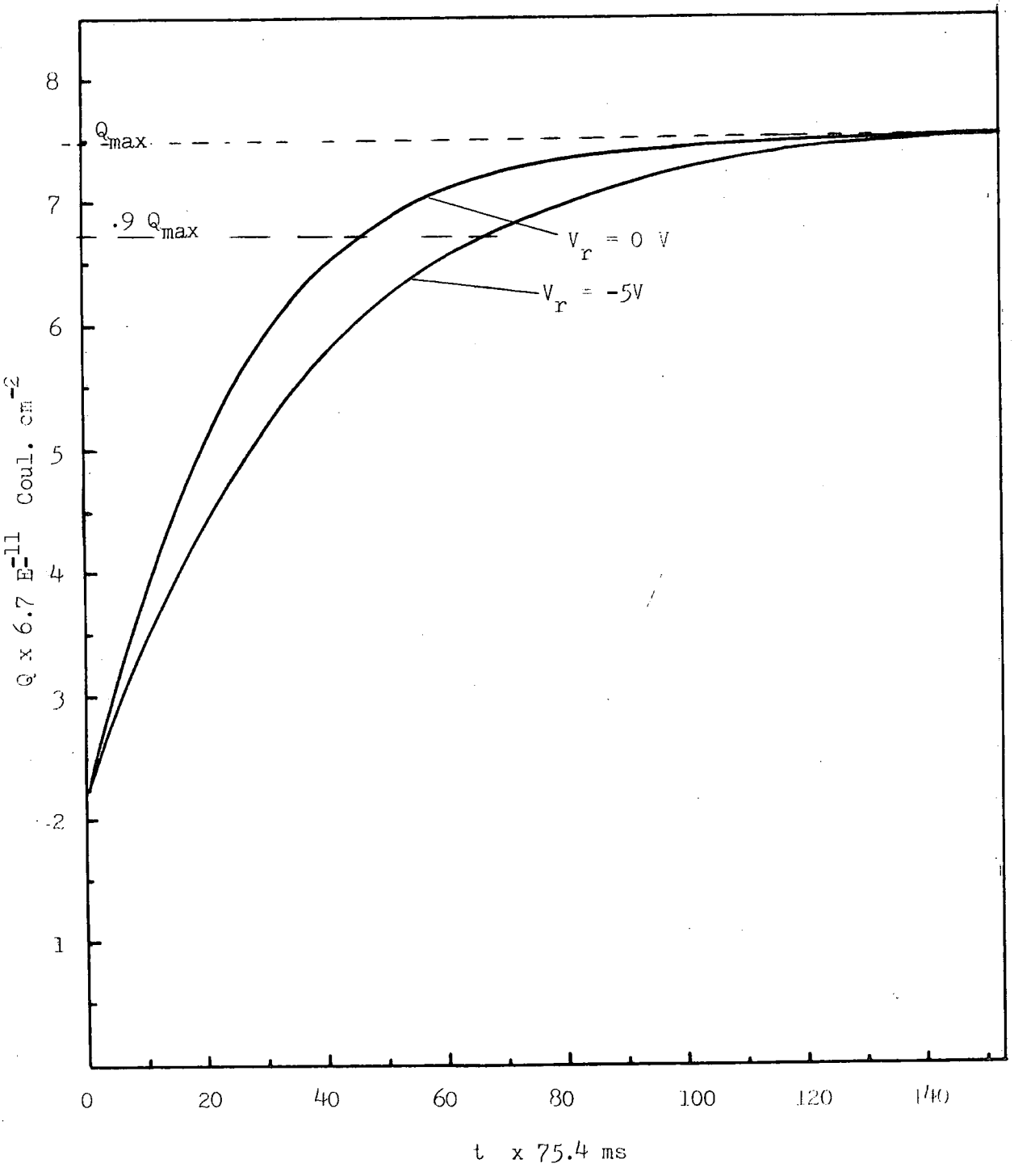

FIG. 4.4 THE Q-t TRANSIENT FOR ITTF#4 WITH DIFFERENT GUARD RING VOLTAGES, V_r (ΔV_a = 25 mV, V_a = +5 V.)

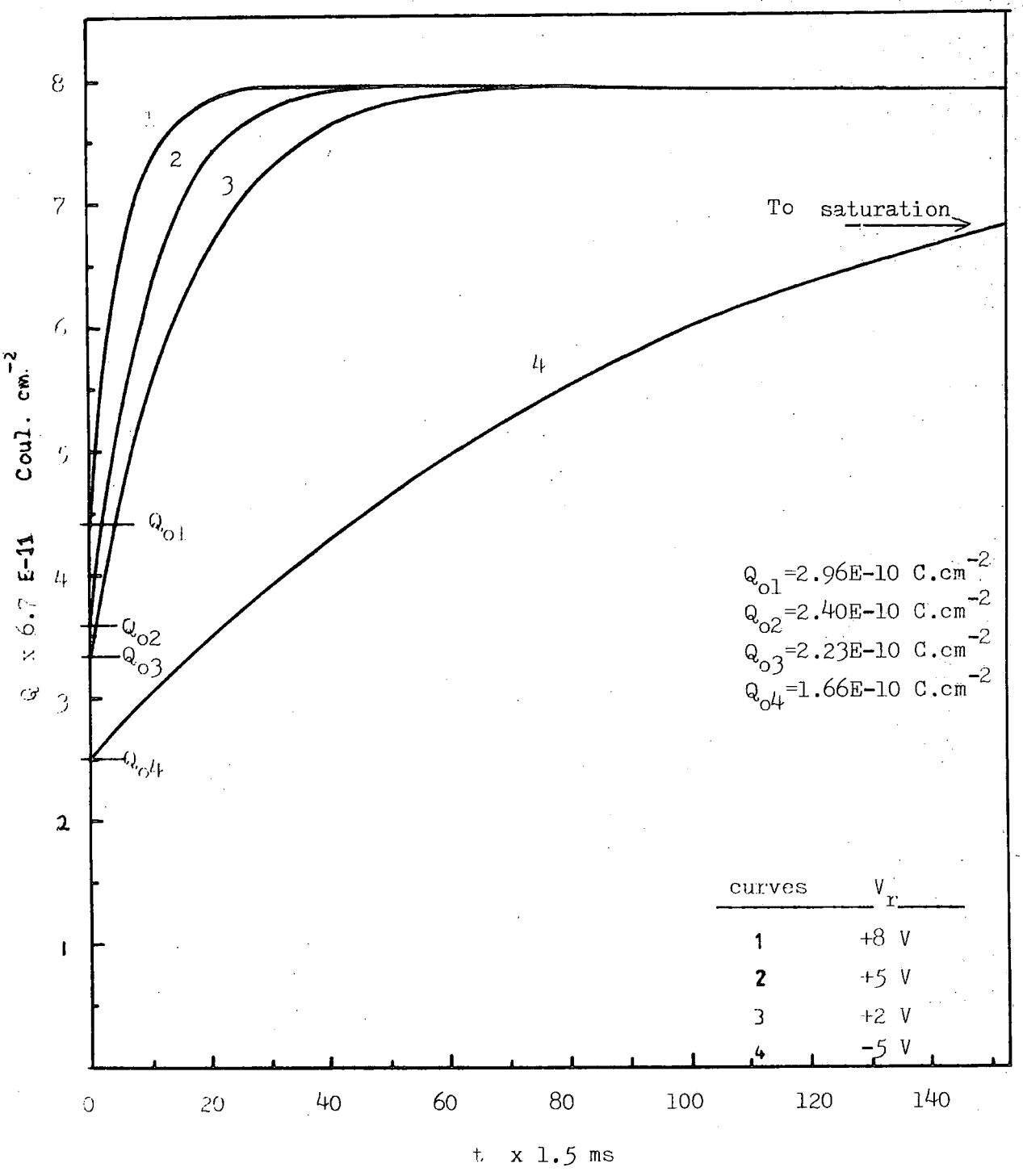

FIG. 4.5 Q-t Transients for ITTF2 Sample with Different Guard Ring Voltages

(ΔV_g = 25 mV, V_g = +5 V)

lateral flow of charge at t = O+ where the initial step Q_{O+} in the transient, due to the displacement current, increases when the surrounding inversion is stronger (i.e. V_r increased positively). The values of Q_{O+} are 2.67×10^{-12} C, 2.16×10^{-12}C, 2.01×10^{-12}C, and 1.50×10^{-12}C respectively and at the same time the transient becomes faster as V_r is increased positively.

Measurements made on the sample ITTG2 for V_r values of +3 V, -2V, and -5V gave a similar trend for the response time and the initial step height as shown in Figure 4.6.

4.1.2 Discussion

The aim of these experiments was to find out how the voltage on the guard ring affects the Q-t transient of a p-type MOS capacitor. They were also to show that by ignoring the role of the guard ring, serious errors can occur in a Q-t experiment aimed at determining the bulk lifetime. The results show that the shape of the Q-t curves is greatly affected by the voltage of the guard ring. For all the samples measured, the Q-t response was faster and it would give a falsely short minority carrier lifetime if the guard ring is not sufficiently negatively biased so as to produce an accumulation beneath it. The error due to not having a guard ring at all would therefore become large if the oxide charge concentration was high. This effect was shown experimentally by the application of positive voltages to the guard ring which reflects the same situation as having a high positive charge concentration in the oxide. The experiment not only showed that the response time was shortened by inversion outside the electrode area but also that the initial step of the Q-t curve was increased. The reason for the latter phenomenon is as follows.

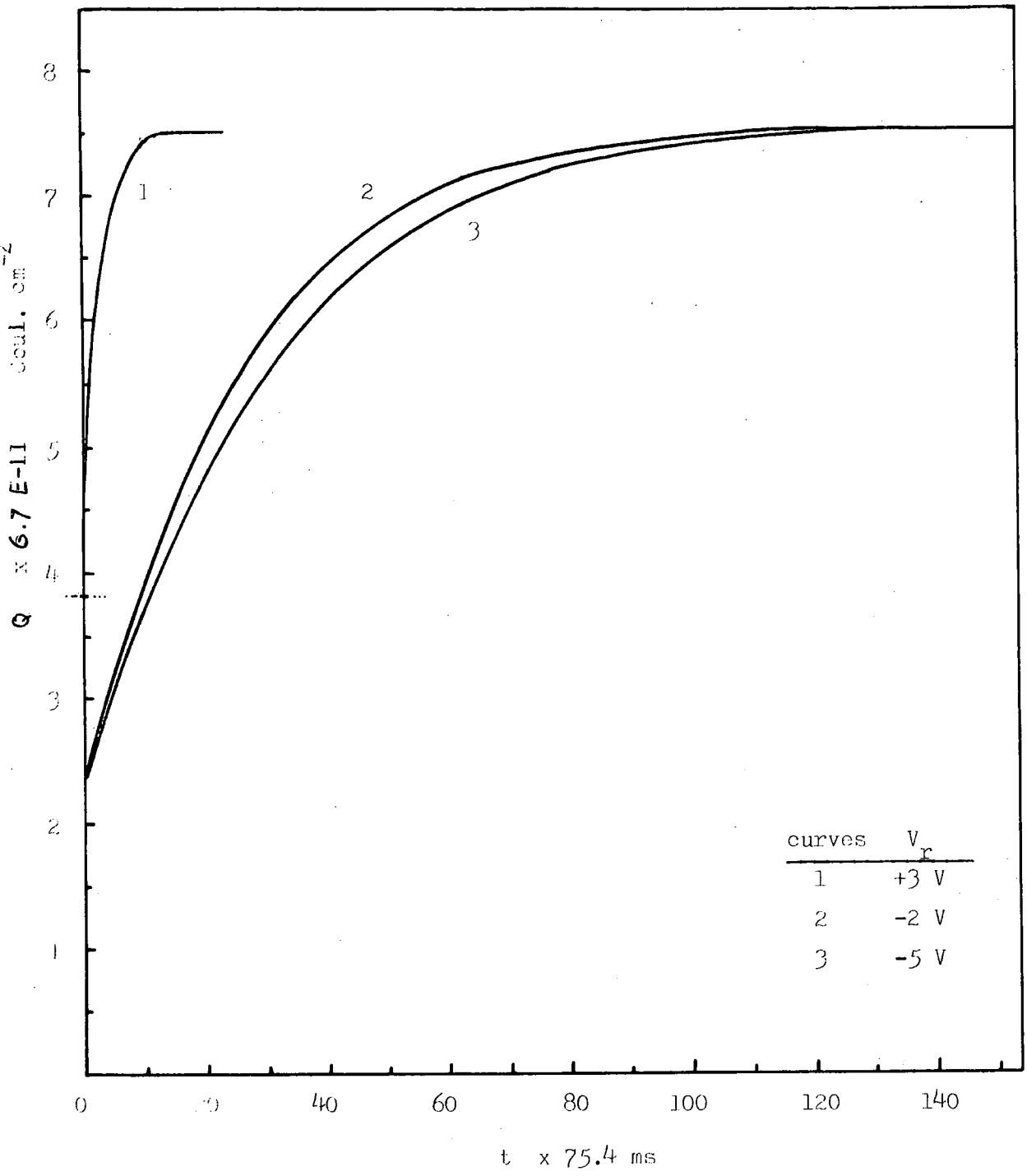

FIG. 4.6 THE Q-t TRANSIENTS FOR ITTG2 WITH DIFFERENT GUARD RING VOLTAGES, V_r

(ΔV_a = 25 mV)

Figure 4.2 shows the depletion layer in a p-type MOS capacitor with a guard ring around its measuring electrode. On the application of the voltage step the depletion width immediately widens into the bulk of the semiconductor giving rise to a displacement current. Ideally this is the only component of the change in the charge in a Q-t experiment at t = O +. However, the presence of electrons in the inversion layer surrounding the electrode provides another component for the charge increment in the sample at t = O + as the electrons move laterally and accumulate at the oxide semiconductor interface. The spacing between these charges and the electrode is less than that between the increment charge at the depletion layer edge and the electrode so that the electron movement has a comparatively large effect resulting in a larger initial step in the Q-t transient.

As time increases (t > O) the return of the depletion width to its equilibrium value is normally due to the thermal generation of electrons (minority carriers) which reduced the magnitude of the surface potential to its equilibrium value. With an inversion layer surrounding the electrode the rate of increase of the inversion charge in the device is assisted by the lateral flow of electrons from the periphery. For this reason the transient becomes faster. The experiments therefore fully confirmed the expectation deduced from other MOS studies.

To avoid the errors discussed above the guard ring must therefore be properly biased to prevent lateral flow of charge. The voltage found to be suitable for the present samples is at least - 5 volts. Even with this bias it should be noted that the gap between the guard ring and the metal electrode might still contribute some lateral charge flow leading to errors.

However, by using a device with large area to perimeter ratio this contribution can be minimised.

In view of the large effect of lateral charge flow in the above Q-t measurements, it is rather surprising that it has not been investigated previously. Also, the published results make no reference to guard rings which appear not to have been used. The present work shows that neglect of the surface could easily lead to errors in apparent bulk lifetime measurements of up to ten times or more.

4.2 The Effect of the D.C. Bias on the Q-t Transient

In a typical Q-t experiment, the bias voltage is one of the most important parameters as it determines the initial equilibrium state of the MOS capacitor. By looking at a C-V plot the reason for the choice of bias is quite obvious. Referring to Figure 4.7, one would expect that a voltage where the capacitance is constant (i.e. in inversion) to be the most suitable choice for investigating minority carrier effects. This is because the initial charge, the surface potential and the depletion width are well defined at $t = 0-$ before the application of the voltage step in a Q-t experiment. Also, the surface potential and depletion width return to almost the same values at $t = \infty$.

All published Q-t experiments have been performed with a steady d.c. to bias the sample into inversion and stimulation by a voltage step into heavier inversion so that the difference between the initial and final states is very small and can be neglected. There are no published results on the very important effect that a difference of d.c. bias could have on the Q-t transient. In the following paragraphs we shall therefore describe the experiments carried out to

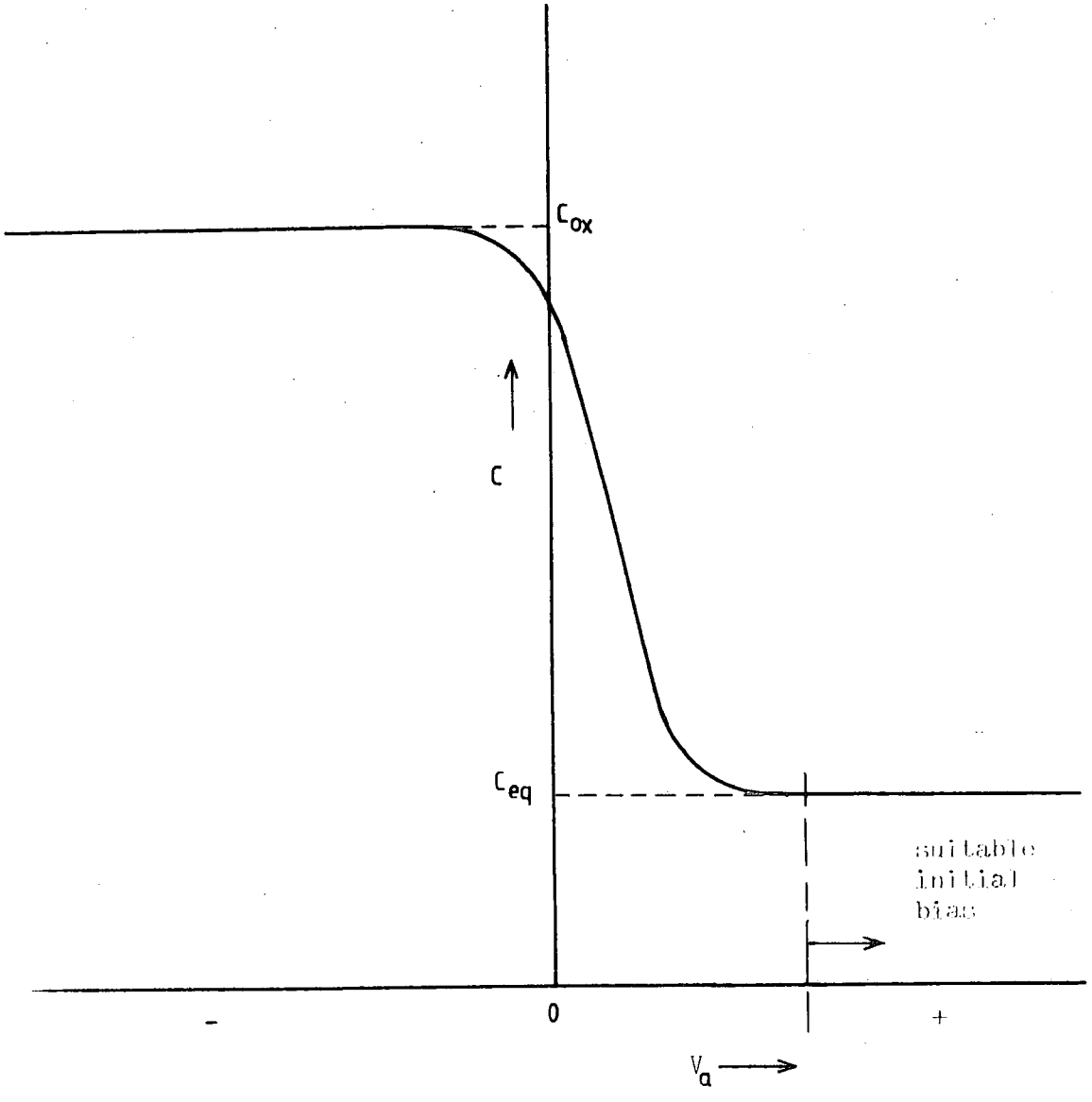

FIG. 4.7 A TYPICAL C-V PLOT FOR A p-TYPE MOS CAPACITOR

investigate this effect.

In the experiments performed, several MOS capacitors of both p- and n-types were used. For the p-type capacitors a guard ring was used biased to -5V to maintain the proper accumulation in the surface around the capacitor to minimise lateral flow of charges. For all measurements a voltage step of 25 mV (equivalent to 1 kT of energy) was used with polarity such as to increase the level of inversion, i.e. a positive step for p-type and negative for n-type. The small voltage step was chosen so that only a small deviation from equilibrium was obtained. According to Hofstein (10) this should give an almost exponential transient response.

4.2.1 Results

In these experiments the Q-t transients were recorded for different applied voltages, using the same experimental set-up as in the previous section. The applied voltages were first kept within the range required to give strong inversion. For the n-type sample TC3-8D3, voltages of -8.3V, -7.3V, and -5.4V were used. The Q-t transients obtained were very close with the times to reach 90% of the final values of 0.15 s, 0.15 s, and 0.16 s, respectively, (Figure 4.8). For the p-type sample, ITTAU1,3 the applied voltages were +10V, +5V, and +2.5V. These too showed little difference in the transient with times required to reach 90% of the maximum of 1.14 s, 1.13 s, and 1.14 s (Figure 4.9). The applied voltages were then changed in both samples to close to the inversion threshold. For sample TC3-8D3 a voltage of -1.7V was used and for ITTAU1,3 + 0.5V. As shown in Figures 4.8 and 4.9 the times taken to reach 90% of the maximum charge were then 0.03 s and 0.73 s for the two samples respectively. It can be seen that these

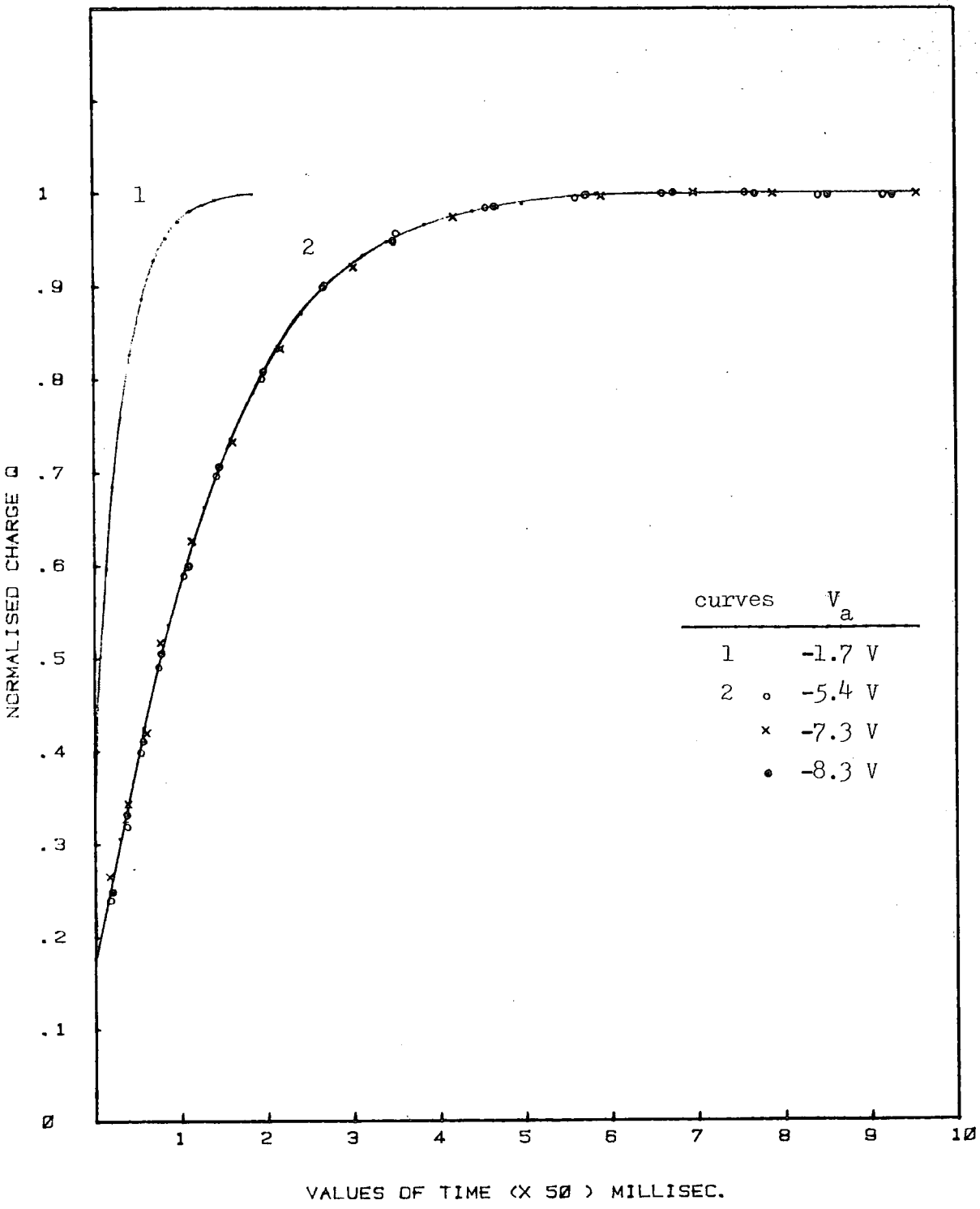

FIG. 4.8 Q-t TRANSIENT FOR SAMPLE TC3-8D3 AT DIFFERENT BIAS VOLTAGES IN INVERSION

(ΔV_a = 25 mV)

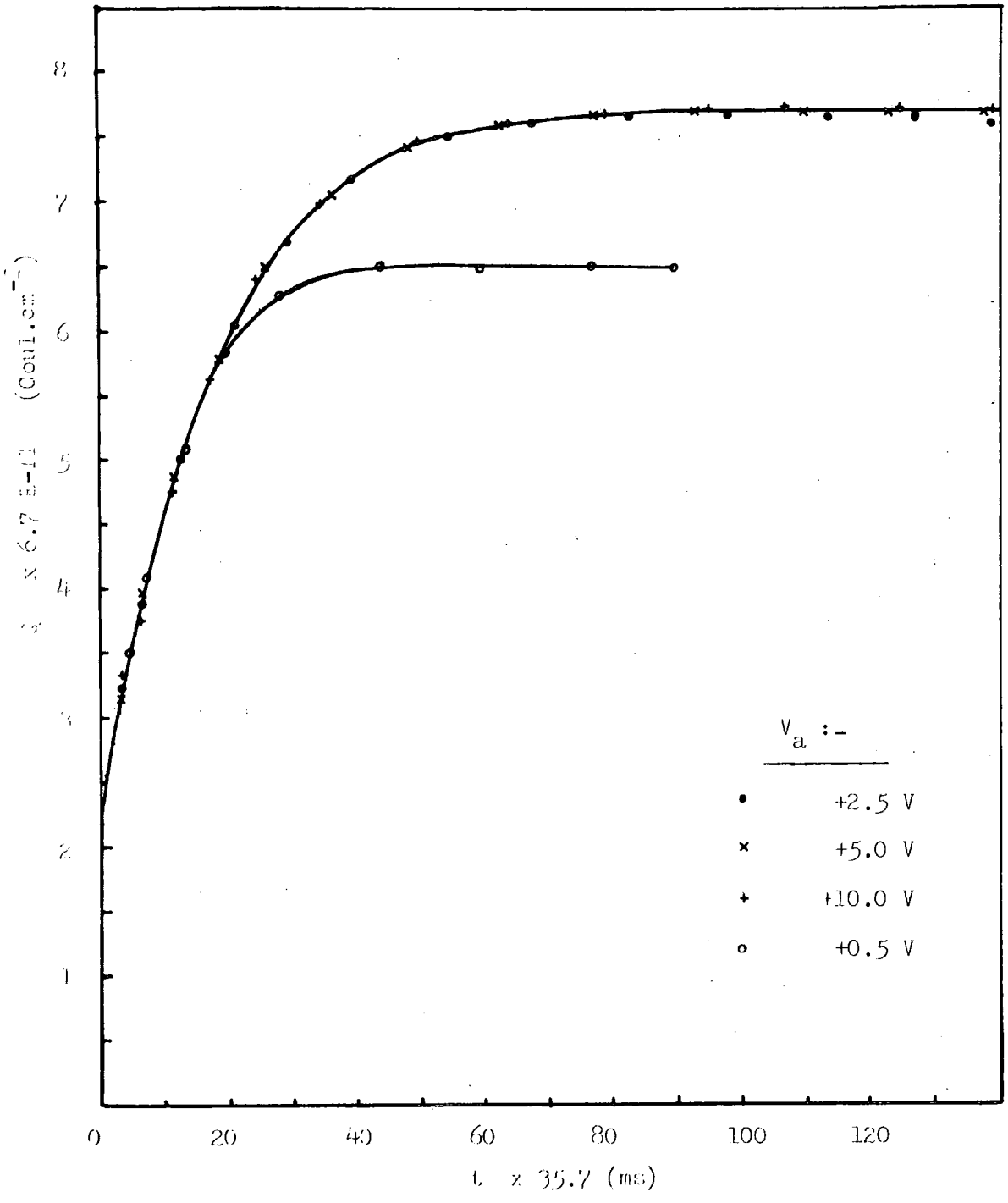

FIG. 4.9 Q-t TRANSIENTS FOR THE SAMPLE ITTAU1,3 AT DIFFERENT BIAS VOLTAGES IN INVERSION

(ΔV_a = 25 mV)

transients were much faster than with the capacitor in inversion.

Measurements were next made on a p-type sample ITTN3,6 for the full range of applied voltage from +5V in inversion through to -0.3V which is in accumulation. It was found that as the voltage was made more negative, i.e. towards accumulation, the maximum charge dropped until a minimum was reached equal to the height of the initial step. It then increased again up to a maximum which was the same as for the inversion case. At the same time the Q-t rise time continued to shorten and when accumulation was reached the response became a step function when displayed on the same time scale as other transients. The capacitance of the sample as measured after each transient with the Boonton 72 BD was plotted against the maximum charge Q_{max} as shown in Figure 4.10. From this it was seen that Q_{max} reached a minimum when the capacitance was 72 pF and that it increased to the oxide capacitance as the sample approached accumulation.

When the MOS capacitor is in accumulation it behaves like a parallel plate capacitor. This was checked by biasing the sample ITTAU1,3 into accumulation to give the transient shown in Figure 4.11. This was compared with the response from a 220 pF mica capacitor. In this mode the response was too fast to be recorded accurately using the present automatic set-up, confirming that the recorded transients were not affected by the rise time of the apparatus.

4.2.2 Discussion

In the first part of the above experiment with applied voltages of -8.3V, -7.3V, and -5.4V for TC3-8D3 and +10V, +5V, and +2V for ITTAU1,3, the samples were well in the heavy

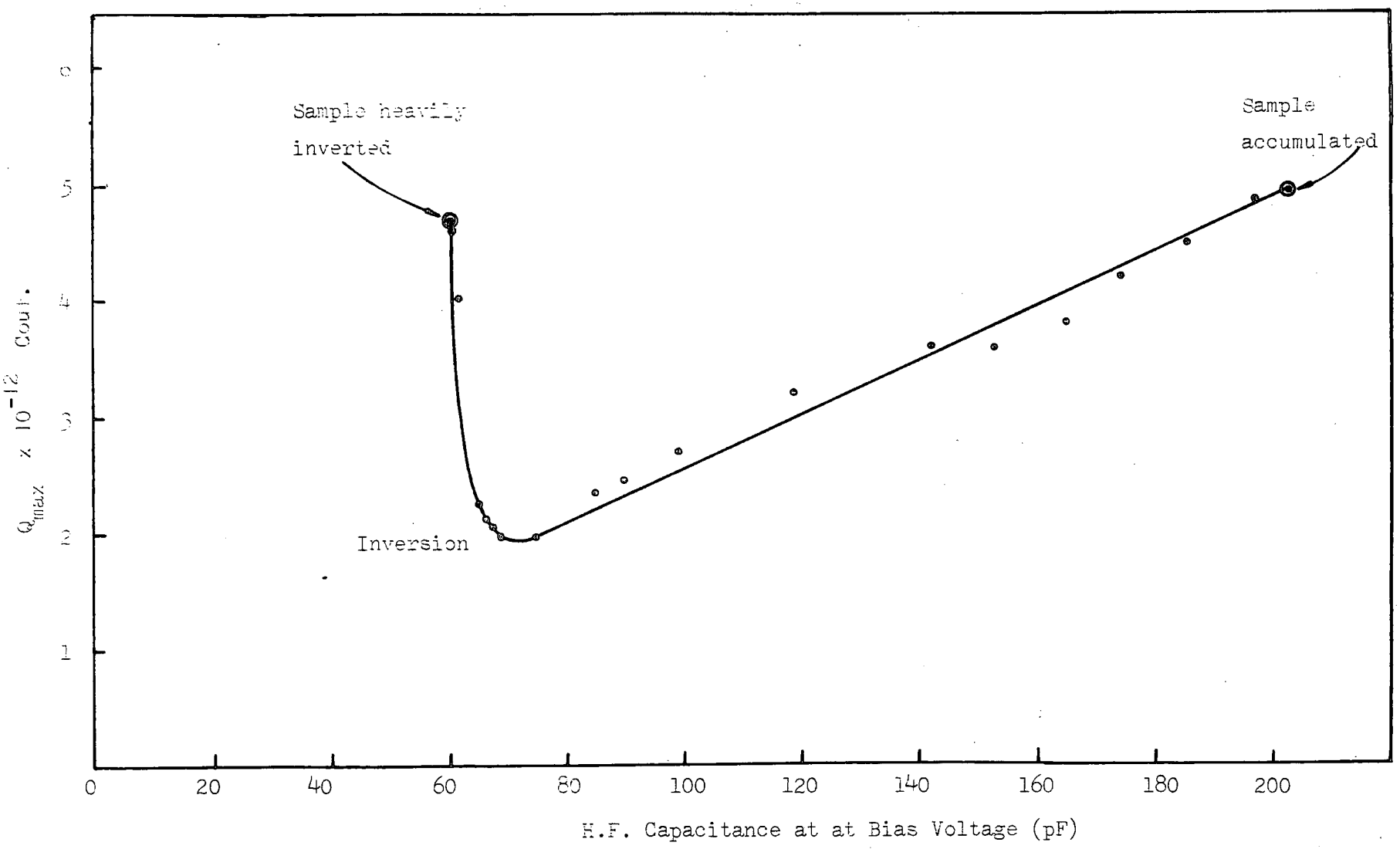

FIG. 4.10(a) PLOT OF Q_{max} AGAINST A.C. CAPACITANCE FOR ITTN3,6 SAMPLE

(ΔV_a = 25 mV)

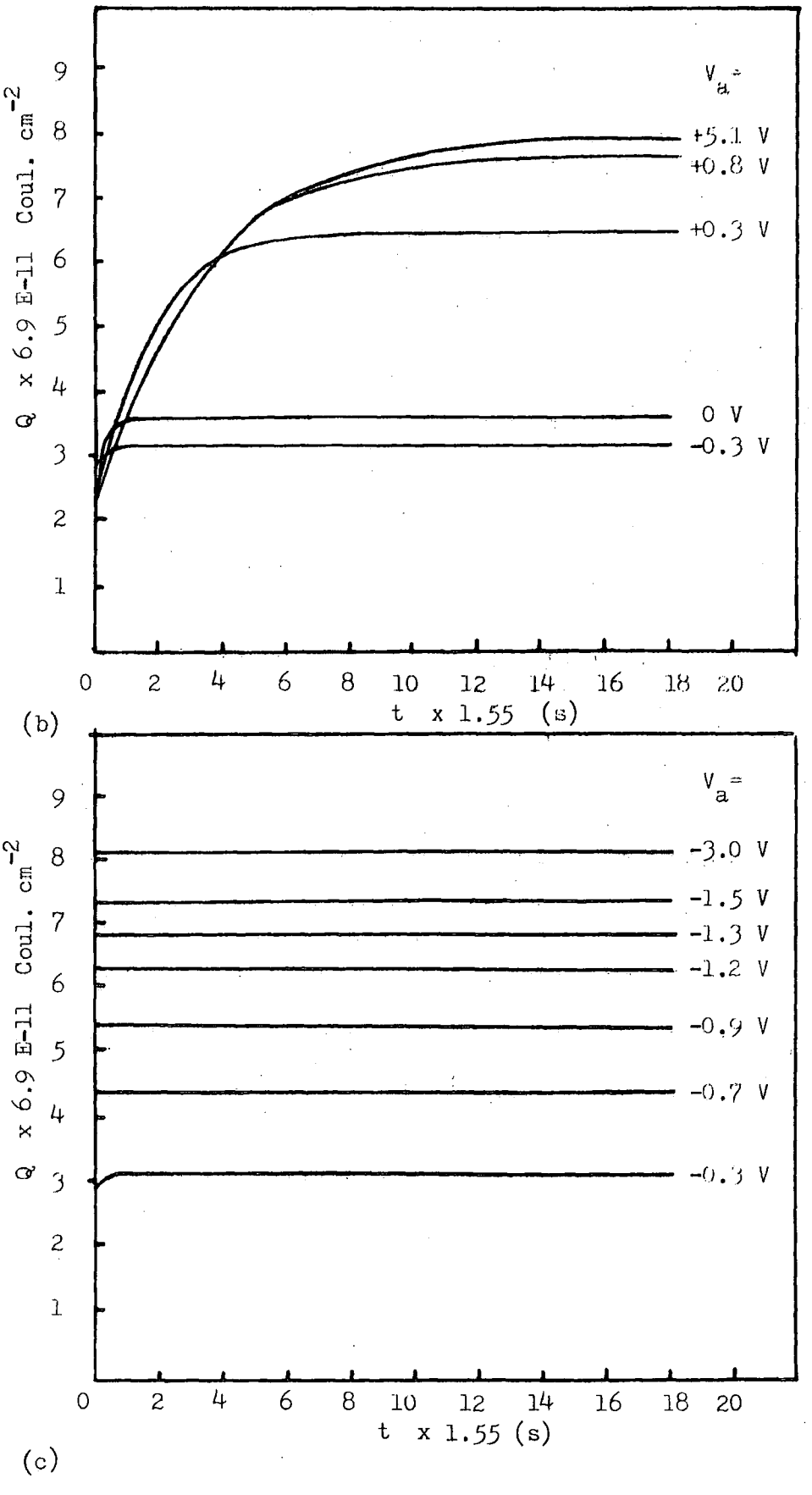

FIG. 4.10(b) & (c) EFFECT OF BIAS VOLTAGE ON Q-t TRANSIENTS. (Sample ITTN3,6)

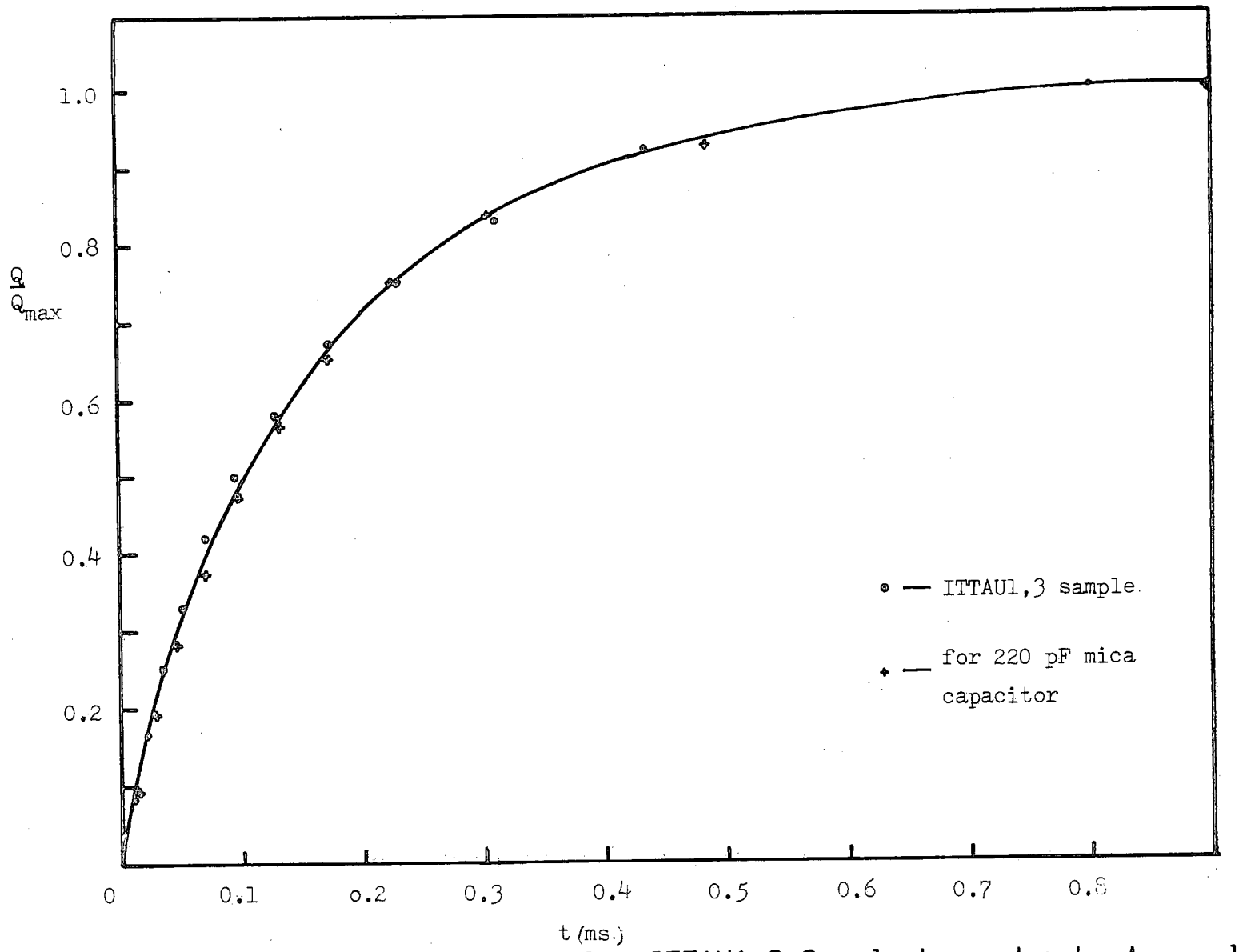

FIG. 4.11 Normalised Q-t Curves for ITTAU1,3 Sample biased into Accumulation

(ΔV_a = 25 mV)

inversion region as can be seen from the h.f. C-V plots of Figures 4.12(a) and 4.12(b) respectively. Under these conditions the surface potential, the depletion width, and the capacitance were almost independent of the voltage. With the application of a step voltage, the surface potential and depletion width will be changed momentarily but they will return to their equilibrium values when sufficient carriers have been generated during the transient. Therefore as long as the voltage before and after the application of the voltage step is greater than the threshold for inversion, the Q-t transient will be independent of voltage, as found. This is true when the carriers are formed mainly by bulk generation. However, with a large surface generation component the Q-t transient shape may vary with the initial voltage because the source of the minority carriers may be affected by the precise value of the surface potential. The results show that this is not the case with the samples used in this experiment, which therefore appear to be dominated by bulk generation.

When the applied voltage is reduced to less than the inversion threshold the Q-t transient is observed to change in shape as well as having a reduced maximum charge. This corresponds to the applied voltages of -1.7V for the sample TC3-8D3 and +0.5 V for ITTAU1,3. Referring to Figures 4.12(a) and 4.12(b), these voltages were very near the inversion threshold although not in the heavy inversion region. In this case a change in the applied voltage will also change the depletion width x_d. Figure 4.13 shows the energy band diagram and the distribution of charge in a p-type MOS capacitor when biased to the onset of inversion. Under this condition the depletion width has not quite reached its maximum value and,

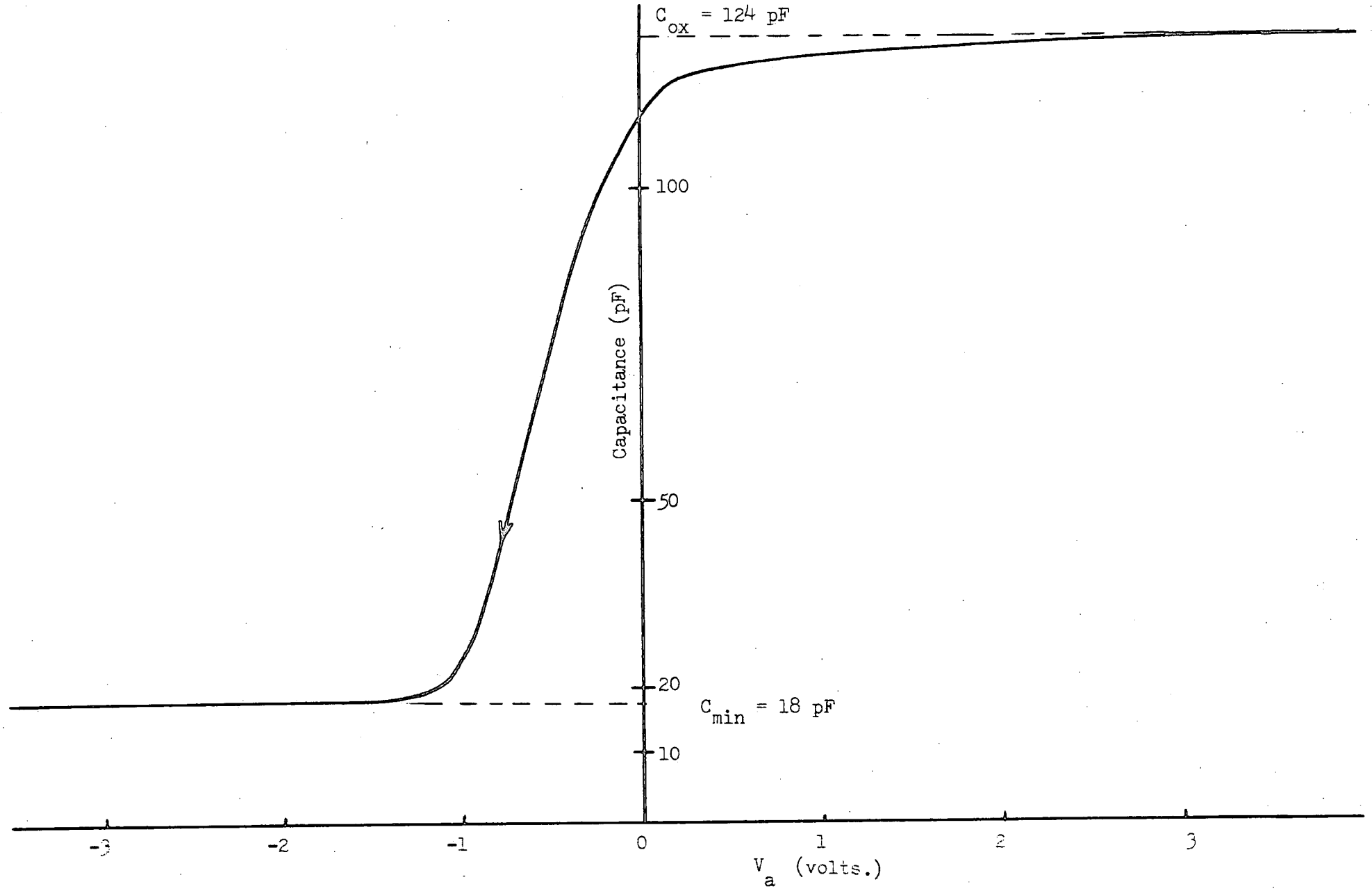

FIG. 4.12(a) C-V PLOT FOR SAMPLE TC3-SD3

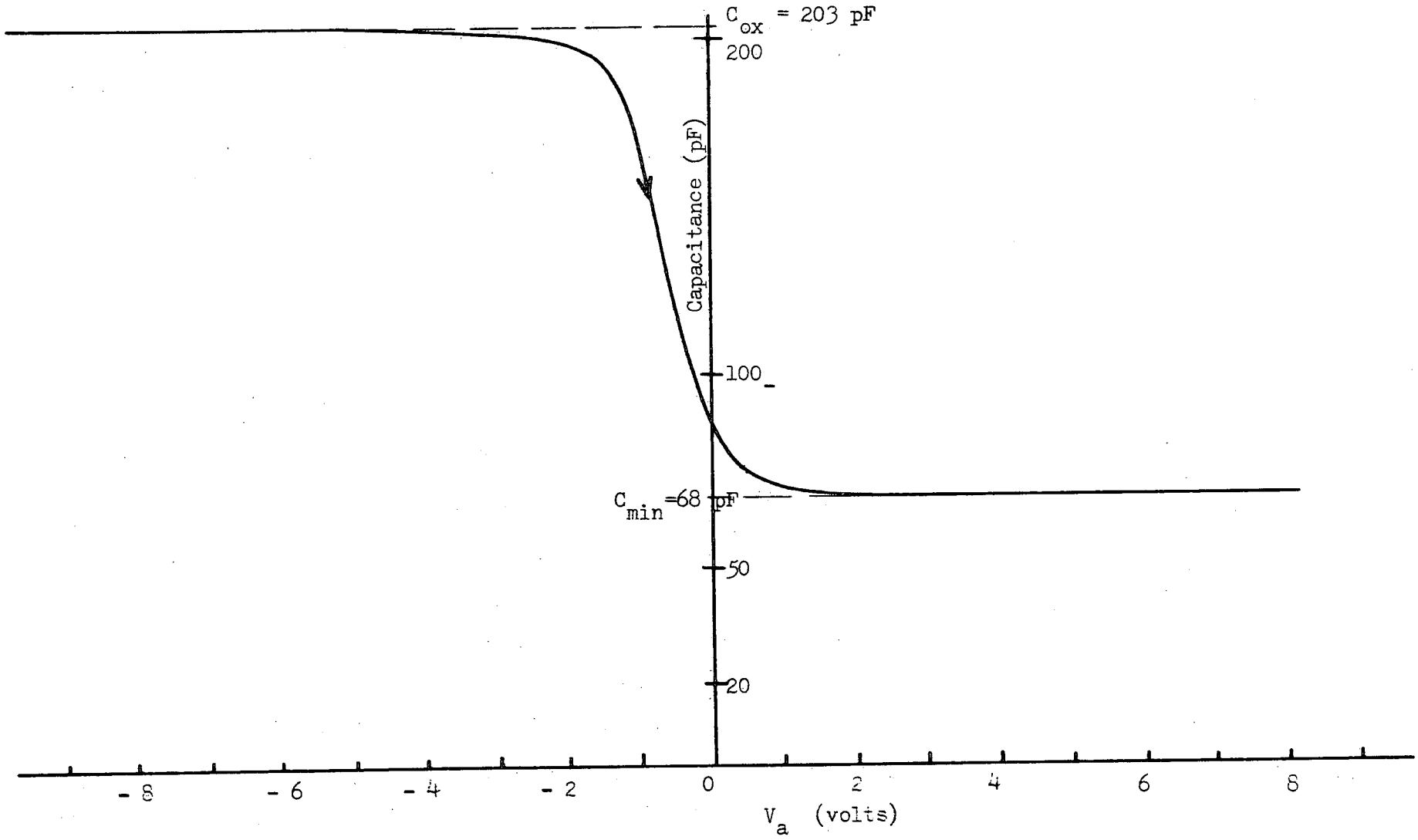

FIG. 4.12(b) C-V PLOT FOR SAMPLE ITTAU1,3

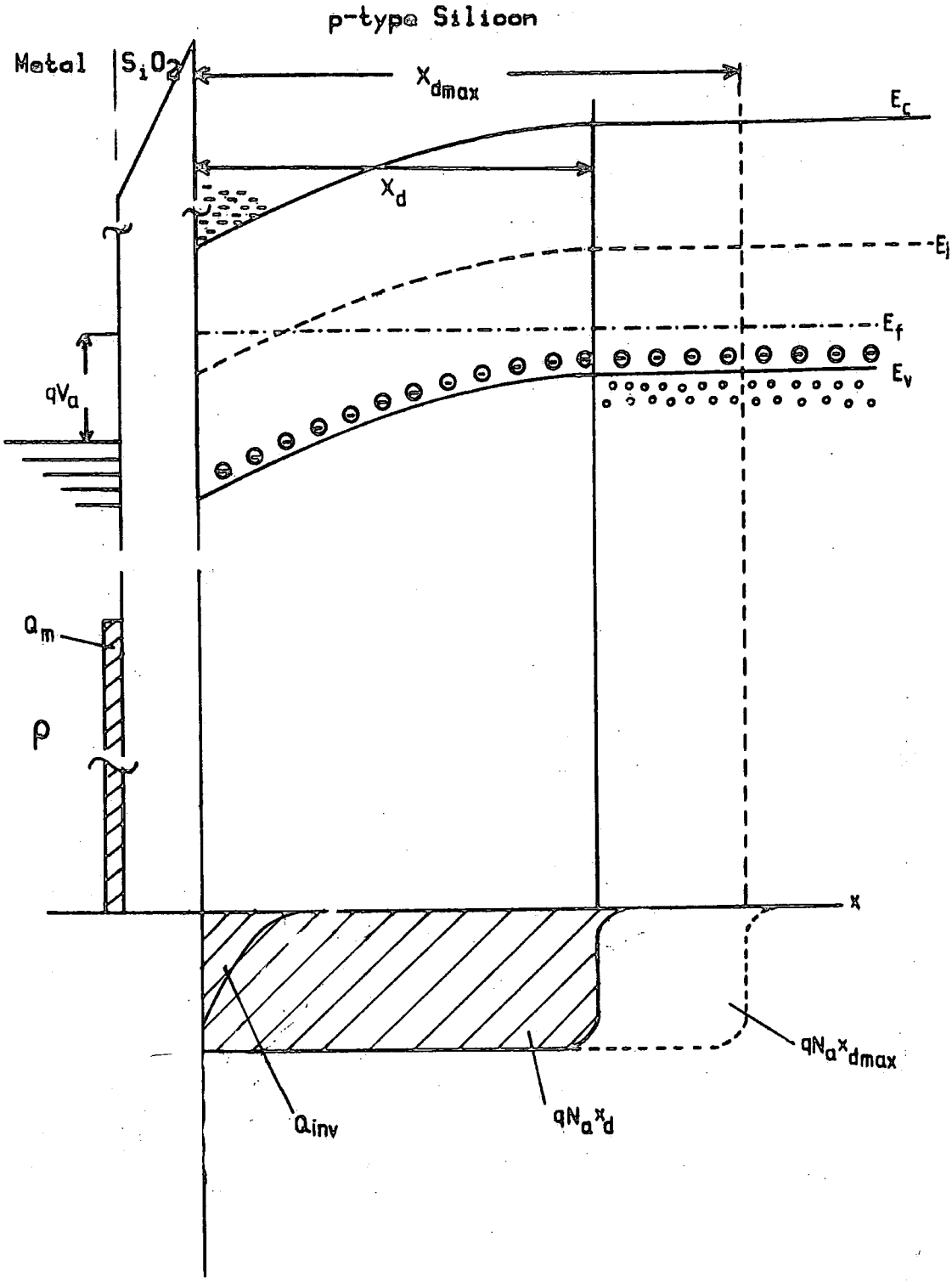

FIG. 4.13 Energy Band Diagram and Charge Distribution in an MOS Capacitor biased into Weak Inversion

although strong inversion has not been reached, there was a reasonably high concentration of minority carriers attracted towards the oxide-semiconductor interface by the charge on the electrode. Thus the electrode charge is balanced by the depletion charge from the uncompensated ionised doping atoms and the minority carrier concentration at the interface. When the step voltage is applied in this case the depletion width will extend into the bulk so that initially the change in charge on the electrode will be totally balanced by the increased depletion charge. The increased voltage will also pull more minority carriers to the interface as they are generated so that the surface potential will be slightly reduced as the depletion width drops back to its new value which is rather greater than the original. The rate of this return is governed by the generation rate which also determines the shape of the Q-t transient. Since the depletion width does not return to its original value in this case the number of minority carriers generated is limited and the maximum charge Q_{max} of the Q-t plot and the time required to reach saturation is reduced compared with the strongly inverted condition. The argument used above to explain the variation of Q_{max} with bias voltage is, of course, the same as that used for the familiar low-frequency small signal a.c. capacitance characteristic and in fact

$$Q_{max} = C_{\ell f}.\Delta V$$

where $C_{\ell f}$ is the low frequency capacitance.

For the sample ITTN 3,6, the voltage range was extended further. In order to discuss these results, Figure 4.10(b) and 4.10(c) will be used. These show the variation of Q_{max} with

the applied voltage V_a. Figure 4.10(b) is a set of transient curves for values of V_a between +5V and -0.3V and Figure 4.10(c) shows them for V_a between -0.3V and the accumulation voltage of -1.2V. The results in Figure 4.10(b) go further than those in Figure 4.8 which have been discussed in the preceding paragraphs. In Figure 4.10(b), Q_{max} dropped to a minimum value and then started to rise again when the voltage was insufficient for inversion so that the depletion width is less than the equilibrium maximum value. When the voltage step is applied in this case the electrode charge increment is mainly balanced by the charge due to the increment of the depletion width, which is due to the movement of majority carriers only, and hence occurs in a very short time. Since no inversion layer is formed there is no further increase in the charge giving an almost flat response with time except for the leading edge which is due to a small build up of electrons of the surface during depletion. As the voltage is further reduced the depletion width falls further so that the edge where the change of charge occurs is closer to the electrode resulting in a larger change of charge from the same voltage step as observed in Figure 4.10(c).

The maximum value of Q_{max} occurs when the applied voltage is sufficient for accumulation as shown in Figure 4.10(c). In this case there will be charges on the electrode on one side and the majority charges in the silicon on the other. The MOS capacitor then behaves like a parallel plate capacitor and the application of a voltage step will change just the majority carrier concentration of the silicon surface. Since this results in a very fast response the time scale had to be reduced in an experiment to show the characteristic

of such a capacitor. This experiment was performed on sample ITTAU1,3 at a bias voltage of -4 volts, with the result shown in Figure 4.11. The Q-t response obtained compared well with that of a 220 pF mica capacitor as expected since the mobility of the carriers in the MOS capacitor is high enough not to have caused any deviation.

From this set of experiments it was found that the Q-t response of an MOS capacitor is very sensitive to the applied voltage if strong inversion has not set in. In agreement with theory this was found to be especially so for the case where the samples are in accumulation or depletion. When the bias is greater than the threshold for strong inversion, the Q-t response shows little change with initial voltage. For the p-type sample it was found that a bias of +5 volts was about right for a Q-t experiment in the strong inversion mode and for the n-type sample this was found to be -5 volts. These figures are only good if the flat band does not shift very much with time otherwise the magnitude has to be changed accordingly. Nevertheless these voltages worked well in the continuation of this investigation.

Although explained in the same way as the a.c. capacitance characteristics, the experimental variation of Q_{max} with bias and voltage does not appear to have been reported previously. The variation of the Q-t transient shape between inversion and accumulation biases, which is far more difficult to explain precisely, will be discussed further in Chapter 8 .

4.3 The Effect of the Voltage Step Magnitude on the Q-t Transient

In the last two sections we have seen how the Q-t transients are affected by the guard ring bias for a p-type MOS capacitor and by the initial applied bias to both p- and n-type samples. So far voltage steps of 25mV were used in all these experiments. The present section is on experiments on the effect of larger voltage steps on the Q-t transients. Larger steps are desirable because the larger charges are easier to measure accurately. However, it is necessary to investigate the extra physical effects that might be associated with larger step voltages.

In a Q-t experiment it is the voltage step that changes the surface potential and the depletion width from their equilibrium values thus altering the rate of generation or recombination of carriers in the semiconductor. For a positive step this then leads to an increase in the minority carrier concentration at the oxide-semiconductor interface. It is the rate of increase of this carrier concentration that gives the Q-t transient.

The choice of a suitable step height is important for the method of analysis because the assumption made in the theoretical treatment of the Q-t transient may be dependent upon the magnitude of the step height. For example,in Hofstein's method of analysis a small voltage step is required for his assumptions to be valid and when the voltage step is increased, his analysis will fail. For the method of analysis used by Viswanathan and Takino, a larger voltage step has to be used as the method fails when the system is close to equilibrium due to their generation expression becoming invalid as

equilibrium is approached.

In this section we shall describe experiments on the Q-t method carried out using different magnitudes of voltage steps to see how they affect the Q-t transients. Two samples were used, one a p-type sample ITTAU2,2 and the other the n-type sample, TC3-8D3. These samples were initially biased into strong inversion. A voltage of +5 volts was used on ITTAU2,2 and -5 volts on TC3-8D3. In addition a voltage of -5 volts was applied on the guard ring of ITTAU2,2 to form an accumulation region around the electrode to prevent lateral flow of charge. Voltage steps of 25 mV, 50 mV, and 100 mV were applied on both samples and Q-t transients were obtained and analysed for each voltage step.

4.3.1 Results

To a first approximation the charge flowing in the sample is proportional to the applied step voltage, so that the Q-t transients had to be normalised to compare the transient shapes. Also log-linear plots was also used to see how close the transients were to exponentials.

Considering the n-type sample TC3-8D3 first, the responses for various voltage steps are given in Figure 4.14(a) which shows their respective magnitudes and in Figure 4.14(b) in normalised form. The general trend observed was that the speed of response decreases with increasing voltage steps. For the voltage step of 25 mV, the time to reach 90% of Q_{max} was 0.16 s, and for 50 mV, it was 0.17s. Although these are quite close, for the 100 mV voltage step the time was 0.22 s, the difference which was more obvious.

A similar behaviour was observed for the p-type sample ITTAU2,2 where the rise times to 90% of Q_{max} were 0.99s, and

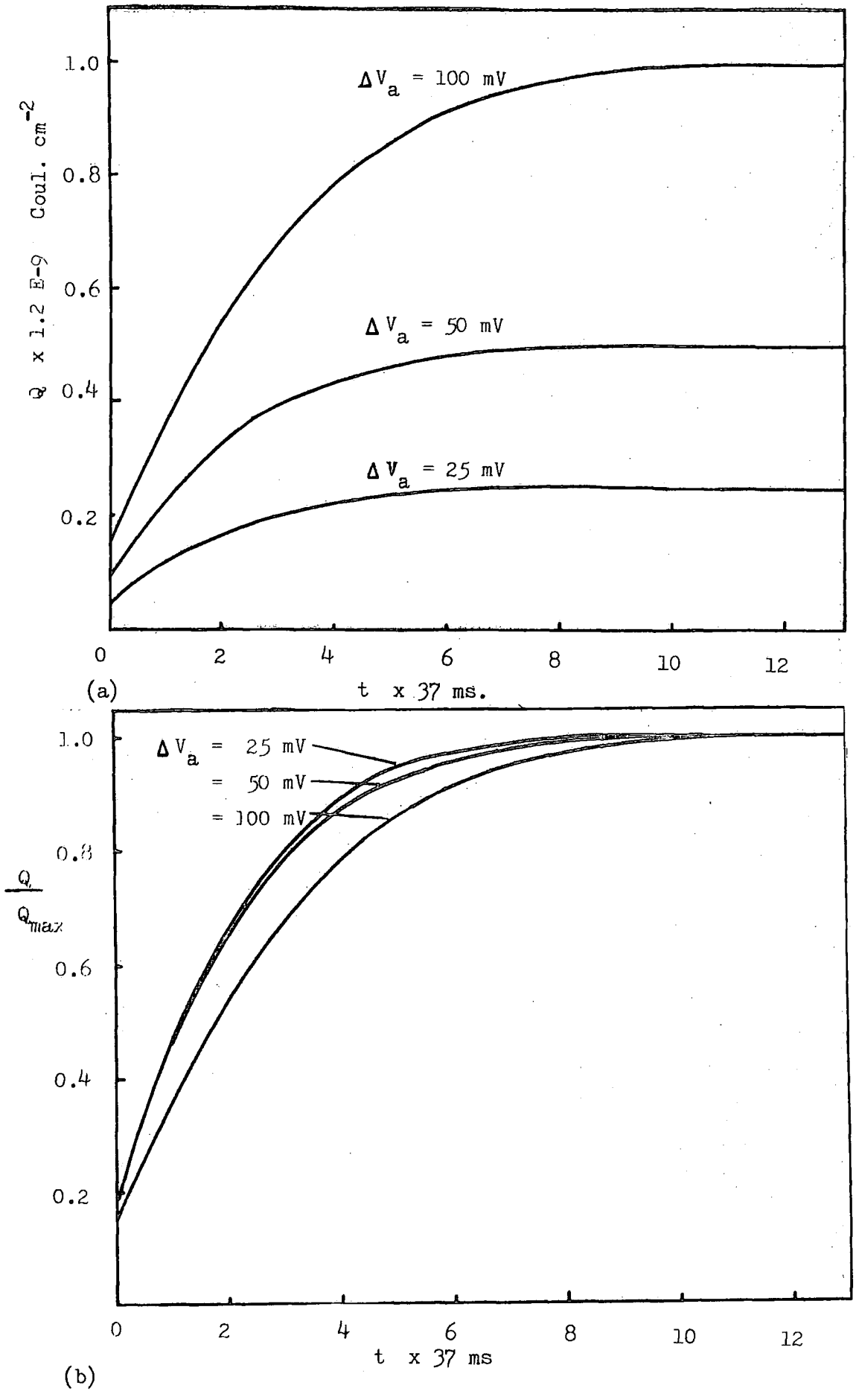

FIG. 4.14 (a) Q-t PLOTS OF SAMPLE TC3-8D3 FOR DIFFERENT VOLTAGE STEPS, ΔV_a

(b) NORMALISED PLOTS OF THE ABOVE

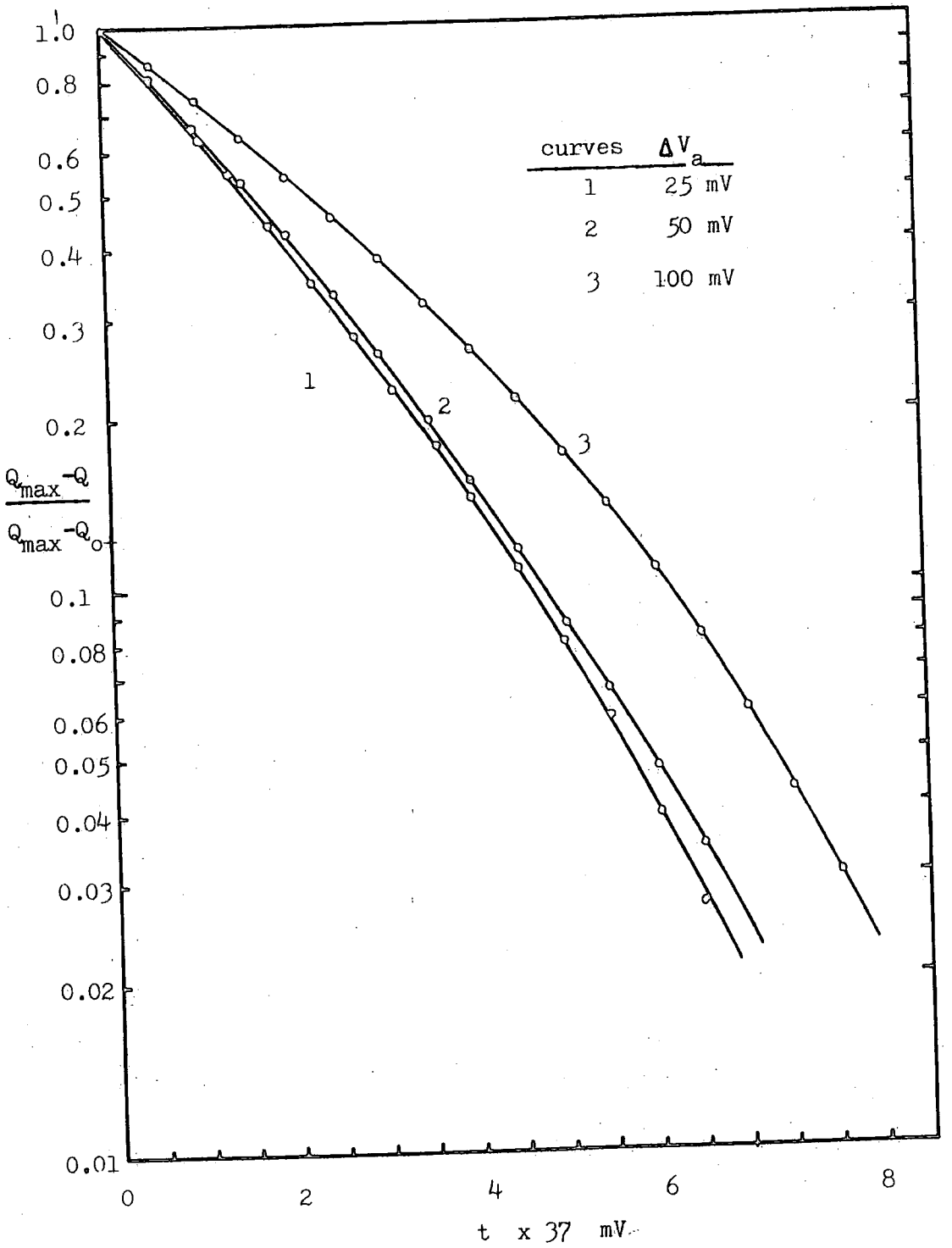

FIG. 4.14(c) PLOT OF LOG $\left(\frac{Q_{max}-Q}{Q_{max}-Q_{o+}}\right)$ VERSUS t FOR TC3-8D3

1.01 s for the voltage steps of 25 mV and 50 mV respectively. The rise time for the 100 mV step was significantly longer at 1.17 sec. The Q-t transients for different voltage steps for the ITTAU2,2 are shown in Figure 4.15(a) and Figure 4.15(b).

Measurements were further carried out on another p-type sample ITTB4,4 with a wider range of voltage steps of 25 mV, 68 mV, 147 mV and 1V. As the scales of the transients differ greatly, only a normalised plot is shown in Figure 4.16(a). The transient for the 68 mV voltage step was omitted in this figure for the sake of clarity, but the response times for all the four voltage steps are shown in Figure 4.16(b). The times to reach 90% of Q_{max} were 14.05 s, 17.32 s, 21.30 s, and 54.39 s, respectively.

The ratios of the initial step Q_{O+} to Q_{max} were also measured. For sample TC3-8D3 it was found to be 0.18 for voltage steps of 25 mV and 50 mV and 0.16 for the 100 mV step. For ITTAU2,2 it was 0.29 for all the three voltage steps. For ITTB4,4 the ratio was 0.29 for the smaller voltage steps of 25 mV, 68 mV, and 147 mV but for the 1 V voltage step it was 0.26. These values will later be compared with expectation in Chapter 8.

4.3.2 Discussion

From the results it was found that the absolute value of the initial charge step at t = o+ increases with voltage step. This is due to the fact that a longer voltage step will initially change the surface potential more, so extending the depletion layer further by the movement of the majority carriers and exposing more uncompensated ionised dopant atoms. For a more meaningful comparison, one should look at the normalised plots. The initial step of these plots is in fact the ratio Q_{O+}/Q_{max}. Figure 4.17 shows how

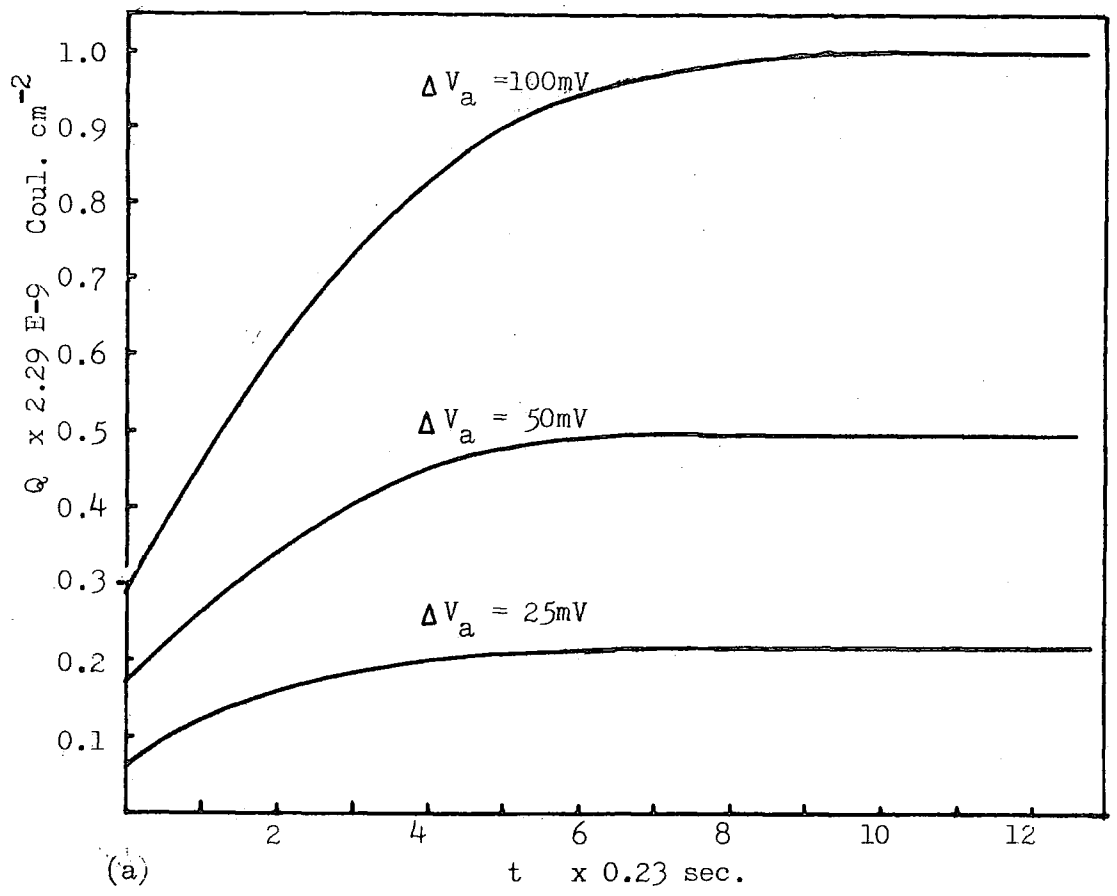

(a)

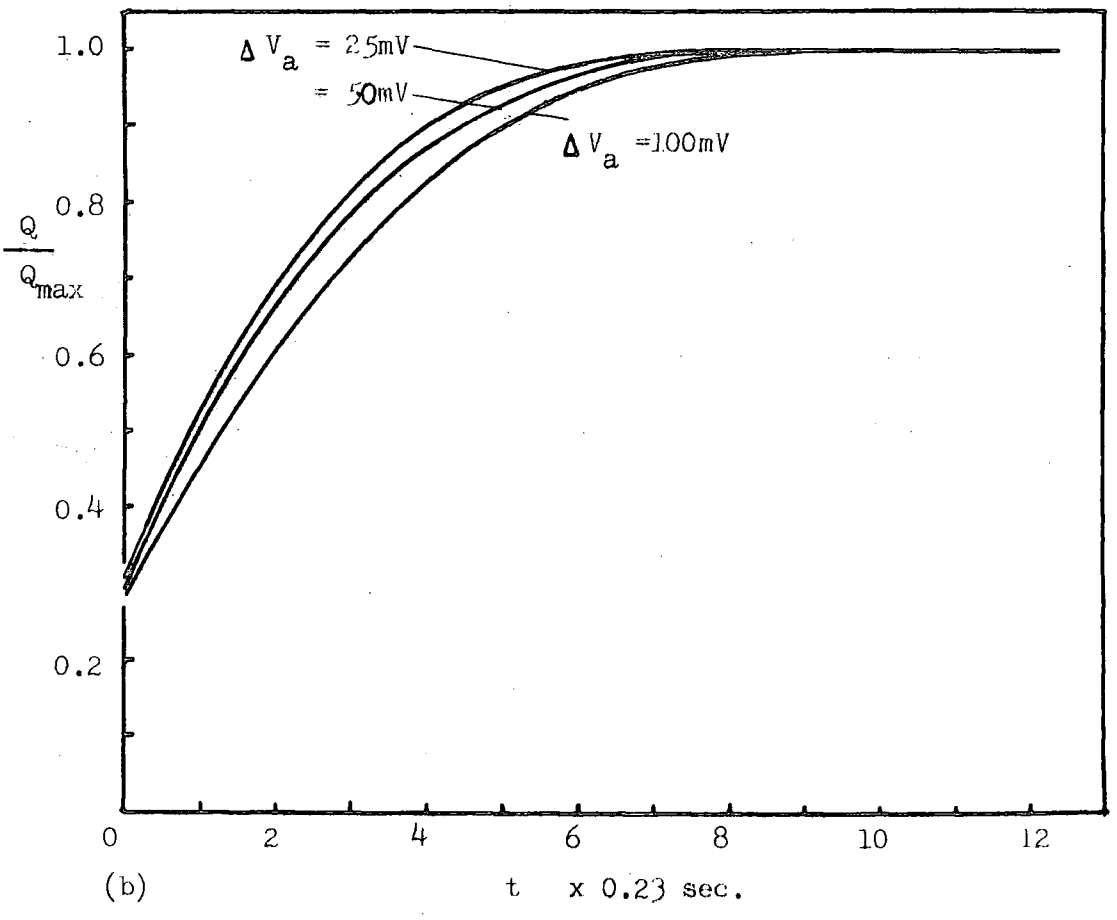

(b)

FIG. 4.15 (a) Q-t PLOTS OF SAMPLE ITTAU2,2 FOR DIFFERENT VOLTAGE STEPS, ΔV_a

(b) NORMALISED PLOTS OF THE ABOVE

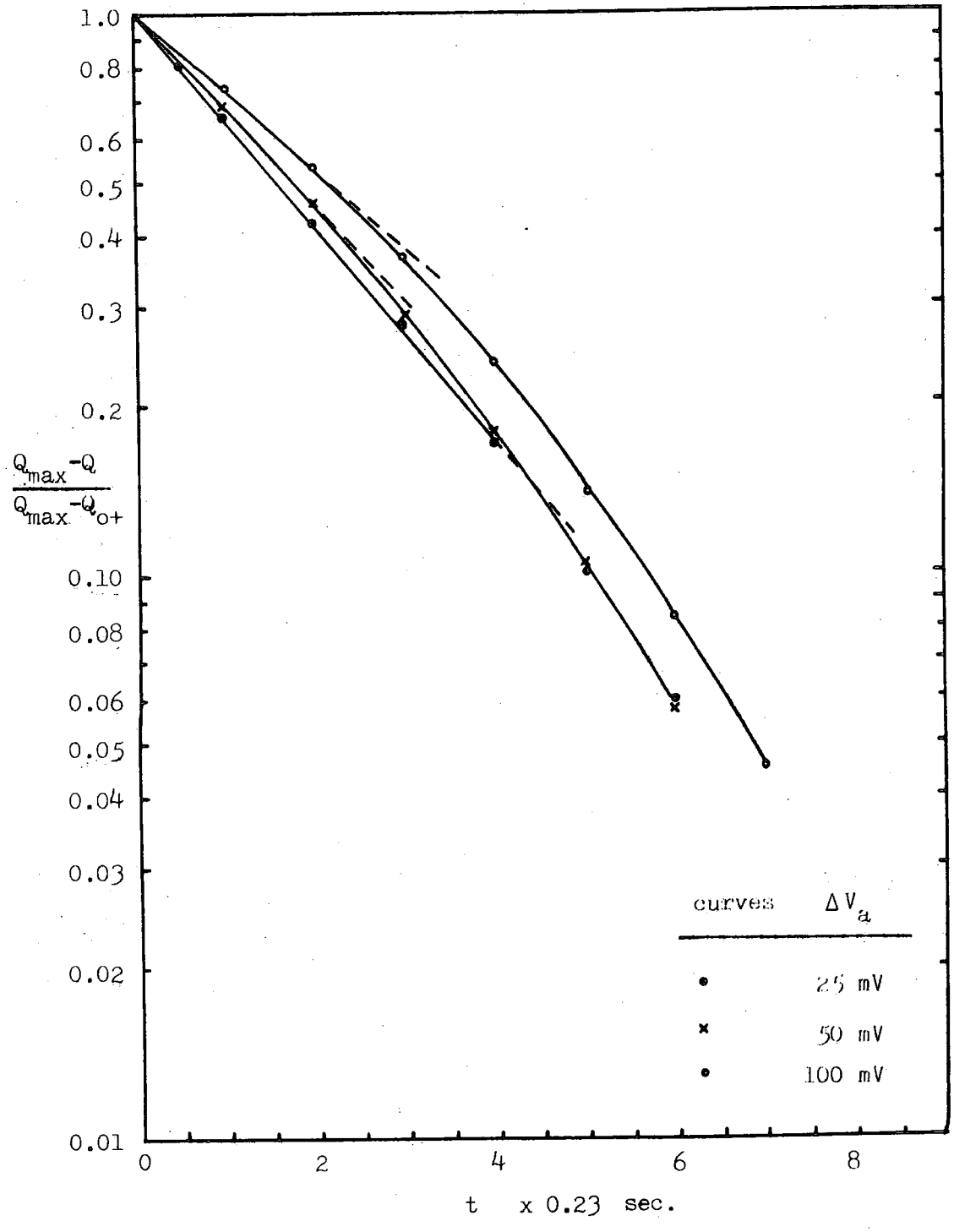

FIG.4.15(c) PLOT OF LOG $\left(\frac{Q_{max}-Q}{Q_{max}-Q_{o+}}\right)$ VERSUS t FOR SAMPLE ITTAU2,2

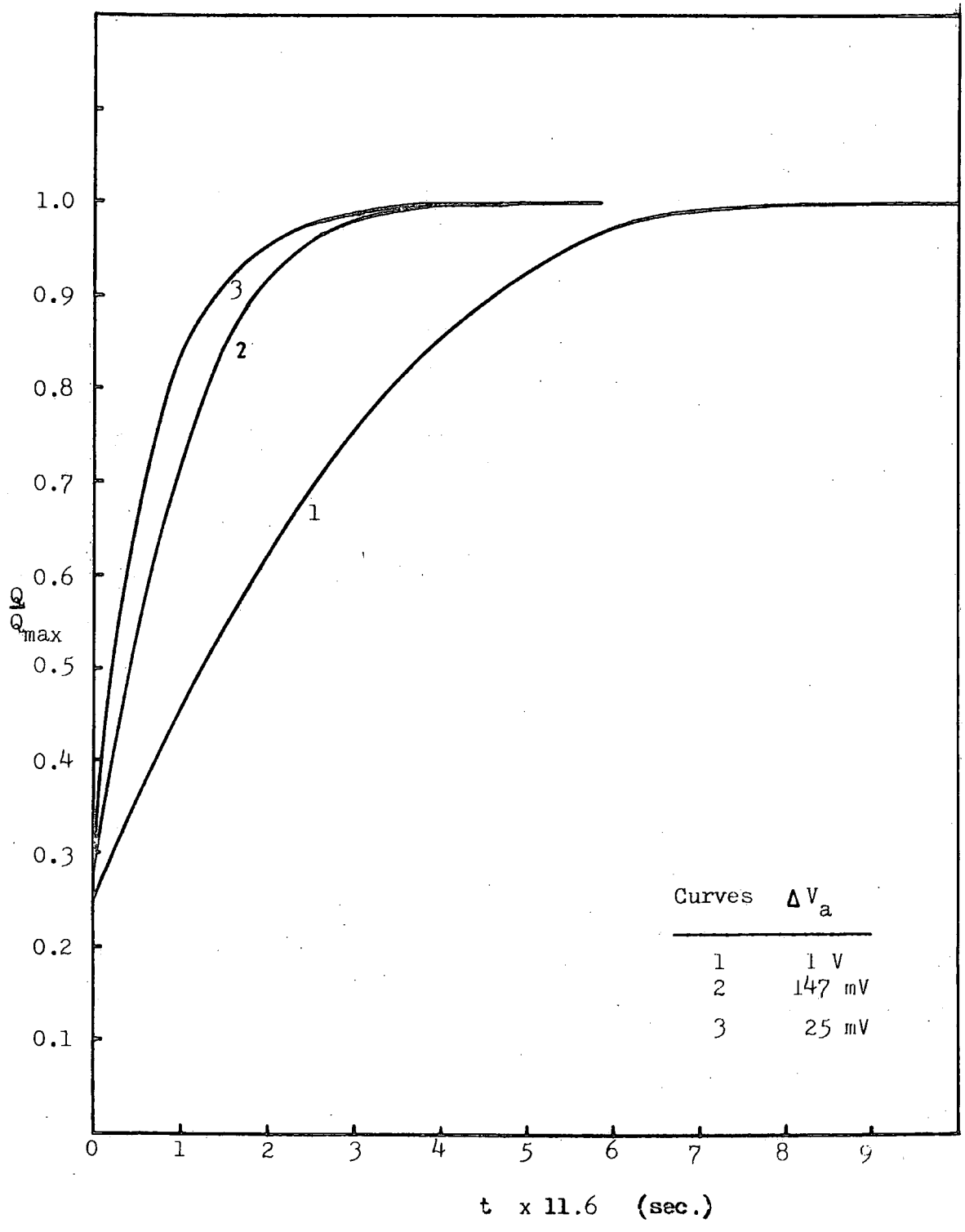

FIG. 4.16(a) Normalised Q-t Plots with Different Voltage Steps for ITTB4, 4

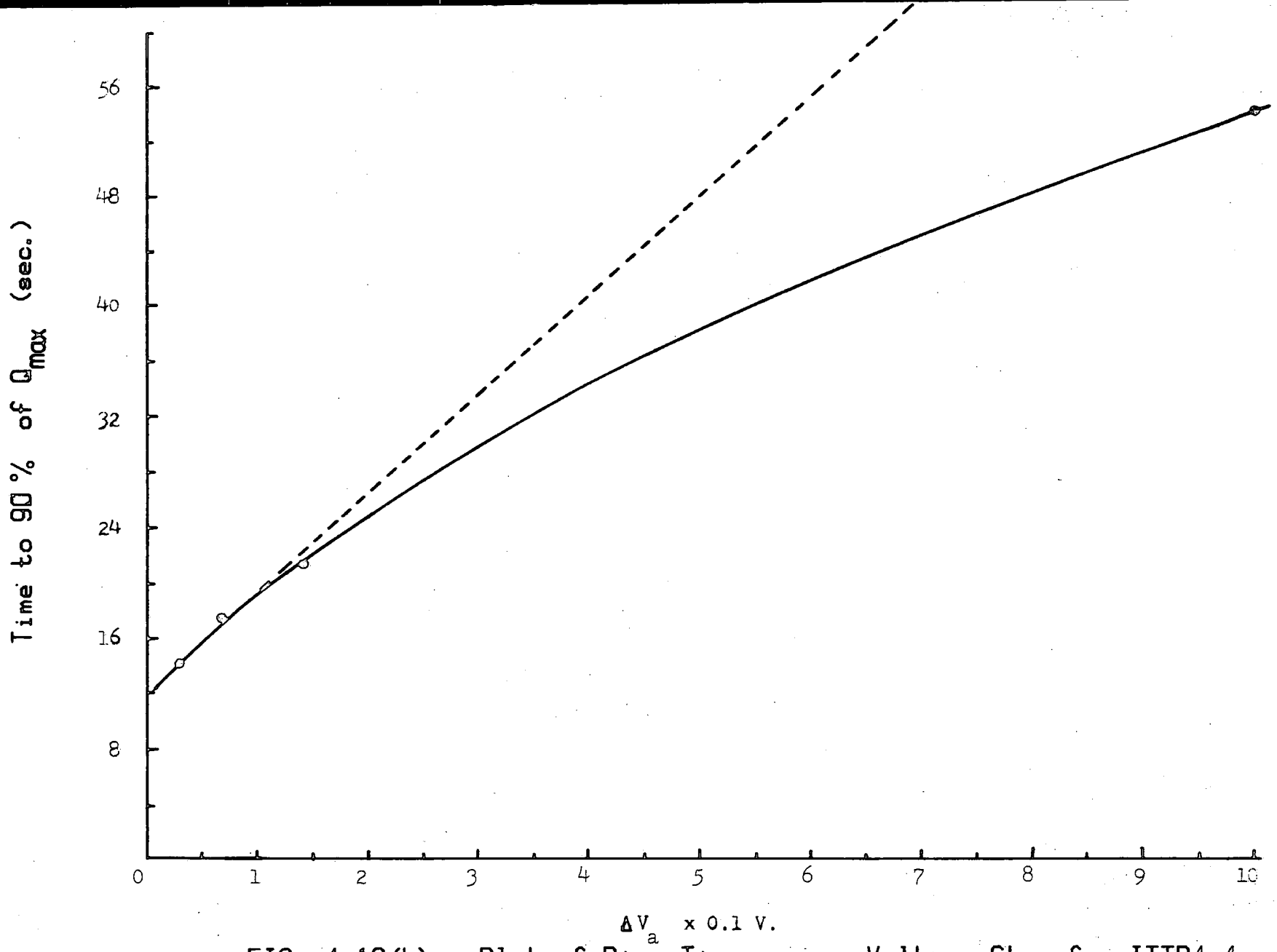

FIG. 4.16(b) Plot of Rise Time versus Voltage Step for ITTB4, 4

the effective h.f. capacitance changes with voltage step magnitude above the bias value. Effectively the instantaneous capacitance falls on a deep depletion type of characteristic below the equilibrium h.f. value. It is therefore expected that the initial step charge will decrease as the voltage step is increased. In the normalised plots of Figures 4.14(b), 4.15 (b), and 4.16, it was found that for small voltage steps, the difference in the initial steps was undetectable but for the larger voltage step of 100 mV for TC3-8D3 and 1V for ITTB4,4 it did in fact decrease.

The results also show that when the voltage step was changed from 25 mV to 50 mV the response time showed little difference but when compared to the plots for the voltage steps of greater than 100 mV, the response time increases slightly with increasing voltage step. The gradient of the Q-t plot gives the net generation current J_{gen} in the depletion layer, as shown in Figure 4.18. The appropriate constancy of the transient duration shows that the gradient at t_{O+} is roughly proportional to the step magnitude as illustrated also in Figure 4.14 and 4.15. Hence it appears that J_{gen} is proportional to ΔV which is not consistent with generation throughout the almost constant depletion layer width. This point will be discussed further in Chapters 5 and 8.

The behaviour of the Q-t transients was also analysed by plotting them on log-linear scales as in Figures 4.14(c) and 4.15(c). For small voltage steps of 25 mV the log plot was linear for most part of the transient except for the part very close to saturation. This is because the re-combination processes becomes more significant as the surface

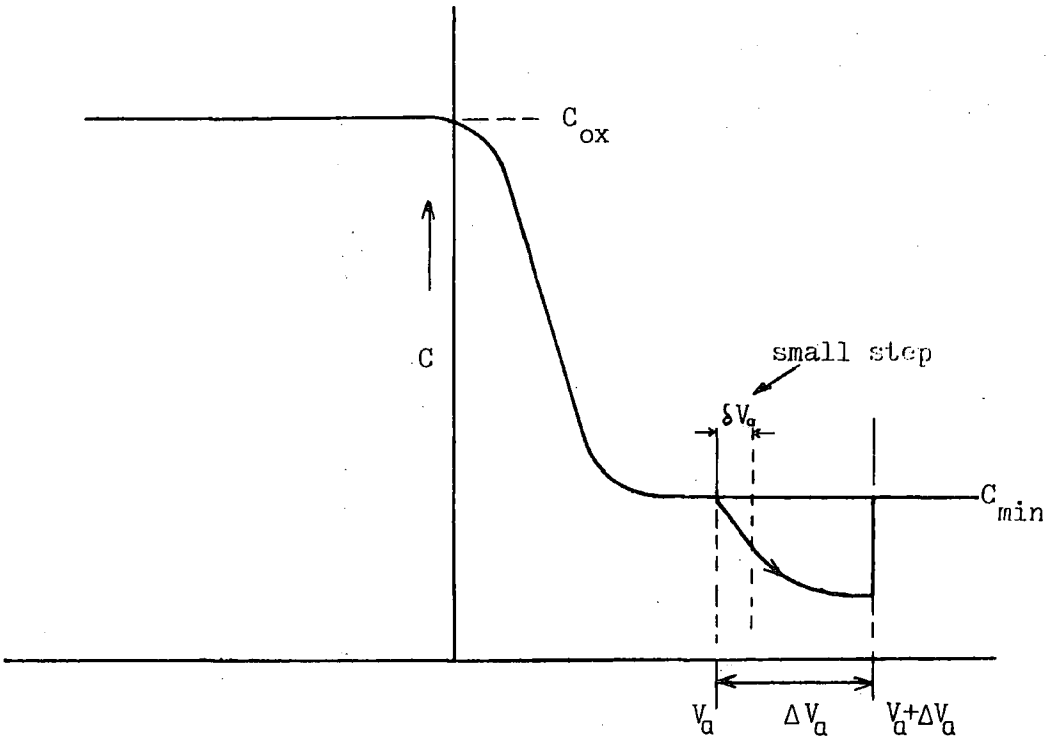

FIG. 4.17 APPLICATION OF VOLTAGE STEP SHOWN ON H.F. C-V PLOT

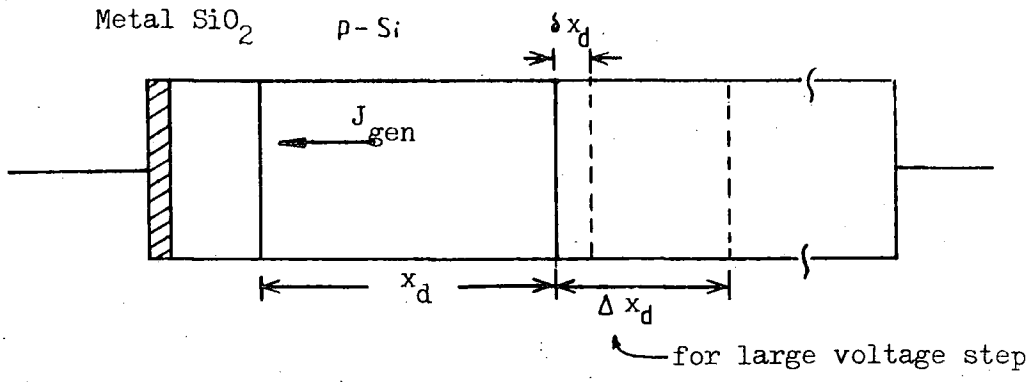

FIG. 4.18 SCHEMATIC CROSS-SECTION OF MOS CAPACITOR SHOWING GENERATION CURRENT AND DEPLETION WIDTH

potential and the energy levels approach their inversion values, hence the exponential behaviour no longer holds. For larger steps the deviation is greater implying that the small signal analysis can no longer be applied. It was also found that the log plots for the larger voltage steps have smaller gradients implying a slower response in agreement with the times to reach 90% of Q_{max} for the actual transients. These experiments therefore show that transient obtained from small voltage steps can be approximated to the simple exponential law as obtained from the small signal analysis of Hofstein. For larger voltage steps the analysis failed and a different approach is needed to reflect a more complex relationship between the charge and time in the Q-t transients.

4.4 The Effect of the Voltage Step Polarity on the Q-t Transient

In the Q-t experiment described in the previous sections, the applied voltage was always changed so that the MOS capacitor was biased from heavy inversion into heavier inversion. For a p-type sample this required the voltage to be changed from a positive value to a more positive value and for the n-type from negative to a more negative value. This is called a "forward" voltage step in this work. However the response can also be studied for the opposite polarity when the voltage is changed from that for heavy to less heavy inversion and this is called the "reverse" voltage step response in this work. The forward response is associated with minority carrier generation in the silicon whereas the reverse response is due to recombination.

The reverse response has been completely neglected in the literature. In the work of Hofstein it was mentioned that large reverse voltage steps gave transients which deviated less from exponentials than for forward steps, but no explanation was given for such behaviour. To date, there has been no other publication on the observation or interpretation of the reverse voltage step Q-t transient.

In this section observations of Q-t transients following the application of the reverse voltage steps are presented. The experiment involved the normal Q-t experimental set up with forward and reverse voltage steps applied from the same bias value. The sample had always reached equilibrium before the application of the new voltage step.

4.4.1 Results

Measurements are given here for the same p- and n-type samples ITTAU2,2 and TC3-8D3 and also on other p-type samples, ITTB4,4 and ITTAU1,3. Throughout the experiments, the d.c. bias was fixed at +5V for the p-type and -5V for the n-type samples except for the d.c. bias experiment.

Figures 4.19(a) and 4.19(b) show typical normalised Q-t transients for TC3-8D3 and ITTAU2,2 respectively for forward and reverse voltage steps of 25 mV and 100 mV. It was found that the Q-t transients were only slightly faster with the reverse voltage drop of 25 mV but were very significantly faster for 100 mV. For the sample TC3-8D3 the times to reach 90% of Q_{max} for the forward and the reverse transients were 0.16s. and 0.14s respectively for the 25 mV voltage step, and 0.22s and 0.10s respectively for the 100 mV step. For the sample ITTAU2,2 the times were 0.99s and 0.78s

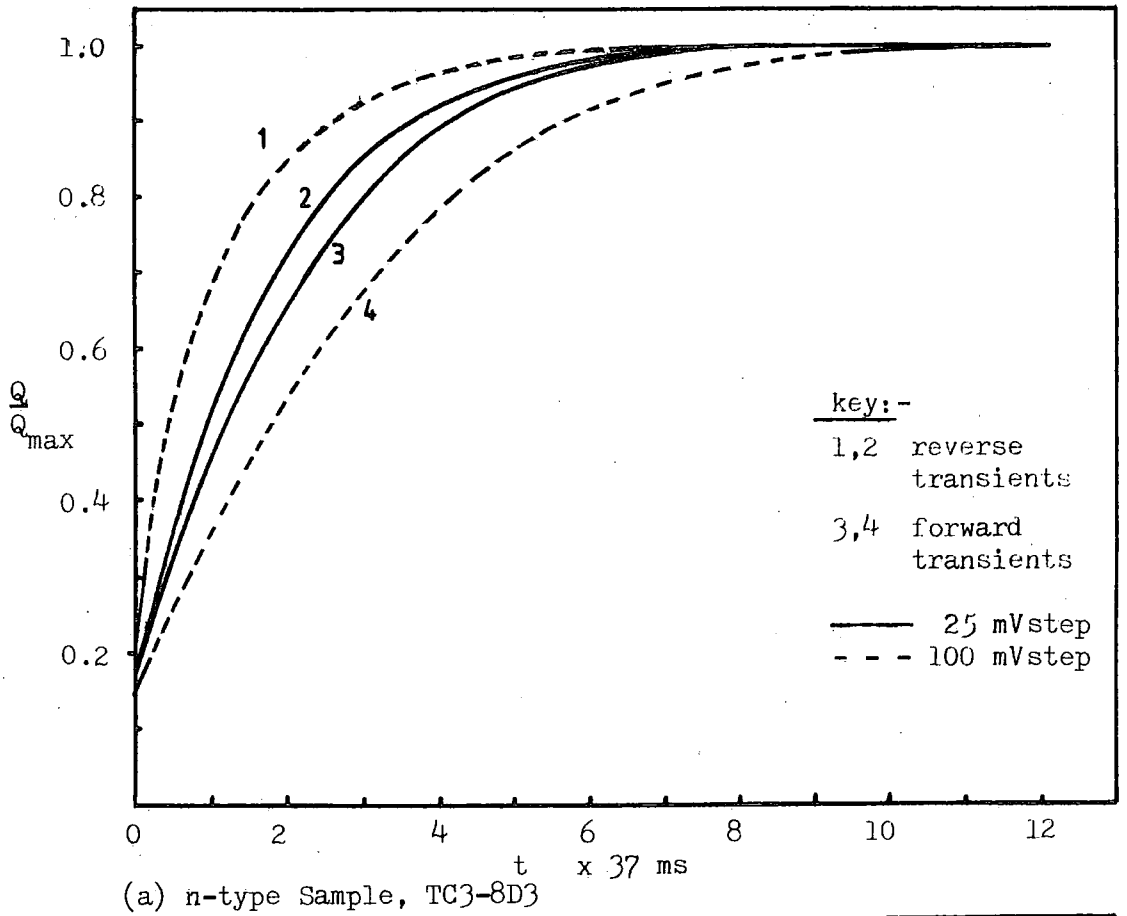

(a) n-type Sample, TC3-8D3

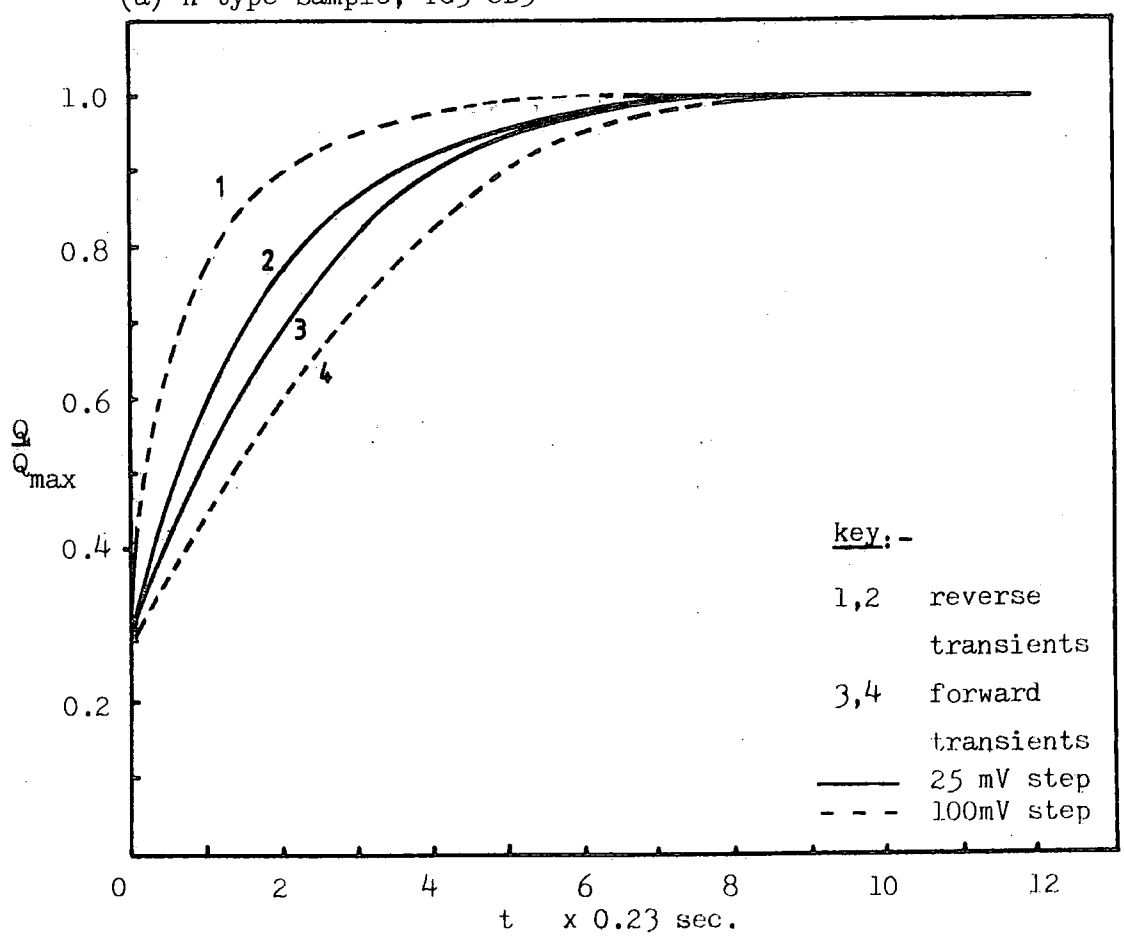

(b) p-type Sample, ITTAU2,2

FIG. 4.19 TYPICAL Q-t TRANSIENTS FOR FORWARD AND REVERSE VOLTAGE STEPS

respectively for the 25 mV voltage step and 1.17s and 0.48s for 100 mV.

The effect of the magnitude of the voltage step was investigated by increasing it to 50 mV and 100 mV. Figures 4.20 (a) and 4.20(b) show normalised Q-t transients for the forward and reverse voltage steps of different magnitudes for samples TC3-8D3 and ITTAU2,2 respectively. The response of the reverse transient was found to be shorter for the larger voltage step. For TC3-8D3, the times to 90% of Q_{max} were 0.14s, 0.12s, and 0.10s for the voltage steps of 25 mV, 50 mV, and 100 mV respectively, and for ITTAU2,2 they were 0.79s, 0.64s, and 0.48s. The values of Q_{O+}/Q_{max} were also noted for the two samples and it was found to increase as the voltage step increased. Both these are the opposite to the case for forward steps which give slower transients and smaller Q_{O+}/Q_{max} as the step voltage is increased. Measurements on the effect of voltage steps were extended to 1 volt for the sample ITTB4,4. The normalised plots for this are shown in Figure 4.21. The response times and the values of the initial steps in the transient are shown in Table 4.1 where it can be seen that Q_{O+}/Q_{max} continues to increase with increasing ΔV_a thus confirming the results for the first two samples. The response time was found to decrease further as the voltage step is increased.

Experiments on the effect of d.c. bias on the reverse transient were carried out on sample ITTAU1,3. The results are summarised in Table 4.2 and the normalised plot in Figure 4.22. It can be seen that it follows the trend of the forward transient where the response time is faster when the bias approaches the deep depletion. For the bias of 5 volts

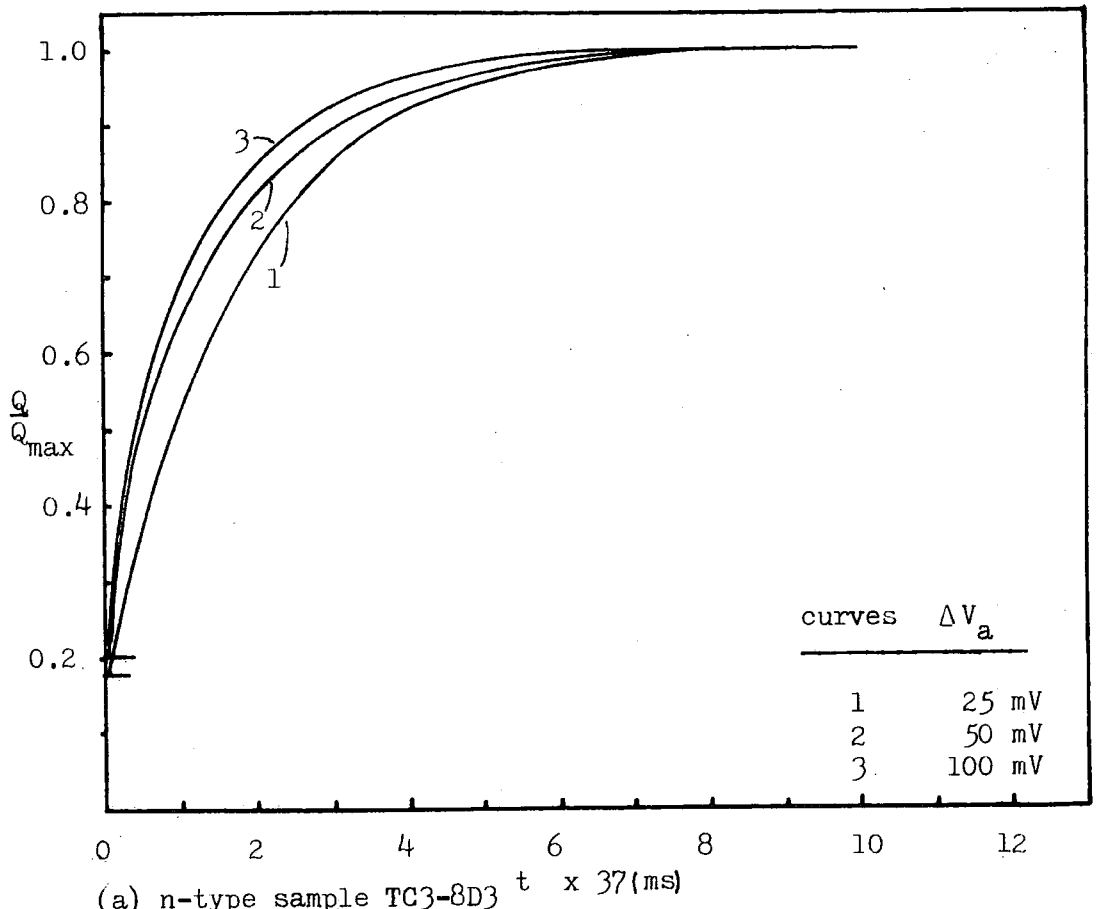

(a) n-type sample TC3-8D3

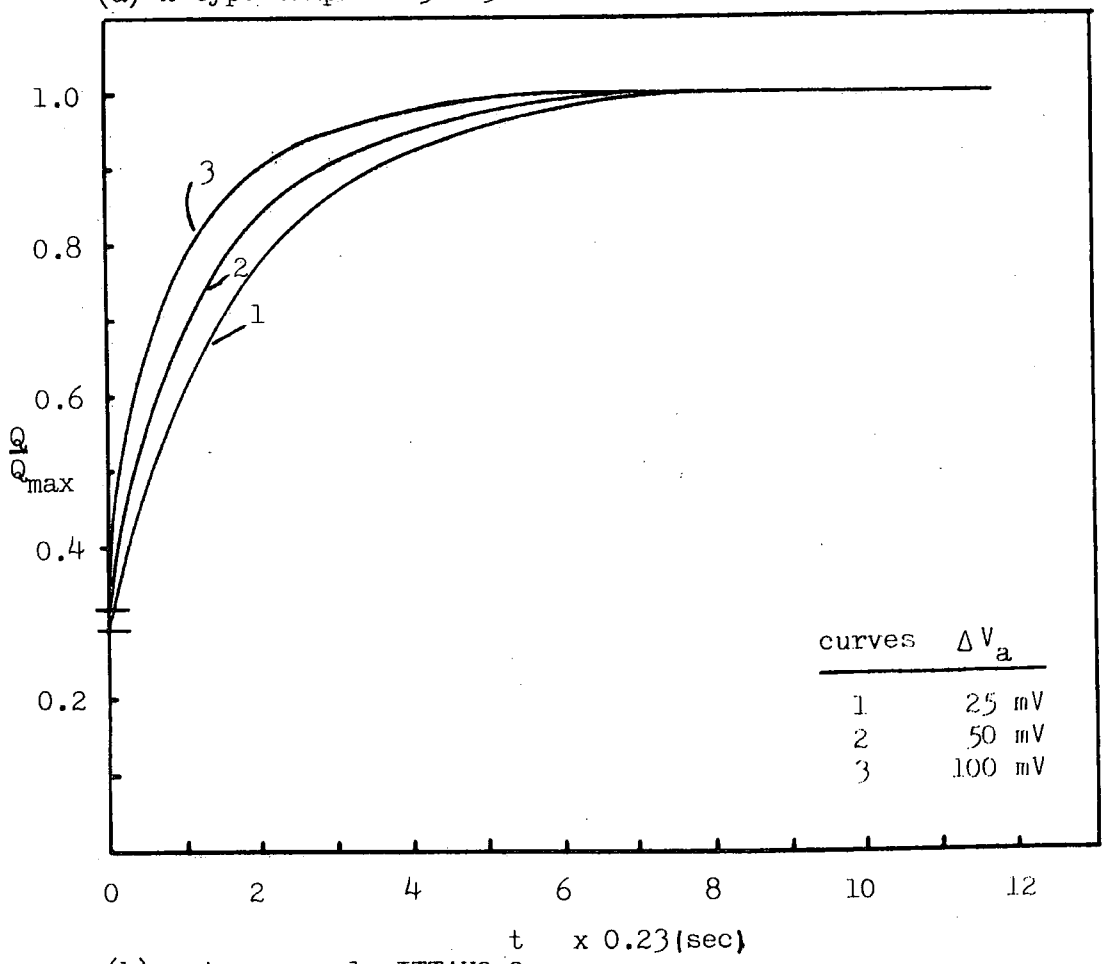

(b) p-type sample ITTAU2,2

FIG. 4.20 TYPICAL REVERSE Q-t TRANSIENTS OF MOS CAPACITOR

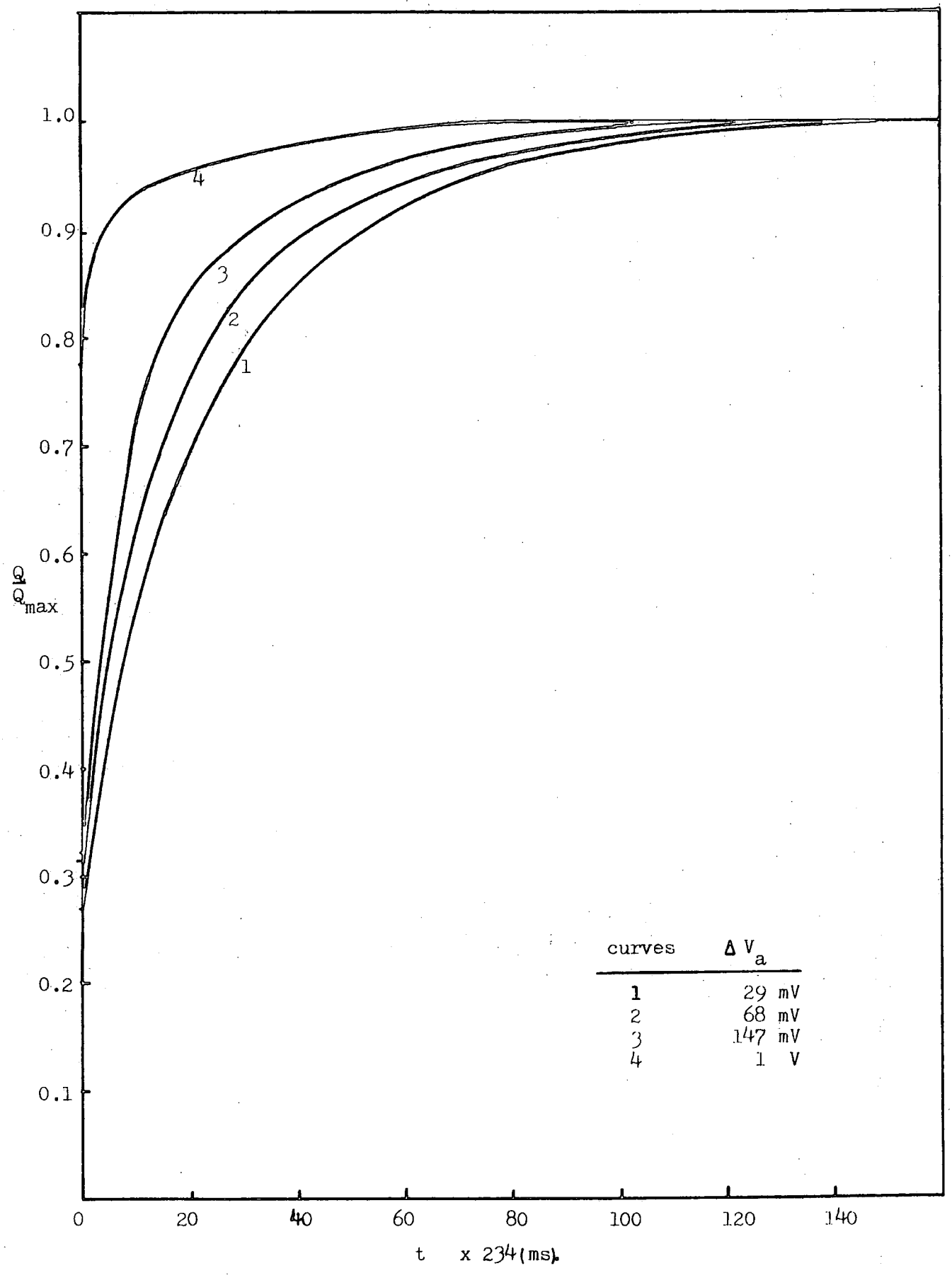

FIG. 4.21 Reverse Q-t Transients for ITTB4, 4 Sample with Different Voltage Steps

ΔV_a	Q_{o+} (Coul.)	$\frac{Q_{o+}}{Q_{max}}$	$t_{90\,\%}$ (s.)
29 mV	1.65×10^{-12}	0.30	12.17
68 mV	4.37×10^{-12}	0.32	10.30
147 mV	9.90×10^{-12}	0.32	7.49
1.0 V	1.79×10^{-10}	0.78	2.36

TABLE 4.1 REVERSE TRANSIENT RESULTS FOR DIFFERENT VOLTAGE STEPS FOR ITTB4,4 SAMPLE

V_a	Q_{o+} (Coul.)	$\frac{Q_{o+}}{Q_{max}}$	$t_{90\,\%}$ (s.)
2.0 V	1.39×10^{-12}	0.31	0.27
2.5 V	1.35×10^{-12}	0.30	0.96
5.0 V	1.38×10^{-12}	0.32	1.07
10.0 V	1.38×10^{-12}	0.30	1.07

TABLE 4.2 REVERSE TRANSIENT RESULTS FOR DIFFERENT APPLIED VOLTAGES FOR ITTAU1,3 SAMPLE

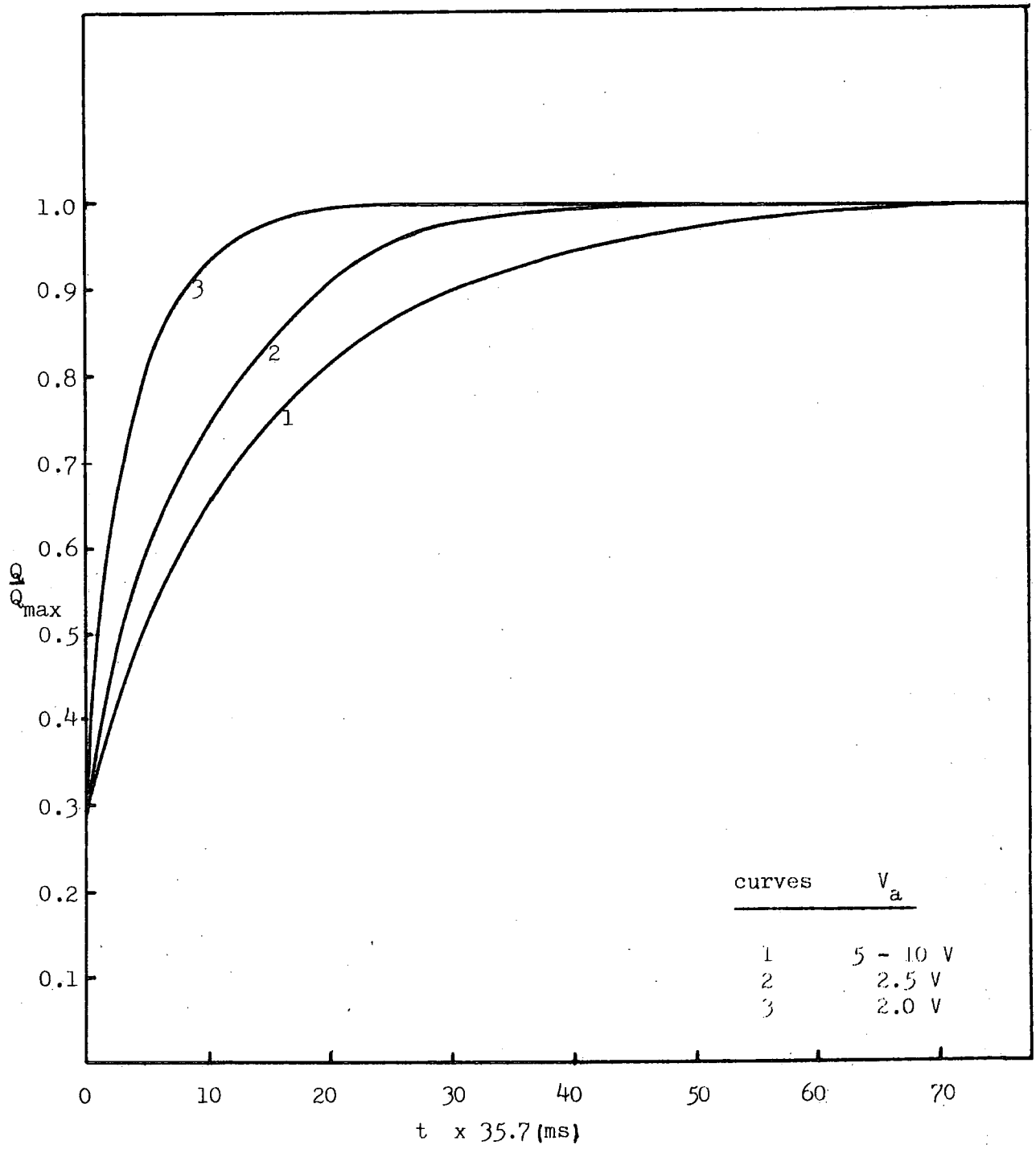

FIG. 4.22 REVERSE Q-t TRANSIENTS FOR SAMPLE ITTAU1,3 WITH DIFFERENT D.C. BIAS.

(ΔV_a = 25 mV)

onwards, the response times are constant.

4.4.2 Discussion

For even a preliminary discussion of the results obtained in this section one has to consider the deviation from equilibrium in an MOS capacitor in the inversion condition. In equilibrium the rate of generation of carriers equals the rate of recombination but during the transient this equality is disturbed. Taking a p-type sample, during the forward voltage step the depletion width initially widens due to the repulsion of the holes, and this attracts more thermally generated electrons towards the oxide-semiconductor interface while generated holes are repelled to the edge of the depletion layer to compensate the exposed doping ions. Since the population of carriers is very low in the depletion region, recombination is suppressed until enough inversion charges are produced to achieve equilibrium once again. Although the depletion layer width and the surface potential are now almost back to their original values, the concentration of the inversion charge is increased.

When a reverse voltage step is applied, the potential across the semiconductor is reduced and so the depletion edge moves towards the oxide from the movement of holes in response to the applied voltage change. The inversion charge will now exceed the new equilibrium value and the excess will move slightly towards the bulk and be lost by the process of recombination near the surface. In contrast to the forward step where the generation of carriers is within the entire width of the depletion region, the recombination process for the reverse step occurs mainly at the surface where the rate is strongly dependent upon the concentration of the excess

inversion electrons. The bigger the voltage step, the higher this excess charge will be and so the rate of recombination is relatively faster. For the forward voltage step on the other hand the generation rate is thermally controlled and independent of the inversion charge although it increases with the excess depletion layer width. As this is less than proportional to the step voltage the time required to form the extra inversion charge will increase with the step magnitude.

Contrary to the case of a forward voltage step the initial charge increment for the normalised negative step transient increases with increasing voltage step magnitude. The movement of majority carriers on the application of the voltage step is towards the interface for the reverse step thus narrowing the separation between the electrode and the semiconductor charges, i.e. reducing the depletion layer width. Since the opposite charges on a capacitor are inversely proportional to the separation between them, the normalised initial charge Q_{o+}/Q_{max} will be more than proportional to the voltage step as shown in Figure 4.23.

The measurements on the effect of the applied voltage on the reverse step Q-t transient showed similar behaviour as for the forward step, where the response time decreases as the applied voltage is reduced. The explanation is similar to that of the low frequency small signal a.c. capacitance characteristics.

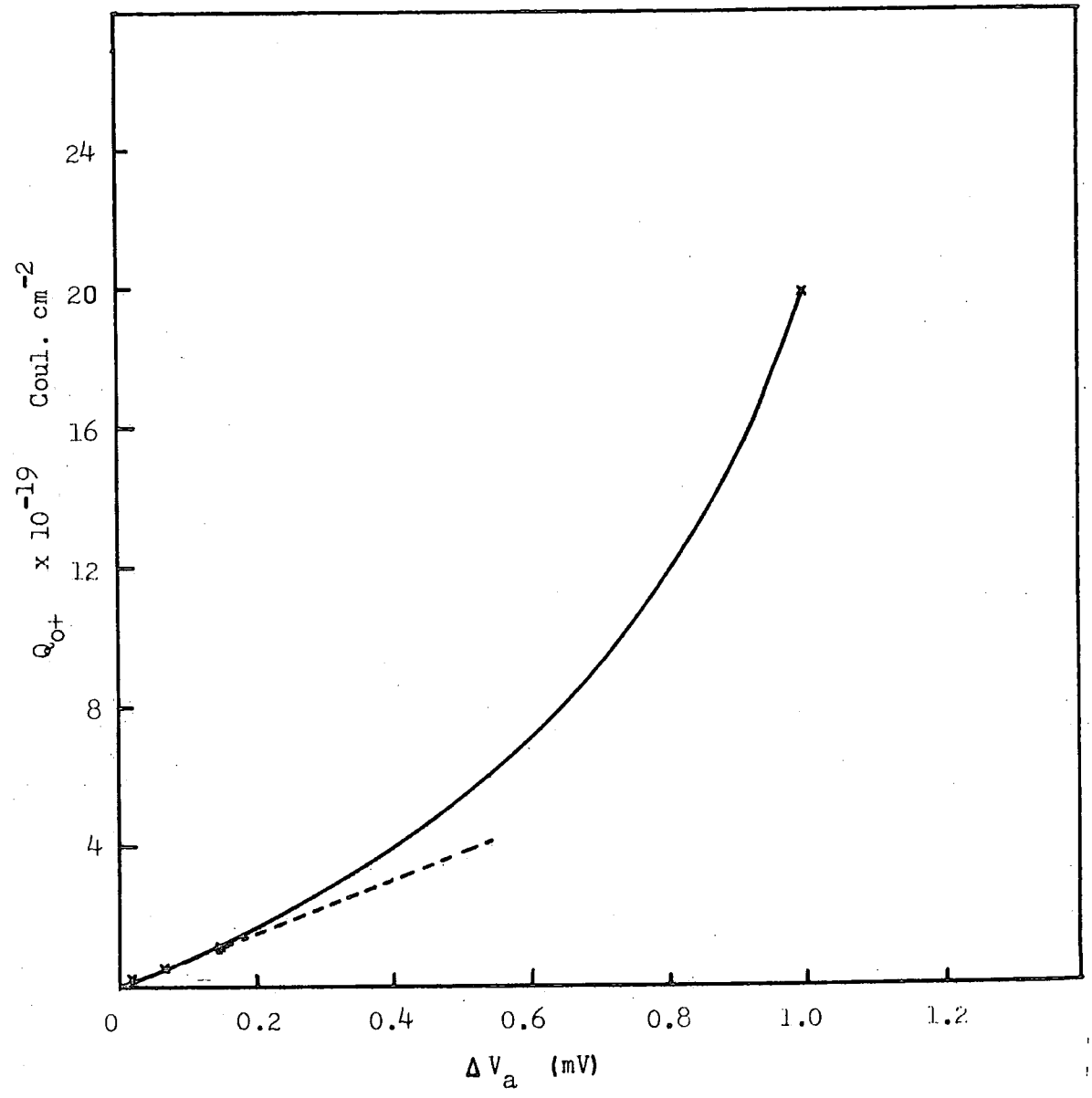

FIG. 4.23 PLOT OF Q_{o+} VERSUS ΔV_a FOR THE REVERSE TRANSIENT OF SAMPLE ITTB4,4

4.5 Conclusion to the Chapter

The aim of the experiments described in this chapter was to investigate the experimental features of Q-t transients on MOS capacitors and to compare the experimental curves with expectation. These basic matters have not been investigated previously although the Q-t method has been used to measure lifetime. Generally the results confirmed qualitative theory and this gives confidence in using the method. The experiments also provided information for the proper setting up of the parameters so that the Q-t experiments can be performed consistently using small signal methods of analysis to obtain the lifetime.

From Section 4.1 it was found that for p-type samples there should be a guard ring surrounding the metal electrode biased so that the semiconductor surface beneath it is in accumulation. This prevents lateral flow of charge and gives reliable Q-t curves. It was also found that sufficiently large voltage must be applied to the guard ring in order for this precaution to be effective. For the p-type samples used in this work, the guard ring voltage of -5V was found adequate.

The results from the work outlined in Section 4.2 shows that C-V plots are needed to decide the proper initial d.c. bias for the MOS capacitors if straight forward measurements of lifetime are required. The effect of too low a d.c. bias had been shown to be an increase in the speed of response of the MOS capacitor thus giving a falsely high generation rate if analysed by the normal assumptions. In the case of the p-type samples a bias of about +5V was found to be sufficient to bias the MOS capacitor well into heavy inversion

and for the n-type samples, a bias of -5V was necessary. The effects on the Q-t curves of biassing below heavy inversion have been explained qualitatively.

In Section 4.3, it was seen that the shape of the Q-t curves depends on the voltage step magnitude and that a voltage step larger than a few kT/q gives a curve that deviates significantly from the exponential thus requiring a different method of analysis as compared to the exponential transient for the small voltage step. This will be dealt with in more detail in Chapter 8.

The general trend observed with varying the polarity of the step, Section 4.4, was that the Q-t transient due to a reverse voltage step has a faster response than that due to the forward step. It was also found that for small voltage steps the difference between the reverse and forward Q-t response is quite small and that as the voltage step is increased the difference between the two traces becomes larger. This agrees qualitatively with expectation as in the case for the voltage step magnitude experiment, the theory of this effect will be dealt with in more detail in Chapter 8.

CHAPTER 5

THEORY OF THE Q-t TRANSIENT

5.1 Introduction

The Q-t transient measurements can be divided into two main categories. One is the small voltage step transient and the other is for the large voltage step. For the small step, the theory is based on small signal analysis and the voltage step magnitude is limited to around 25 mV. The assumption made here is that for a small enough voltage step the Q-t transient can be approximated to an exponential which has been confirmed experimentally. However it is found that on increasing the voltage step, the exponential relationship no longer holds. This limitation has been overcome only by Viswanathan and Takino (23) whose method of analysis breaks down towards the end of the transient. In both methods the contribution to the minority carrier concentration in the depletion region due to the diffusion of electrons from the bulk substrate has not normally been considered. At the same time all previous measurements of Q-t transients have been for increasing inversion, i.e. when generation predominates, while the recombination process which is observed by the application of a reverse voltage step has not been considered.

It is the purpose of this chapter to discuss some of these omissions by proposing a model to explain the behaviour of the Q-t response for which a mathematical expression is obtained. This is solved using a microcomputer and thus the

theoretical Q-t plots are presented. In the first part of the chapter, a qualitative description of the movement of the charges and the change in the band diagram during the transient is given. The theoretical plots are then analysed and discussed at the end of the chapter. For reasons discussed in Chapter 1, we shall consider only the ideal MOS capacitor.

In modelling the Q-t response, we shall be considering the charge movement in the MOS capacitor after a voltage step is applied. First a simple picture is used to explain the response where we consider a simple diagram to show the concentration of carriers and the electric field that are developed due to the applied voltage. The behaviour of the carriers is described under the two conditions of equilibrium and of non-equilibrium, and for both forward and reverse voltage steps, where as explained in the last chapter, the forward voltage step refers to the voltage step that increases the bias and brings the sample towards heavier inversion, and the reverse direction is where the voltage step decreases the bias to less heavy inversion.

5.2 The Equilibrium Condition

First, the equilibrium condition before the application of the voltage step is considered. Figure 5.1 is the cross-section of the p-type MOS capacitor biased into inversion and in equilibrium. The figure shows the depletion width and the charge concentration in the device under equilibrium where the depletion width x_d is at its maximum equilibrium value. In Figure 5.2 the energy band diagram for this condition is given showing the surface potential and the energy profile under the applied bias. The surface potential is proportional to the square of the maximum depletion width x_{do} and since the

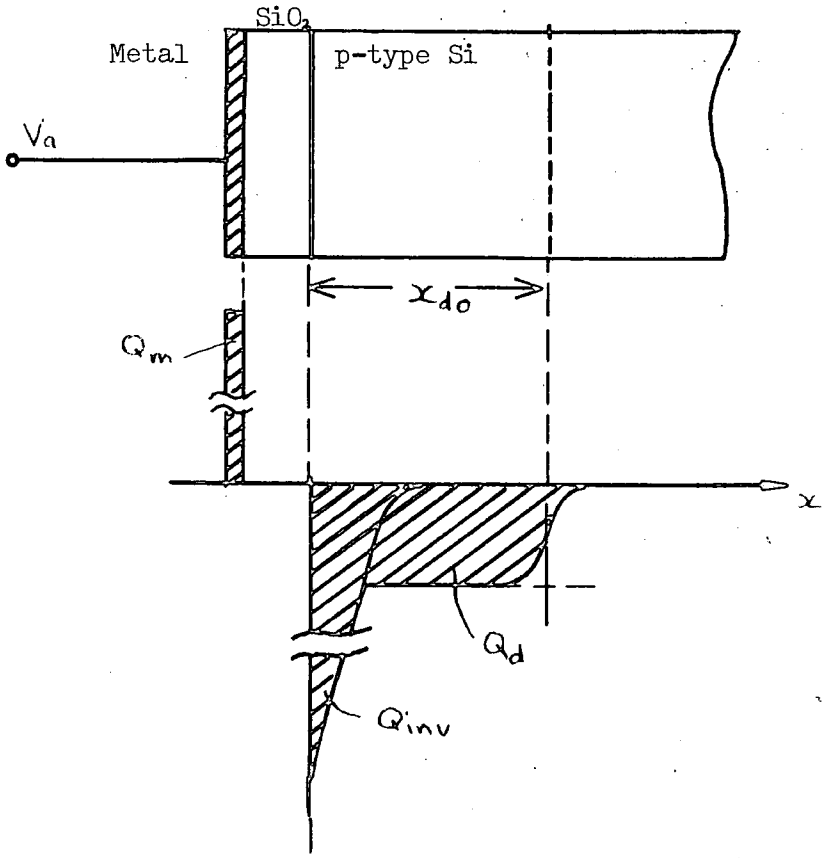

FIG. 5.1 Cross-section Representation of the MOS Capacitor in Inversion

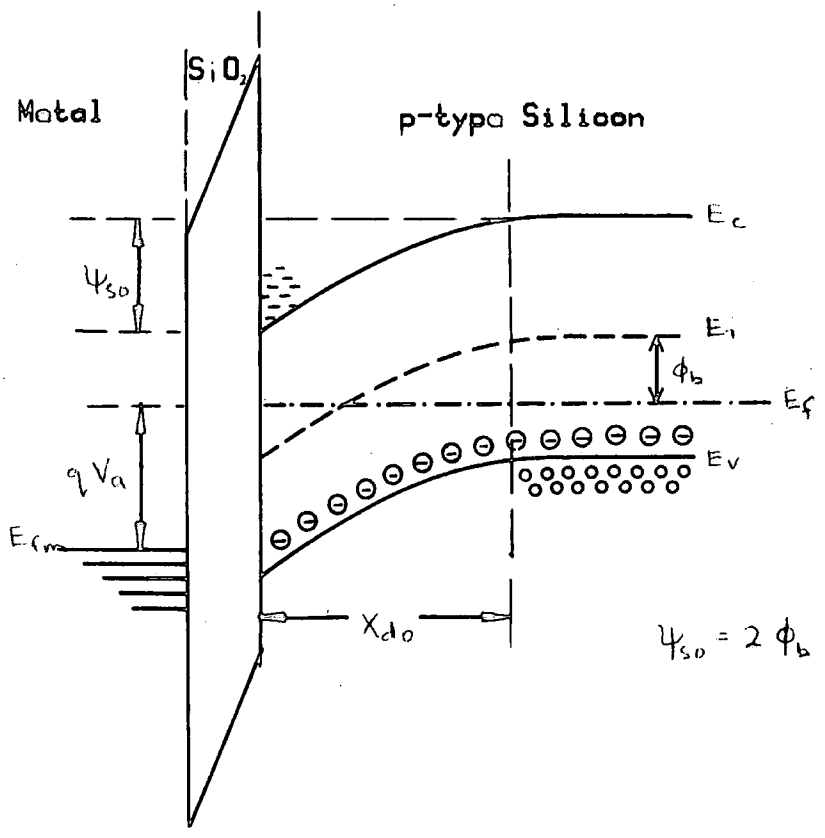

FIG. 5.2 The Energy Band Diagram of the MOS Capacitor in the Inversion Condition (Equilibrium)

capacitor is in strong inversion, the relation $\psi_s = 2\phi_b$ holds where ϕ_b is the difference between the intrinsic energy E_i and the Fermi level E_f in the neutral bulk of the semiconductor. In Figure 5.3(a) we show a logarithmic profile of the electron and the hole concentrations in the inversion and depletion regions. This follows from the relations

$$p = n_i \exp\left(\frac{E_i - E_f}{kT}\right) \tag{5.1}$$

$$n = n_i \exp\left(\frac{E_f - E_i}{kT}\right) \tag{5.2}$$

To have a more exact picture of the carrier profile we have to look at a linear plot of these concentrations. In Figure 5.3(b), linear plots of hole and electron concentrations against distance are shown for the p-type capacitor. It is seen that the concentration of electrons forms an inversion layer at the silicon surface while the region between the surface and the depletion layer edge, is depleted of both carriers. The hole concentration rises up to the value N_a at the edge of the depletion layer. The total charge concentration profile of the depletion layer is that of the fixed dopant ions and the minority carriers as shown in Figure 5.3(c). The voltage applied across the sample is the sum of the voltages dropped across the oxide and across the semiconductor, where the latter is the surface potential.

The potential profile inside the depletion region is given by the solution of Poissons equation as $\psi = \frac{qN_a}{2\epsilon_s}(x_d - x)^2$. At the surface it is the surface potential ψ_s and at the inner edge of the depletion region it drops to zero. Electrons

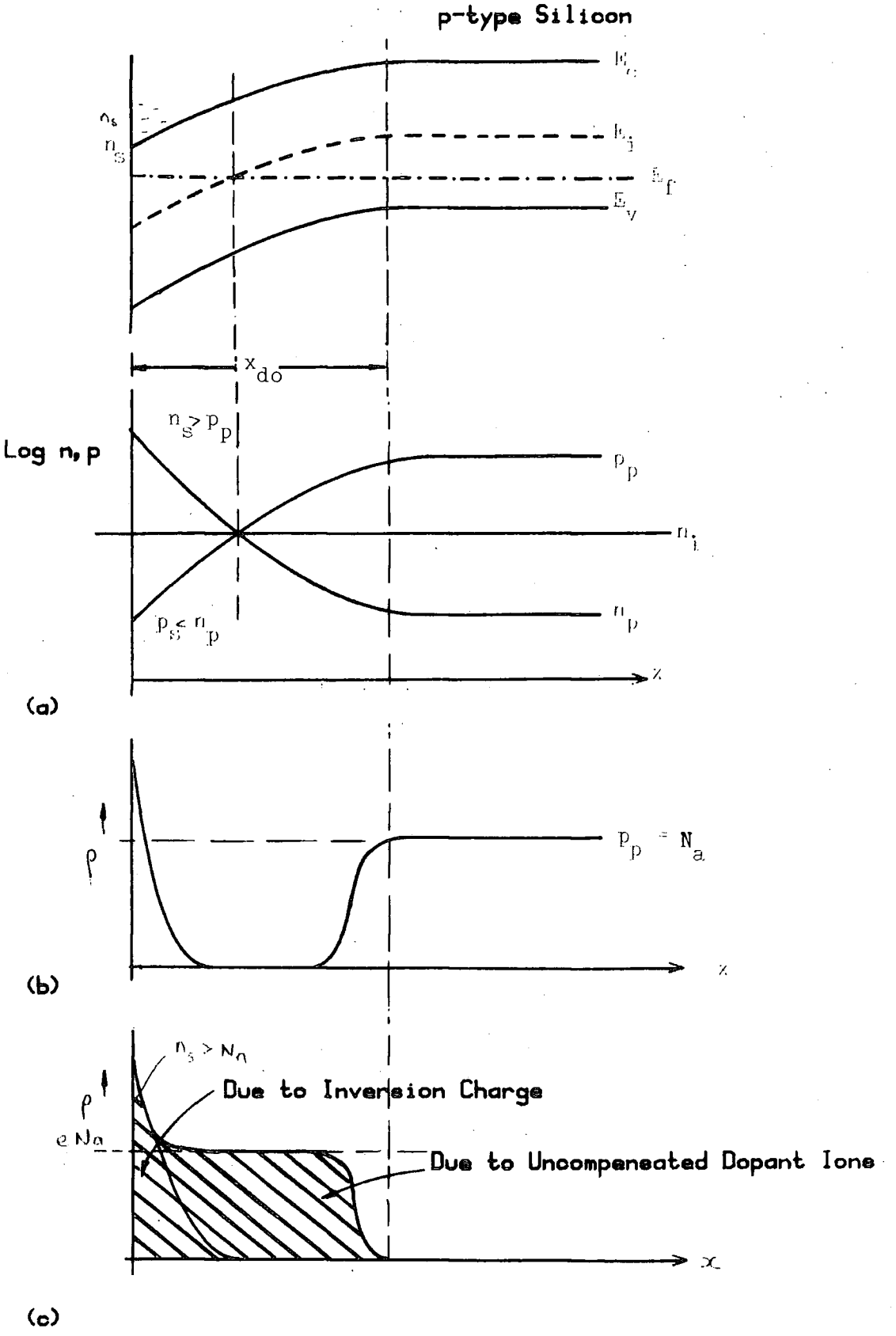

FIG. 5.3 The p-type MOS Capacitor in Equilibrium showing: -

a) Log Plot of the Carrier Concentration
b) Linear Plot of the Carrier Conc.
c) Net Charge Concentration

and holes will move in opposite directions in the electric field in the depletion layer. They will also tend to move by diffusion due to their varying concentrations. However, in equilibrium, the drift and the diffusion components of both carriers currents must cancel each other and as a result the net current is zero everywhere.

The processes of generation and recombination go on all the time in equilibrium at rates that are equal to each other but in opposite directions. Referring to Figure 5.4 we try to show the actual processes of generation and recombination that might occur in the MOS capacitor in equilibrium. Generation and recombination are assumed to occur predominantly through Shockley-Read traps in the forbidden gap. As is well known, traps with energies E_t near the centre of the gap are by far the most active in generation and recombination (45) so that these will be the only ones considered. From Figure 5.4 we can divide the depletion width into various regions according to the energy levels of the traps with respect to the Fermi level, E_f (2). The region where E_t is greater than E_f, called Region I, has the trap energy levels higher than E_f, so that they will be empty most of the time. Since the conduction band is almost empty, generation and recombination will go on predominantly between the valence band and the trap levels in Region I. The concentration of carriers in the conduction and the valence bands will remain constant at a given position x, as equilibrium is maintained. This causes the rate of generation to be equal to the rate of recombination.

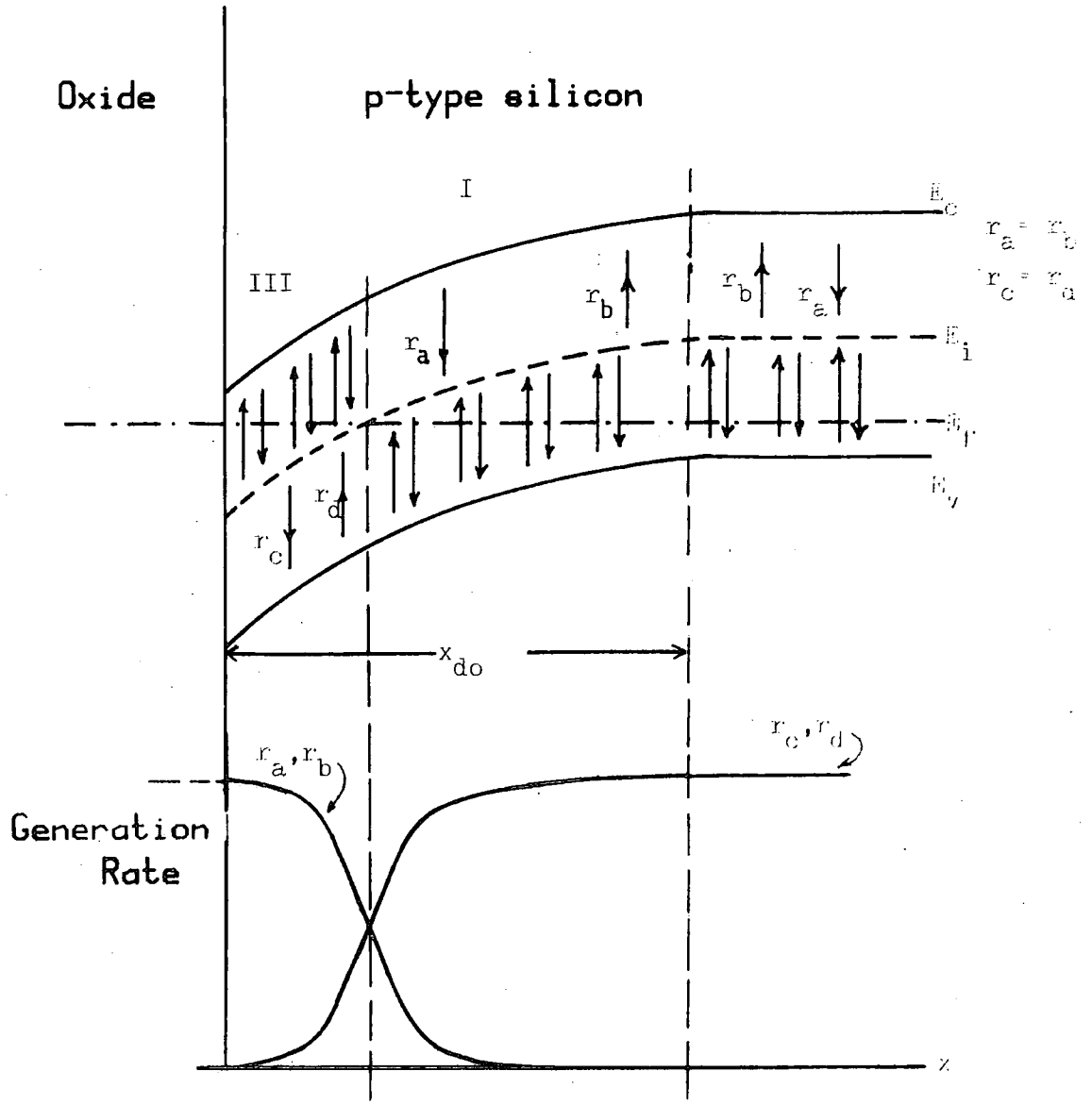

FIG. 5.4 Generation and Recombination in a p-type MOS Capacitor in Equilibrium

That is

$$r_a = r_b$$

and

$$r_c = r_d$$

where r_b and r_a are the electron capture and emission rates to and from the conduction band respectively, and r_c and r_d are the emission and capture rates to and from the valence band respectively.

The region where E_t is less than E_f is named Region III. Here the traps are filled with electrons and, since the hole concentration is very low in the valence band in this region, the generation- recombination processes occurs mainly between the conduction band and the generation centres.

Transitions between the bands via the traps occur at a rate which is the lowest of the transition rates between one band and E_t. Figure 5.4 shows that the net generation and recombination rates are therefore negligible except in the vicinity of the position where the trap energy crosses the Fermi energy where r_a, r_b, r_c and r_d are all equal and opposite in equilibrium.

5.3 The Non-Equilibrium Condition

In the earlier chapters we have briefly discussed the effect of a voltage step applied to the MOS capacitor originally in the equilibrium condition. Here we shall deal with the situation in more detail. The forward voltage step will be discussed first, followed by the reverse step analysis in detail.

5.3.1 The Forward Voltage Step Transient

Before going into a detailed description of the generation-recombination processes, we shall look at the charge movement in an MOS capacitor out of equilibrium. Figure 5.5 shows the changes in the charge distribution for a forward voltage step on a p-type MOS capacitor. For simplicity we omit the charges that exist at t = 0 in equilibrium and concentrate only on the changes in the charge concentrations. The equilibrium depletion width is x_{do}. Figure 5.5(b) shows the case immediately after the application of the voltage step, where the depletion width is extended beyond x_{do} so that it exposes more ionised dopant atoms to balance the electrode charge Q_m. This appears as a step increase in the Q-t plot because of the fast movement of holes, which being the majority carriers, have a very short time constant. The increased charge in the electrode is therefore initially balanced by the increased charge due to the extended depletion width ΔQ_d. From Poisson's equation, taking a one dimensional case we have

$$\frac{d}{dx}\left(\frac{dV}{dx}\right) = -\frac{\rho}{\varepsilon_s} \tag{5.3}$$

where ρ is the charge concentration (= qN_a) in the semiconductor. Integrating the above equation we have,

$$\int_{x=x_d}^{x=0} d\left(\frac{dV}{dx}\right) = -\int_{x_d}^{0} \frac{\rho}{\varepsilon_s}\, dx \tag{5.4}$$

Therefore $$|F| = \frac{dV}{dx} = \frac{\rho x_d}{\varepsilon_s}, \qquad F = \text{field strength}$$

$$\rho = \frac{qN_a x_d}{\varepsilon_s}$$

$$= \frac{Qd}{\varepsilon_s} \tag{5.5}$$

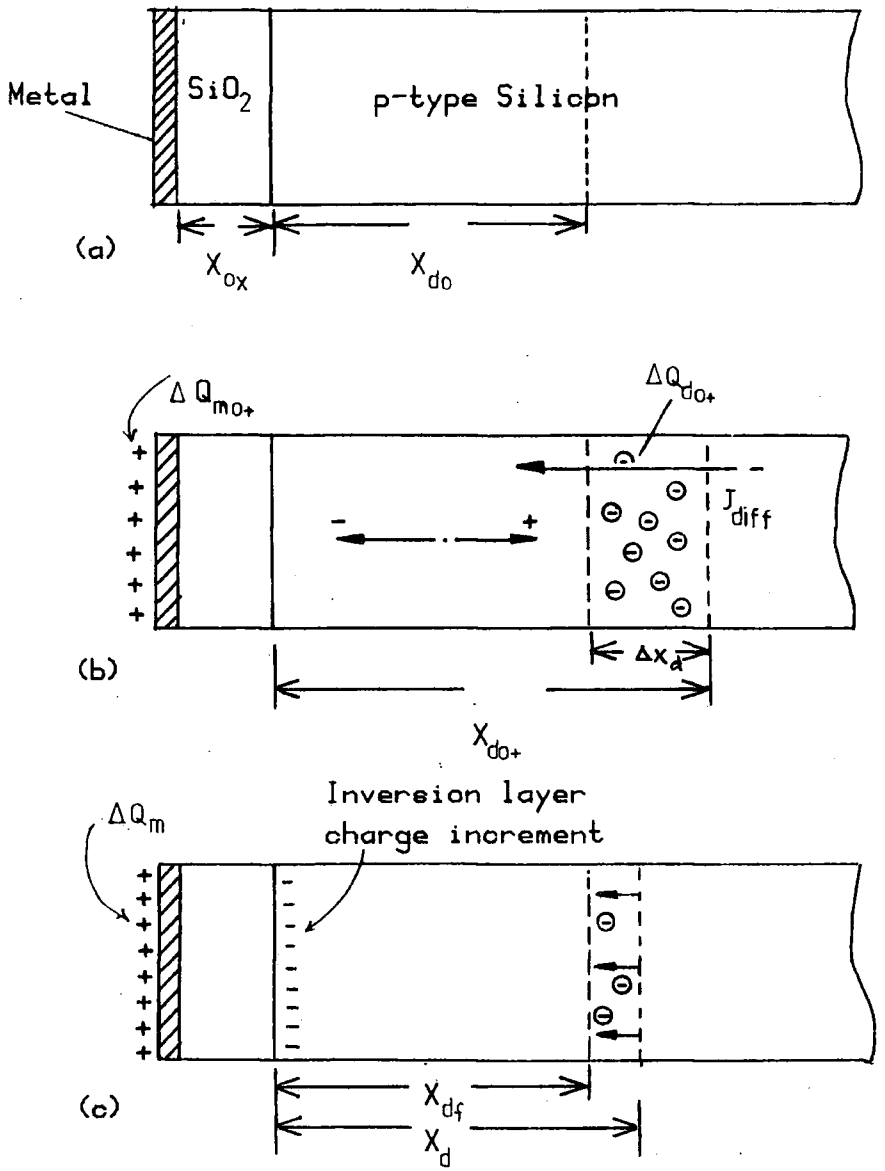

FIG. 5.5 Cross section of a p-type MOS Capacitor

(a) In Equilibrium

(b) Immediately After a Voltage Step (t=0+)
(showing only the charge difference)

(c) After the Voltage Step (t>0+)
(non-equilibrium condition)

Therefore, for a given value of the applied voltage the charge that is required to maintain the potential increases as the separation decreases. This explains the increase in the charge Q_m as the depletion layer collapses and its charge is replaced by the inversion charge which is closer to the electrode.

The Q-t transient can be described by considering the band bending due to the application of the voltage step. The transient can be divided into two parts. One is immediately following the application of the voltage step when the depletion width and band bending are at their maxima, and the depletion region is further depleted of carriers as electrons are swept to the interface and the holes repelled into the bulk of the semiconductor. We denote this time as t_{O+}. The second is when the time is greater than t_{O+} during which the minority carriers are generated in the depletion region and the system is moving back towards a new equilibrium state. This is known as the equilibration time (3).

(a) The Initial Step $t = t_{O+}$

When the forward voltage step is first applied, a period of non-equilibrium occurs where the metal electrode is charged up rapidly and the energy levels at the semiconductor-oxide interface are pulled downwards thus increasing the surface potential ψ_s of the semiconductor. The holes, which are all the time in equilibrium with the valence band, as they are the

majority carriers, move almost instantaneously into the bulk leaving the uncompensated dopant ions and increasing the depletion layer width beyond its maximum equilibrium value. This changes the carrier concentration profile in the depletion region due to electrostatic interaction with the charge on the metal.

In Figure 5.6 the energy band diagrams before and immediately after the voltage step are shown. From this figure it is seen that as the energy levels are bent downwards, more trap levels are pulled below the Fermi energy E_f. Comparing the two diagrams in Fig.5.6, we can visualise the extension of the depletion width as the addition of Region II in between Regions I and III in the depletion layer. This is defined as the region where the traps which were initially empty, are suddenly filled as they are pulled below E_f. This filling of the traps occurs in the first few microseconds for the normal values of trap cross-section (2). The traps in this region can alternatively be considered as filled with holes when they were above E_f. When they go below E_f it is as though holes are emitted to the valence band by the process of capturing electrons. In the Q-t experiment this occurs during the initial step of the transient and well within the response time of the recording equipment, as is the time for the changing of the depletion layer width by the displacement current. The sudden change in the applied potential also changes the electron concentration profile in the depletion region as illustrated in Figure 5.7 where the electrons are shown to be pulled strongly into the interface. At the same time the electron concentration at the edge of the depletion layer and the bulk will be decreased to almost zero, so creating a con-

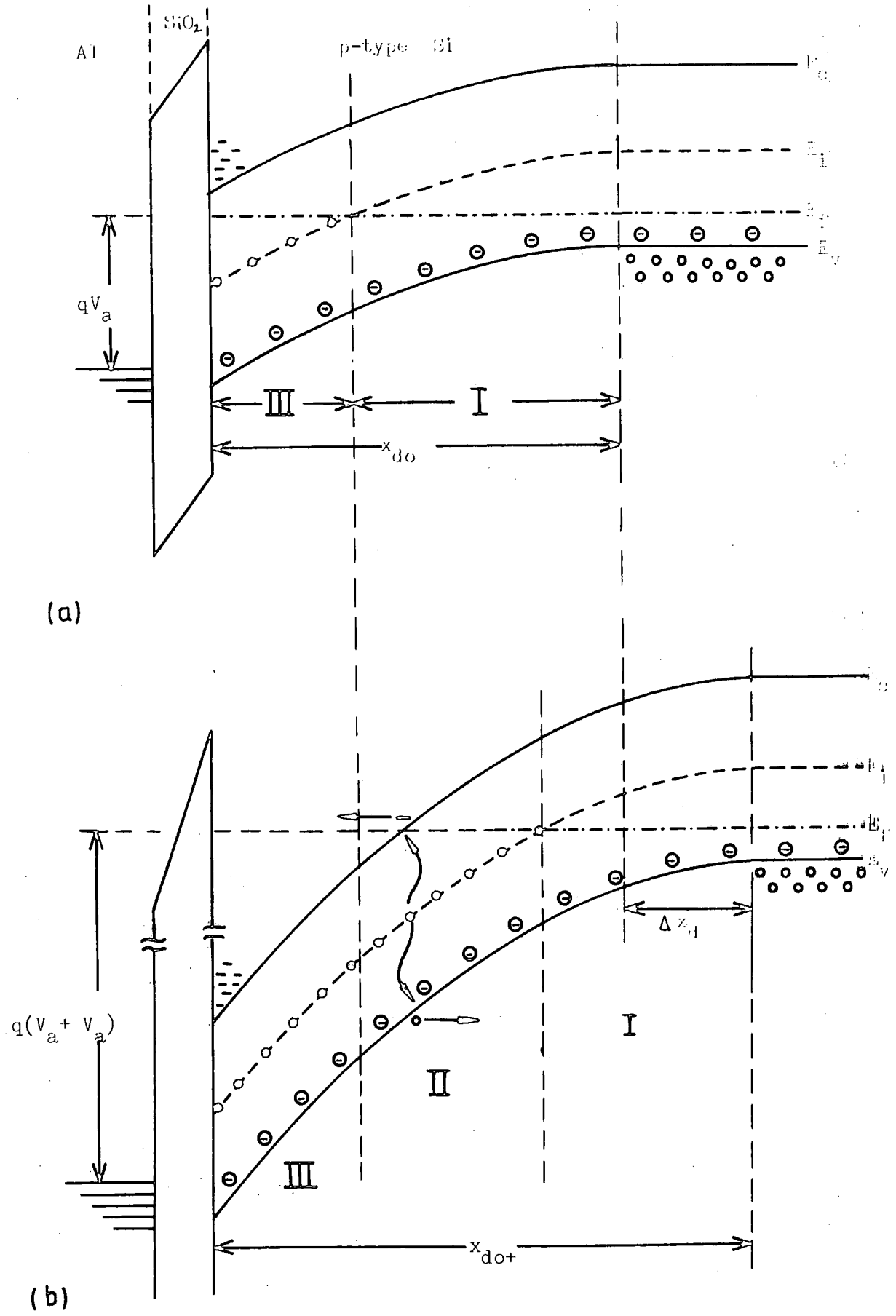

FIG. 5.6 Band Diagram for p-type MOS Capacitor
(a) In Equilibrium ($t<0$)
(b) Immediately After Voltage Step Application ($t=0+$)

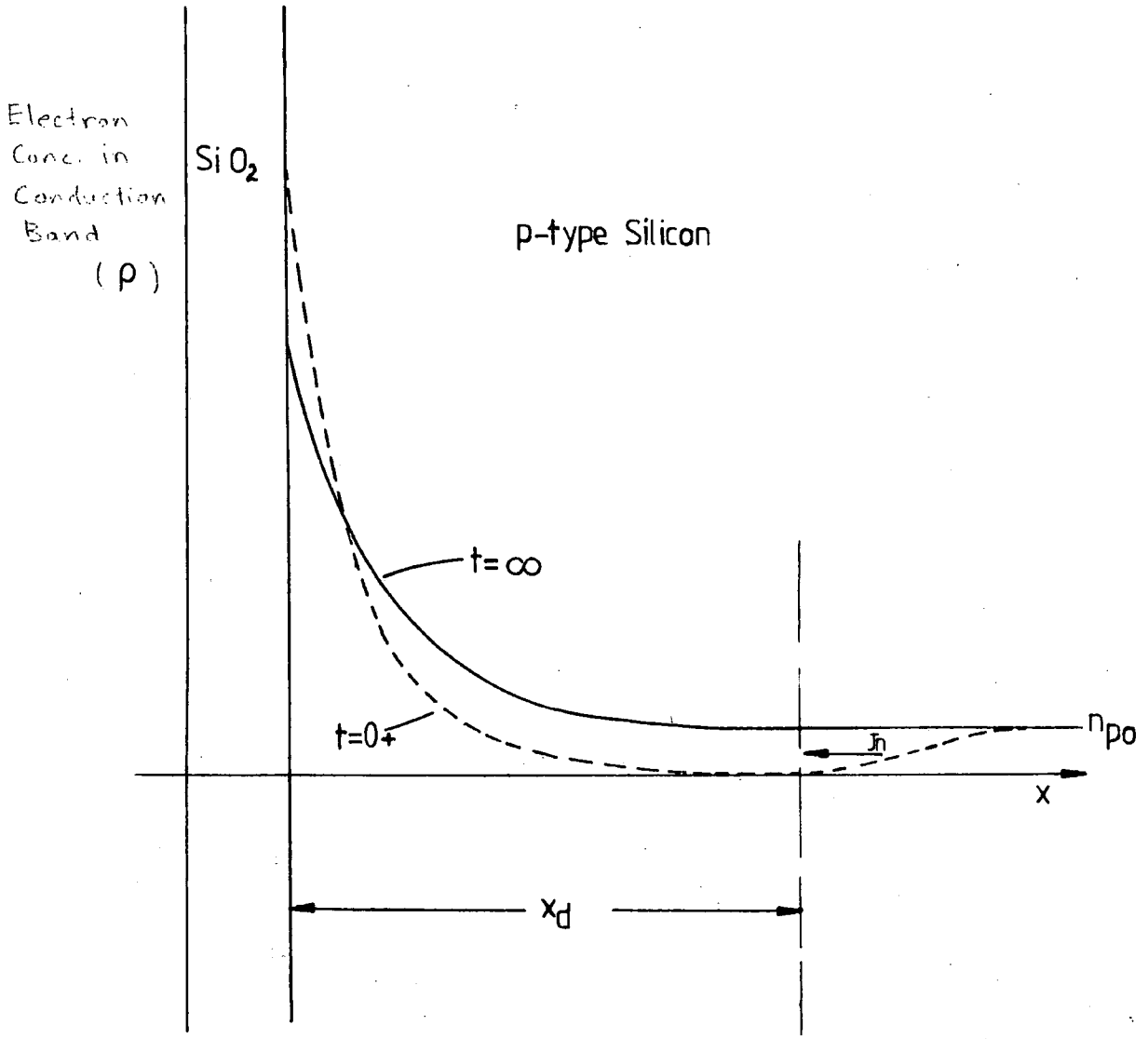

FIG. 5.7 Concentration of Free Electrons in the Depletion Region of a p-type MOS Capacitor Immediately after a Voltage Step application.

centration gradient in the bulk. This will cause electrons to diffuse into the depletion region from within a diffusion length L_d beyond the depletion layer ($x > x_d$).

It can be shown that at room temperature this diffusion current is negligible compared to the generation current in the depletion region (47,48). The minority carrier concentration in the bulk is given by

$$n = n_{po}(1 - e^{-(x-x_d)/L_d}) \tag{5.6}$$

where $n_{po} = \frac{n_i^2}{N_a}$ is the equilibrium minority carrier concentration of the p-type semiconductor.

The electron diffusion current due to the concentration gradient is

$$J_{ndiff} = - q D_n \frac{dn}{dx} \tag{5.7}$$

where D_n is the diffusion coefficient for the electrons.
At the edge of the depletion layer $x = x_d$, and substituting for n, this becomes

$$J_{ndiff} = \frac{q D_n n_i^2}{L_d N_a} \tag{5.8a}$$

or since $L_d = \sqrt{D_n \tau_g}$ where τ_g is the bulk lifetime

$$J_{ndiff} = q \frac{L_d}{\tau_g} \frac{n_i^2}{N_a} \tag{5.8b}$$

Now the actual generation rate U_g in the depletion layer itself is

$$U_g = \frac{n_i}{2 \tau_g} \tag{5.9}$$

which gives the generation current, J_g as

$$J_g = q U_g x_d$$

$$= \frac{q x_d n_i}{2 \tau_g} \qquad (5.10)$$

From Equation 5.8(b) and 5.10

$$\frac{J_g}{J_{ndiff}} = \frac{q x_d n_i}{2 \tau_g} \cdot \frac{1}{q} \cdot \frac{\tau_g}{L_d} \cdot \frac{N_a}{n_i^2}$$

$$= \frac{1}{2} \cdot \frac{x_d}{L_d} \cdot \frac{N_a}{n_i} \qquad (5.11)$$

Putting in some values, we have for $N_a = 10^{15}$ cm^{-3}, $x_d \simeq 6 \times 10^{-5}$ cm and for $D_n \simeq 20$ cm^2 s^{-1}

$$L_d = 4.5 \times 10^{-3} \text{ cm} \quad \text{for } \tau_g = 1 \ \mu s$$

$$L_d = 1.4 \times 10^{-2} \text{ cm} \quad \text{for } \tau_g = 10 \ \mu s$$

$\therefore$ $\frac{x_d}{L_d}$ 1.33×10^{-2} to 4.30×10^{-3}

$\therefore$ $\frac{J_g}{J_{ndiff}} = 1.33 \times 10^{3}$ to 4.30×10^{2}

That is

$$\frac{J_g}{J_{ndiff}} >> 1 \quad \text{in all cases}$$

and so the diffusion term is negligible. The physical reason for this is that although L_d may be $>> x_d$, the generation rate in the depletion layer is far greater because it is proportional to n_i as both electrons and holes are absent.

In the bulk, the generation rate is proportional to $\frac{n_i^2}{Na}$ which is the minority carrier concentration n_p ($n_p << n_i$).

At higher temperatures, $n_i = \sqrt{N_c N_v}\ e^{-E_g/2kT}$, will increase. Only above $\sim 100^{\circ}C$ will the diffusion term become important and this is outside the range of the present experiments.

Similarly it can be shown that the surface generation term can be neglected when compared to the bulk generation in the depletion layer. The surface generation expression can be written as (48)

$$G_s = \frac{1}{2} S\, n_i$$

where G_s is the generation rate at the surface.

S is the surface recombination velocity.

The current density due to surface generation J_s is given by

$$J_s = \frac{1}{2} q\ S\, n_i$$

from Equation 5.10 we can write the ratio

$$\frac{J_g}{J_s} = \frac{\frac{1}{2} .q. \frac{x_d}{\tau_g} . n_i}{\frac{1}{2} .q. S. n_i}$$

$$= \frac{x_d}{2.\tau_g}$$

For τ_g = 10μs and x_d = 10 μm

J_g = 10 x J_s for S = 1 cm s^{-1}

and J_g = 100 x J_s for S = 0.1 cm s^{-1}

That is J_g is more than 10 times greater than J_s for values of S up to 1 cm s^{-1}. The typical value of S for device grade MOS capacitor is less than 1 cm s^{-1} therefore one can neglect the surface generation term in the present model.

(b) $t > t_{0+}$

As time increases the inversion charge concentration will increase until the final equilibrium value is reached. This is the main part of the Q-t transient and it is due to the generation of electrons which will flow rapidly to the surface to increase the inversion charge concentration and decrease the depletion width. Of the two sources of electrons flowing in the depletion region, those diffusing from the bulk have been shown above to be negligible compared with the other which is from thermal generation from centres lying near the intrinsic level. The net generation rate eventually decreases as the recombination component increases. Initially there are very few carriers away from the surface thus preventing recombination. As time increases the generation process due to thermal excitation goes on unaffected but the recombination rate rises as carriers build up in the depletion region.

For this time period the depletion width is decreasing as electron-hole pairs are being generated. As more carriers are generated the energy levels and the depletion width return towards the equilibrium values. The trap levels of Region II (Figure 5.8) also move above E_f thus reducing the occupancy function. This causes the traps to emit electrons to the conduction band which are then swept to the interface. The extra charge contributed by emptying the traps is, however, small compared with the total thermally generated charge and it does not affect the transient shape.

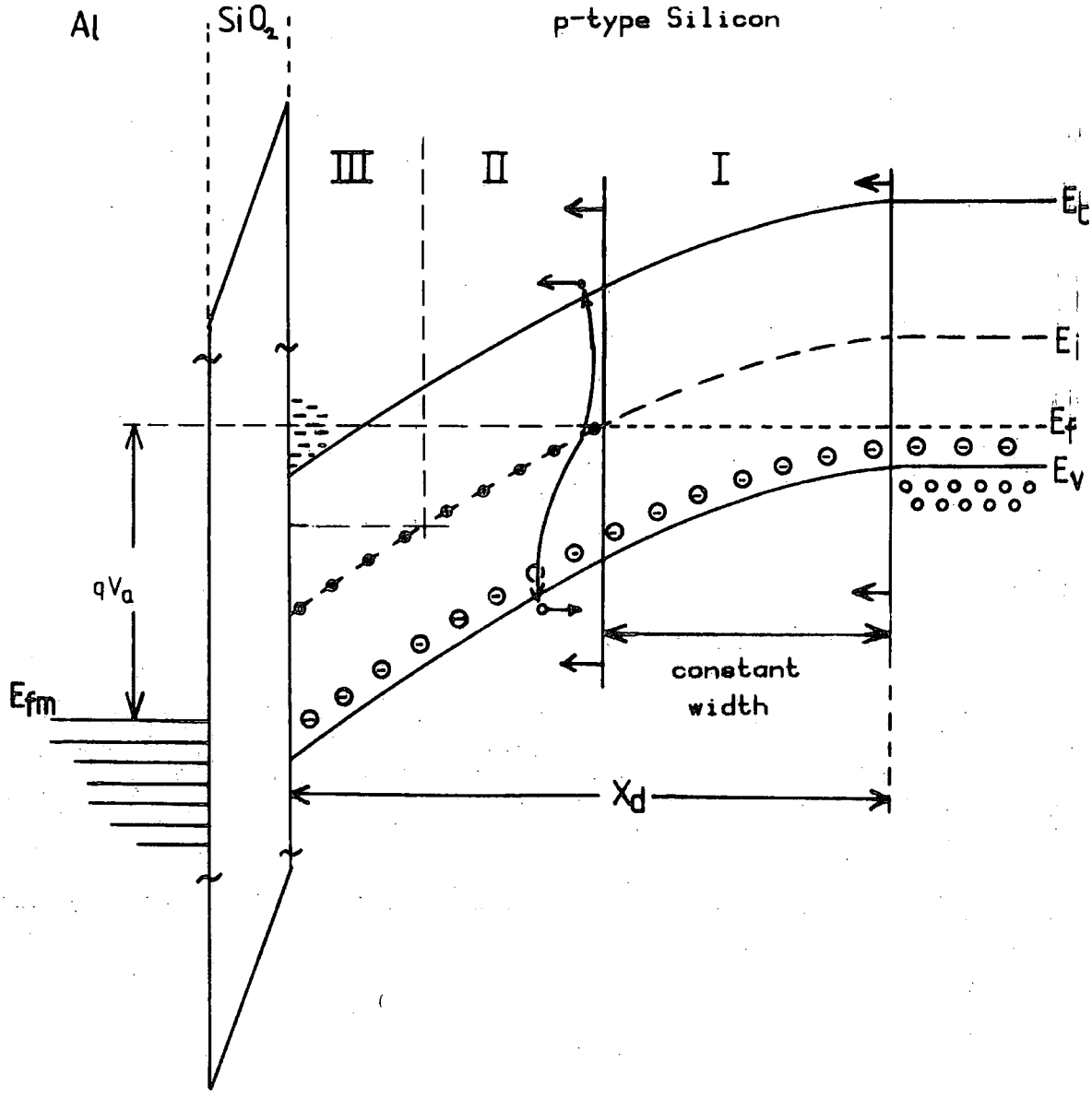

FIG. 5.8 Relaxation of Depletion Width after the Forward Voltage Step Application

5.3.2 The Reverse Voltage Step Transient

The description of the charge transient so far given is for the application of the forward voltage step where the device is taken from heavy inversion to heavier inversion. In a typical Q-t experiment, after the device has returned to equilibrium from this step it is taken back to the initial potential for the next forward transient to be observed. However, during the return to the initial potential, which is achieved by applying a reverse step potential, the device responds with a similar but reverse Q-t transient. This must be explained by a different process from net generation as the boundary conditions are now quite different. Several authors (18-20) have worked on this process but they have been concerned only with capacitance measurements and the use of short duration pulses instead of a step voltage. To date nobody has published results or analysis of the Q-t transient following a reverse voltage step.

It is the purpose of this section to try to explain this phenomena qualitatively. A suggestion for a quantitative analysis will be found later in the chapter. Similar to the forward voltage step discussion, we will divide the description into two periods, one immediately after the application of the voltage step and the other during the main transient.

(a) $t = t_{0+}$

Referring to Figure 5.9, it is seen that when the voltage step is initially applied, the depletion width is almost immediately reduced to a value less than the maximum equilibrium width by the sudden movement of holes towards the oxide-semiconductor interface. The hole charge is now needed to balance the negative charge in the semiconductor

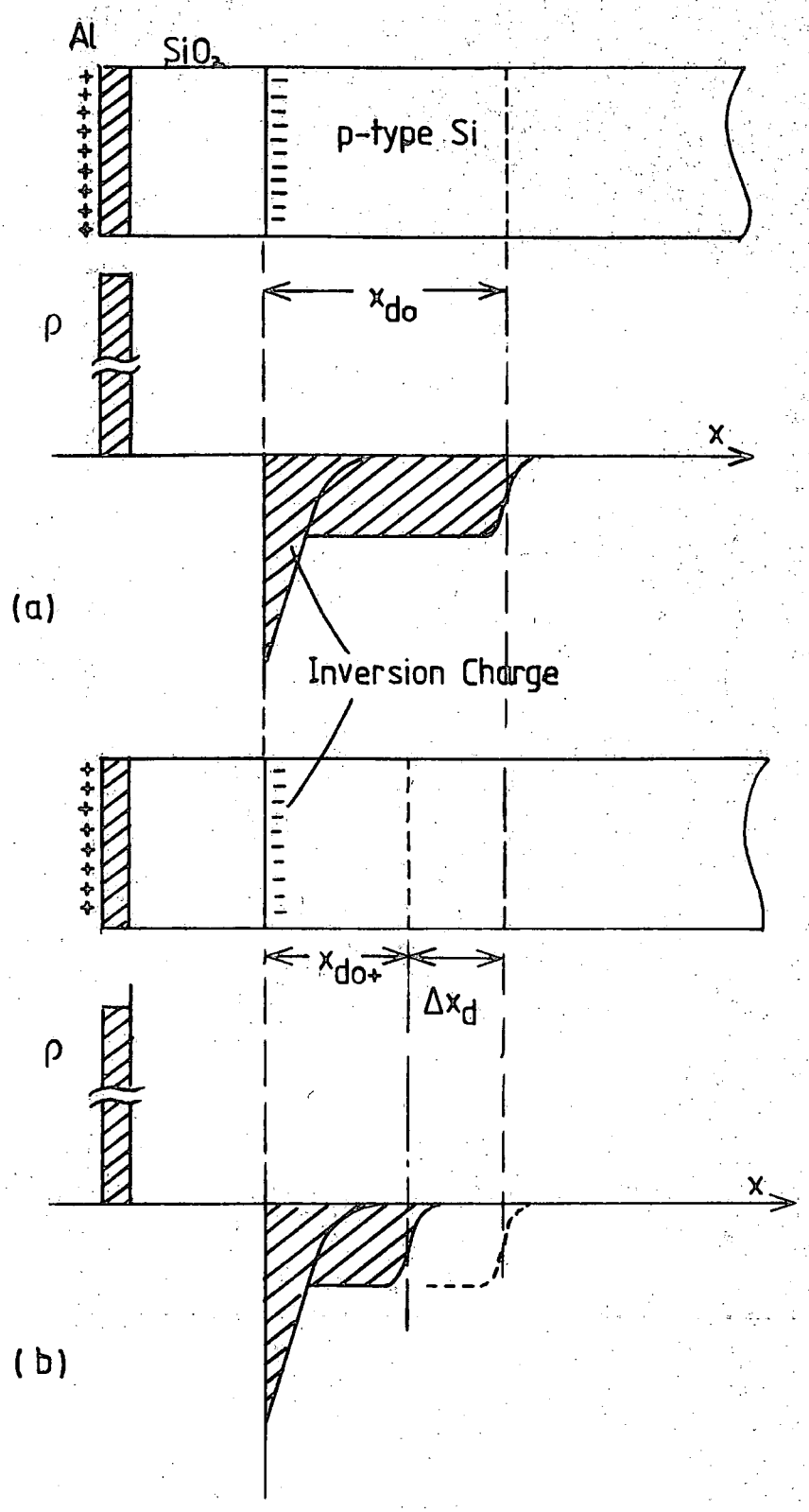

FIG. 5.9 MOS Capacitor before and after the Reverse Voltage Step application

(a) In Equilibrium

(b) Immediately after Application of the Reverse Voltage Step

which is reduced by the sudden decrease in the positive applied voltage. At this first moment, the excess inversion charge have not had time to recombine so that the surface potential is also reduced suddenly and the depletion layer width is temporarily reduced. For voltage steps that are small enough as to affect only the depletion charge initially, the positive charge on the electrode is balanced by the remaining depletion charge and the inversion charge.

On the Q-t plot the sudden decrease of the depletion charge appears as the initial step in the charge change. As the movement of the depletion layer edge is towards the oxide, there is a maximum voltage step that can be applied before the depletion layer collapses totally at the beginning of the transient. If the applied voltage step is greater than this then the transient will become far more complicated as it would involve the immediate movement of the inversion charge To avoid this the magnitude of the voltage step has to be carefully chosen. The maximum voltage that can be applied for the transient to be of the simplest form is given by the expression

$$\Delta V_{max} = \frac{q N_a x_{do}}{C_{ox}} + \frac{q N_a x_{do}^2}{2 \epsilon_s} \qquad (5.12)$$

(b) $t > t_{0+}$

After the initial step, the depletion layer will have reached a minimum value and the system is out of equilibrium as the excess inversion charge decreases through the recombination process. During the transient the depletion layer increases again to its equilibrium value. The excess charge is lost by the net recombination of electrons.

This occurs because although the generation rate in the inversion layer is constant, the excess concentration of electrons in the conduction band makes the recombination increase. The net rate of recombination is proportional to the change in the depletion layer width away from the equilibrium value. During the recombination process, the inversion concentration is steadily decreasing, while the depletion width is increasing so as to balance the charge on the metal electrode. This process continues until the equilibrium depletion width is reached once more.

5.4 The Concept of the Minority Carrier Lifetime

The minority carrier lifetime, τ_g is the average time the electrons of a p-type semiconductor for example spend in the conduction band before recombining with the holes in the valence band. When carriers are injected into a semiconductor, equilibrium will be disturbed due to the presence of excess carriers. The characteristic time for the excess carriers to readjust to achieve the final equilibrium state is equal to τ_g. In equilibrium, the recombination rate is equal to the net generation rate, U_g, which is given by

$$U_g = \frac{\Delta n}{\tau_g} \qquad (5.13)$$

where Δ_n is the excess minority carrier concentration.

In the transient measurements for the MOS capacitor the situation is slightly different. Here the depletion layer is initially expanded resulting in a condition where there are insufficient minority carriers for the given applied voltage. Charge neutrality is temporarily maintained by the uncompensated ionised dopant atoms. During the return to equilibrium, minority

carriers are generated and their concentration in the depletion region increases. The expression that relates the minority carrier lifetime to the generation rate in a depletion layer has been studied by Sah, Noyce, and Schockley (5). Initially, the ideas were developed for p-n junctions in the reverse bias condition. They were then applied to MOS devices for which the accepted expression is

$$U_g = \frac{n_i}{2\tau_g} \tag{5.14}$$

Some workers (2,3,22) have suggested however that the generation-recombination expressions have to result from a non-steady-state analysis if they are to be applied to all situations. For example Simmons and Wei derived time dependent generation rates which are different for holes and electrons. These rates differ through the depth of the depletion layer but they converge to the same value after a short time. By using the time dependent generation rate, they re-evaluated the Zerbst plot and showed that the Zerbst method is erroneous as it uses only one time constant for the generation time. The difficulty with their analysis is that the Zerbst plot obtained from this calculation curved in the wrong way at the beginning of the transient when compared to all experimental Zerbst plots. In their calculation the gradient at the beginning of the transient is zero while in the actual plot it is greater than the gradient of the linear portion. The other significant difference is that the generation width according to Simmons and Wei is just the region from the oxide-semiconductor interface to the point where the trap level crosses E_f (i.e. Regions II

and III of Figure 5.8). According to Zerbst and several other authors, it is only the additional width from the equilibrium value (i.e. Region II) that contributes to generation. The inclusion of Region III in the generating width leads to more error in the physical model of the transient measurement because in this region the traps are always in the same condition (i.e. filled with electrons) both before and after the step voltage application. Hence these traps are unlikely to generate carriers. These arguments show that the argument of Simmons and Wei needs to be approached cautiously and that the generation width as defined by Zerbst is the better of the two. The Zerbst generation region is the region that is in excess from the equilibrium value. In Region I the traps are always empty so that the net generation is small while Region III is always filled so here too the generation process does not occur.

Under transient conditions, the behaviour of electrons and holes in the MOS capacitor cannot be described by Fermi-Dirac statistics. Collins et al (3) did extensive computer modelling of the transient response of the device following the application of a voltage step using exact equations. They used the continuity, Poisson and the generation-recombination relations in their numerical calculations, pulsed from flatband to inversion. Thus they were concerned with large voltage steps. The time scale involved ranged from the charging up of the depletion layer, which occurs in less than 10^{-12} s, to the final equilibrium state. This time is divided into three main periods - (i) the dielectric relaxation time, (ii) the depletion time and (iii) the equilibration time as described

previously. Most of the experimental methods concerned with MOS capacitor transients involve only the equilibration time. It was also shown by Collins et al that although the rise in the carrier concentrations follows different time paths between the exact analysis and the steady-state approximation, this difference occurs before the equilibration time. For this reason the steady-state expression for the generation lifetime can be used in the present experiment.

Comparison with the Zerbst plot as obtained from Collins et al's computer calculation showed that with zero bulk generation centre concentration, giving $\tau_g = \infty$, the exact analysis gave a finite value for the generation rate. When not including surface generation in their calculations a finite value for the surface recombination velocity was apparently obtained from a Zerbst plot. These two discrepancies make the Zerbst method erroneous if no correction is included. This phenomenon can however be explained as follows.

There are two possible sources that contribute to the increase in the minority carrier concentration in the depletion layer. One is the thermal generation from generation centres and the other is due to the diffusion of electrons from the bulk as described earlier. When the generation centres are absent, the diffusion term must dominate and this will produce an apparent generation rate as though recombination centres were present because the inversion charge still increases. The bulk diffusion term was neglected by Collins et al and hence their Zerbst plot analysis gave the wrong result.

As for the surface generation velocity, the Zerbst expression does not in fact give a true value of s since the curvature of the plot for large values of t is due to the build

up of the hole concentration at the surface towards the end of the transient. The presence of true surface generation centres would only help in achieving the final equilibrium in a shorter time, and would not affect the shape as assumed in the conventional analysis of the Zerbst plot. By applying the voltage step when the device is already in heavy inversion, as in most of the present Q-t measurements, any surface effect will be eliminated in any case as the surface potential is almost constant during the transient.

In the qualitative model discussed above various changes have been made, which may affect the analysis of the parameters of the transient. Firstly it was shown that in earlier calculations, the bulk diffusion term and the surface recombination velocity were neglected which has an effect when bulk generation is small. Secondly the expression for the generation width was now chosen from the work of Rabbani and Lamb (12) which is a refinement over that suggested by Zerbst, taking into consideration the narrowing of Region III due to the extra band bending when the system is out of equilibrium. Finally a simpler approach than that of Collins et al has been taken which makes this model less complicated to evaluate. The inclusion of these improvements will be shown in the development of a new simplified quantitative model in the following section.

5.5 The Mathematical Formulation

5.5.1 The Forward Voltage Step Transient

To maintain charge neutrality in the MOS capacitor at all time the following equation always holds

$$Q_m = - (Q_{inv} + Q_d) \qquad (5.15)$$

where Q_m, Q_{inv}, and Q_d are the charges per unit area of the metal electrode, the inversion layer, and the uncompensated dopant ions in the depletion region. For this analysis we will divide the time t into 3 parts (a) the time before the voltage step is applied or $t < 0$ where the device is in equilibrium (b) the time immediately after the voltage step or when $t = t_{0+}$ and (c) the time after the voltage step application until the final equilibrium state is reached or $t_\infty > t > t_{0+}$. The latter is the time duration of the actual transient.

(a) At Equilibrium ($t < 0$)

$$Q_{mo} = -(Q_{io} + Q_{do}) \tag{5.16}$$

where Q_{do} and Q_{io} respectively are the depletion and inversion charges in equilibrium. By taking the equilibrium depletion width as X_{do} we have

$$Q_{do} = -q N_a X_{do} \tag{5.17}$$

$$Q_{io} = -q\int_0^\infty n_i \exp(q\phi_b/kT)\, dx \tag{5.18}$$

where ϕ_b is the potential difference between the Fermi level and the intrinsic level.

(b) Immediately after the Voltage Step ($t = t_{0+}$)

$$Q_{mO+} = -(Q_{io+} + Q_{do+}) \tag{5.19}$$

where $Q_{io+} = Q_{io}$ because the inversion charge ~~starts~~ is initially unchanged and $Q_{do+} = qN_a x_{do+}$ where x_{do+} is the depletion width immediately after the voltage step.

(c) Equilibration Period ($t > t_{o+}$)

During the return of the depletion width to its final equilibrium value the total charge per unit area $Q_m(t)$ in the semiconductor is given by

$$Q_m(t) = Q_{mo} + qN_a(x_{do+}-x_{do}) + qU_g \int_o^t x_{gen}dt - qN_a(x_{do+}-x_d) - \quad (5.20a)$$

where x_{gen} is the generation width given by (32)

$$x_{gen} = \sqrt{(x_d^2 - \frac{x_{do}^2}{2})} - \frac{x_{do}}{\sqrt{2}} \quad (5.20b)$$

and U_g is the generation rate.

The last term of (5.20a) is due to the decrease in the depletion charge during the relaxation time. Subtracting (5.16) from (5.20a) yields the increment in the charge in the MOS capacitor. Thus

$$\Delta Q_m(t) = qN_a(x_{do+} - x_{do}) + qU_g \int_o^t x_{gen}\, dt - qN_a(x_{do+}-x_d) \quad (5.21)$$

On differentiation, the following expression is obtained:-

$$\frac{d}{dt} \Delta Q_m(t) = qN_a \frac{dx_d}{dt} + q\, U_g\, x_{gen} \quad (5.22)$$

From the voltage equation

$$V_a = V_{ox} + \psi_s \quad (5.23)$$

where $V_{ox} = \frac{Q_m}{C_{ox}}$ and $\psi_s = \frac{qN_a}{2\varepsilon_s} x_d^2$

Therefore before the voltage step, the voltage V_{a1} is

$$V_{a1} = \frac{Q_{mo}}{C_{ox}} + \frac{qN_a}{2\epsilon_s} x_{do}^2 \qquad (5.24)$$

After the voltage step is applied, the total voltage remains constant throughout the transient. Thus the final voltage equation is

$$V_{a2} = \frac{Q_m(t)}{C_{ox}} + \frac{q N_a}{2\epsilon_s} x_d^2 \qquad (5.25)$$

Taking the difference of the last two equations gives :-

$$\Delta V_a = \frac{\Delta Q_m(t)}{C_{ox}} + \frac{qN_a}{2\epsilon_s} (x_d^2 - x_{do}^2) \qquad (5.26)$$

Therefore

$$x_d = \sqrt{\frac{2\epsilon_s}{qN_a}\left(\Delta V_a - \frac{\Delta Q_m(t)}{C_{ox}} + \frac{qN_a}{2\epsilon_s} x_{do}^2\right)} \qquad (5.27)$$

$$\frac{d x_d}{dt} = -\frac{1}{C_{ox}} \cdot \frac{1}{2} \sqrt{\frac{2\epsilon_s}{qN_a}\left(\frac{1}{\Delta V_a - \frac{\Delta Q_m(t)}{C_{ox}} + \frac{qN_a}{2\epsilon_s} x_{do}^2}\right)} \frac{d}{dt} \Delta Q_m(t) \qquad (5.28)$$

Substituting into 5.22 and using 5.20(b)

$$\frac{d}{dt} \Delta Q_m(t) = -\frac{1}{C_{ox}} \sqrt{\frac{q N_a \epsilon_s}{2}\left(\frac{1}{\Delta V_a - \frac{\Delta Q_m(t)}{C_{ox}} + \frac{qN_a}{2\epsilon_s} x_{do}^2}\right)} \frac{d}{dt} \Delta Q_m(t)$$

$$+ qU_g \sqrt{\frac{2\epsilon_s}{qN_a}\left(\Delta V_a - \frac{\Delta Q_m(t)}{C_{ox}} + \frac{qN_a x_{do}^2}{2\epsilon_s}\right)} - \frac{x_{do}^2}{2} - \frac{qU_g x_{do}}{\sqrt{2}} \qquad (5.29)$$

Rearranging and using $\psi_s = \left(\Delta V_a - \frac{\Delta Q_m(t)}{C_{ox}} + \frac{qN_a}{2\epsilon_s} x_{do}^2\right)$

we have

$$\left[1 + \frac{1}{C_{ox}}\sqrt{\frac{q\ N_a\ \epsilon_s}{2\ \psi_s}}\right] \frac{d\Delta Q_m(t)}{dt} = q\ U_g \sqrt{\frac{2\ \epsilon_s}{q\ N_a} \cdot \psi_s - \frac{x_{do}^2}{2}} - \frac{q\ U_g x_{do}}{\sqrt{2}} \qquad (5.30)$$

From this final expression it is possible to obtain a theoretical Q-t plot by an iterative method which is performed on a microcomputer. The details are given in section 5.6.

5.5.2 The Reverse Voltage Step Transient

The equations for the device in equilibrium are the same as for the forward voltage step case so that only the non-equilibrium situation will need to be considered. It should be noted that in this case the charge is decreasing from the initial equilibrium values. Following a similar approach to that of the forward voltage step situation, we obtain the following equations.

(a) Immediately after the Voltage Step ($t = t_{0+}$)

$$Q_{mo+} = Q_{mo} - q\ N_a(x_{do} - x_{do+}) \qquad (5.31)$$

By writing $\Delta Q_{mo+} = Q_{mo} - Q_{mo+}$

we have $$\Delta Q_{mo+} = q\ N_a(x_{do} - x_{do+}) \qquad (5.32)$$

(b) Equilibration Period ($t > t_{0+}$)

$$Q_m = Q_{mo} - q N_a(x_{do} - x_{do+}) - qR \int_o^t x_r dt + qN_a(x_d - x_{do+}) \tag{5.33a}$$

where R is the net rate of recombination

x_r is the region where the net recombination is most likely to occur. For simplicity we shall assume that generation occurs in the region which is the difference in the depletion layer width from its equilibrium value.

That is

$$x_r = x_{do} - x_d \tag{5.33b}$$

On differentiating (5.33a)

$$\frac{d}{dt}\left(\Delta Q_m\right) = - q R(x_{do}-x_d) + q N_a \frac{dx_d}{dt} \tag{5.34}$$

Considering the voltage equation before the application of the voltage step, this is

$$V_{a1} = V_{ox1} + \psi_{so} \tag{5.35}$$

After the voltage step, the applied voltage remains the same throughout the transient giving

$$V_{a2} = V_{ox2} + \psi_s \tag{5.36}$$

Subtracting (5.36) from (5.35) and by writing $V_{ox1}-V_{ox2}$ as

$\Delta Q_m/C_{ox}$ and $V_a = V_{a1} - V_{a2}$, we obtain

$$\Delta V_a = \frac{\Delta Q_m}{C_{ox}} + (\psi_{so} - \psi_s)$$

or
$$\Delta V_a = \frac{\Delta Q_m}{C_{ox}} + \frac{qN_a}{2\epsilon_s}(x_{do}^2 - x_d^2) \tag{5.37}$$

This gives x_d which is

$$x_d = \sqrt{\frac{2\epsilon_s}{qN_a}\left(-\Delta V_a + \frac{\Delta Q_m}{C_{ox}} + \frac{qN_a}{2\epsilon_s} x_{do}^2\right)} \tag{5.38}$$

and
$$\frac{d\,x_d}{dt} = \frac{1}{2} \cdot \frac{1}{C_{ox}} \cdot \sqrt{\frac{2\epsilon_s}{qN_a}\left(\frac{1}{-\Delta V_a + \frac{\Delta Q_m}{C_{ox}} + \frac{qN_a}{2\epsilon_s} x_{do}^2}\right)} \cdot \frac{d}{dt}\Delta Q_m \tag{5.39}$$

Substituting this into (5.34) gives

$$\frac{d}{dt}\Delta Q_m(t) = \frac{1}{C_{ox}}\sqrt{\frac{qN_a\epsilon_s}{2}\left(\frac{1}{-\Delta V_a + \frac{Q_m}{C_{ox}} + \frac{qN_a x_{do}^2}{2\epsilon_s}}\right)} \cdot \frac{d}{dt}\Delta Q_m$$

$$+ q\,R\left[\sqrt{\frac{2\epsilon_s}{qN_a}\left(-\Delta V_a + \frac{\Delta Q_m}{C_{ox}} + \frac{qN_a}{2\epsilon_s} x_{do}^2\right)} - x_{do}\right] \tag{5.40}$$

Finally writing $\psi_s = -\Delta V_a + \frac{\Delta Q_m}{C_{ox}} + \frac{qN_a}{2\epsilon_s} x_{do}^2$

$$\left[1 - \frac{1}{C_{ox}}\sqrt{\frac{qN_a\epsilon_s}{2\psi_s}}\right]\frac{d\Delta Q_m}{dt} = R\sqrt{\frac{2q\,\epsilon_s}{N_a}\psi_s} - q\,R\,x_{do} \tag{5.41}$$

5.6 Method of Solution

A numerical method is adopted here to solve the Q-t problem. The method to be described and the mathematical equations themselves are not as elaborate as in the work of Collins et al (3). The intention here is to provide a simplified model that is more closely related to the experiments and which can be used for both step polarities. The method is based on several assumptions inherent in the equations of section 5.5. These are (i) that the dopant concentration is uniform in the semiconductor (ii) that the interface state effects are negligibly small because the device was initially in heavy inversion and (iii) the generation rates for holes and electrons are equal during the time that we are interested in and that any dissimilarity between the two occurs only in the initial step.

From the previous section it is seen that the basic equation for charge, Eqn. (5.21), cannot be solved either analytically or numerically because there are too many unknowns and the depletion width x_d is a function of time. Since this function is not known independently, Equation (5.22) is used instead with the approximation made that the charge increment in the device is to be calculated from the gradient $\frac{d}{dt} \Delta Q_m(t)$ of the previous value. By taking a reasonably small time interval Δt the charge can be calculated by taking the product $\Delta t, \frac{d}{dt} \Delta Q_m(t)$ hence the theoretical Q-t plot can be obtained This calculation was done using a microcomputer with the following algorithm:-

(i) Calculate the equilibrium values of ψ_s, Q_m accurately for the initial applied voltage V_a.

(ii) Plot the value of ΔQ_m against t or ψ_s against t at $t = t_{o+}$. (For the initial step increase in the Q-t plot).

(iii) Calculate $\frac{d}{dt} \Delta Q_m(t)$ at $t = t_{o+}$ using Equation (5.30).

(iv) For an increment in Δt, extrapolate the value of $\Delta Q_m(t)$ using the relation $\Delta Q_m = \Delta t . \frac{d}{dt} \Delta Q_m(t)$.

(v) For this value of ΔQ_m calculate the values of ψ_s and x_d.

(vi) Plot ΔQ_m for an increased Δt or plot ψ_s for the Δt.

(vii) Check to see if x_d equals the equilibrium depletion width for the applied voltage of $V_a + \Delta V_a$.

(viii) If not equal repeat steps (iii) to (vii).

(ix) If step (vii) is true then end.

The important part of the program is in calculating the initial values of ψ_s and Q_{mo} as the accuracy of subsequent calculated values of ΔQ_m and eventually of the Q-t plots themselves depend on these values. Thus the exact expression for the charge concentration per unit area in the semiconductor derived from Poissons equation is used for the initial calculation of Q_{mo} (49). This equation is,

$$Q_{mo} = \sqrt{2 \varepsilon_s N_a kT} \left[\left(e^{-q\psi_s/kT} + \frac{q\psi_s}{kT} - 1 \right) + \frac{n_i^2}{N_a^2} \left(e^{q\psi_s/kT} - \frac{q\psi_s}{kT} - 1 \right) \right]^{1/2} \quad (5.42)$$

From this expression, it is possible to calculate the space-charge density Q_{mo} in any state of the MOS capacitor. In accumulation, ψ_s is negative and the value of Q_{mo} is dominated by the first term of the expression. If ψ_s is zero then Q_{mo} is

zero giving the flat-band situation. For positive ψ_s, and where ψ_s is smaller than ϕ_b, the potential difference between the Fermi level and the intrinsic level of the bulk, then Q_{mo} is dominated by the second term. This is the depletion condition. When ψ_s is greater than ϕ_b as in our case, we have the inversion condition where Q_{mo} is dominated by the fourth term.

To calculate the value of Q_{mo}, first we select an arbitrary value of the surface potential ψ_s and from (5.42) obtain Q_{mo}. Then the applied voltage V_a is calculated from (5.24). This is then compared with the actual V_a and the process is repeated by changing ψ_s until the calculated V_a agrees with the actual one. From this equilibrium value of Q_{mo}, the subsequent charge can be calculated. First, immediately after the voltage step where $t = t_{O+}$, the change in the semiconductor charge due to the increased depletion width to a maximum, is calculated. This appears as the step increase in the Q-t plot, the increment in the charge ΔQ_{dO+} being given by

$$\Delta Q_{do+} = qN_a (x_{do+} - x_{do}) \qquad (5.43)$$

Then the gradient $\frac{d}{dt} \Delta Q_m(t)$ is calculated at $t = t_{O+}$ and so on until a complete Q-t plot is obtained.

Another part of the program includes the way the surface potential can be quickly determined to calculate the applied voltage. This involves testing to see when the calculated V_a passes the required value. This is first done using large increments in ψ_s initially but when the test gives a positive value ψ_s is changed back to the previous value and the increment is reduced in magnitude so as to give a higher sensitivity for the change of ψ_s. The process is repeated until the required

accuracy is obtained. If the chosen ψ_s gives V_a values diverging from the actual one, a small routine is used to detect this and to adjust the direction of the increment. This technique proves to be efficient in obtaining good accuracy in a very short time. Use of small steps throughout would give a very long calculation time and large increments in ψ_s by themselves would greatly reduce the accuracy. The actual process involved in this technique is as shown in the algorithm below:-

(i) Take a rough estimate of the surface potential ψ_s.

(ii) Set the initial increment magnitude of ψ_s ($\Delta\psi_s$).

(iii) For the above surface potential calculate the applied voltage V_{a1}.

(iv) Calculate the difference between the actual applied voltage and the calculated one (i.e. $\Delta V_1 = V_{a1} - V_a$).

(v) Increment ψ_s by $\Delta\psi_s$ ($\psi_s = \psi_s + \Delta\psi_s$).

(vi) Calculate the second applied voltage value V_{a2} for the new ψ_s.

(vii) Calculate the difference between the actual applied voltage and the calculated one in (vi) (i.e. $\Delta V_2 = V_{a2} - V_a$).

(viii) Check to see if ΔV_1 and ΔV_2 are of the same sign.

(ix) If step (viii) is not true then change ψ_s to its value just before the test and reduce the increment magnitude. Then go back to step (v).

(x) If step (viii) is true then check for accuracy.

(xi) If accuracy is not enough check first to see if V_a is converging towards V_a. If not, change the direction of the increment and go to step (v).

(xii) If V_a is converging then continue to repeat step (v).

(xiii) If accuracy is enough in step (x) then the latest ψ_s

and Q_{mo} are the required surface potential and the charge concentration in the semiconductor for the given applied voltage V_a.

(ix) End.

The whole of the program for obtaining the theoretical Q-t is summarised in the flow chart of Figure 5.10 and the full program is given in the Appendix 2 .

5.7 The Theoretical Q-t Plots

Figures 5.11(a) and 5.11(b) give the calculated plots of Q-t following a forward voltage step of 25 mV for various lifetime values from 5 μs to 20 μs and 20 μs to 120 μs respectively. The time scales for the two figures are difference because of different ranges of lifetime covered. A further analysis was made using a lifetime of 100 μs with a 25 mV voltage step, as in Figure 5.12(a) for which the theoretical Q-t plot has also been normalised and plotted on a log-linear graph in Figure 5.12(b). It is found that the logarithmic plot gives a straight line except when approaching saturation where a slight deviation from linearity is obtained. This shows that the Q-t transient is not entirely exponential even for small voltage steps. The reason for this is the fact that recombination, which becomes significant towards the end of the transient, is not taken into consideration in the equation. The linear portion of the log plot implies that the solution to Equation (5.30) is an exponential only during the part before saturation.

Figure 5.13 shows a theoretical Q-t plot for the reverse voltage step and Figure 5.14 is a comparison of the theoretical Q-t plots for the forward and reverse voltage steps for a chosen lifetime value of 30 μs. The difference in the transients follows

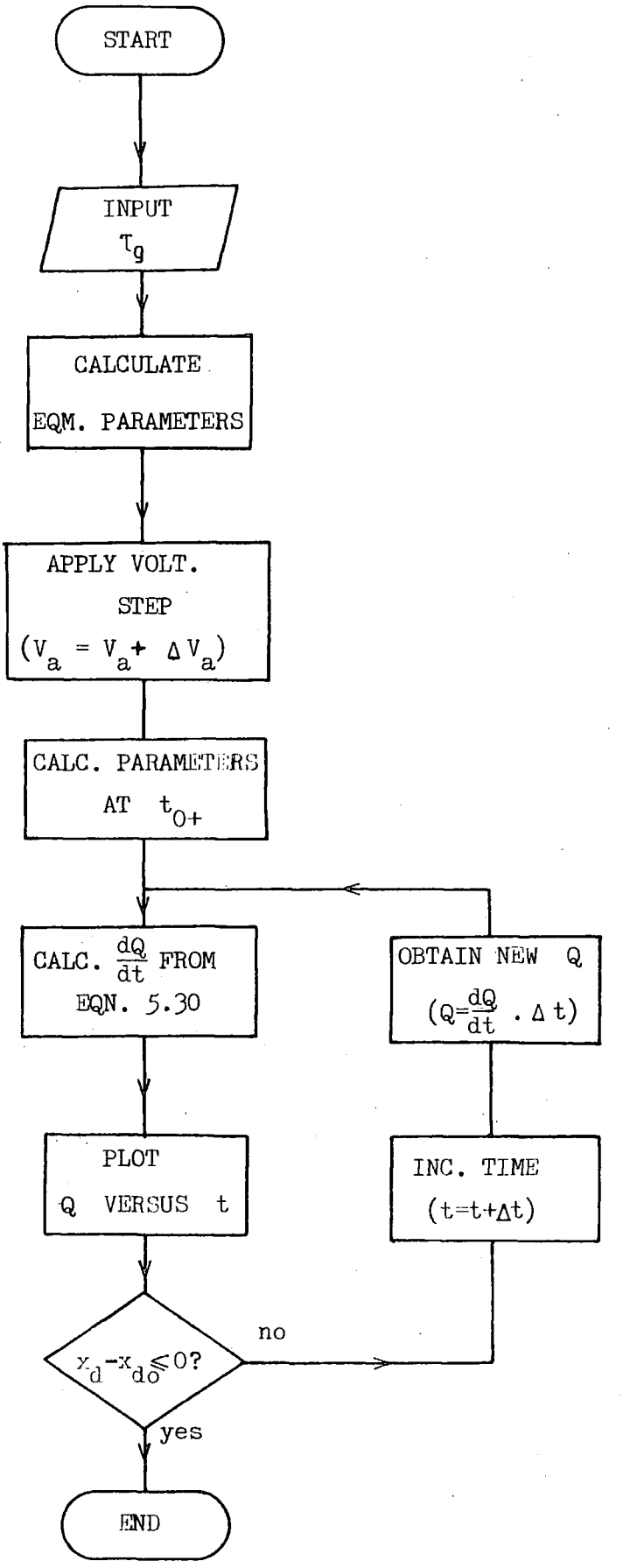

FIG. 5.10 FLOWCHART FOR CALCULATING THE THEORETICAL Q-t TRANSIENTS FROM THE PRESENT THEORY

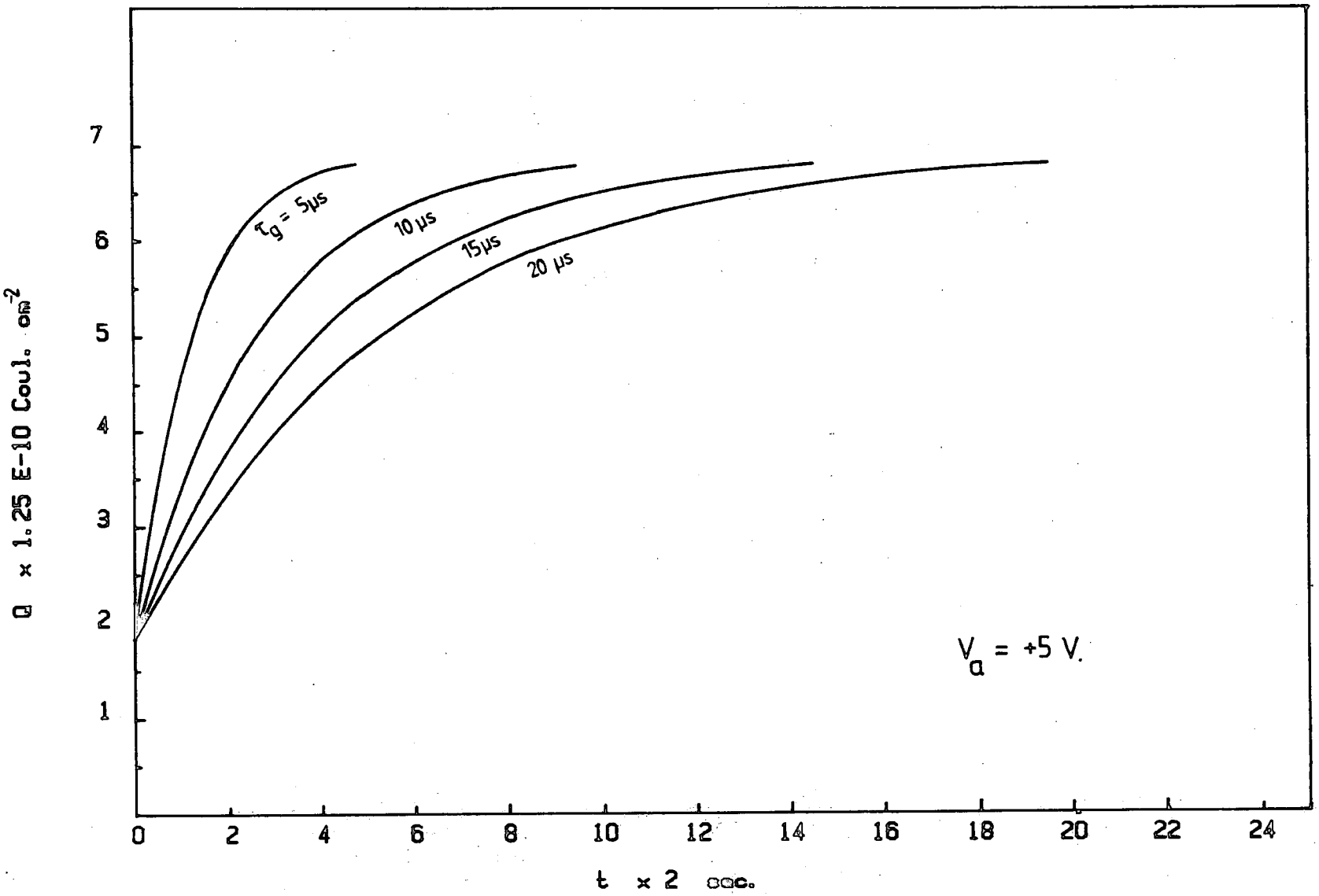

FIG. 5.11(a) Theoretical Q-t Plots for τ_g= 5 to 20 μs for ΔV_a= 25 mV

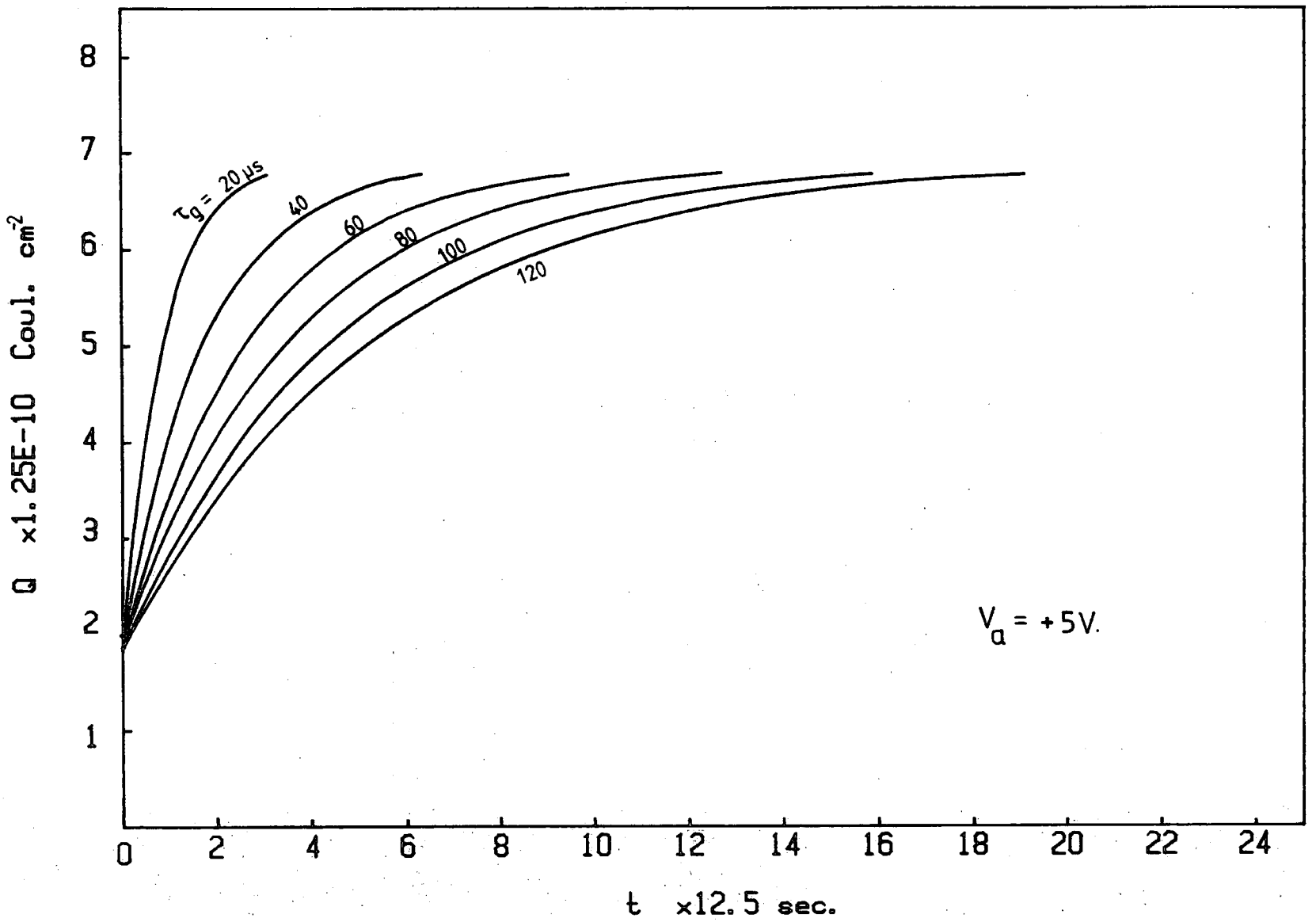

FIG. 5.11(b) Theoretical Q-t Plots for Tg=20 to 120 µs for Δ Va=25mV

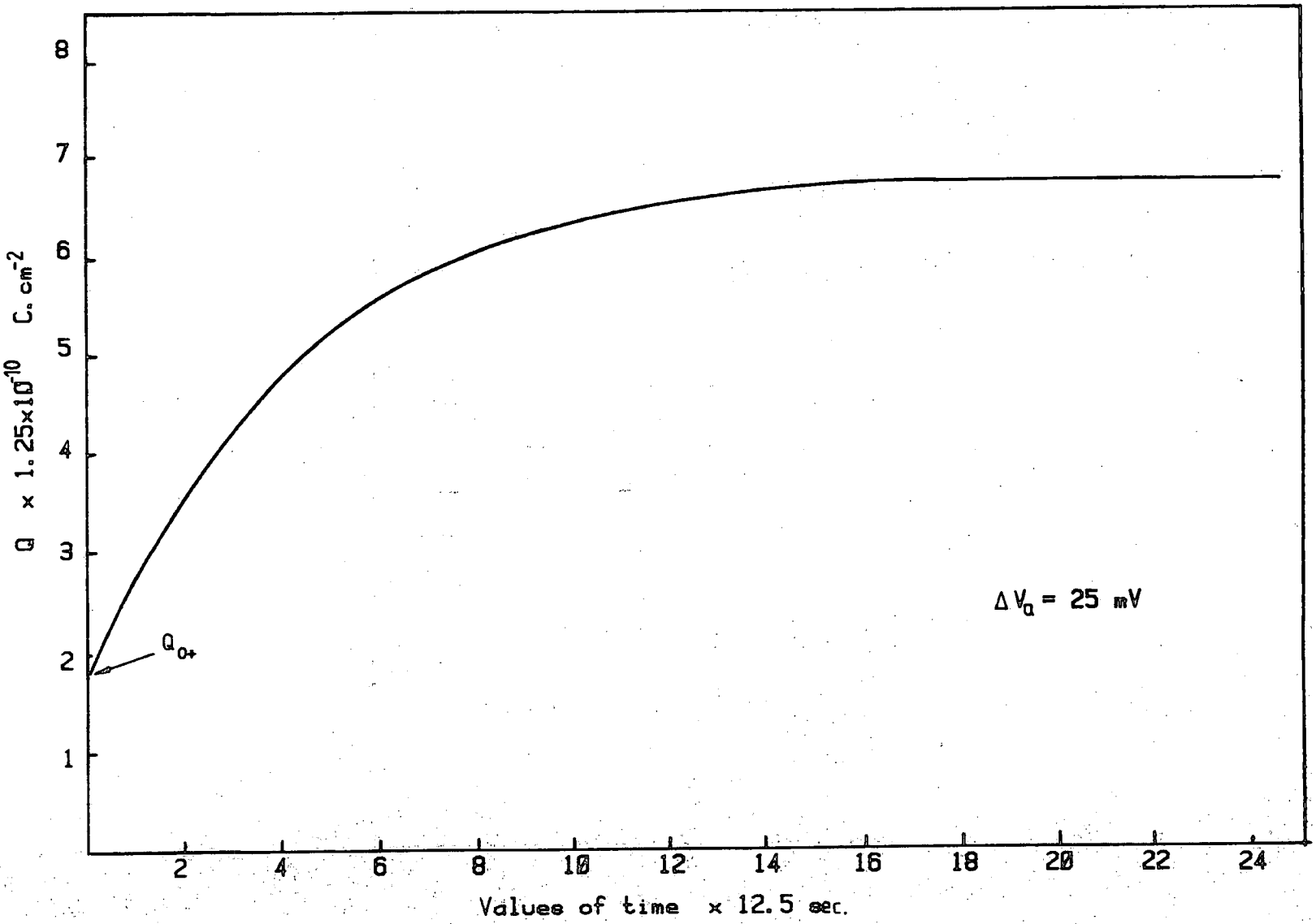

FIG. 5.12(a) Theoretical Q-t Plot for τ_g = 100 μs

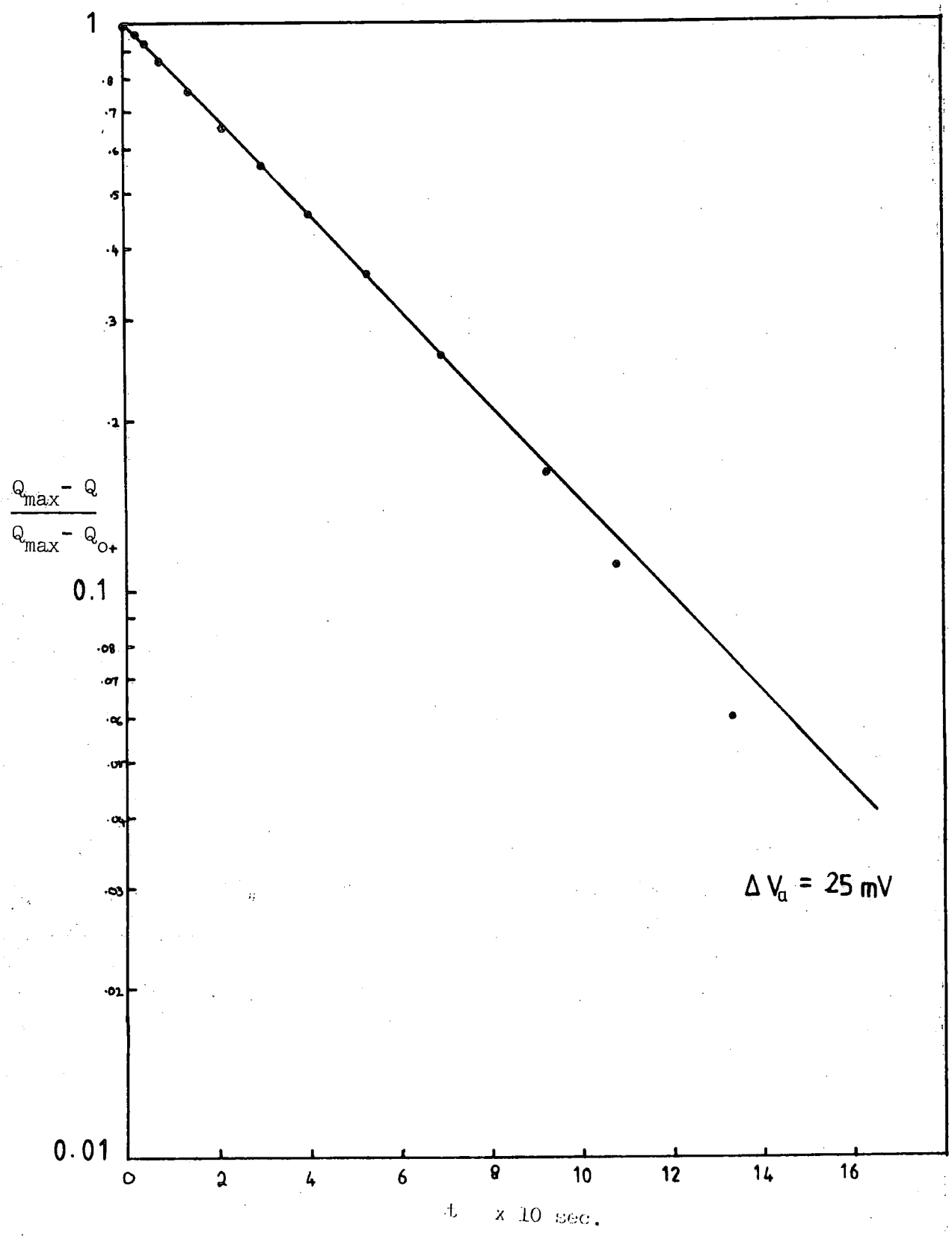

FIG. 5.12(b) Log Plot of the Theoretical Q-t Curve for τ_g= 100 μs

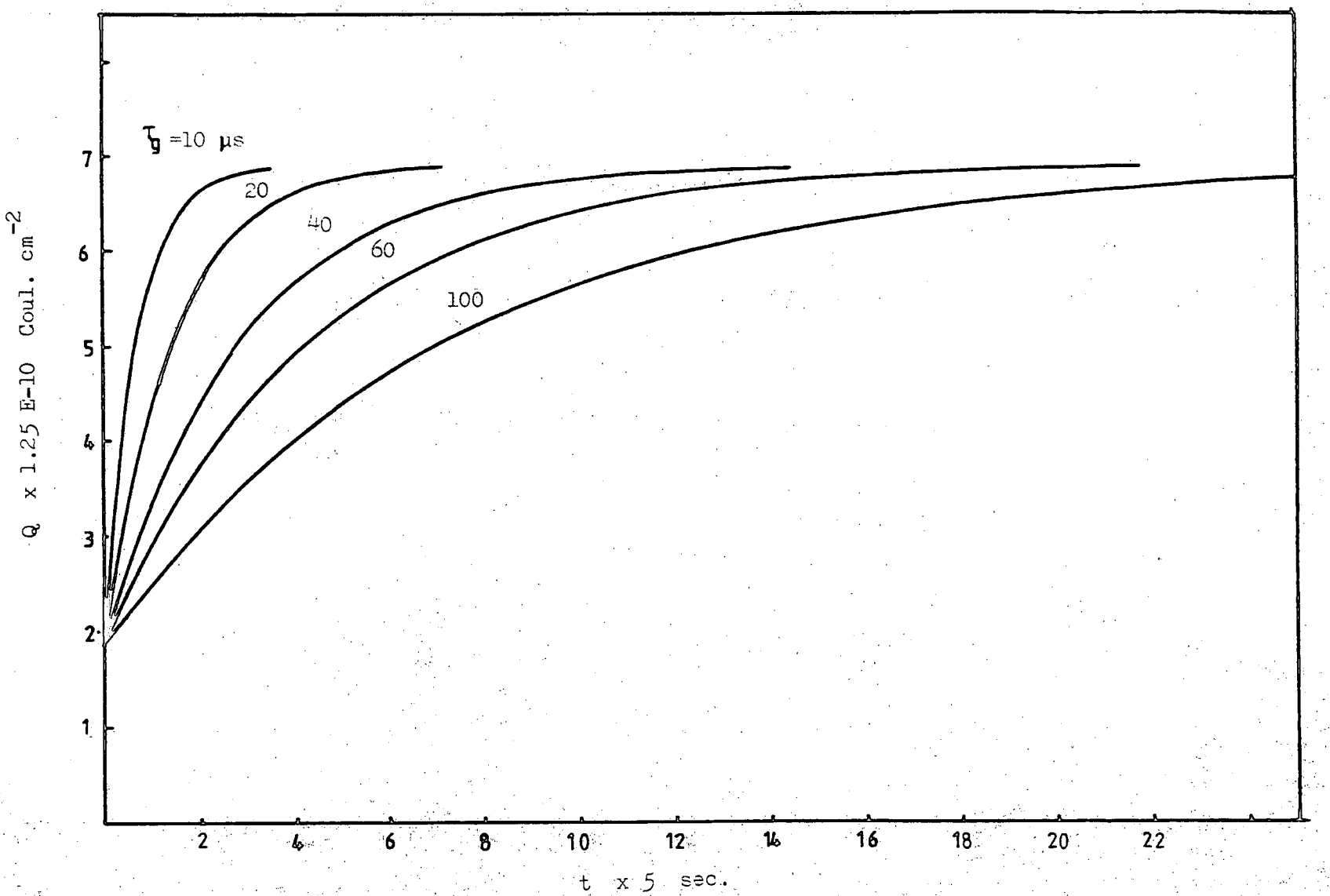

FIG. 5.13 Calculated Reverse step Transient for different τ_g's (ΔV_a = 25 mV)

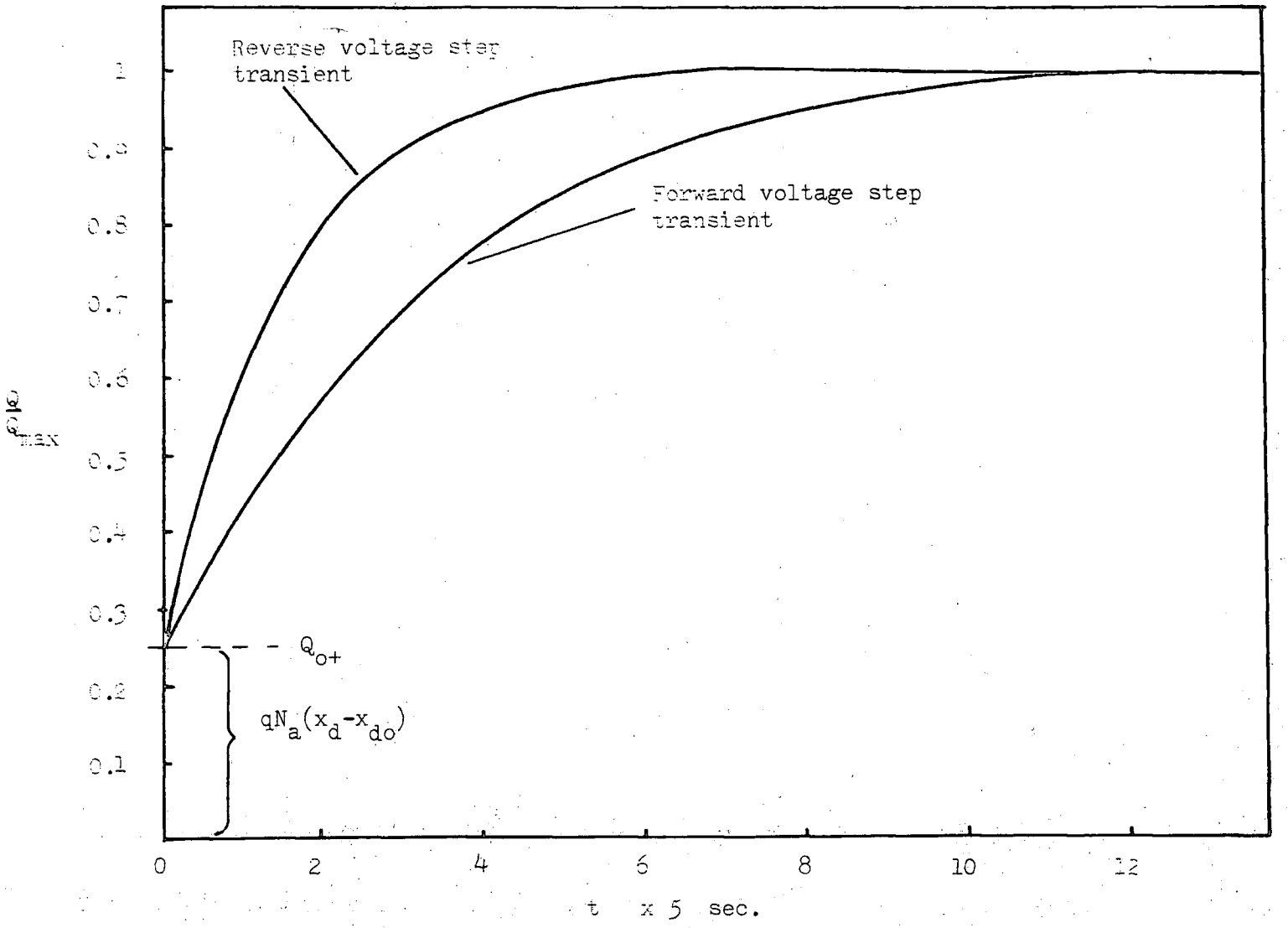

FIG. 5.14 THEORETICAL Q-t PLOTS FOR FORWARD AND REVERSE VOLTAGE STEPS FOR τ_g OF 30 μs, AND ΔV_a = 25 mV

the same trend as in the experimental plots. Further discussion of the comparison of theory and experiment will be given in Chapter 8.

5.8 Discussion

In this chapter, theoretical expressions for the Q-t transient have been presented following a different approach from those used previously. The present theory is based on the following assumptions. (i) That the depletion approximation holds where the concentration of carriers in the depletion region is taken to be very small with respect to the dopant concentration except for a very thin layer at the surface where the minority carriers accumulate to form the inversion layer. (ii) That the dopant concentration is uniformly distributed throughout the depletion region. (iii) That surface states and the metal semiconductor work function difference are assumed negligible for reasons already explained in the earlier chapters, and this implies that the MOS capacitor is an ideal one. (iv) That the minority carrier lifetime is taken to be independent of time. This follows from the results obtained by the exact work of Collins et al where it was shown that the overall response is as though there is only one constant value of lifetime because the exact time dependent lifetime coincides with the time independent one during the equilibration time and they only differ in a very short time interval immediately after the voltage step and before the equilibration time. (v) That in the heavy inversion condition, the surface effects are screened off by the inversion layer so that they do not affect the transient in any way, and finally (vi) the net generation or net recombination occurs mostly in one particular region of the depletion layer.

The present theory differs from Hofstein's in that small signal analysis is used in the latter method where the MOS capacitor is represented by a linear equivalent circuit as shown earlier and the transient response is treated as in an RC circuit. The region where the net generation occurs is assumed to be the entire depletion layer width. Also the expression for the generation rate used by Hofstein is $\frac{n_i}{\tau_g}$ without the factor of 2 in the denominator.

Comparing the present theory with that of Viswanathan and Takino, there are some similarities in the expression used as in both cases the differential charge rate $\frac{dQ_m}{dt}$ is evaluated thus requiring graphical differentiation of the transient. However in the present method the analysis is mainly done by curve fitting between the theory and experiment. In contrast to the method of Viswanathan and Takino, the surface effect has now been neglected and also the choice of the generation width is different in the two theories.

The present method, though not as involved as that of Collins et al where the actual generation-recombination and the continuity equations are used, provides a more simplified analysis of the Q-t transient and it is also easier to perform the analysis especially with a microcomputer.

The theoretical plots obtained from this analysis follow the same shape as the experimental ones. By comparing the plots to the experimental ones it is a simple matter to obtain the lifetime of the minority carriers. The evaluation of the experimental curves will be done in Chapter 8.

In the present work theoretical expressions for both the forward and the reverse voltage steps have been obtained

for the first time and as observed experimentally the initial charge increment step for the reverse voltage step is bigger than the forward one. This is especially so for the larger steps and it is due to the difference in the separation between the initial step change in the depletion charge and the electrode charge. For the reverse voltage step measurement, this separation is smaller than that for the forward step. For a given step height, the forward step is shown to provide a slower transient from that of the reverse step and this is also observed experimentally. The comparison of theory and experiment will be discussed in greater detail in Chapter 8.

CHAPTER 6

THE H.F. C-V METHOD OF LIFETIME DETERMINATION

6.1 Introduction

In this chapter the method of evaluating the minority carrier lifetime from high frequency (h.f.) C-V plots is described. The use of the conventional C-V technique to evaluate the MOS surface state density was first reported by Kuhn (50). Since then other authors (28 - 33) have also investigated certain aspects of the generation-recombination processes using the C-V measurement technique. The method of Taniguchi (30) is the latest and this will be described in more detail in the following sections. This method requires C-V plots at two different voltage sweep rates. From, the equations developed, a set of curves for different τ_g and S values can be computed for each sweep rate for a constant oxide thickness and dopant concentration. Using this plot the values of τ_g and S for all devices from the same wafer can be determined merely by performing the normal h.f. C-V measurements at two sweep speeds and referring to the theoretical graph for the resulting values of τ_g and S.

In the present work the C-V technique was used on some of the same samples as in other measurements in order to obtain comparative values of τ_g and to compare the ease of using the techniques.

6.2 Theory

To see how small-signal C-V measurements are affected by the rate of minority carrier generation we need to consider how the normal C-V curve of an MOS capacitor is affected by the voltage sweep speed. Considering the depletion situation, when the voltage is increased positively at a certain rate, the holes are repelled by the electric field into the bulk of the p-type semiconductor and the depletion layer width increases. This corresponds to points A to B in Figure 6.1. As the charges that respond to the small a.c. signal are at the edge of the depletion layer, the increasing bias voltage causes the capacitance to drop because their effective separation from the charges on the metal electrode increases. The capacitance drops until point C of Figure 6.1 is reached. This corresponds to the maximum depletion width x_{do} in equilibrium, beyond which the capacitance remains constant with voltage in the inversion mode of the MOS capacitor.

For a sample that has very low generation rate and/or the voltage sweep rate is sufficiently fast, the constant capacitance portion C D of Figure 6.1 does not occur and the capacitance drops below the inversion value following the trace C E instead. This is due to the fact that the inversion charge cannot increase fast enough for the rising bias voltage so that the depletion layer width increases beyond the maximum equilibrium value x_{do} to compensate the charge on the metal electrode.

When the voltage sweep direction is reversed the depletion width stops increasing and the carriers generated in the depletion layer begin to neutralise the uncompensated dopant ions, resulting in a decrease in the depletion width. The

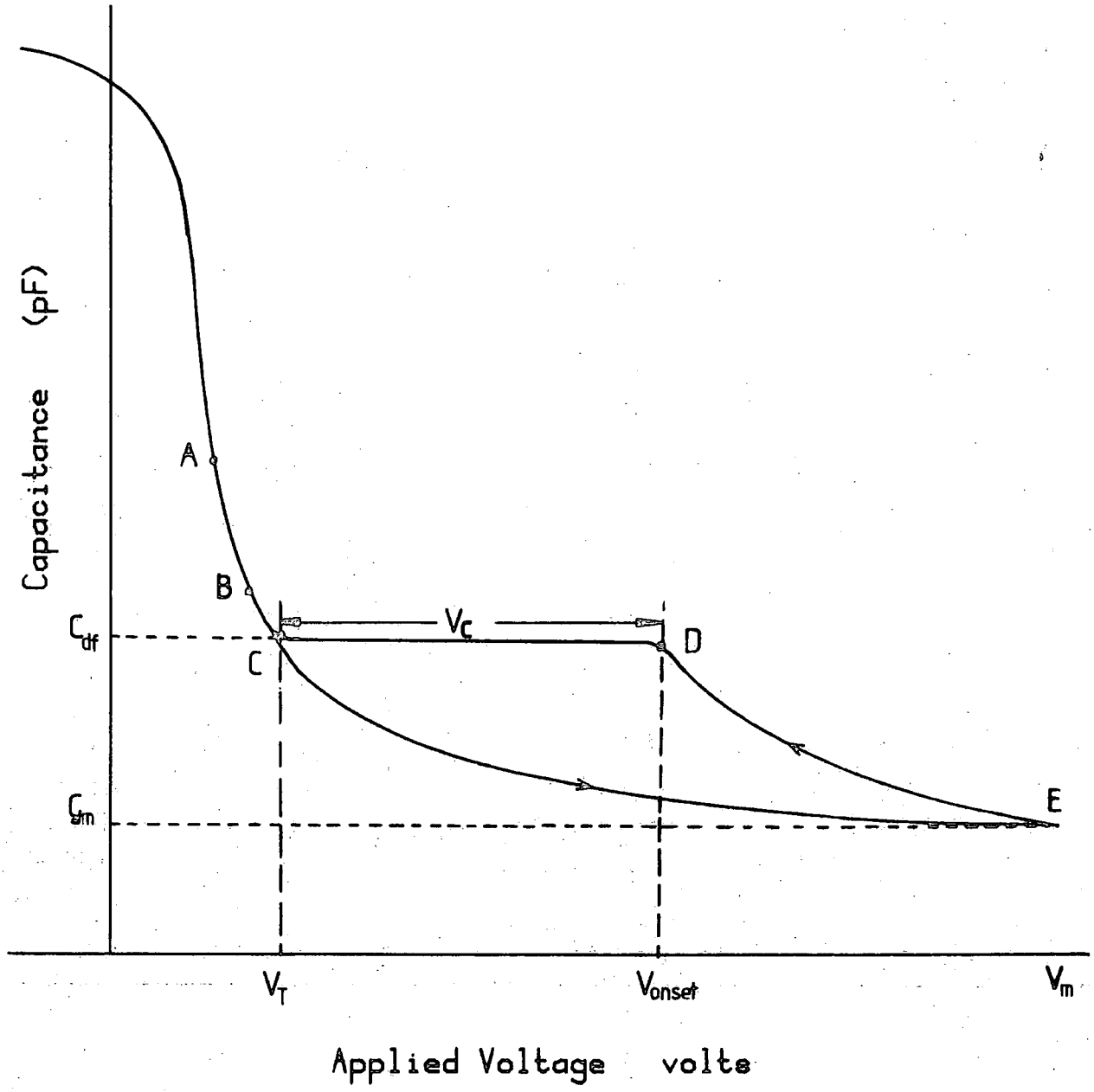

FIG. 6.1 H.F. C-V Plot in the Inversion Region

capacitance therefore increases with falling bias voltage as indicated by the curve E D of Figure 6.1. At Point D the depletion width has decreased to the equilibrium value of x_{do} and the capacitance thereafter remains constant. The capacitance will stay constant until all the inversion charges have recombined which is at the onset of inversion (point C) again. When the bias voltage falls below the value for the onset of inversion, the capacitance increases along the normal depletion curve again. The measurement of the voltage range V_c of Figure 6.1 during which the capacitance is constant is used to calculate the lifetime τ_g by means of a suitable analysis. The value of V_c clearly depends on τ_g because the smaller the lifetime the more the minority carriers will be in equilibrium and the broader will be the constant capacitance range V_c. The same argument applies for the surface recombination velocity.

For this method two equations were developed by Taniguchi (30) and the full derivation will not be repeated here. The first equation is

$$\left(\frac{1}{x} - \frac{1}{x_m}\right) - \left(\frac{1}{A^*} + 1\right)\left[\ell n \frac{x}{x-A^*} - \ell n \frac{x_f}{x_f-A^*}\right] + \frac{A}{\alpha}(V-V_T) = 0 \quad (6.1)$$

which applies for a forward sweep rate α volts/sec which brings the MOS capacitor into deep depletion until the maximum voltage V_m is reached. The second equation is

$$\left(\frac{1}{x} - \frac{1}{x_m}\right) - \left(\frac{1}{A^*} + 1\right)\left[\ell n \frac{x}{x-A^*} - \ell n \frac{x_m}{x_m-A^*}\right] + \frac{A}{\alpha}(V-V_m) = 0 \quad (6.2)$$

which is for the reverse sweep from V_m to the onset of the

equilibrium capacitance. The symbols used are :

$x = \frac{C_d}{C_{ox}}$ where C_d is the depletion capacitance

$x_f = \frac{C_{df}}{C_{ox}}$ where C_{df} is the inversion capacitance

$x_m = \frac{C_{dm}}{C_{ox}}$ where C_{dm} is the lowest capacitance at $V = V_m$.

$A = \frac{n_i}{2 \tau_g N_a}$

$A^* = \frac{A}{(A+B)} \cdot \frac{C_{df}}{C_{ox}}$ where $B = \frac{C_{ox}\left(\alpha - \frac{q n_i S}{C_{ox}}\right)}{\epsilon_s q N_a}$

V_T = Threshold voltage as shown in Figure 6.1.

Details of the derivation for the equations above can be found in the reference mentioned. Using the above equations, the values of τ_g and S can be calculated from the experimental results as described in the Sec. 6.3.

6.3 The Experimental Set-Up

The equipment used is the same as for any typical C-V measurement and the usual precautions are necessary. In a normal C-V measurement only one voltage sweep rate is usually used whereas this method requires two different sweep rates. As the region of interest is entirely in the inversion mode the voltage cycle was confined to bias the sample only from depletion to heavy inversion in this work. This was done by adjusting the d.c. offset on the ramp generator to give a voltage swing from -1 volt to +8 volts.

For each sweep rate the value of V_c was obtained this being the only measurement required. In this method the values of V_c are compared with values calculated from the equations of Sec. 6.2 by entering an experimental point on a chart calculated for a range of values of τ_g and S. This enables the values of τ_g and S to be obtained very easily once the theoretical plot has been produced.

6.3.1 Calculation Technique

The chart that will be used to obtain τ_g and S from the experimental values of V_c is a theoretical plot of $(V_{c2}-V_{c1})$ against V_{c2} for different values of τ_g and S as shown in Figure 6.2. In this, V_{c2} and V_{c1} are the values of V_c for the two sweep rates α_2 and α_1 respectively. The theoretical curves are produced from equations 6.1 and 6.2 using the values of C_{ox}, C_{dm}, C_{df} and V_m appropriate to the particular sample and measurement. The calculation is not a straight forward one and the following numerical algorithm is used to obtain the curves :-

The calculation starts by assigning values to the surface recombination velocity, S , and lifetime τ_g. Using these, the equations are solved to give values of $(V_{c2}-V_{c1})$ and V_{c2} and hence a point on the chart. The value of τ_g is then changed and the point recalculated. After covering a suitable range of τ_g, the value of S is changed and the process repeated. This algorithm is shown in the flow charts of Figure 6.3(a) and 6.3(b). These formed the basis of the BASIC program given in Appendix 3 which gave results which were plotted directly on an H.P. plotter as charts similar to Figure 6.2 .

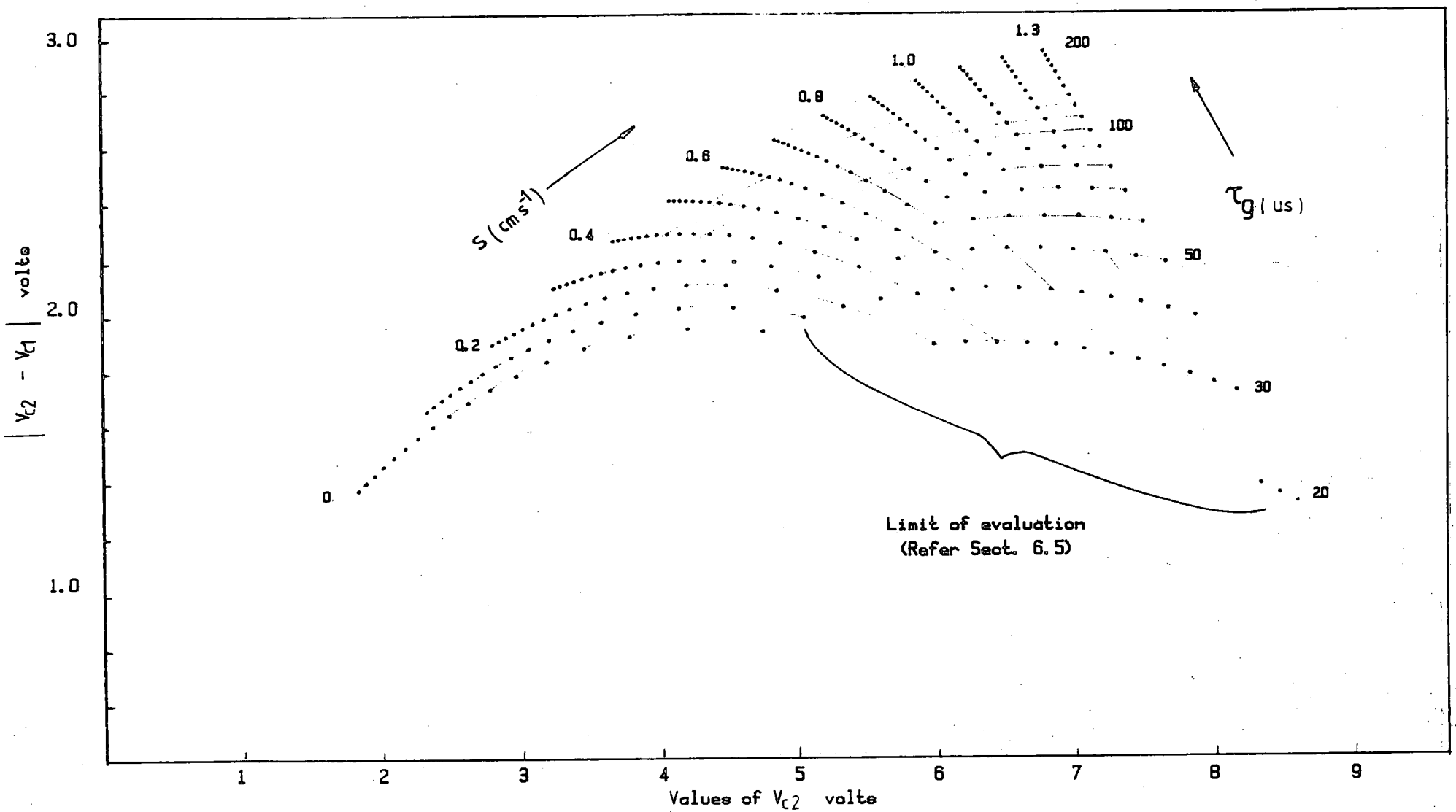

FIG. 6.2 A Typical $|V_{c2} - V_{c1}|$ versus V_{c2} Chart

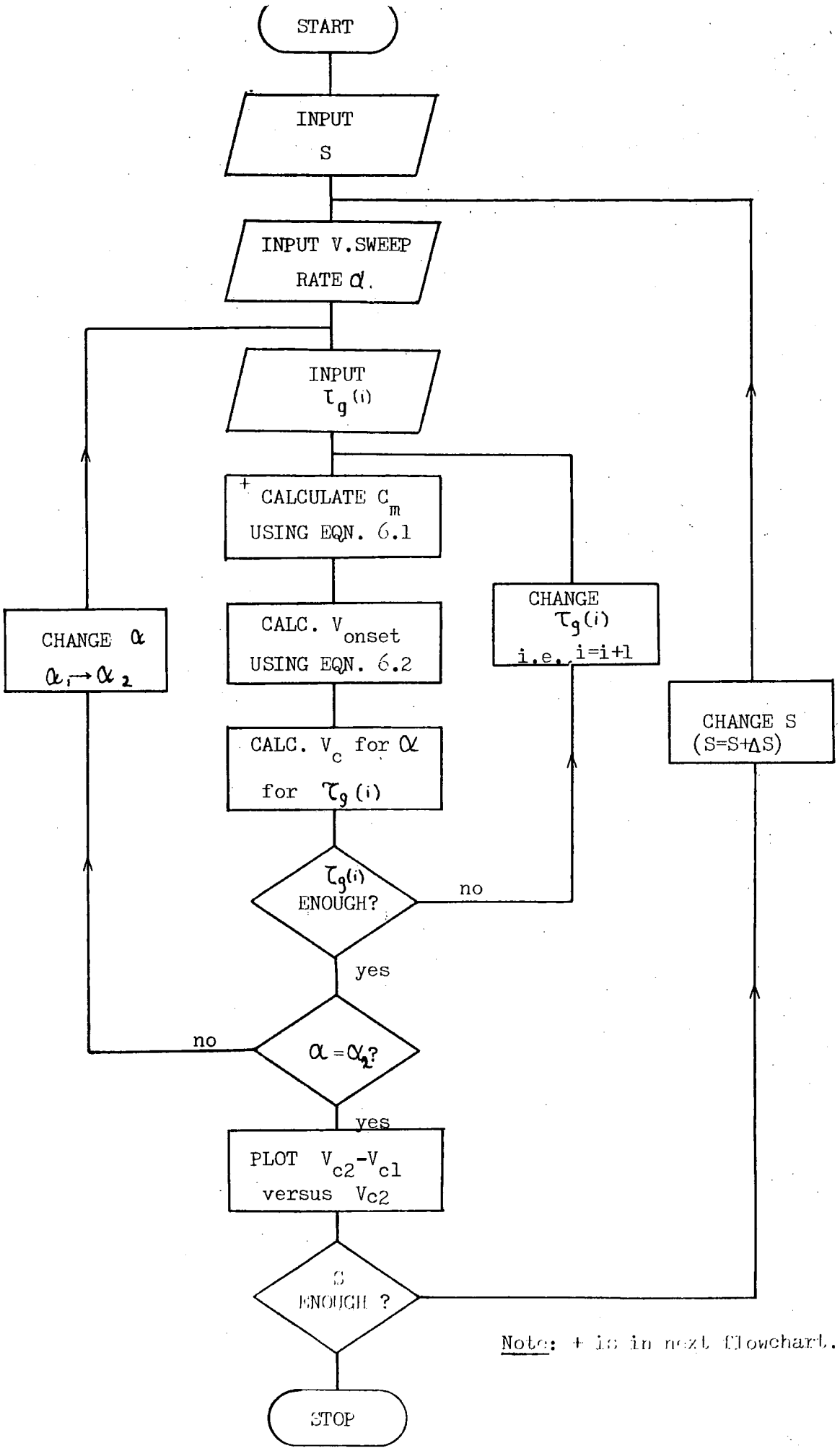

FIG. 6.3(a) Flowchart to Produce Charts for obtaining and S from C-V Plots.

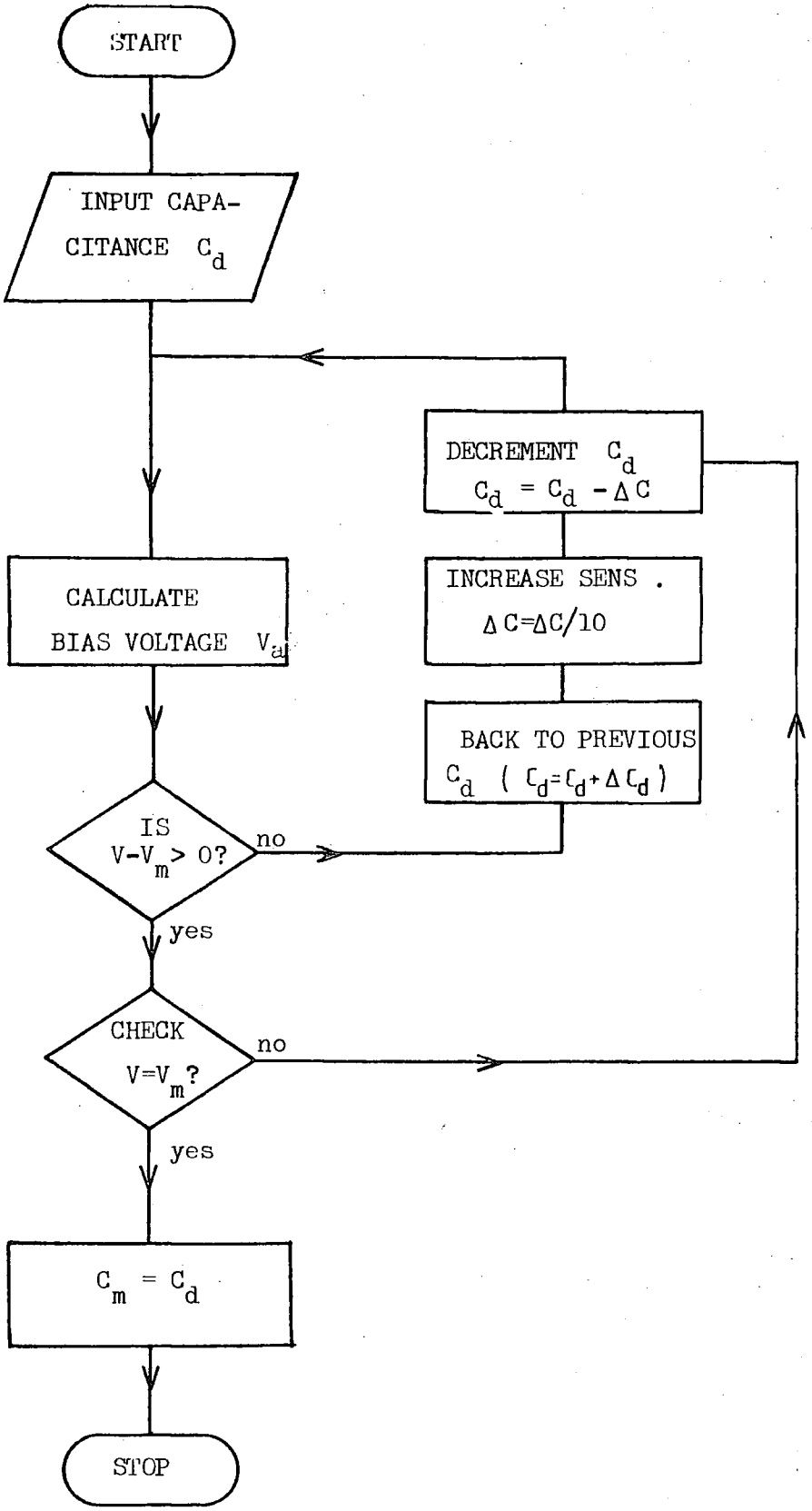

FIG. 6.3(b) Flowchart of Subroutine(+) for Calculating C_m

The experimental value of $(V_{c2}-V_{c1})$ and V_{c2} is entered as a point on the chart, enabling the corresponding values of S and τ_g to be obtained.

6.4 Results

Measurements were done on different p-type samples ITT14, ITT134, and ITT135. The maximum voltage swing for all the measurements was 8.3 v. which was found to give adequate inversion to the samples. The C-V plots for the inversion capacitance for these samples are given in Figures 6.4(a), 6.4(b), and 6.4(c) respectively. The voltage sweep rates were 1.16 v s^{-1} and 3.36 v s^{-1} for ITT14, 0.66 v s^{-1} and 1.61 v s^{-1} for ITT134, and 0.15 v s^{-1} and 0.69 v s^{-1} for ITT135. For the first two samples it was found that the point corresponding to $V_{c2}-V_{c1}$, V_{c2} was outside the $S-\tau_g$ chart showing that it was not possible to find values of S and τ_g by this method for these samples. This is shown in Figures 6.5(a) and 6.5(b).

For sample ITT135 the $S-\tau_g$ chart is shown in Figure 6.5(c). For this sample it was found that the intercept of the lines $(V_{c2}-V_{c1})$ and V_{c2} is in the range of the chart giving values of τ_g of 250 μs and S of 0.31 cm^{-1}. As a check, the measurement on ITT135 was repeated with different voltage sweep rates of 0.06 v s^{-1} and 0.69 v s^{-1} and this gave τ_g and S as 265 μs and 0.31 cm s^{-1} in good agreement with the previous result (Figure 6.5(d)).

6.5 Discussion

The general shape of the C-V plots at high sweep rates was found to agree with the explanation given in Section 6.2. The effect of sweep speed is to vary the deviation from the normal equilibrium C-V curve. During the forward sweep $\left(\frac{dV_a}{dt} > 0\right)$ the capacitance falls below the equilibrium

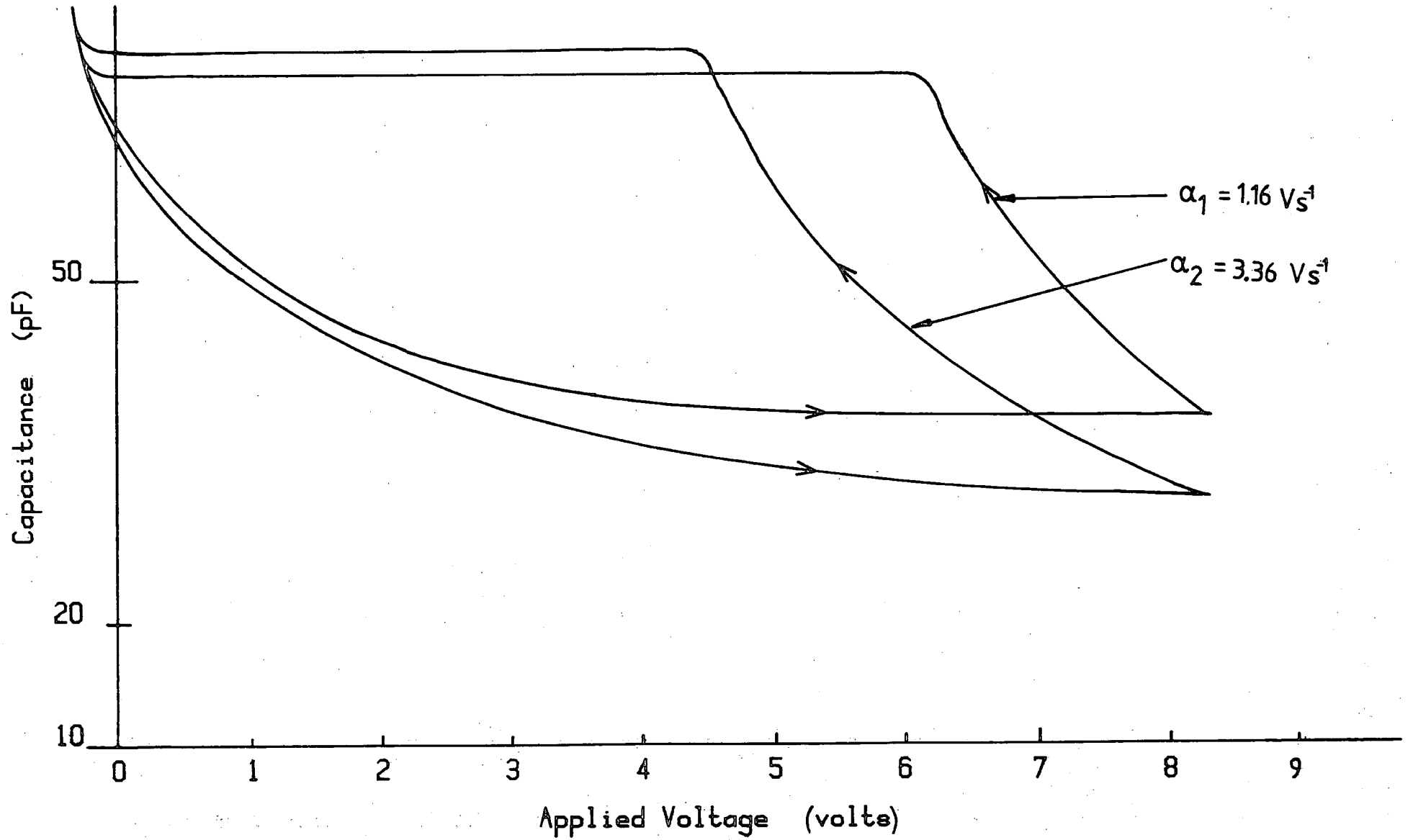

FIG. 6.4 (a) H-F C-V Plots for ITT14

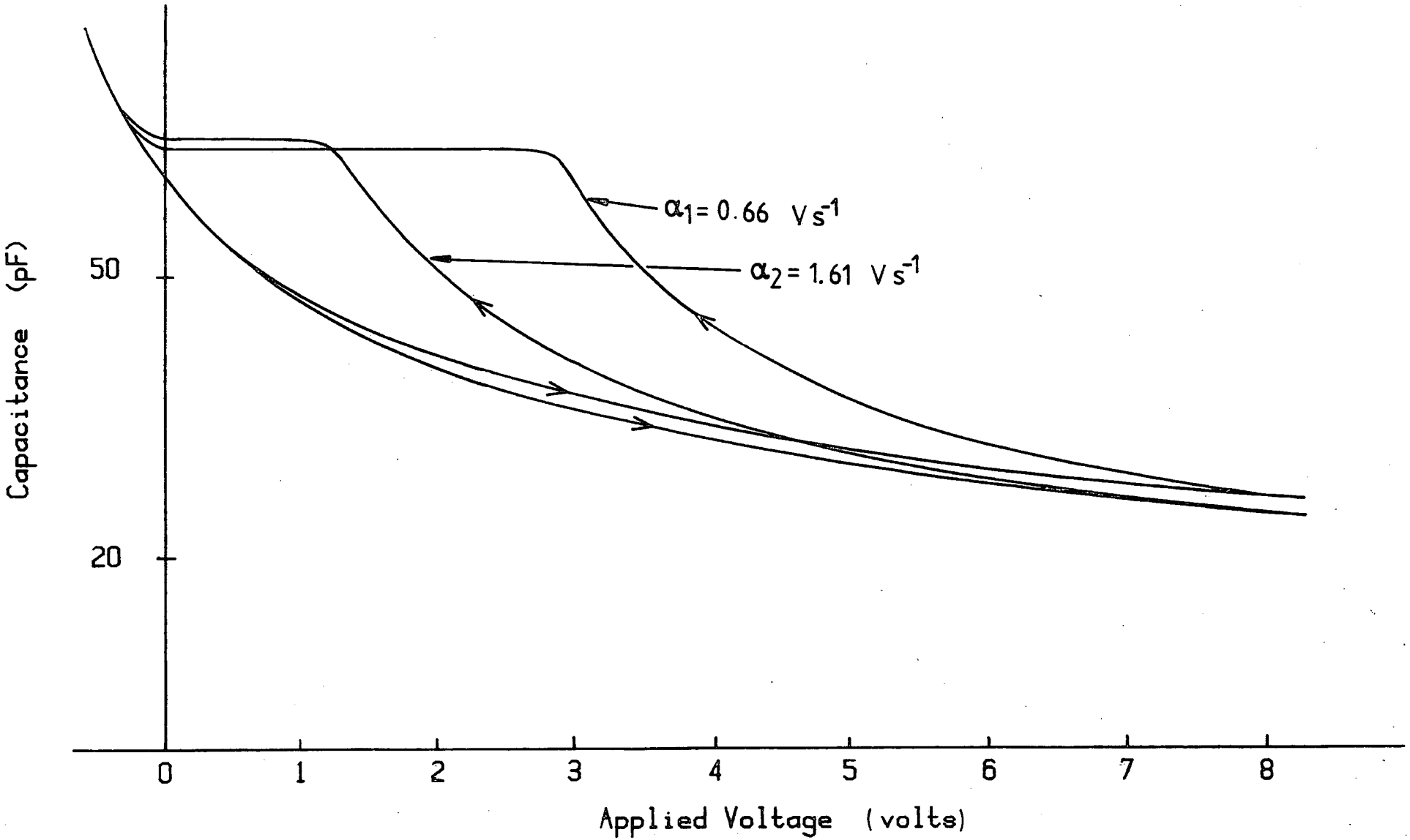

FIG. 6.4 (b) H.F. C-V Plots for ITT134

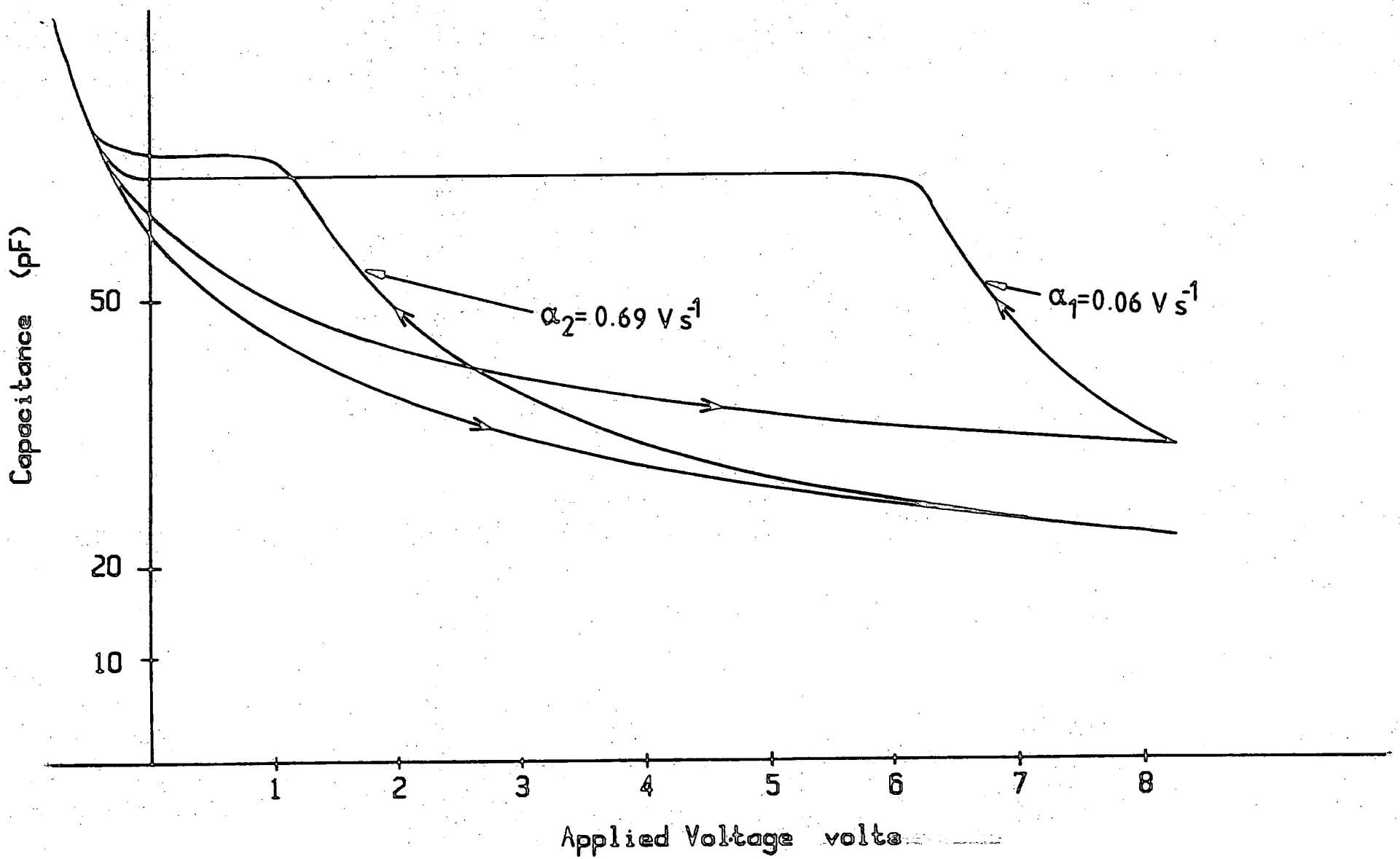

FIG. 6.4(c) H.F C-V Plots for IIIV35

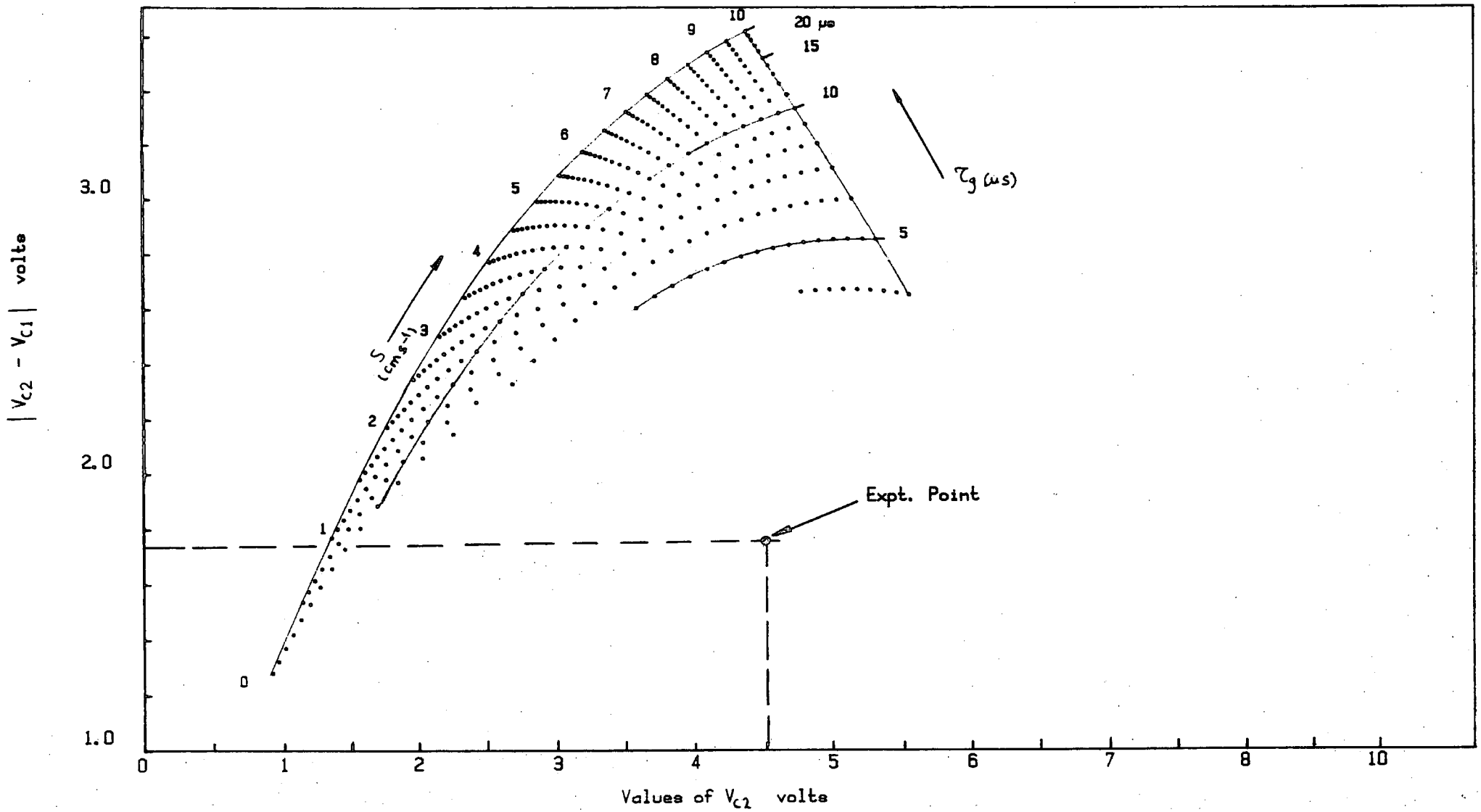

FIG. 6.5(a) $|V_{C2} - V_{C1}|$ versus V Chart for ITT14 for $\alpha_1 = 1.16\ Vs^{-1}$ and $\alpha_2 = 3.36\ Vs^{-1}$

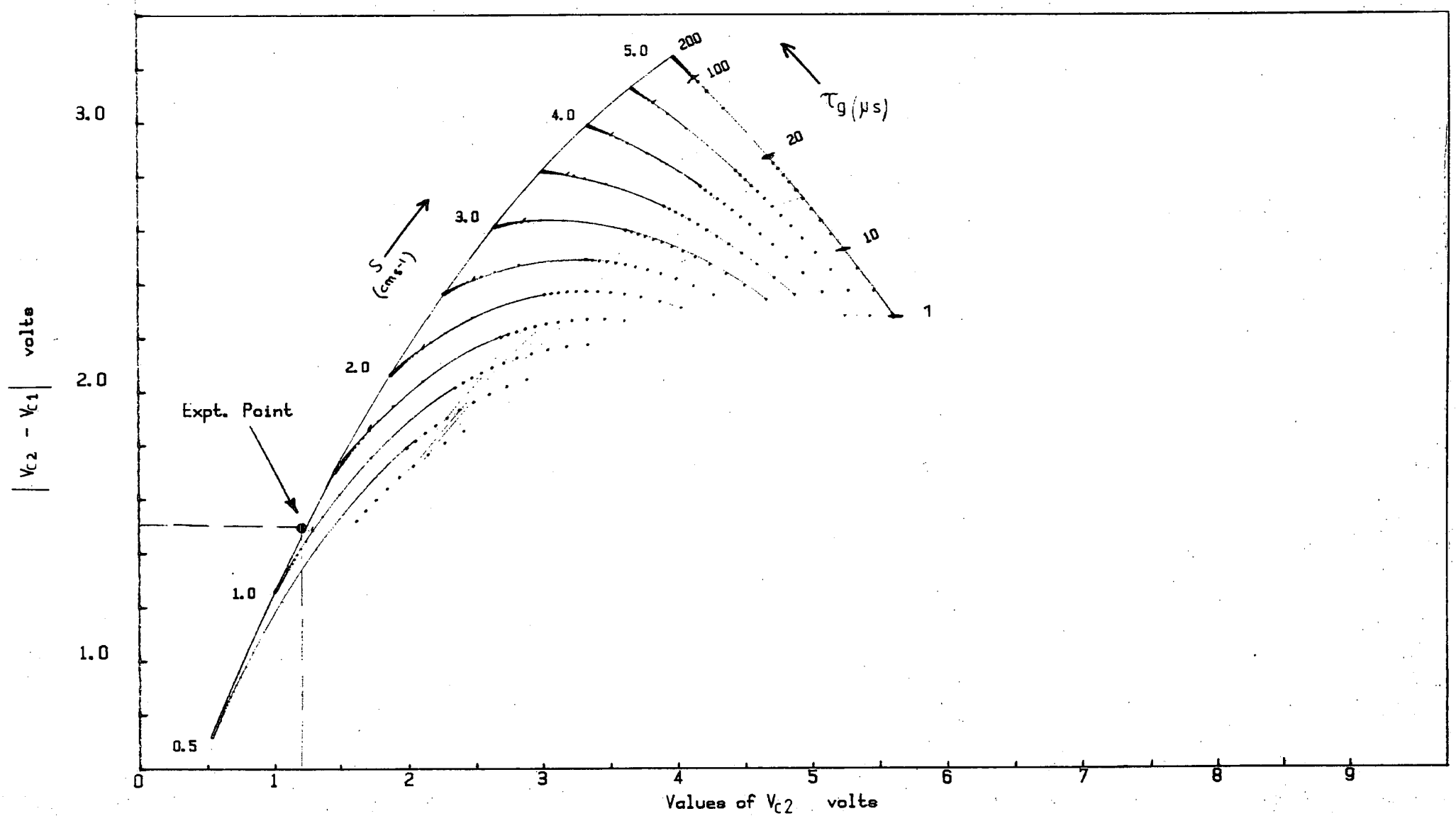

FIG. 6.5(b) $|V_{c2} - V_{c1}|$ versus V Chart for ITT134 for $\alpha_1 = 0.66\ Vs^{-1}$ and $\alpha_2 = 1.61\ Vs^{-1}$

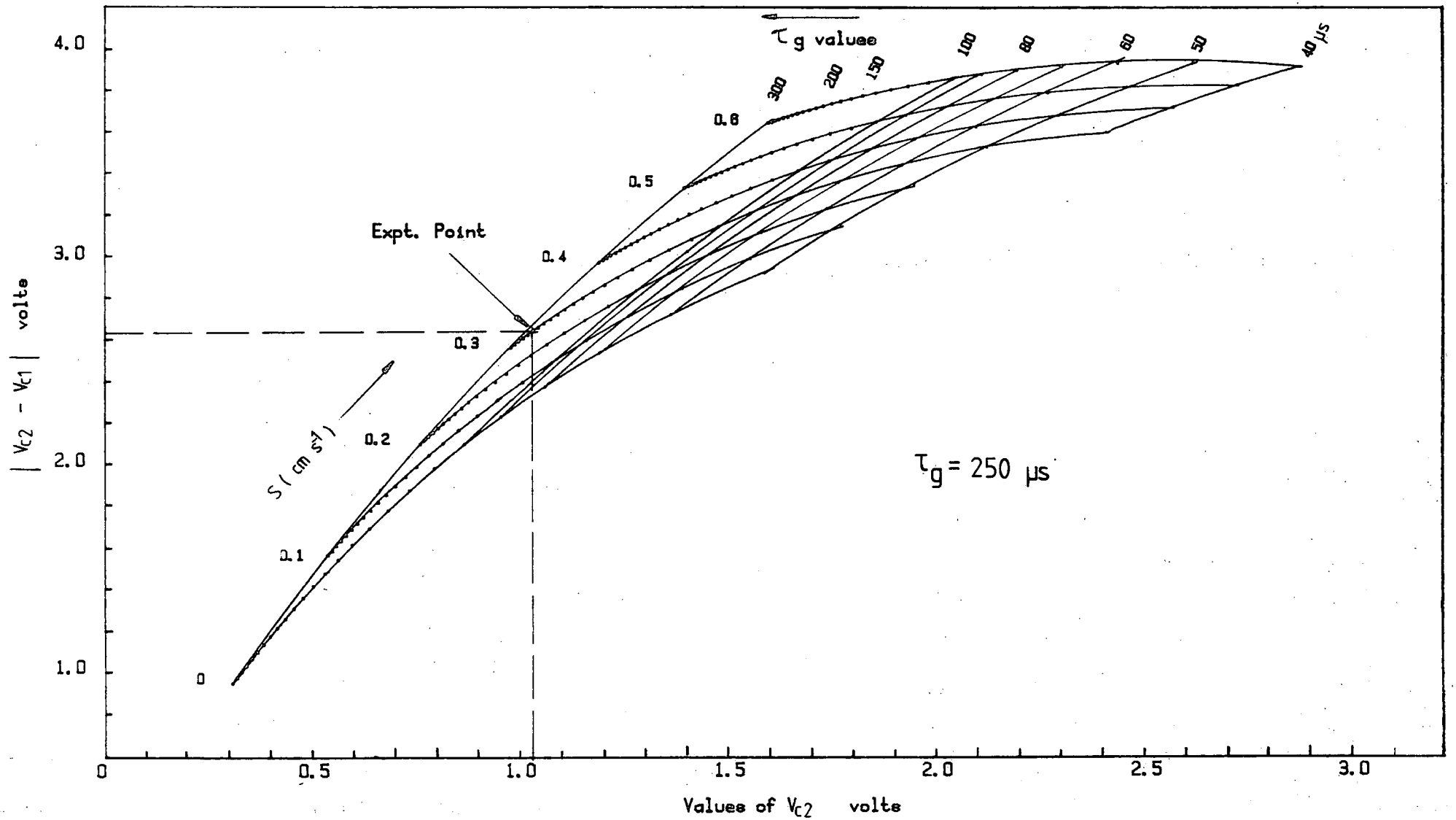

FIG. 6.5(c) $|V_{c2} - V_{c1}|$ versus V_{c2} Chart for ITT135 for $\alpha_1 = 0.15\ Vs^{-1}$ and $\alpha_2 = 0.69\ Vs^{-1}$

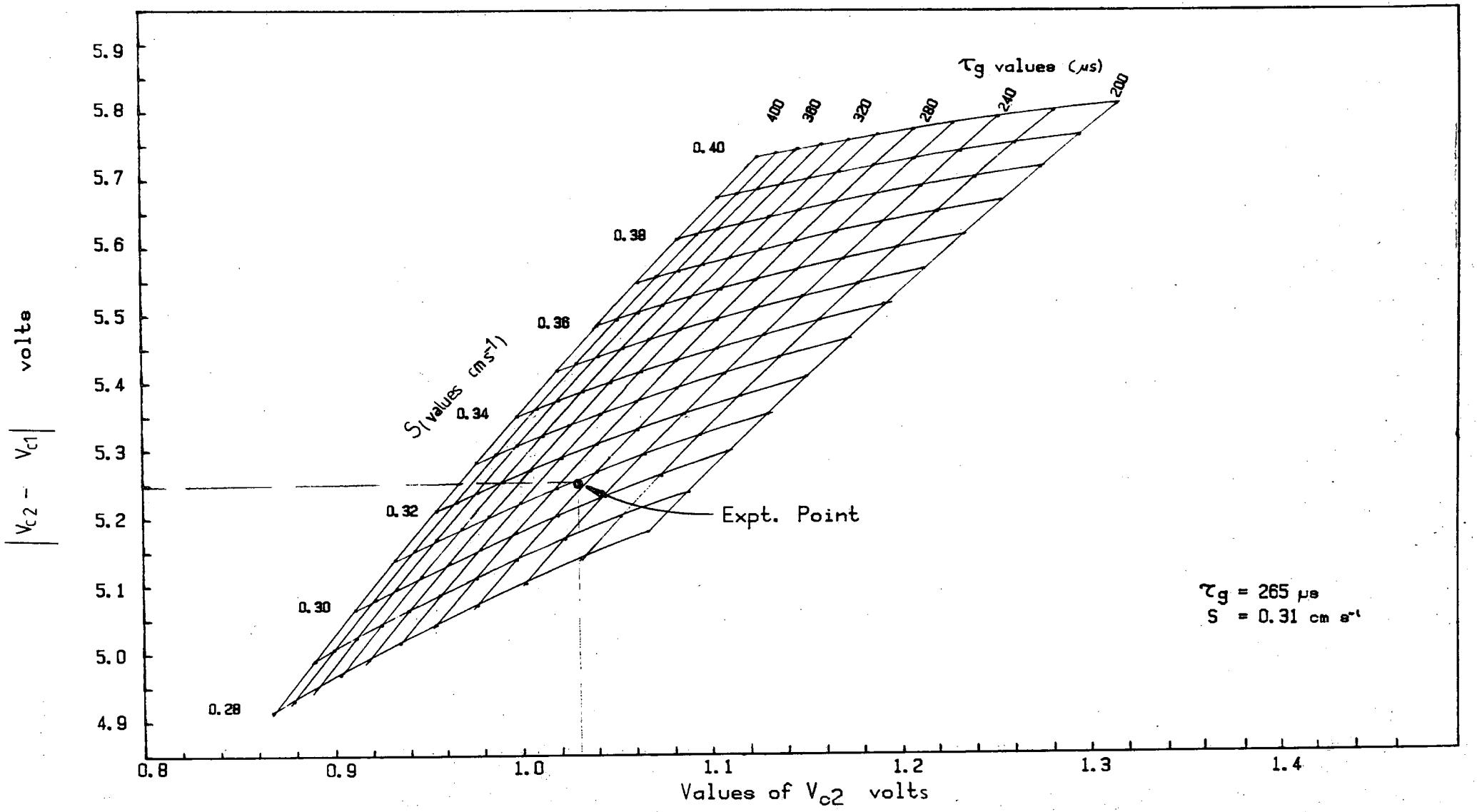

FIG. 6.5(d) $|V_{c2} - V_{c1}|$ versus V_{c2} Chart for ITT135 for $\alpha_1 = 0.06\ Vs^{-1}$ and $\alpha_2 = 0.69\ Vs^{-1}$

inversion value due to the increased width of the depletion layer. When the maximum voltage V_m is reached the depletion layer width begins to decrease as the generated minority charge increases resulting in an increased capacitance. If the voltage were to remain fixed at V_m, the capacitance would increase along a vertical line to reach the equilibrium inversion value C_{df}. This would give the maximum possible value for V_c. With the applied voltage decreasing as in the negative sweep situation the capacitance reaches C_{df} at a lower value of V_a thus decreasing the magnitude of the straight portion V_c. If the sweep rate is higher, following a similar argument, V_c will be smaller.

For samples with different values of τ_g and S, the value of V_c at a constant sweep rate will be different. For higher τ_g the capacitance will be closer to the deep depletion value during the positive going voltage sweep as the generation of inversion change is reduced. Also during the negative voltage sweep the capacitance will reach the equilibrium value at a lower voltage thus reducing the magnitude of V_c. On the other hand the value of S, the surface generation rate, is the opposite to that for τ_g, a high value increasing the value of V_c.

In the numerical solution of the equations given by Taniguchi it was found that certain combinations of τ_g and S cannot be found for certain voltage sweep rates. This is because the argument of the natural logarithm term in the equations, should always be positive and it accounts for the discontinuity found on the S-τ_g charts of Figures 6.2 and 6.5. Looking at equations (6.1) and (6.2) the following conditions

must hold for the log term to be definable:-

$$\frac{x}{x-A^*} > 0$$

$$\frac{x}{x_f-A^*} > 0$$

and

$$\frac{x}{x_m-A^*} > 0$$

From these conditions the requirement for the equations to be solvable is

$$\alpha > \frac{qn_i}{C_{ox}} \left[s + \frac{\varepsilon_s}{2\tau_g} \cdot \left(\frac{C_{df}}{C} - 1 \right) \right]$$

The second term on the right-hand side of the expression is very small ($< 10^{-5}$) even for small values of τ_g so the criterion for the validity of the equations becomes approximately

$$\alpha > \frac{q\, n_i S}{C_{ox}}$$

Because of this limitation the value of α has to be carefully chosen but there is no means of knowing the S_i value before the measurement so that α has to be chosen from experience. Therefore this method does not actually provide an easy way of determining τ_g.

From the results on samples ITT14 and ITT134, the success of the method clearly depends greatly on the particular

samples used because it failed completely for these samples by giving an experimental point well outside the region that could be plotted on the chart. This failure was not investigated further since this thesis is not mainly concerned with the voltage ramp technique. For the sample ITT135 the values of τ_g obtained by this method are also too high. This however will be discussed in Chapter 8 when the results of the C-V method are compared with the others.

In view of the above problem, it was found that the method is not as straight forward as claimed by its author. Although the idea of having a chart that is applicable to all devices of the same wafer looks promising as a method for monitoring device fabrication, the accuracy and validity of the result are greatly affected for values in the extremities of the chart. Furthermore, the calculation and plotting of the $S-\tau_g$ chart is very slow even using a microcomputer and a digital plotter. For these reasons it is realised that the pulsed Q-t technique is at least as good for the determination of τ_g.

CHAPTER 7

C-t AND FAST-RAMP MEASUREMENTS

7.1 Introduction

As mentioned in earlier chapters, there are several other methods that have been used to measure the minority carrier lifetime in MOS capacitors. Many of these were developed from the Zerbst method (1) which is based on pulsed C-t transient measurements, while others use a linear voltage ramp and analyse either the capacitance or the gate current of the device with respect to the instantaneous applied voltage. In each case the methods differ rather more in their theoretical analysis than in the experimental techniques employed.

In this work two of these methods of measuring lifetime were used for comparison with the Q-t method from the points of view of experimental technique, analysis and results. This Chapter therefore briefly describes the use of the basic Zerbst C-t transient method and the non-equilibrium fast ramp technique which were chosen as being two of the simplest. The comparison with the Q-t method will be discussed in Chapter 8.

7.2 The C-t Method

The change in capacitance of an MOS capacitor with time after the application of a voltage step was first studied by Jund and Poirier (51). In their analysis they assumed that the capacitance relaxation followed a simple exponential with time. However, it was Zerbst who first developed the method of analysis that allows the minority carrier lifetime as well as the surface recombination velocity to be deter-

mined from the C-t transient. In his analysis Zerbst assumed that in the non-equilibrium situation following the application of a voltage step the change in the inversion charge concentration during the capacitance relaxation is due to generation at the surface as well as the net bulk generation in the depletion layer.

Following Zerbst's paper, a number of other authors looked into variations of the method. In particular, Schroder and Nathanson (17) suggested a correction to be made to the Zerbst expression used in the analysis. They showed that when the MOS capacitor is biased into depletion, the depletion layer does not only extend into the bulk but also laterally. The surface recombination velocity immediately beneath the gate electrode is different from that at the laterally depleted region, and this has an effect on the measured lifetime. Therefore the Zerbst method does not give the true lifetime τ_g but an effective lifetime . Schroder and Nathanson derived a relationship between the true bulk lifetime and this effective lifetime. Despite this and other criticisms, the Zerbst method without modification is still being used as a standard reference technique whenever the minority carrier lifetime and surface recombination velocity of MOS capacitors are measured.

7.2.1 Theory

A typical high frequency C-V curve for an MOS capacitor is shown by the full line in Figure 7.1(a). On applying a positive voltage step with the capacitor already in inversion, the response is as shown by the broken line, where V_a is the initial applied voltage and ΔV is the voltage step.

Immediately after the voltage step is applied the additional electric field repels majority carriers further into the bulk thus extending the depletion width and causing the capacitance to drop from its equilibrium value C_f to the minimum value C_m. Subsequently, the applied voltage remains constant at $(V_a + \Delta V)$ and as minority carriers are generated the depletion width relaxes back to its new equilibrium value which is almost the same as the initial value. The capacitance variation with time is therefore as shown in Figure 7.1(b) where the values correspond with those in Figure 7.1(a). Figure 7.1(b) is the familiar C-t curve for the MOS capacitor. By analysing this curve as shown below one obtains the so-called Zerbst plot from which the lifetime can be evaluated.

By solving the charge neutrality, voltage, capacitance, and surface potential equations, Zerbst derived an expression for the inversion charge Q_{inv} per unit area. For p-type silicon this is

$$Q_{inv} = C_{ox} V_a - q \frac{N_a \epsilon_s}{2 C_{ox}} \left(\frac{C_{ox}^2}{C^2} - 1 \right) \qquad (7.1)$$

where C is the capacitance per unit area, at any time, t The derivation of this equation is given in Appendix 4. Differentiating the expression with respect to time gives the rate of change of the inversion charge concentration, that is

$$\frac{d Q_{inv}}{dt} = - q \frac{N_a \epsilon_s}{2 C_{ox}} \cdot \frac{d}{dt} \left(\frac{C_{ox}^2}{C^2} \right) \qquad (7.2)$$

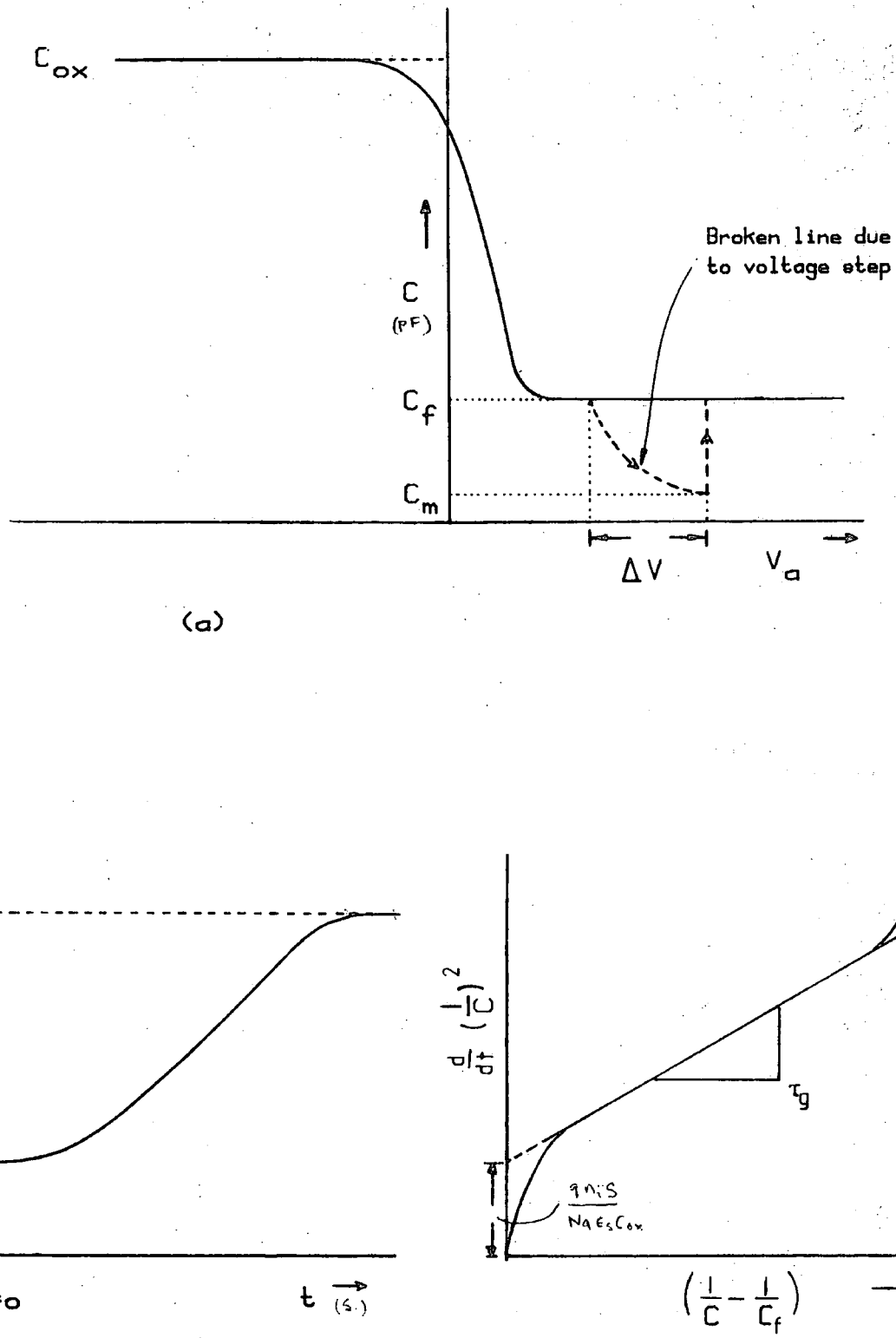

FIG. 7.1 (a) A Typical C-V Plot for p-type MOS-C showing the effect of a Step Voltage.
(b) A C-t Transient following a Voltage Step.
(c) A Typical Zerbst Plot.

This rate of change is due to generation in the bulk and at the surface which are assumed to be given by the two terms in the equation

$$\frac{d\,Q_{inv}}{dt} = \frac{q\,n_i}{\tau_g}\,(x_d - x_f) + q\,n_i S \qquad (7.3)$$

Equating (7.2) and (7.3) gives the Zerbst expression

$$-\frac{d}{dt}\left(\frac{1}{C}\right)^2 = \frac{2\,n_i}{N_a C_{ox} \tau_g}\left(\frac{1}{C} - \frac{1}{C_f}\right) + \frac{2\,n_i S}{N_a C_{ox}} \qquad (7.4)$$

and by plotting $\frac{d}{dt}\left(\frac{1}{C}\right)^2$ against $\left(\frac{1}{C} - \frac{1}{C_f}\right)$ one gets the Zerbst plot as shown in Figure 7.1(c). The gradient of the linear portion of the plot yields τ_g, while the intercept gives S.

7.2.2 Experimental Details

The Zerbst technique was set up to provide a direct comparison with the Q-t method for some of the samples. The experimental lay-out is as shown in Figure 7.2, where the sample was placed in the probing box which was described in Chapter 3. The leads from the prober and the sample base plate were connected to the input of the Boonton 72BD capacitance meter. The step voltage was applied by programming the Commodore microcomputer through the IEEE port and a digital to analogue converter as for the Q-t method but with an additional amplifier to allow for finer adjustment of the analogue voltage which was applied to the MOS capacitor through the polarising connections on the capacitance meter. The magnitude of the voltage step and the pulse duration were both controlled by the microcomputer, but the digital

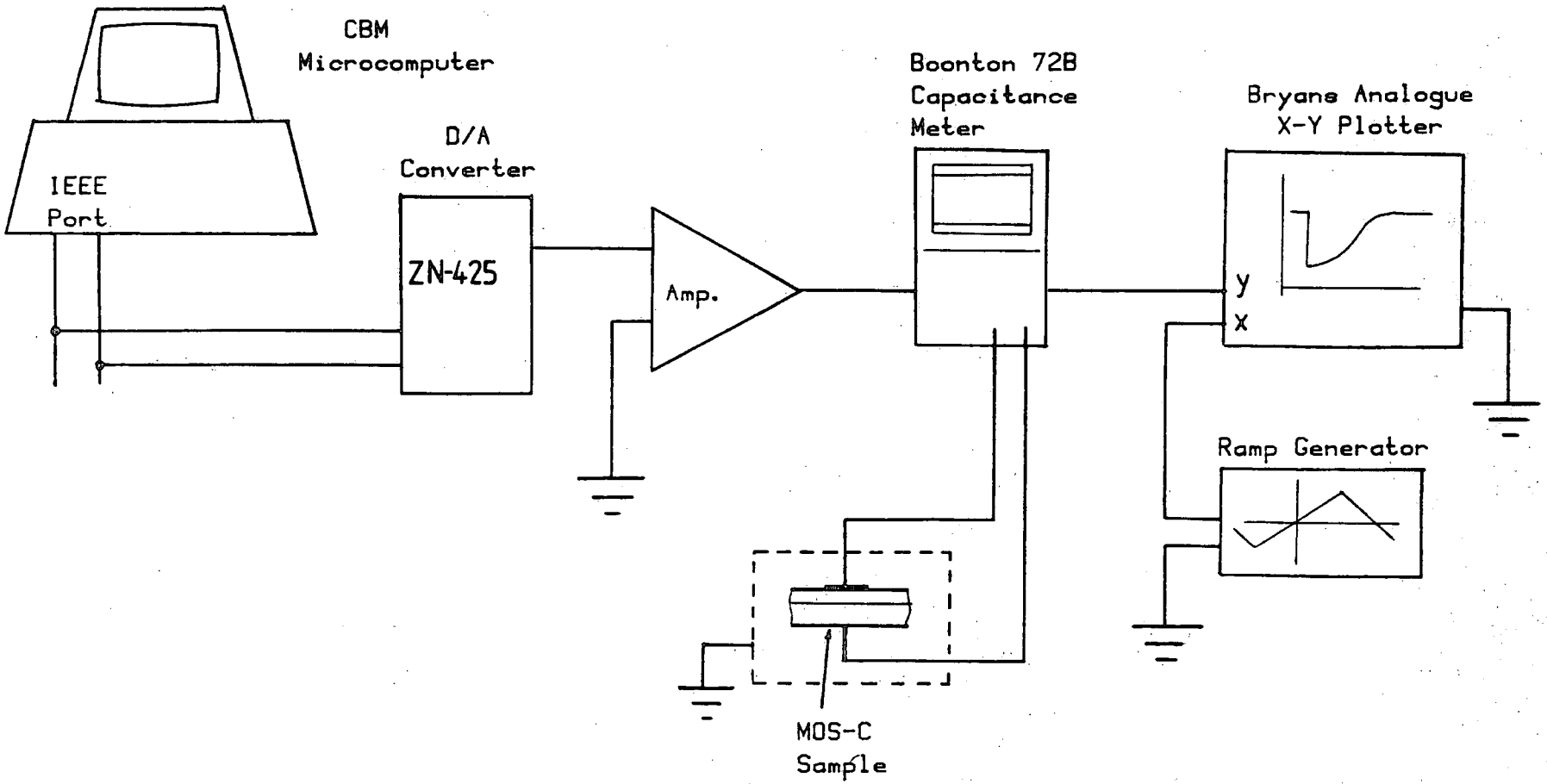

FIG. 7.2 Experimental layout for C-t Transient Measurements

output of the capacitance meter responded too slowly for the transient to be recorded digitally. Instead an analogue x-y plotter was attached to the analogue output of the capacitance meter with the capacitance information connected to the y-input while the x-input was driven by an external ramp generator. As with the Q-t experiments careful screening was observed to minimise extraneous noise pick-up and the measurements were done in total darkness by ensuring that the probing box was light-tight.

7.2.3 Results and Discussion

Measurements were carried out for a number of samples and the results are summarised in Table 7.1. The detailed results given below are for the p-type sample ITT135 previously used for Q-t experiments. The oxide capacitance of this sample, 2.29×10^{-8} F cm^{-2}. was obtained from a high frequency C-V measurement and this value was used throughout the analysis.

The general shape of the capacitance transient obtained was similar to that obtained by Zerbst. Figure 7.3 shows the transient for a voltage step of 2.50 volts with the high frequency equilibrium inversion capacitance, C_f, of 61.8 pF. The applied voltage was from 2.55 volts to 5.05 volts, which ensured the device in heavy inversion both before and after the voltage step. Immediately after the voltage step, the capacitance dropped to 37.5 pF, returning to its equilibrium value in about 100 sec. The plot of $-\frac{d}{dt}\left(\frac{1}{C^2}\right)$ against $\left(\frac{1}{C}-\frac{1}{C_f}\right)$ is shown in Figure 7.4. According to Equation (7.4), a linear plot was expected but since this equation fails as the transient reaches saturation, a deviation from linearity was observed on the plot as the capacitance C

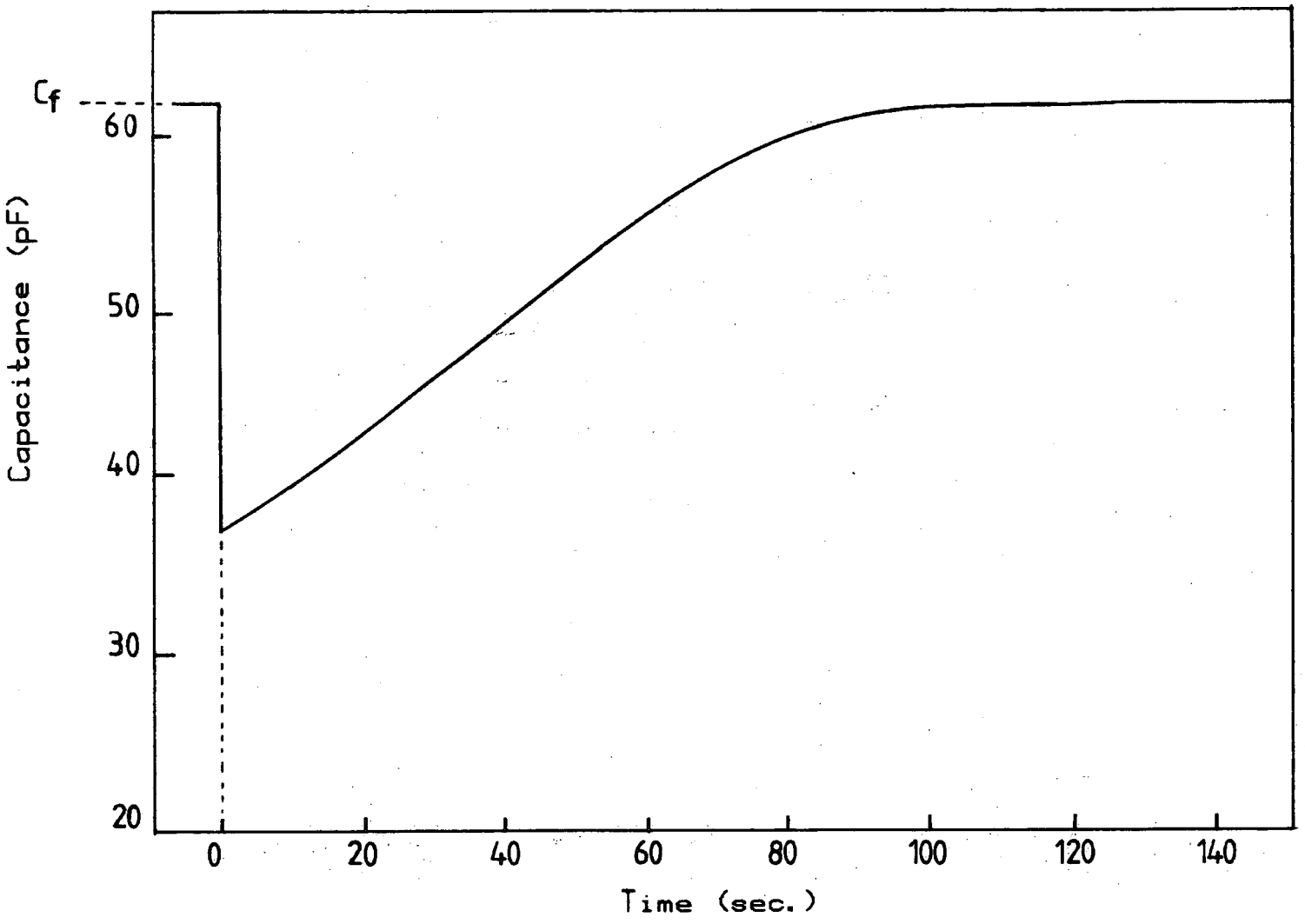

FIG. 7.3 The C-t Transient for ITT135 Sample

approached C_f value. This may be due to the fact that recombination processes become significant as the depletion width approaches its original equilibrium value. The slope of the linear portion of the plot in Figure 7.4 gave the value of τ_g as 65 μsec, and from the intercept with the y-axis the value of S was obtained as 0.25 cm s^{-1}.

From this experiment it was found that the C-t transient measurement was relatively easy to perform and it is quite similar to the Q-t method. The difference between the two methods is that instead of using a simple electrometer, for the Q-t transient measurement, a capacitance bridge was needed in the C-t experiemnt. In both methods a voltage step was required to change the bias from strong to stronger inversion. As the C-t method is not the main concern of this work, the Zerbst experiment was not automated as in the Q-t measurement and so the results are not as consistent, e.g. there is no averaging. Also the analysis required to obtain the result from a C-t transient is not as simple as the Hofstein's Q-t method as it requires manual differentiation of the trace. This is rather similar to the Q-t methods of Takino, and Viswanathan and Takino where differentiation of the trace is also required. However in contrast to their technique, the C-t method does not require the calculation of the surface potential which varies with time during the transient.

The limitation of the C-t method can be seen in the extreme case where the doping concentration is high. Thus with the same voltage step, the change in the depletion width x_d, and hence the capacitance change, will be small but

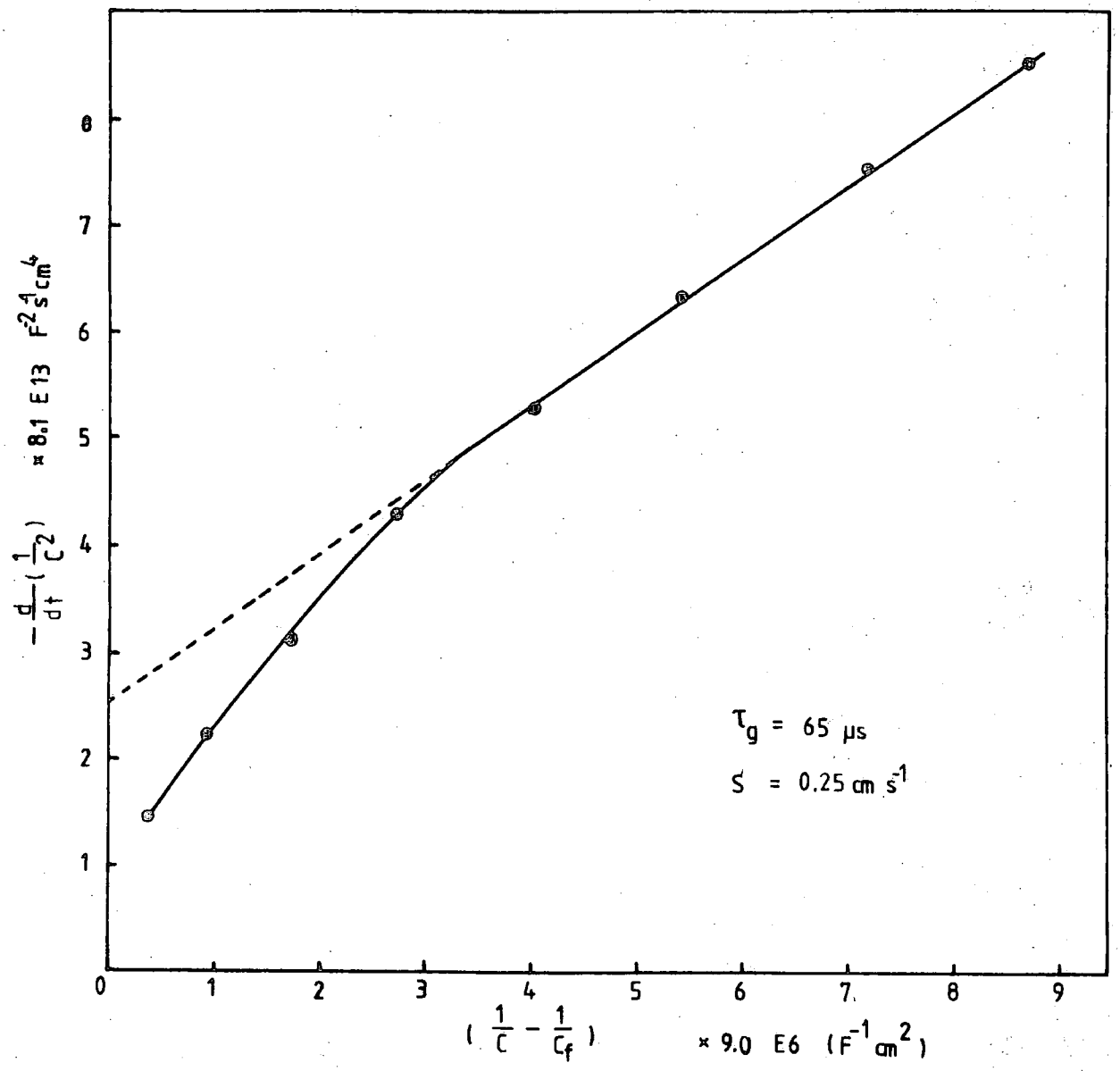

FIG. 7.4 The Zerbet Plot for ITT135 eample.
(ΔV_a = 2V)

the change in charge in the depletion region will be larger. The reason for this is that for higher doping concentrations only a small change in x_d will accompany the necessary change in the depletion charge to balance the charge on the electrode.

Another disadvantage of the C-t method is that because an a.c. signal is required on top of the d.c. bias the response speed is limited by the frequency of the signal if the lifetime is extremely short. This is not the case in the Q-t method as it requires only d.c. voltages and the measuring gear can be easily improved should an extremely fast response be encountered.

It is concluded that on the whole the C-t method shows some limitations compared to the Q-t measurement but these are mostly in extreme conditions. The main disadvantage it has over the simpler Q-t method of Hofstein is the need to differentiate the C-t transient which introduces the main cause of error. The values of the lifetime τ_g obtained by this method will be compared with other methods in the next chapter.

7.3 The Fast Ramp Method

Methods employing a linear voltage ramp to study MOS capacitor characteristics have long been used by several authors. Most of these methods involve capacitance-voltage (C-V) measurements, although some measure the gate current against the applied voltage (53-55). In the latter case there are two sets of conditions to be considered depending on the ramp speed. If the ramp is slow enough to keep the capacitor in equilibrium throughout the voltage cycle the current, $i = C \cdot \frac{dV}{dt}$, will give the equilibrium C-V curve. This

method was used by Kuhn (50) when he studied the interface states in MOS devices. The other extreme is to apply a fast linear voltage ramp as in the method of Kuper and Grimbergen (52). The method to be described here is based on the work by Board and Simmons (27) on the fast ramp current measurement where the devices do not reach equilibrium at all during the voltage cycle. The technique will be briefly described and the results from the joint work with Abdullah (56) in the same research group will be given. From the theoretical analysis it will be shown that the minority carrier lifetime can be extracted easily from the current characteristics.

7.3.1 Theory

Figure 7.5 shows a typical plot of the current in an n-type MOS capacitor resulting from the application of fast voltage ramp. The response is in two parts, one for the forward voltage sweep (i.e. negative dV/dt) while the other is the reverse sweep (positive dV/dt).

The Forward Voltage Sweep

In following the I-V trace from point A to B, the device is in accumulation at point A with a constant current level as there are abundant electrons (majority carriers) in the silicon surface. When the applied voltage passes the flat-band point depletion begins to set in and the current starts decreasing due to limited charge concentration in the silicon surface. As the applied voltage increases in the negative direction the depletion width increases to a maximum value and the current reaches its lowest value at point B. From here on, if the ramp was slow enough, there would be time for the generation current to increase thus increasing

the sample current to B. But since we are here dealing with a fast voltage ramp the carrier generation rate is unable to cope with the voltage change, and the current does not increase to its equilibrium value but to a lower value as shown by the point C in Figure 7.5. The current flowing in the device is made up of the displacement current and the generation current. During this part of the voltage sweep these current components are in the same direction. As shown in Appendix 5 the expression for the gate current is then

$$I_{G_f} = \alpha C_{ox} \left[Z + \frac{1 - Z}{\frac{C_{ox}}{\varepsilon_s} (x_o - ZL_E)} \right] \qquad (7.5)$$

$$\text{and } L_E = \frac{\alpha C_{ox}}{q U_q}$$

$$\text{where } Z = \frac{x_d - x_o}{L_E}$$

α is the ramp speed in volt/sec

and U_g is the generation rate per unit volume.

The Reverse Voltage Sweep

When the magnitude of the applied voltage is reduced the I-V curve follows the lower path DEFG shown in Figure 7.5. The gate current now becomes

$$I_{G_r} = \alpha C_{ox} \left[Z - \frac{1 + Z}{\frac{C_{ox}}{\varepsilon_s} (x_o - ZL_E)} \right] \qquad (7.6)$$

As can be seen from the two equations 7.5 and 7.6

$$I_{G_r} \leq I_{G_f}$$

This is because the displacement and the generation currents are now in opposite directions so that the net effect is the difference of the two. Due to this difference there is initially an abrupt fall from C to D on the plot. From D to E the generation current I_g is greater than the displacement current I_d. When $I_d > I_g$ the net current

$$I_G = I_g - I_d$$

becomes negative as shown on the plot by point E. At F, sufficient minority carriers have been generated for the surface to be just inverted so that the part of the curve from F to G represents the equilibrium displacement current again. This is a mirror image of the equilibrium curve ABB'.

In this experiment, samples having different generation rates will have the portions BCDEF different from one another. For a higher generation rate, thus lower τ_g, the portion BC will be higher and the points E and F will be shifted to a more negative value as shown in Figure 7.5(b). This is caused by the increased sample current due to the increased generation of minority carriers. Conversely for a lower generation rate, the curve will look like B $C_2D_2E_2F_2$ of Figure 7.5(b).

To obtain the value of τ_g one needs to match the I-V curve calculated from the theoretical expression using an estimated value of τ_g to the experimental one. If these curves do not match then another value of τ_g is used until the best fit is obtained. The value of τ_g thus obtained is the lifetime of the sample. This calculation is easily done on a microcomputer and the results can be plotted manually.

From the work of Rahman (57) and Allman (58) who were working in the same research group, it is possible to calculate the lifetime τ_g directly from the I-V plot. In their method the step CD observed in the I-V plot of Figure 7.5(a) is measured. This is the point at the end of the forward sweep ramp where the ramp gradient dV/dt changes sign. From this value, τ_g can be calculated.

7.3.2 Experimental Details

The experimental set up used for the fast ramp method is shown schematically in Figure 7.6. It is similar to that for the Q-t method except for the voltage ramp generator instead of the voltage step source. The electrometer used was the Keithley 600 B switched to current measurement instead of the Coulomb range as in the Q-t measurement. The fast ramp method was not automated and so the result was recorded on a Bryans analogue x-y recorder when the ramp frequency is not too fast. Otherwise a storage oscilloscope was used and the trace was photographed for analysis. Normal experimental precautions were taken as with other methods. The calculations of the theoretical curve to obtain the best fit with the experimental plot was done numerically on a microcomputer and the results were plotted manually.

7.3.3 Results and Discussion

The fast ramp technique was developed in Durham by Dr. P.G.C.Allman (58) and by Abdullah (56). Part of the latter's work was to compare the fast ramp results with the author's Q-t results, and some measurements using both techniques were done jointly.

Measurements were made on both p- and n-type samples. The oxide thickness and the doping concentration were determined

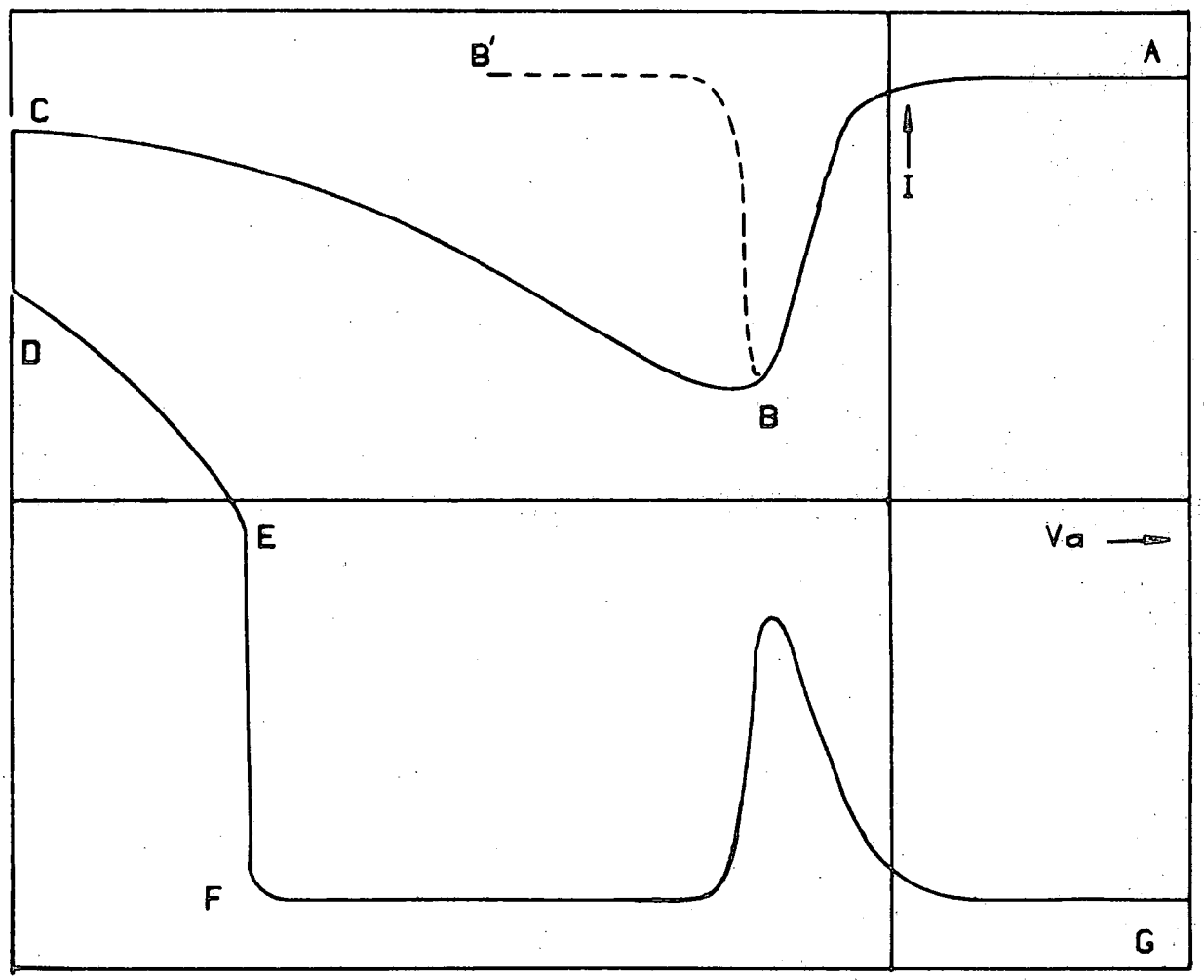

FIG. 7.5(a) A Typical Fast Ramp I-V Plot

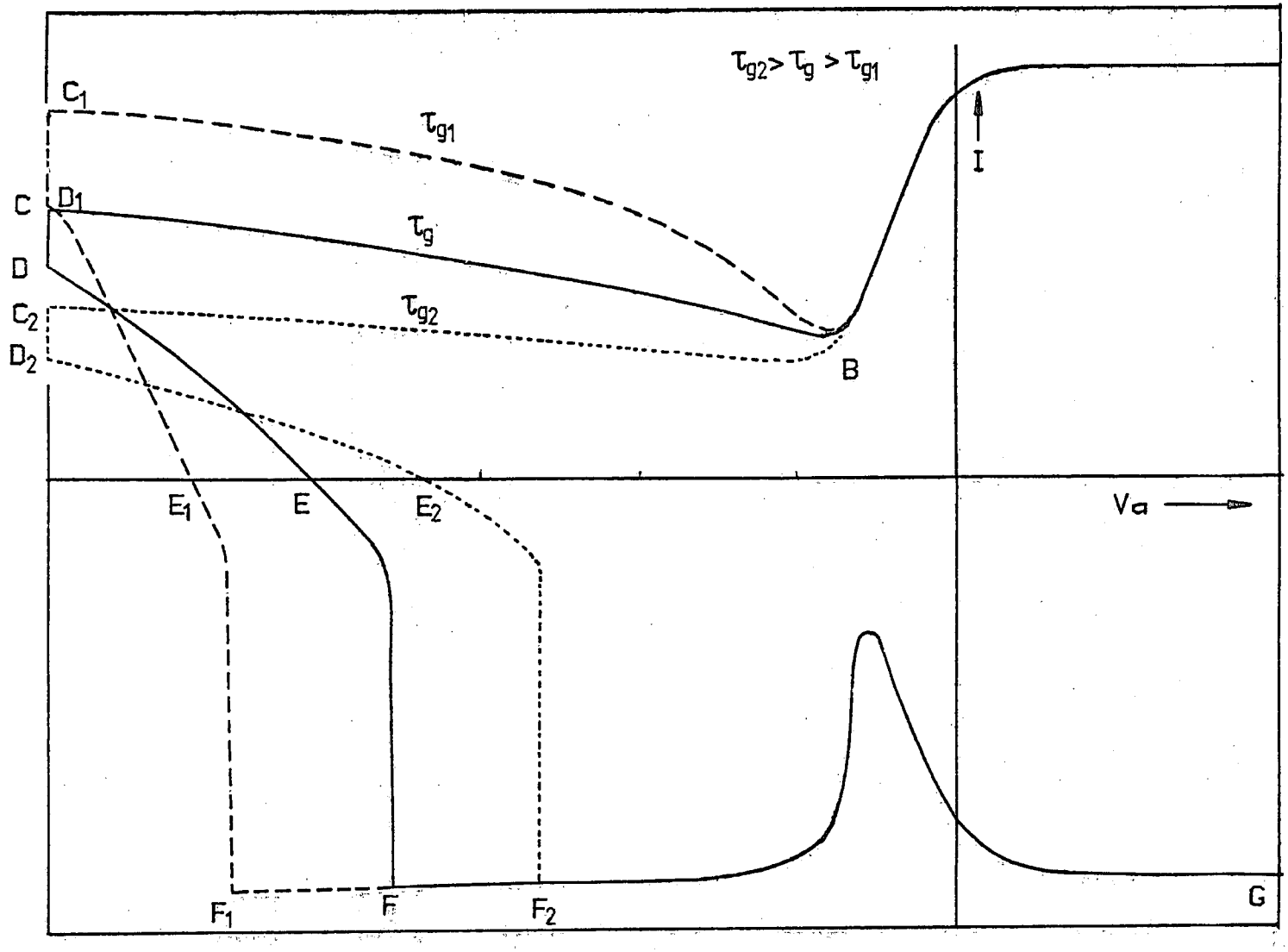

FIG. 7.5(b) The Fast Ramp Plots for n-type MOS Capacitor with Different τ_g's

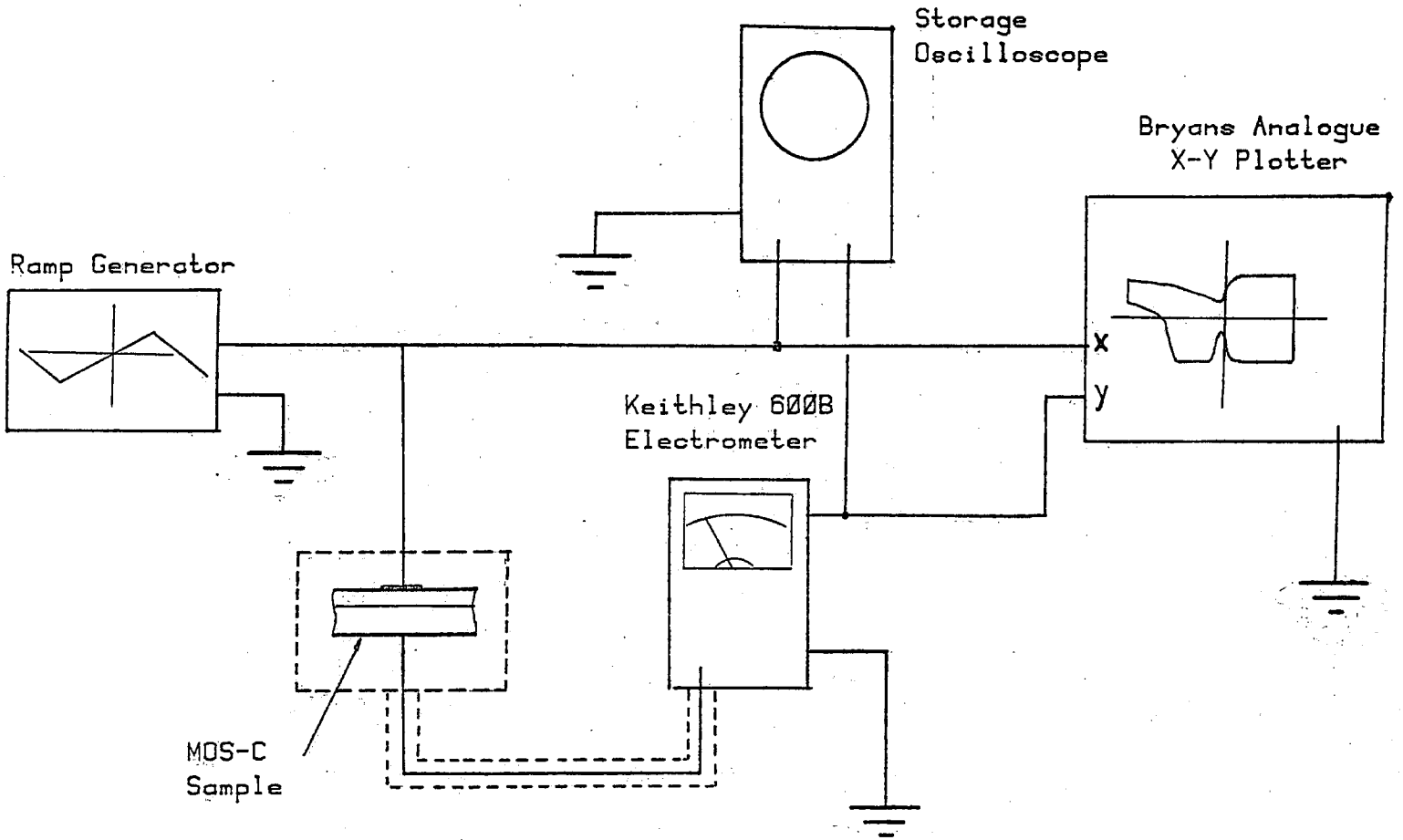

FIG. 7.6 Experimental set-up for Fast Ramp Measurements

from a high frequency C-V measurement. The minority carrier lifetime was obtained by comparing the theoretical plots with the experimental ones. The value of τ_g was changed until the best fit was obtained. The results shown in Table 7.2 and in Figures 7.7(a) and 7.7(b) are for both n- and p-type samples NI-1 and EN-1 respectively.

By this method although the theory fits very well to the experimental plots for the forward going voltage ramp, where the depletion widths are widening, the deviation from the experiment was obvious on the reverse ramp. This may be explained by the fact that as the depletion width collapses, the recombination processes becomes more significant but was not taken into consideration in the theoretical expression, and hence the error. Since the lifetime was obtained by numerical calculation, the method is therefore not easily performed for the purpose of τ_g determination. The main source of uncertainty is in deciding when the best fit is obtained, since this is very subjective.

In spite of these disadvantages the fast ramp experiment is easily set up as its instrumentation is similar to the Q-t method except that it requires a voltage ramp generator instead of the simpler voltage step generator. The comparison as to how well the values of τ_g obtained by this method agree with the Q-t measurement will be discussed in the following chapter.

Sample	τ_g	S
p-type ITT521	66.1 μs	0.16 cm s^{-1}
" ITT523	70.0 μs	0.27 "
" ITT135	65.0 μs	0.25 "

TABLE 7.1 Results obtained from C-t Method

Sample	N_a or N_d (cm^{-3})	τ_g
n-type NI-1	6×10^{14}	6.0 μs
p-type EN-1	7×10^{14}	16.0 μs

TABLE 7.2 Results Obtained by the Fast Ramp Method

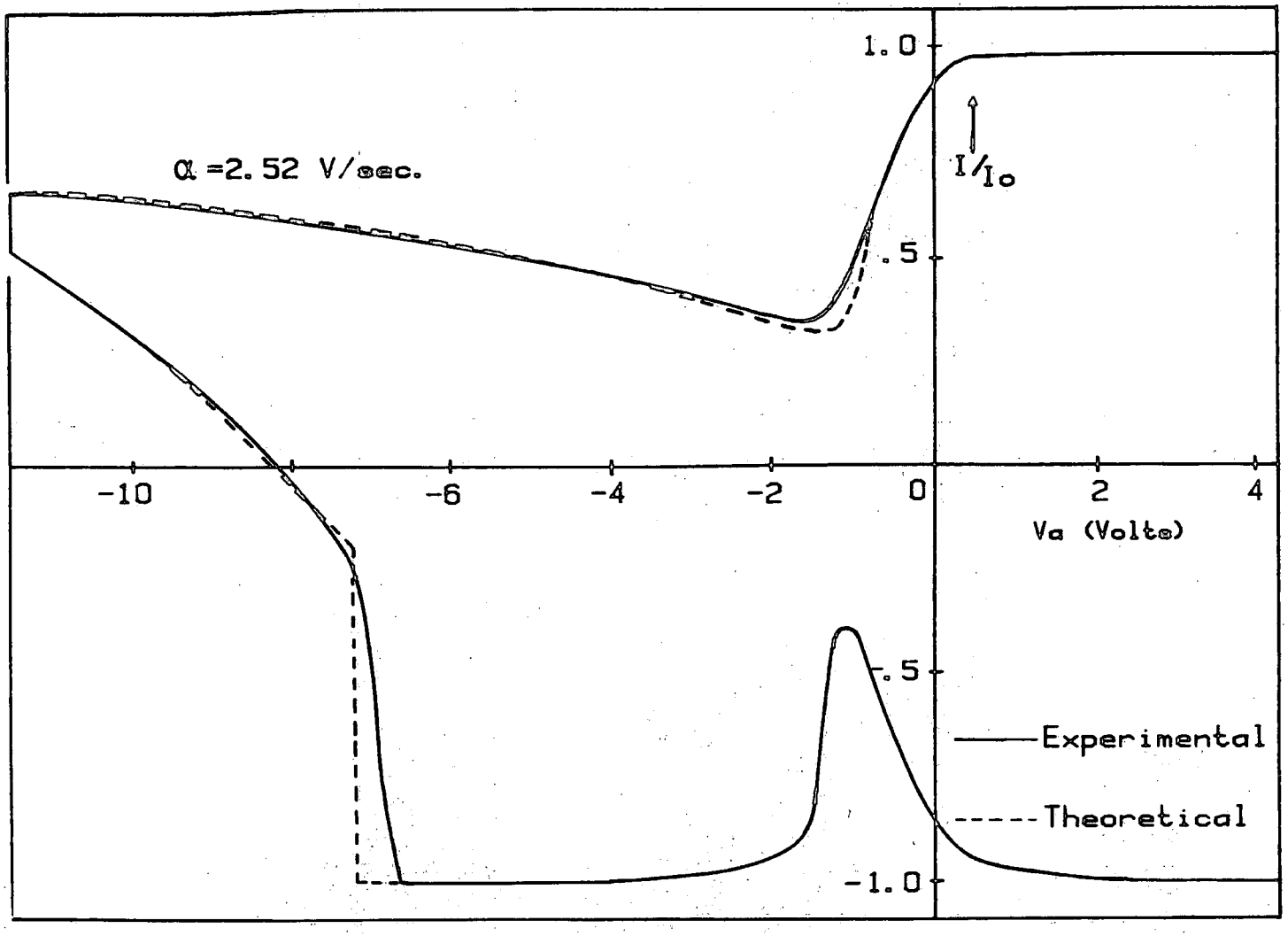

FIG. 7.7(a) Fast Ramp I-V Characteristic for n-type Sample NI-1

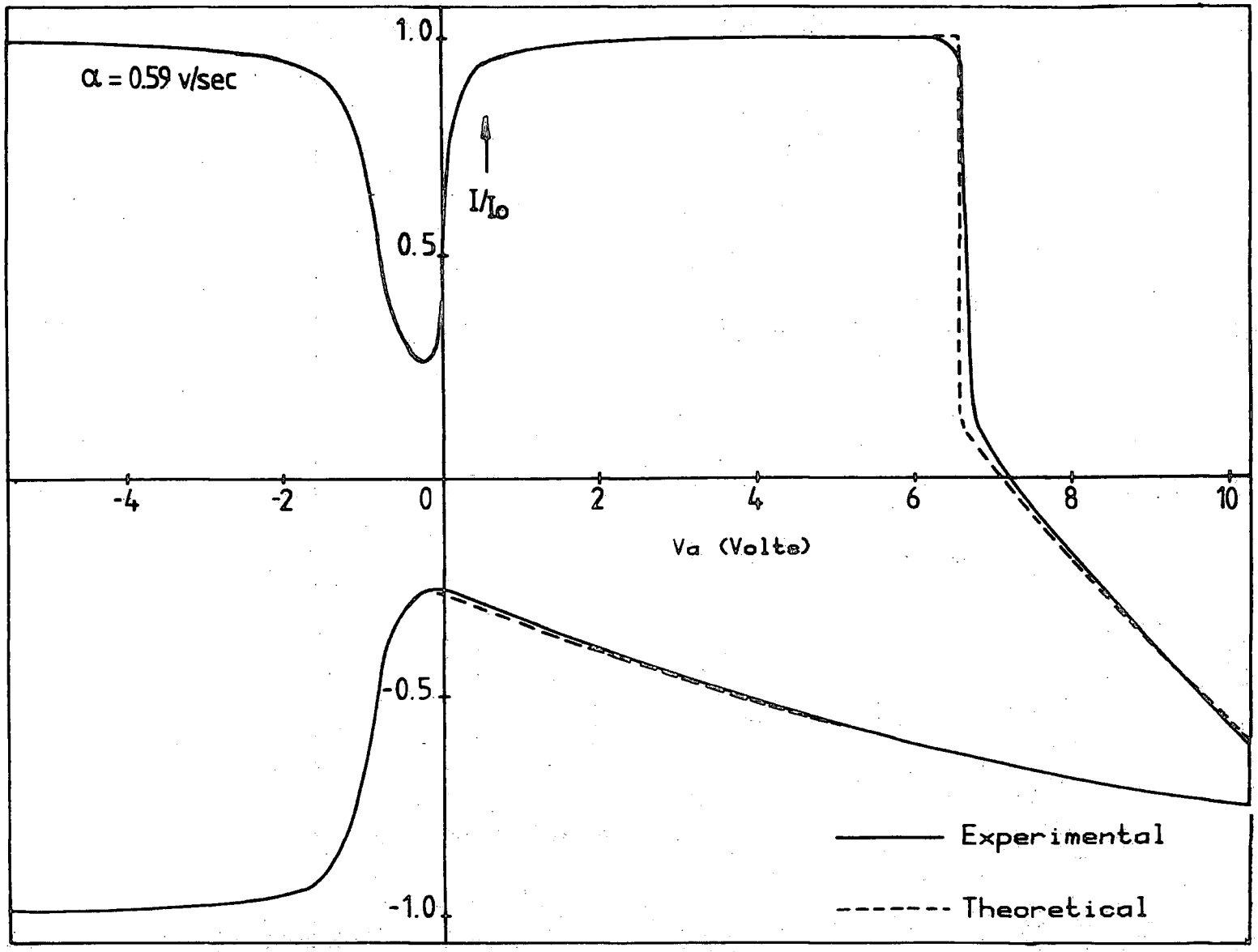

FIG. 7.7(b) Fast Ramp I-V Characteristic for p-type Sample EN-1

CHAPTER 8

ANALYSIS AND DISCUSSION

8.1 Introduction

The theme of the work in this thesis is in linking the small and large signal Q-t methods and others for the determination of the minority carrier lifetime both in theory and experiment. This includes the first work on both the theory and experimental result for the Q-t recombination transient.

In Chapter 4, the various effects on the Q-t transients were shown by typical experimental curves selected from well over five hundred obtained in this part of the investigation. In Chapters 6 and 7 the values of τ_g were obtained by other methods for a few of these samples. In this chapter the corresponding values of the generation lifetime τ_g are calculated using the theory developed in Chapter 5 and compared with those obtained by other Q-t methods and also with the methods described in Chapters 6 and 7. Finally the recombination lifetime, τ_r, is calculated using the new theory developed in this work.

8.2 Comparison of Theoretical and Experimental Results

In this section the theory developed in Chapter 5 will be evaluated to see how it compares with the experimental results. The comparison is made with regard to the actual transient shape, the initial charge increment, and the effect of changing the voltage step. For the voltage step effect, the trend for the variation of the transient shape is also compared with theory. In Section 8.2.3(b) the

present theory and experiment will be compared for the reverse step Q-t transients.

8.2.1 The Generation Layer Width

The first thing to determine in evaluating the theoretical plots is the effect of different assumptions about various parameters put into the theory. These are mostly in the expressions for the generation width and the generation rate.

The generation current is definitely proportional to the generation width x_{gen} in the silicon. However the expression chosen for x_{gen} differs in the various previous publications on MOS transients. The following expressions have been used in different papers :-

$$x_{gen1} = \sqrt{\left(x_d^2 - \frac{x_{do}^2}{2}\right)} - \frac{x_{do}}{\sqrt{2}} \qquad (8.1)$$

$$x_{gen2} = x_d - x_{do} \qquad (8.2)$$

$$x_{gen3} = x_d - \frac{x_{do}}{\sqrt{2}} \qquad (8.3)$$

and $$x_{gen4} = x_d \qquad (8.4)$$

where x_{gen1} is the generation width used by Rabbani and Lamb (12)

x_{gen2} is that of Zerbst (1)

x_{gen3} is that of Simmons and Wei (2)

and x_{gen4} is that of Hofstein (21)

In this comparison only the first three generation layer width expressions will be considered because the last one obviously gives the absolute generation without considering recombination, and this is essential for the sample ever to approach equilibrium. The generation widths 8.1 to 8.4 are compared in Figure 8.1.

Figure 8.2(a) shows theoretical Q-t plots evaluated using the different generation layer widths for a value of τ_g of 20 μs. It is found that x_{gen2} gives the slowest response because it has the lowest value and the smallest net generation current at any time up to saturation. The expression x_{gen1} produces a steeper rise in the transient and with x_{gen2}, a shape which converges for large values of time. This is because these two generation widths become zero as x_d approaches x_{do}, the equilibrium depletion width. The generation width x_{gen3} is the largest of the three and so its Q-t transient has the steepest gradient at any time. In contrast to x_{gen1} and x_{gen2}, this value does not produce a converging transient because it does not become zero as x_d approaches x_{do}, but converges to a finite value of $\left(1 - \frac{1}{\sqrt{2}}\right) x_{do} = 0.29\ x_{do}$.

Between the first two generation widths the first expression is more favourable because it takes into consideration the extra bending of the energy bands at the surface when the MOS capacitor is out of equilibrium. It is for this reason that x_{gen1} is used in the present theory for the Q-t transient.

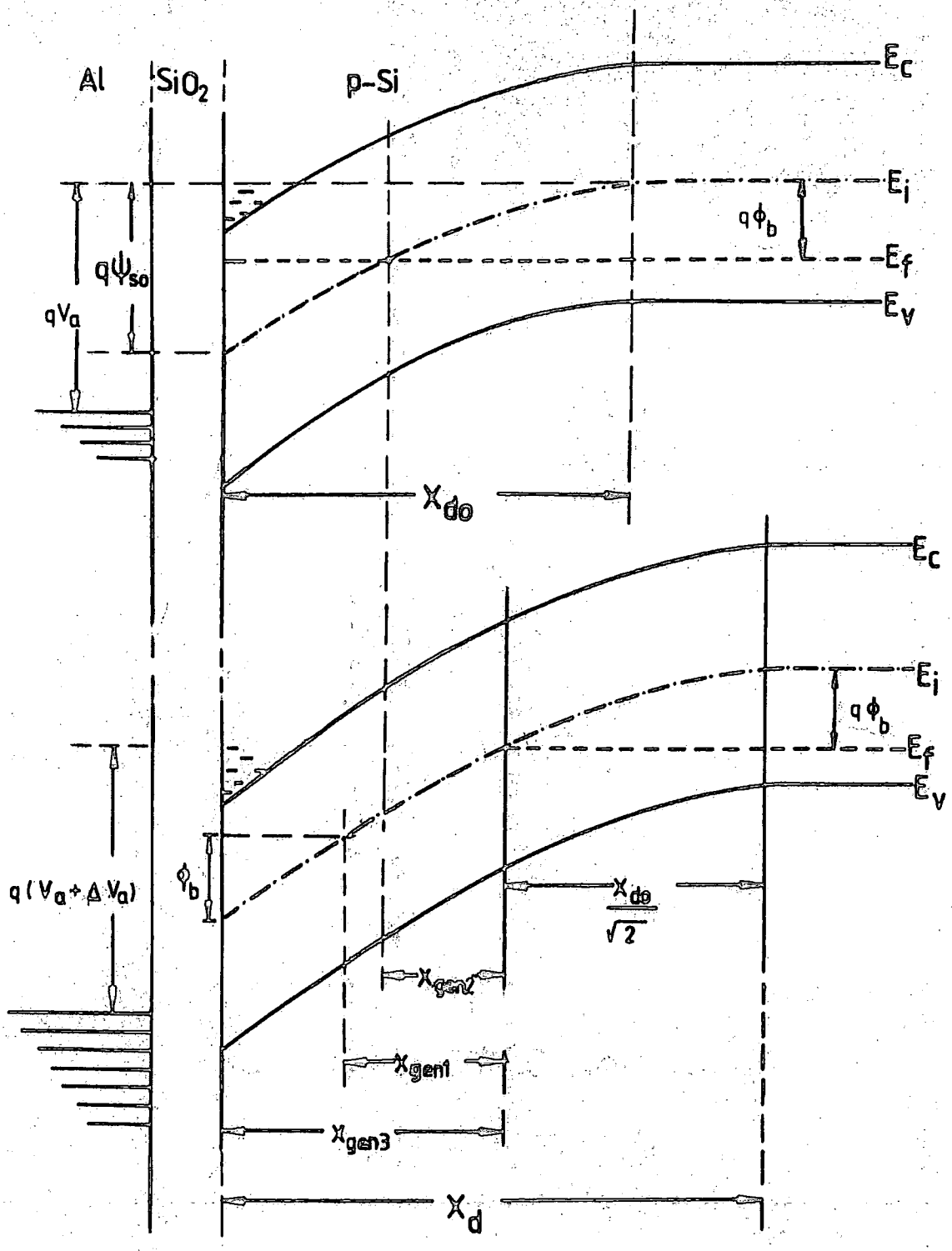

FIG. 8.1 Energy Band Diagram of an MOS Capacitor Showing Various Generation Regions

8.2.2 The Generation Rate Expression

The generation rate of carriers is given in general by the expression (31)

$$U_g = \frac{\sigma_p \sigma_n V_{th} N_t (pn-n_i^2)}{\sigma_n \left[n + n_i e^{(E_t-E_i)/kT}\right] + \sigma_p \left[p + n_i e^{(E_i-E_t)/kT}\right]} \qquad (8.5)$$

where σ_n, σ_p are the capture cross-section for holes and electrons

N_t is the trap density

E_t is the energy of the trap level

V_{th} is the thermal velocity of the electrons.

In the generation layer of the depletion region $p,n << n_i$ and taking $\sigma_p = \sigma_n = \sigma$, and traps at the middle of the energy band gap, Equation (8.5) becomes

$$U_g = \sigma V_{th} N_t \frac{n_i}{2} \qquad (8.6)$$

or $$U_g = \frac{n_i}{2\tau_g} \qquad (8.7)$$

where $$\tau_g = \frac{1}{\sigma U_{th} N_t}$$

In the work of Hofstein and of Zerbst the generation rate expression is

$$U_g = \frac{n_i}{\tau_g} \qquad (8.8)$$

although it is used without justification and appears to be incorrect. However, Equation 8.7 and 8.8 were both used in the present theory and the Q-t transients obtained are compared in Figure 8.2(b) for a lifetime value of 20 μs. The transient with U_g from Equation 8.8 shows a steeper rise as expected. For the subsequent analysis of the experimental results the expression 8.7 is used following the work of Collins et al (3,4) where it was shown that the generation rate never reached the value $\frac{n_i}{\tau_g}$ but only $\frac{n_i}{2\tau_g}$.

8.2.3 Voltate Step Magnitudes

Using the theory developed in Chapter 5 and the appropriate expression for the generation current obtainable from Sections 8.2.1 and 8.2.2, the Q-t transients were calculated for both forward and reverse voltage steps of different magnitudes for a given value of τ_g. These plots are normalised for the purpose of comparison in Figures 8.3 and 8.5. For the forward transient, voltage steps of 25 mV, 50 mV, 100 mV, 1 V, 2 V, and 5 V were used but for the reverse transient the voltage step cannot be as big as explained in Chapter 5, so steps of up to 1 V only were used so as to make a physically acceptable analysis. The forward transient will be discussed first in the following section. For all the calculations here the value of τ_g used was 20 μs.

(a) The Forward Voltage Step Transient

From the normalised theoretical Q-t transients of Figure 8.3 it is seen that the ratio, $\frac{Q_{o+}}{Q_{max}}$, of the initial charge at t = o+ to the maximum charge, decreases with increasing voltage step. The initial charge, Q_{o+} was plotted against the voltage step ΔV_a in Figures 8.4(a) and 8.4(b) for small and for larger voltage ranges respectively. In

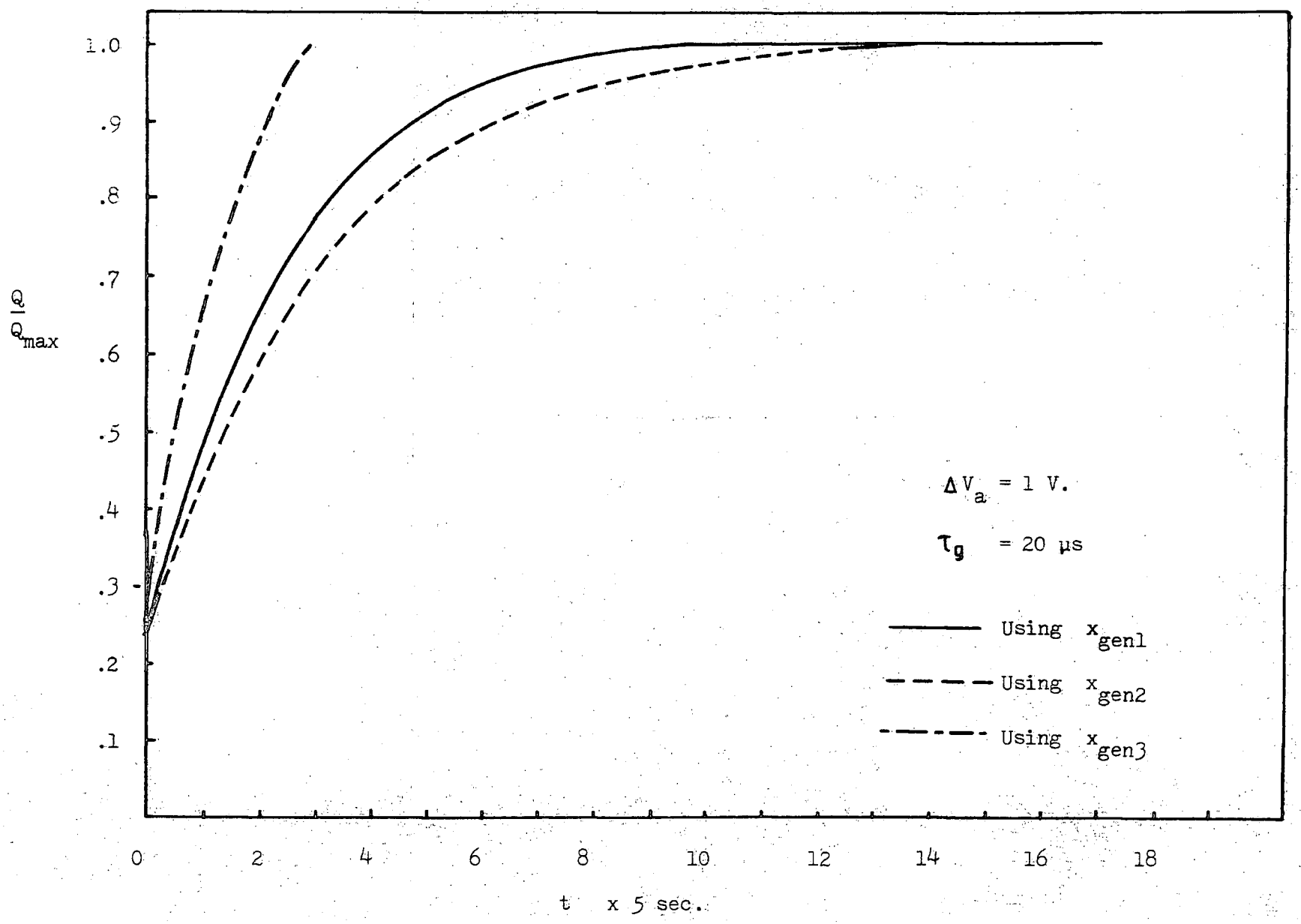

FIG. 8.2(a) EFFECT OF THE GENERATION WIDTH EXPRESSION ON THE THEORETICAL Q-t TRANSIENT

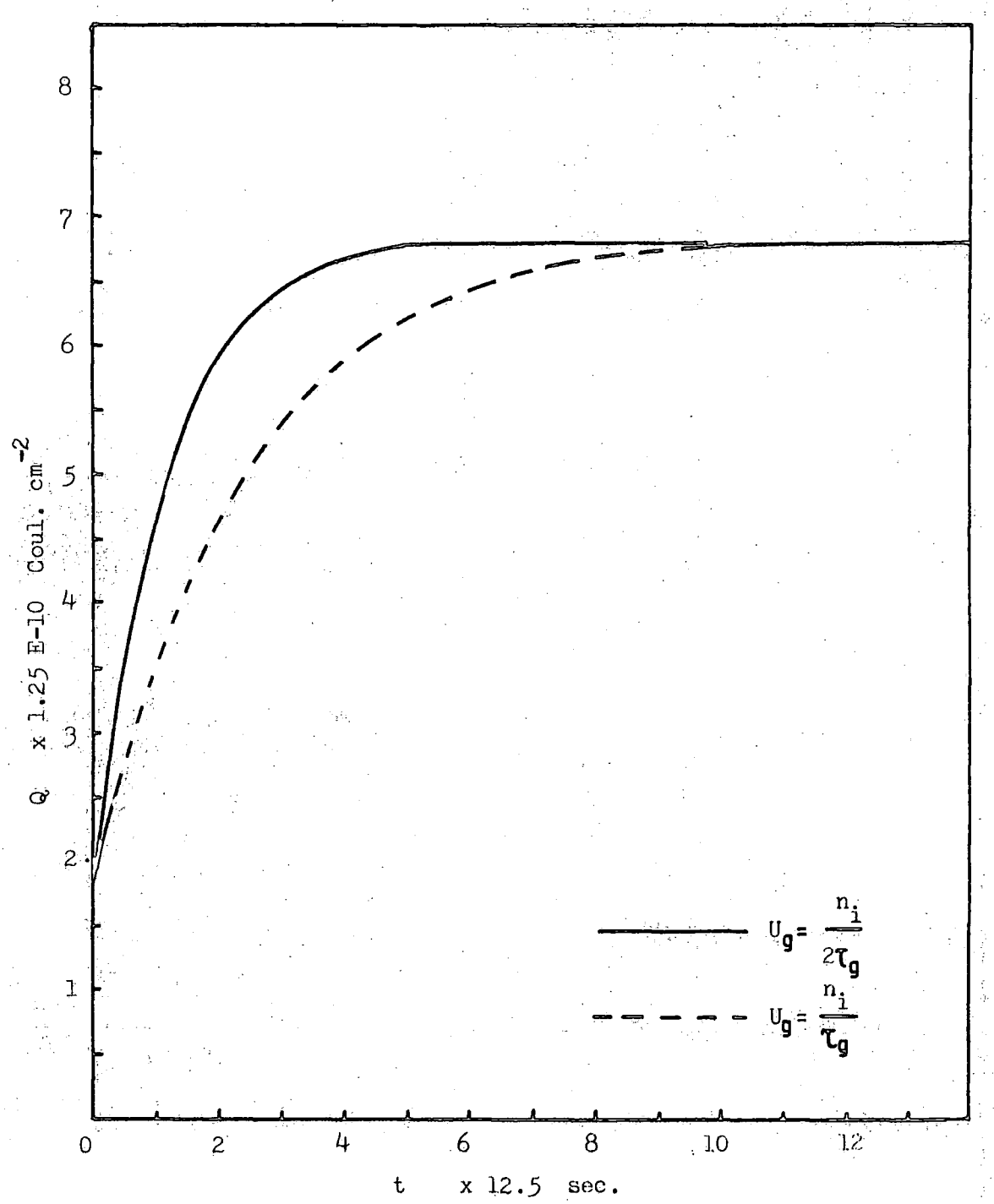

FIG. 8.2(b) THE THEORETICAL Q-t PLOTS FOR DIFFERENT EXPRESSIONS OF THE THE GENERATION RATE

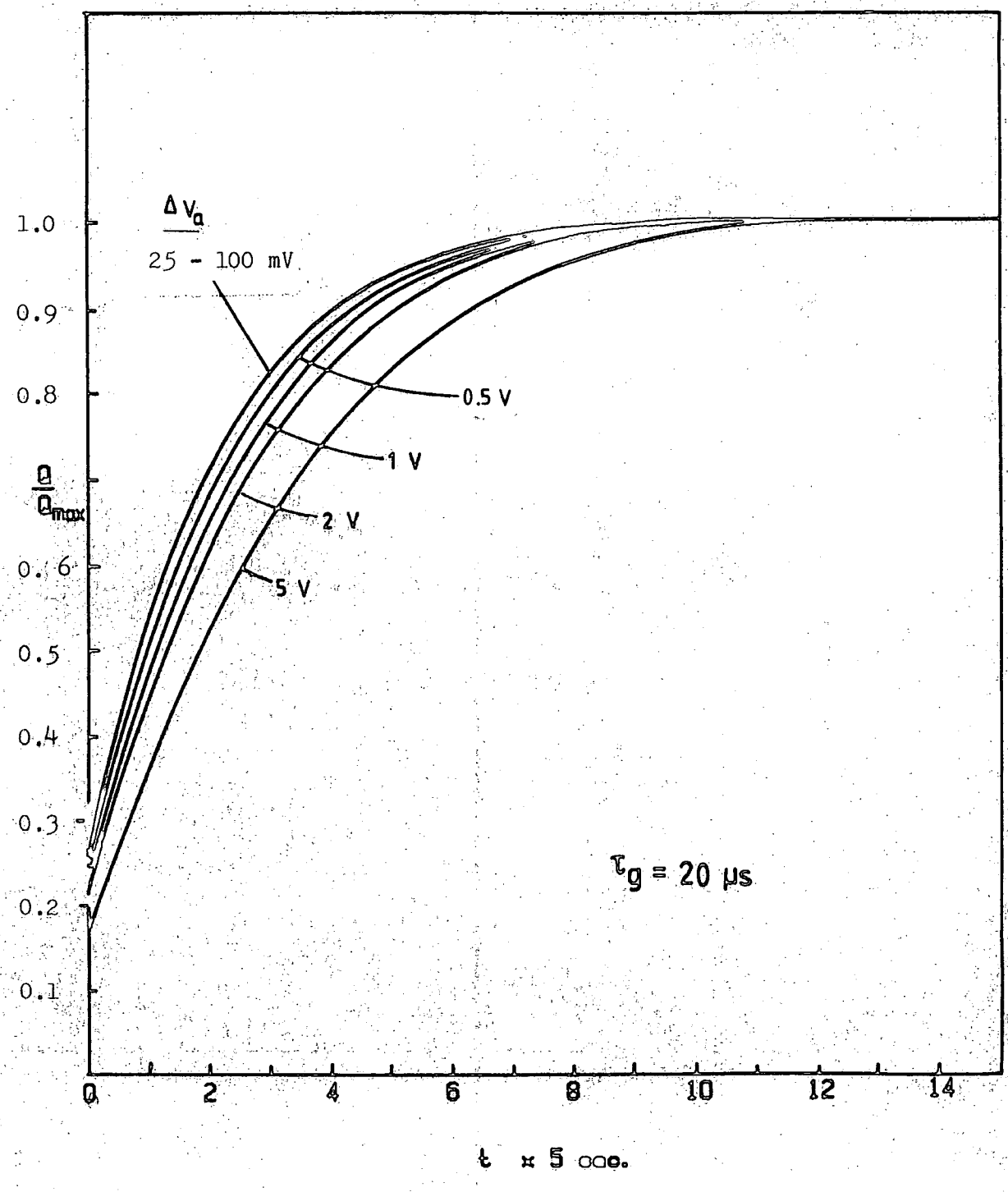

FIG. 8.3 Normalised Theoretical Q-t Plots for the Forward Voltage Steps.

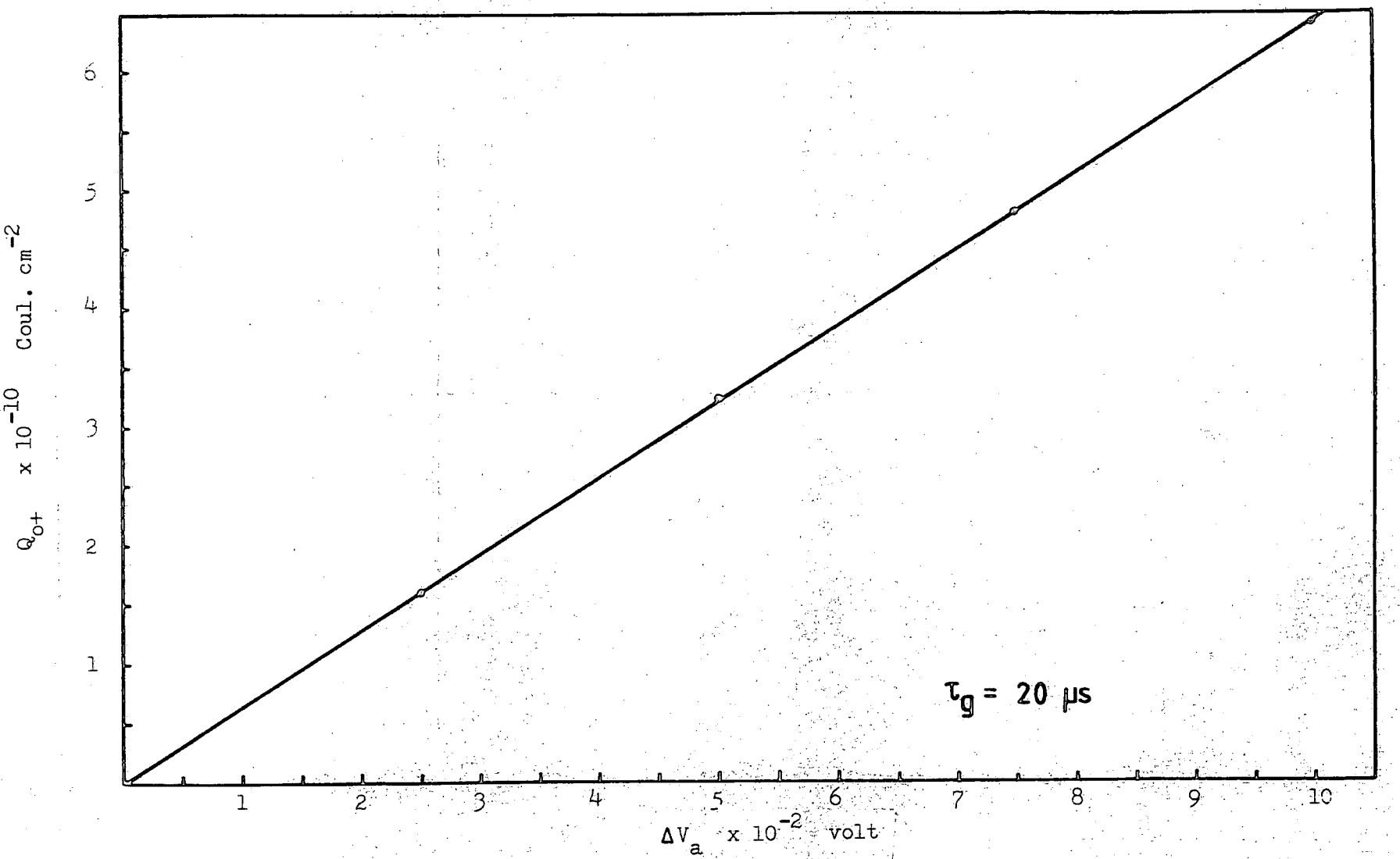

FIG. 8.4(a) Theoretical Plot of Q_{o+} versus Voltage Step
(for small voltage steps)

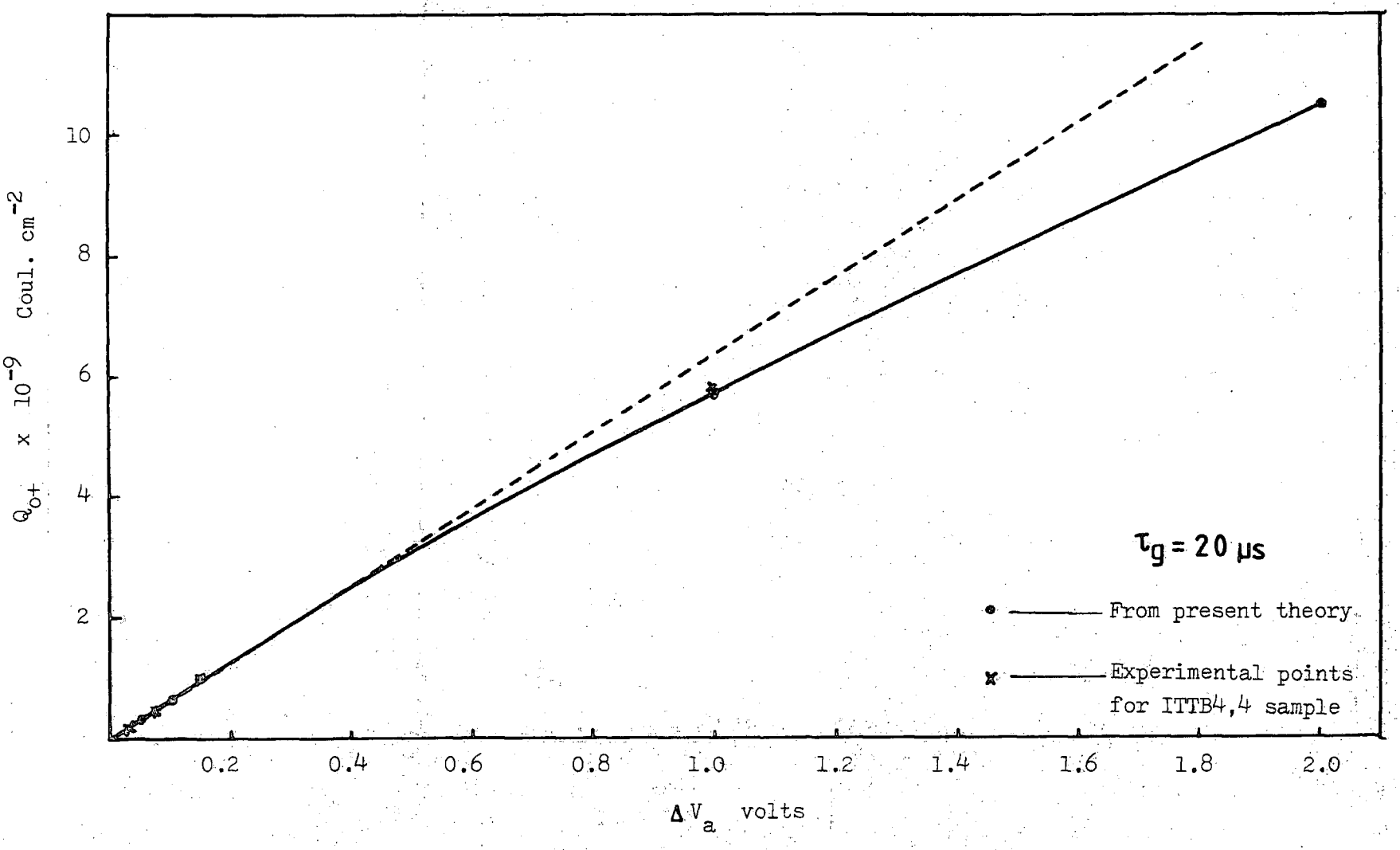

FIG. 8.4(b) THEORETICAL AND EXPERIMENTAL PLOTS OF Q_{o+} VERSUS VOLTAGE STEP
(FOR LARGE VOLTAGE STEPS)

Figure 8.4(a) the voltage step was kept to less than 100 mV. Within this range of voltage step the initial charge increment is proportional to the increase in the voltage step. When the voltage step was further increased to 2 V as in Figure 8.4(b), the increment in Q_{o+} becomes less than proportional to the voltage step increment. This agrees well with the experimental results given in Section 4.3. The experimental results for sample ITTB4,4 are compared with the theoretical plot of Figure 8.4(b) which shows that the experimental points on the graph agree very well with the theory.

Also in Figure 8.3, it is seen that the normalised Q-t transients for voltage steps of 25 mV to 100 mV are very close. This indicates that for the small voltage step range, the increase in charge at any time, is almost proportional to the voltage step increment. However, as the voltage steps were further increased this proportional behaviour does not hold any longer. For larger voltage steps, the charge increment of the forward transient is generally less than proportional to the voltage step increment, except when the final equilibrium is approached, thus giving a slower transient response. This behaviour was also found in the experimental results. The physical reason is that the change of depletion width is less than proportional to the step magnitude when the latter is appreciable. Thus the relative generation current is reduced for large steps and a longer time is required to generate the required charge.

(b) The Reverse Voltage Step Transient

For the reverse voltage step, the behaviour of the Q-t transient is different from the forward case. Figure 8.5 shows the normalised reverse transient for different voltage steps of up to 1 V. Similar to the forward transient, the curves for ΔV_a of 25 mV to 100 mV were very close again indicating approximate proportionality between the charge increment and the voltage step. Contrary to the forward transient condition the ratio of $\frac{Q_{o+}}{Q_{max}}$ increases with increasing voltage step (Figure 8.5). Also for larger steps the charge increment due to the increased voltage step is more than proportional to the step magnitude thus resulting in a faster Q-t response. This is because with larger steps there is more charge to recombine in a smaller depletion layer width, with the increased concentration increasing the recombination current.

For these reasons the difference between the forward and the reverse Q-t transient is more pronounced for large signal Q-t measurements as shown in Figure 8.6.

8.3 Comparison of Results using the Present Q-t Theory and Other Methods

In this section, the value of τ_g is evaluated for typical samples by applying the present theory to the experimental Q-t transient. The values of the lifetime are then compared with those obtained by other Q-t methods. As the method of Hofstein was the simplest to perform, this was chosen as a basis for comparison against other methods and the present theory. Hofstein's method is only valid for small voltage steps and many of the measurements performed were of this type, including all those for the reverse step

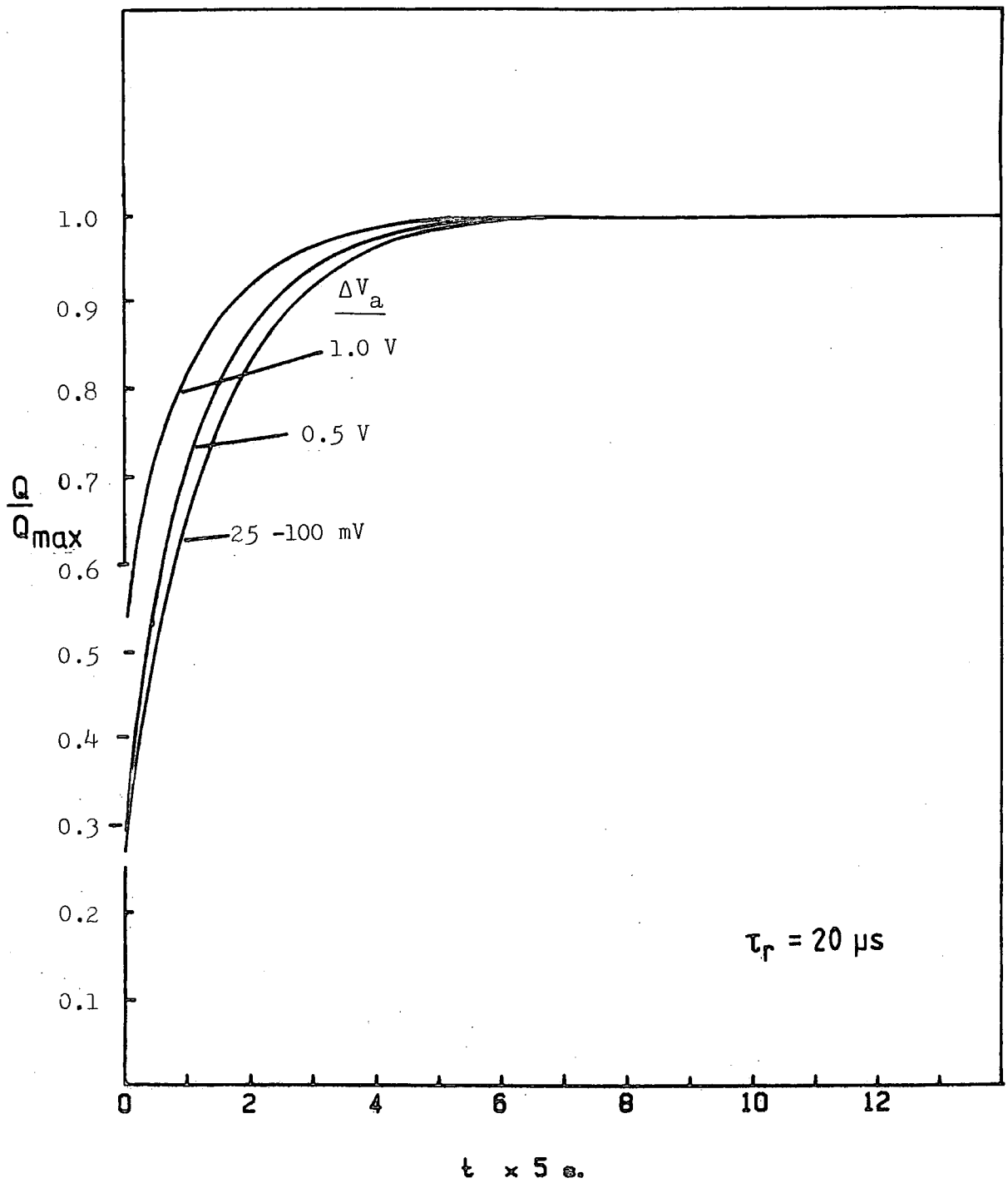

FIG. 8.5 Normalised Theoretical Q-t Plots for the Reverse Voltage Steps.

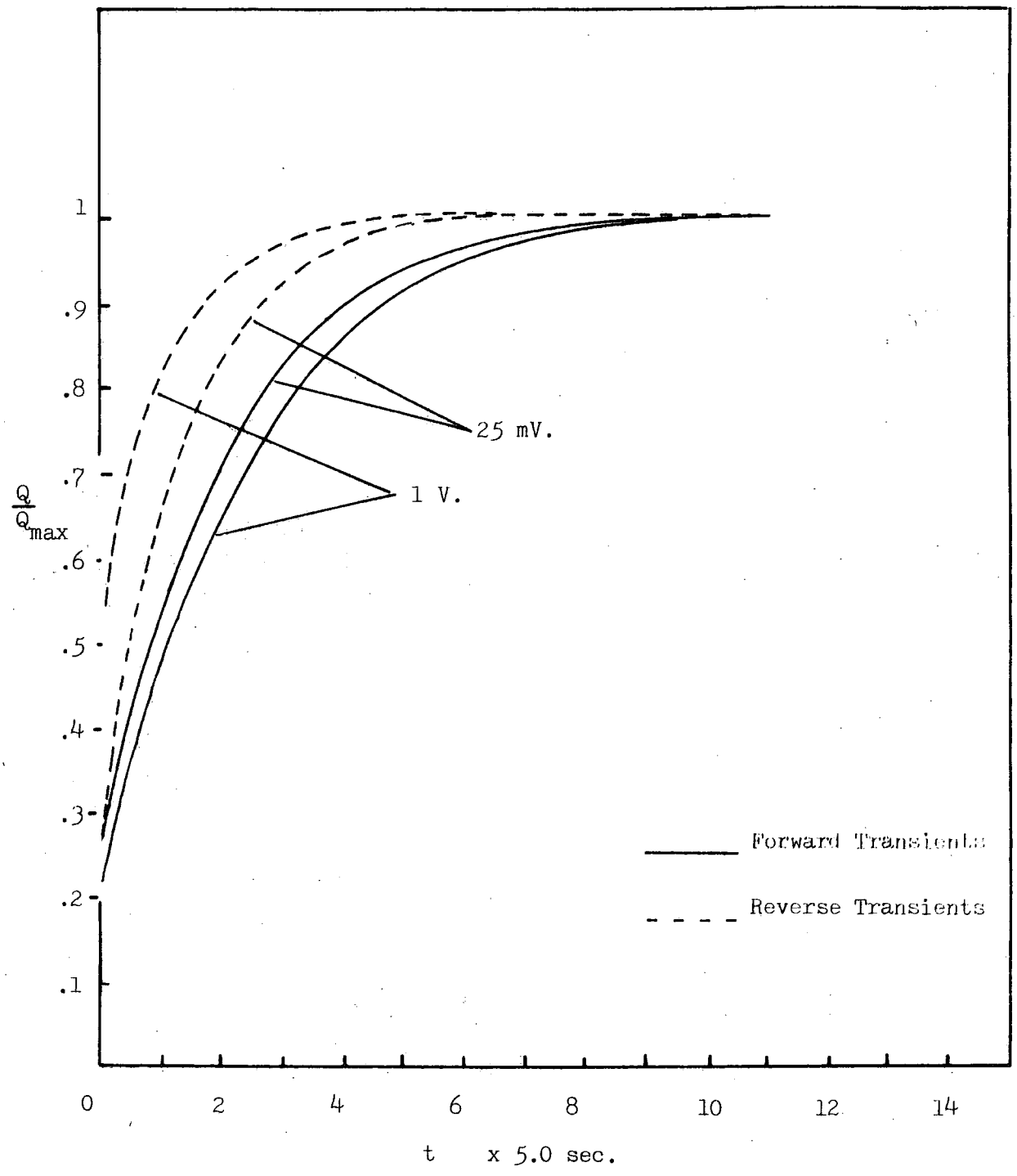

FIG. 8.6 COMPARISON OF THE THEORETICAL Q-t TRANSIENTS FOR THE FORWARD AND REVERSE VOLTAGE STEPS OF 25 mV AND 1 V. (τ_g = 20 μs)

transient which are restricted to relatively small signal in the present theory.

A very large number of samples was used for Q-t measurements in this work and many hundreds of accurate transients were recorded. The results given in the thesis refer mostly to the small number of samples that were also used for measurements by the other techniques. Investigation of the other techniques was rather limited due to shortage of time and because they were peripheral to the main investigation on the Q-t method.

8.3.1 Evaluation of the Minority Carrier Lifetime by the Present Method

The lifetime was obtained from the experimental Q-t plots by comparison with theoretical Q-t plots for a range of values of τ_g obtained using the present theory. Before calculating a set of theoretical plots, the experimental Q-t transient is examined to get the value of the actual dopant concentration N_a, and the oxide capacitance per unit area, C_{ox}. These values are obtained from the value of the initial charge step Q_{o+} and the maximum charge increment Q_{max} by using the following equations.

$$N_a = \frac{Q_{o+}}{q\,\Delta x_{do+}}$$

and $$C_{ox} = \frac{Q_{max}}{\Delta V_a}$$

where ΔV_a is the voltage step magnitude

Δx_{do+} is the change in the depletion layer width at $t = o+$, which can be determined using Equation 5.27.

Using these values of N_a and C_{ox}, the theoretical Q-t curves were generated for a range of values of τ_g using the program described in Section 5.6. This method is shown applied to the Q-t transients for the p-type samples ITT135 and ITTG2 for which the theoretical and experimental plots are compared in Figures 8.7(a) and 8.7(b) respectively. The voltage step used was 25 mV in both cases. From these comparisons, the values of the lifetime τ_g are found to be 27.0 μs and 7.7 μs for the two samples.

The lifetime values for several other samples were also evaluated using the present theory and reasonable results were obtained. For the n-type sample TC3-8D3 and the p-type ITTAU2,2, the evaluation was carried out for the two voltage step magnitudes of 25 mV and 100 mV to test the accuracy of the larger signal theory. The theoretical and experimental plots are shown in Figures 8.8 and 8.9, and the results obtained are :

Voltage Step	TC3-8D3 (n-type)	ITTAU2,2 (p-type)
25 mV	2.2×10^{-8}s	2.5×10^{-6}s
100 mV	3.2×10^{-8}s	2.5×10^{-6}s

Again the values of the lifetime obtained are consistent with the actual transients. For the p-type ITTAU2,2 sample the values of τ_g for both 25 and 100 mV voltage steps are identical indicating that there is a uniform concentration of generation centres within the regions of the silicon measured.

For the n-type TC3-8D3 sample, the value of the lifetime apparently increases with the voltage step magnitude.

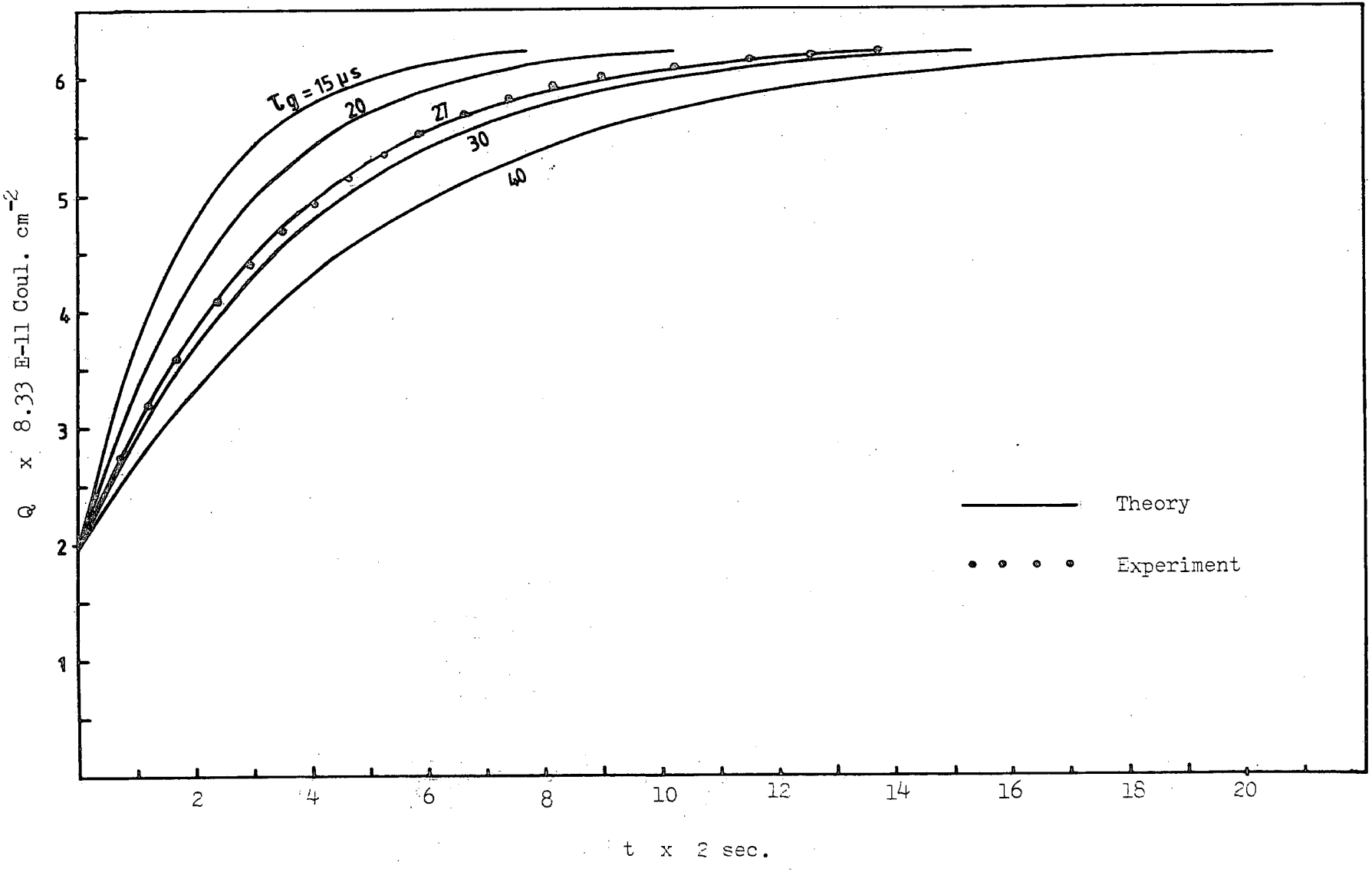

FIG. 8.7(a) Theoretical and Experimental Q-t Transients for ITT135 Sample (ΔV_a = 25 mV)

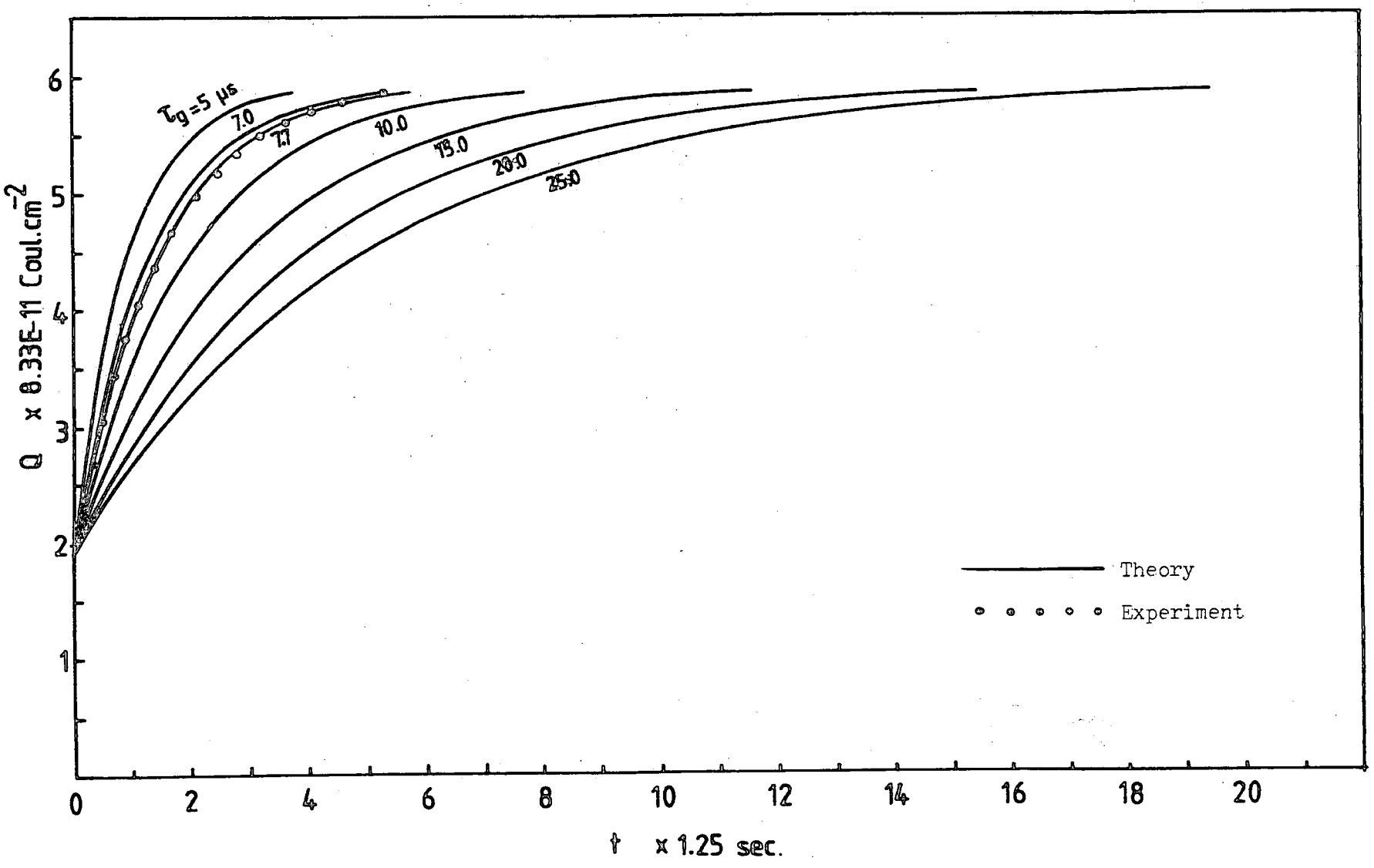

FIG. 8.7(b) Theoretical and Experimental Q-t Transients for ITTG2 Sample (ΔV_a = 25 mV)

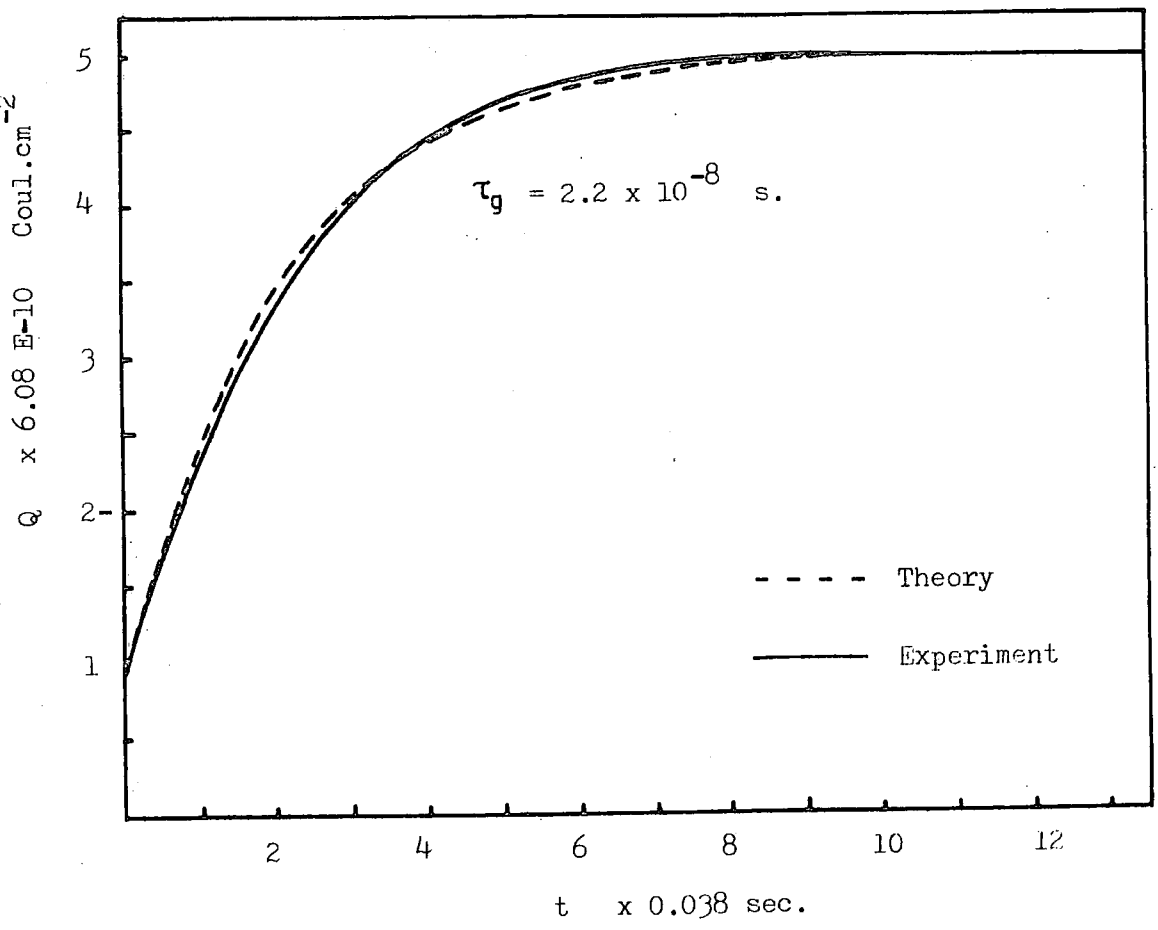

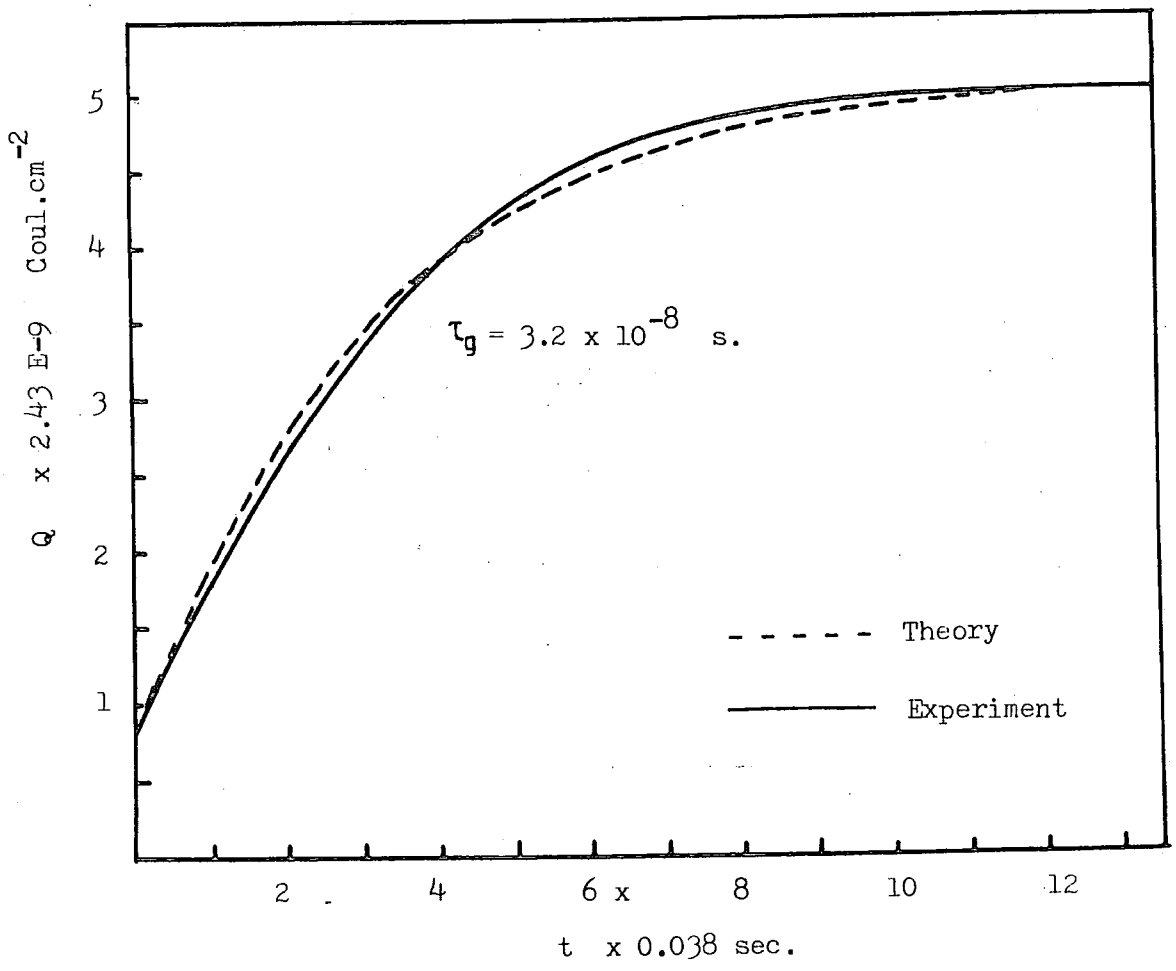

FIG. 8.8 The Theoretical and Experimental Q-t Transients for TC3-8D3 Sample
(a) ΔV_a = 25 mV
(b) ΔV_a = 100 mV

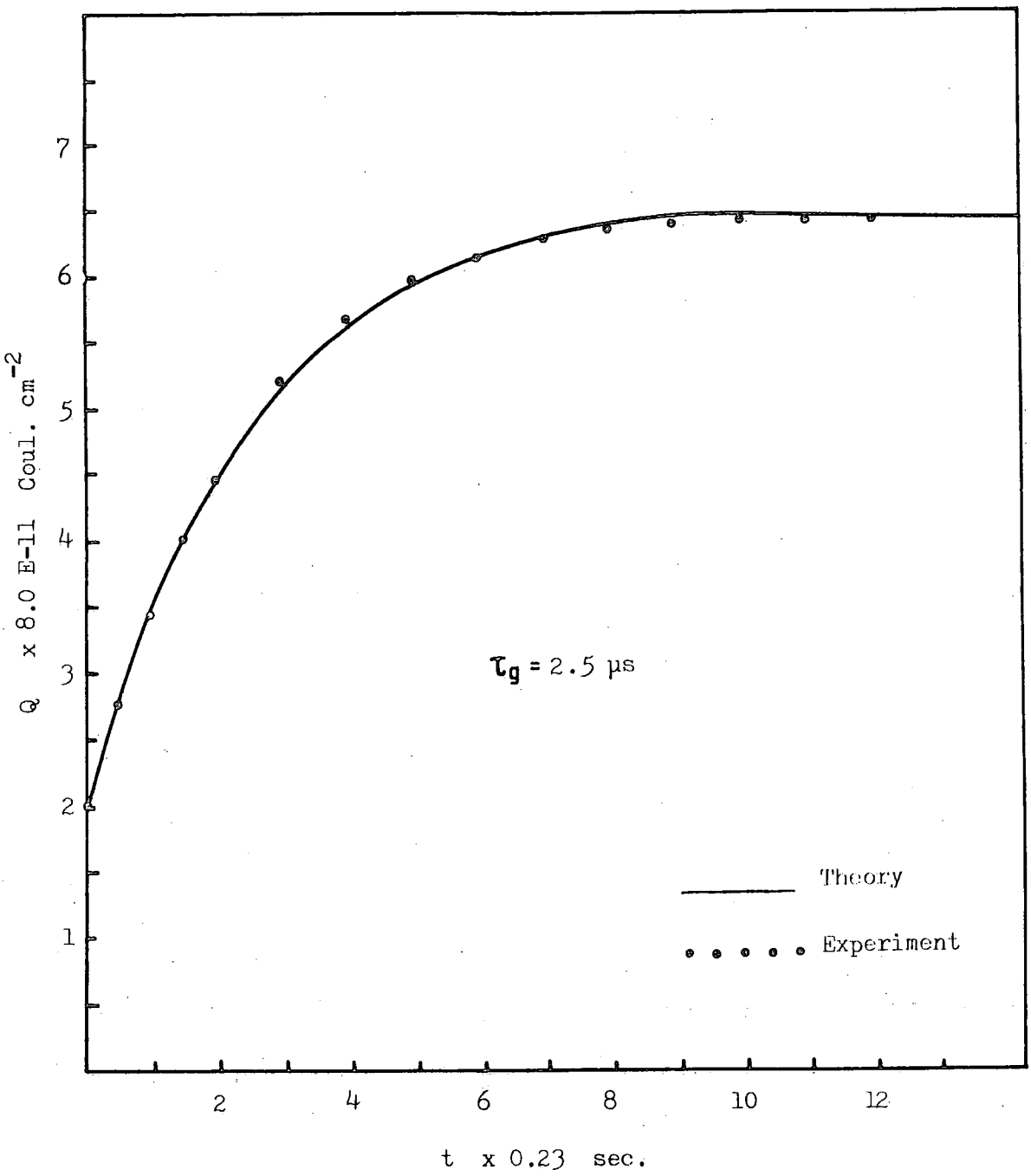

FIG. 8.9(a) The Theoretical and Experimental Q-t Transients for ITTAU2, 2 with ΔV_g = 25 mV

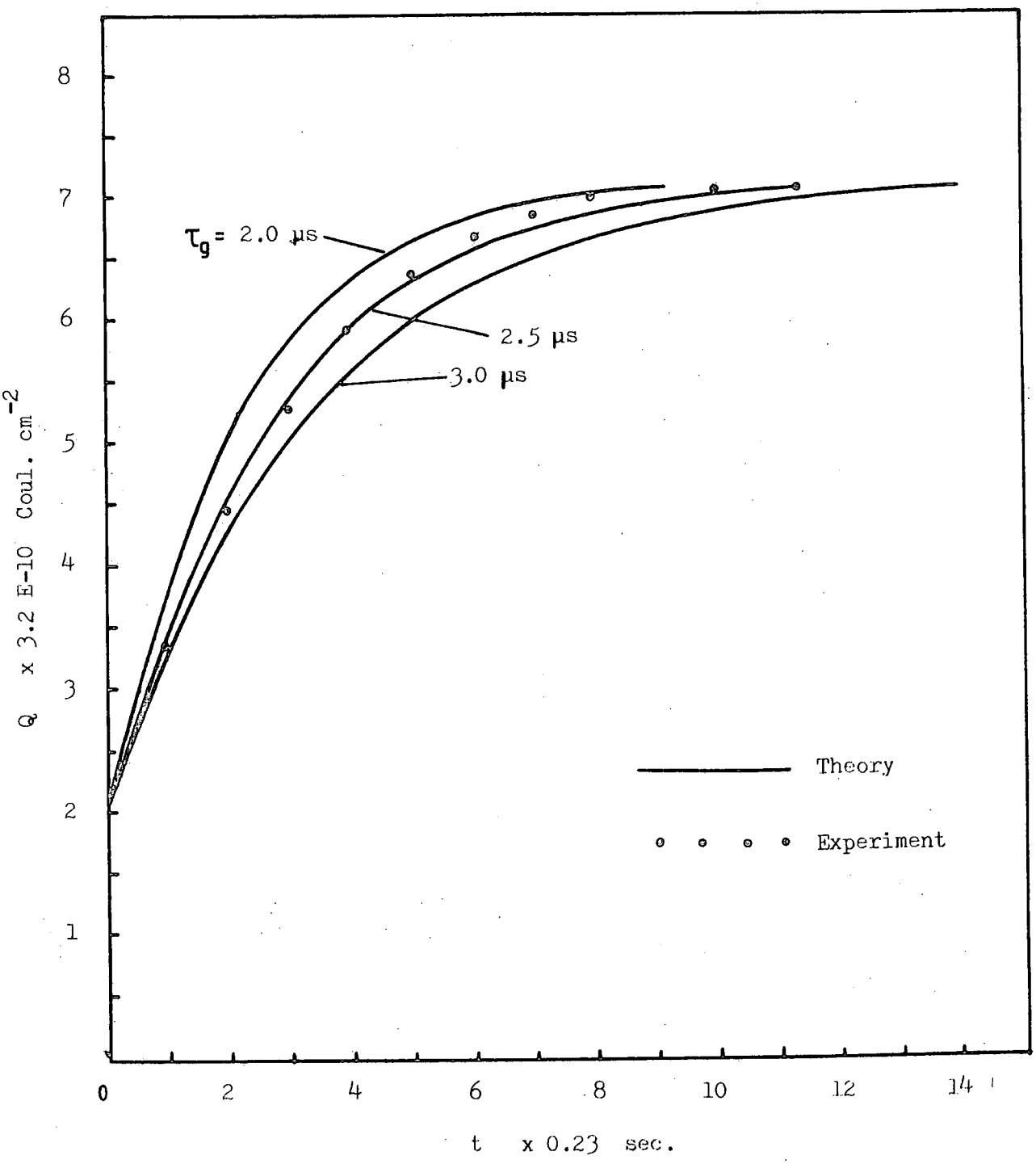

FIG. 8.9(b) The Theoretical and Experimental Q-t Transients for ITTAU2, 2 with ΔV_g = 100 mV

Assuming that the theory holds accurately, and using

$$\tau_g = \frac{1}{\sigma V_{th} N_t}$$

for mid-gap generation centres, this indicates that the generation centre concentration N_t, was higher at the surface. This, combined with a very low lifetime value, would not be surprising for an old sample made in Durham and almost certainly subjected to surface contamination.

8.3.2 Comparison with the τ_g Values from Other Q-t Theories

The results obtained in Section 8.3.1 were subsequently compared with those obtained using the other Q-t methods of analysis, i.e. those of Hofstein and Viswanathan and Takino (Figures 8.10 and 8.11). As Hofstein's method uses a different expression for the lifetime, a correction had to be made to the τ_g value for the final comparison. This comparison is given below for the 25 mV voltage step results

Sample	Hofstein's Method	Hofstein's Method (corrected)	Viswanathan and Takino	Present Theory
ITT135	79.5 μs	39.8 μs	13.7 μs	27.0 μs
ITTG2	19.4 μs	9.7 μs	3.3 μs	7.7 μs

It is seen that as expected Hofstein's method became closer to the present theory after correcting the generation rate expression. The method of Viswanathan and Tanino was found to be in error because of the small voltage step used (Figure 8.11) where the surface recombination velocity S is negative. For this reason the calculation of their method was repeated

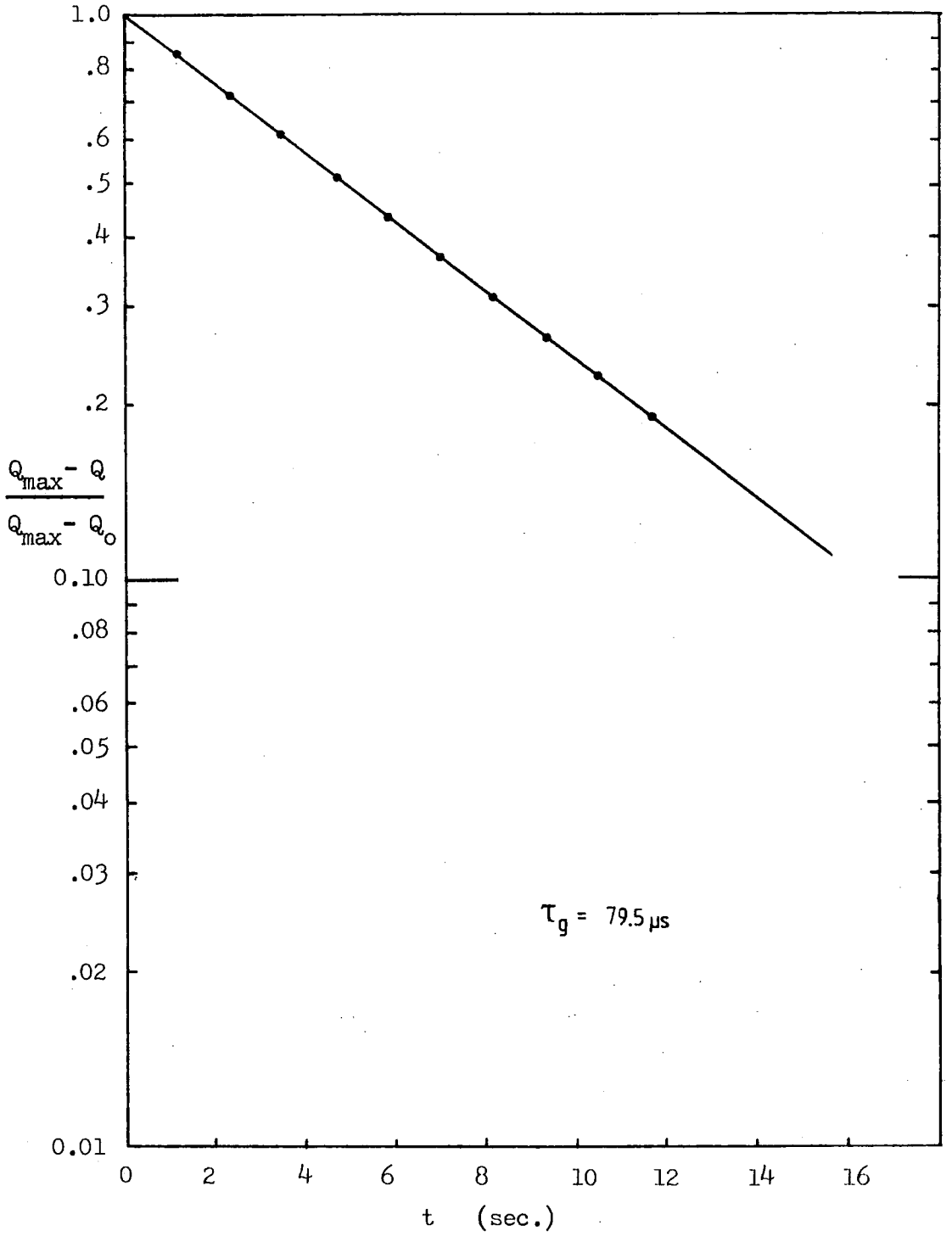

FIG. 8.10(a) LOG. PLOT FOR THE FORWARD TRANSIENT OF ITT135 WITH ΔV_a = 25 mV (FOR HOFSTEIN'S METHOD)

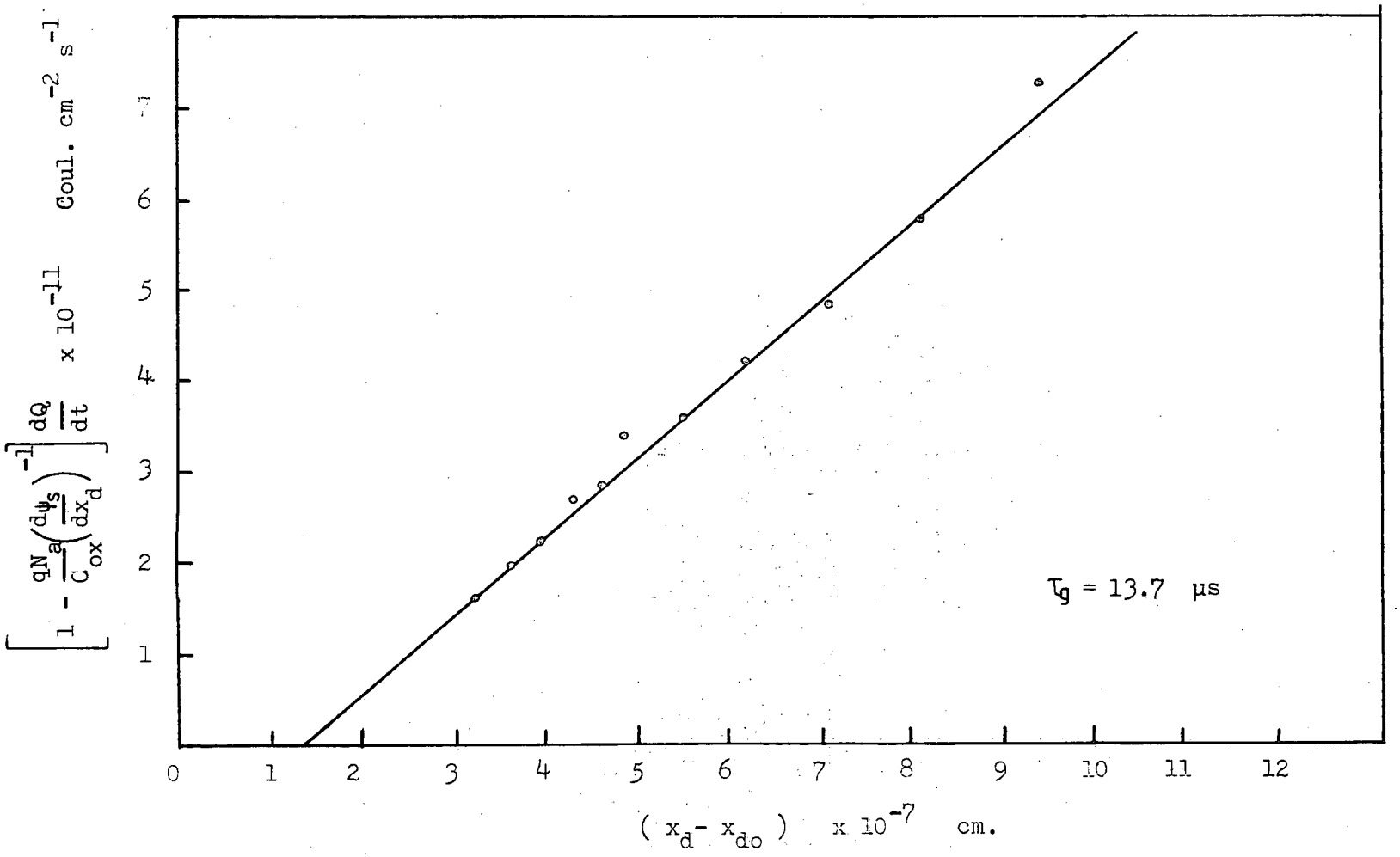

FIG. 8.10(b) THE PLOT FOLLOWING THE METHOD OF VISWANATHAN AND TAKINO FOR ITT135 SAMPLE WITH ΔV_a = 25 mV

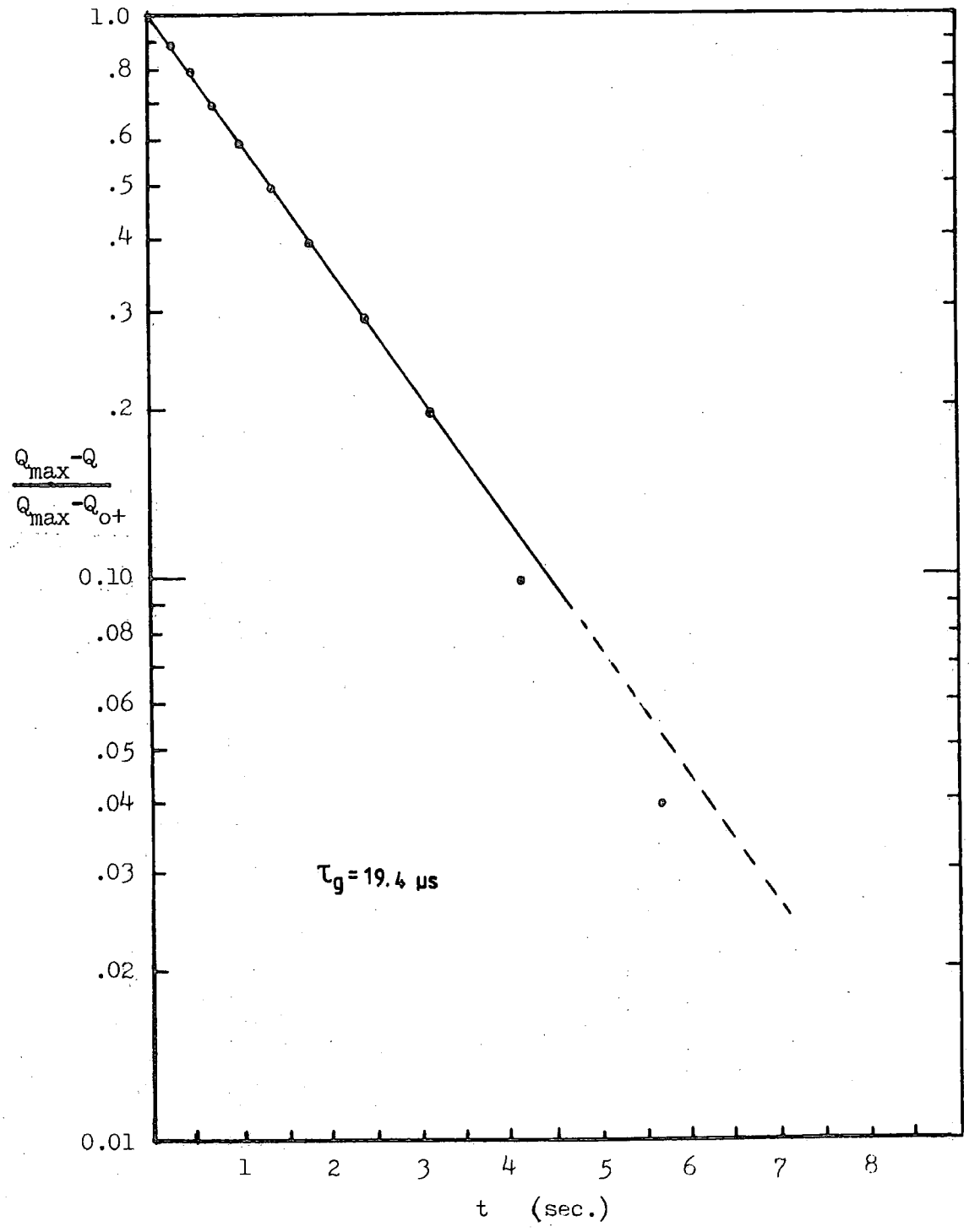

FIG. 8.11(a) LOG. PLOT FOR THE FORWARD TRANSIENT OF ITTG2 WITH $\Delta V_a = 25$ mV

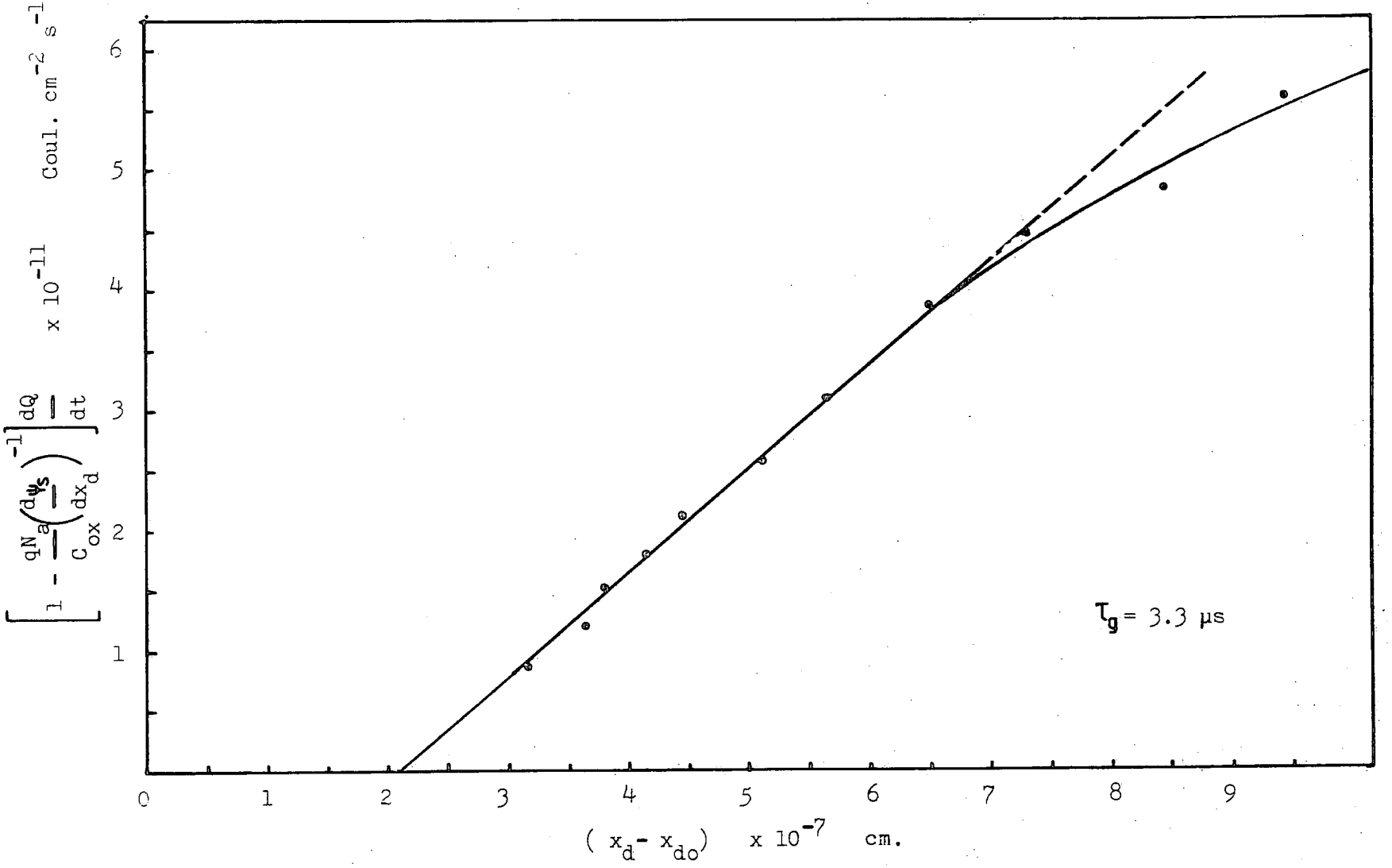

FIG. 8.11(b) THE PLOT FOLLOWING THE METHOD OF VISWANATHAN AND TAKINO FOR ITTG2 SAMPLE WITH ΔV_a = 25 mV

with a bigger voltage step of 0.2 V (Figure 8.12). Only the ITT135 sample was used in this evaluation. The new values of τ_g are as follows :

Sample	Hofstein's Method at 25 mV (with correction)	Viswanathan and Takino Mthd. at 0.2V	Present Theory at 0.2V
ITT135	39.8 μs	39.3 μs	38.0 μs

The result obtained was closer to the value from Hofstein's analysis and nearly three times the small signal value whereas using the present theory the result changes by only about 40%. This suggests that the present theory is more accurate in its ability to give a correct result for all step magnitudes.

Evaluating τ_g on other samples at different voltage steps according to the requirement of their theory (that is small steps for Hofstein's method and larger ones for the methods of Viswanathan and Takino and the present theory), the results are as shown in Figures 8.12, 8.13 and 8.14 and are summarised as follows :-

Sample	Hofstein's (corrected)	Viswanathan and Takino	Present Theory
ITTB4,4	71.3 μs	93.5 μs	75.0 μs
ITTAU2,2	2.7 μs	2.9 μs	2.5 μs
ITT135	39.8 μs	39.3 μs	38.0 μs

This shows that the present method is consistent in giving values of the lifetime in close agreement with other Q-t methods particularly Hofstein's.

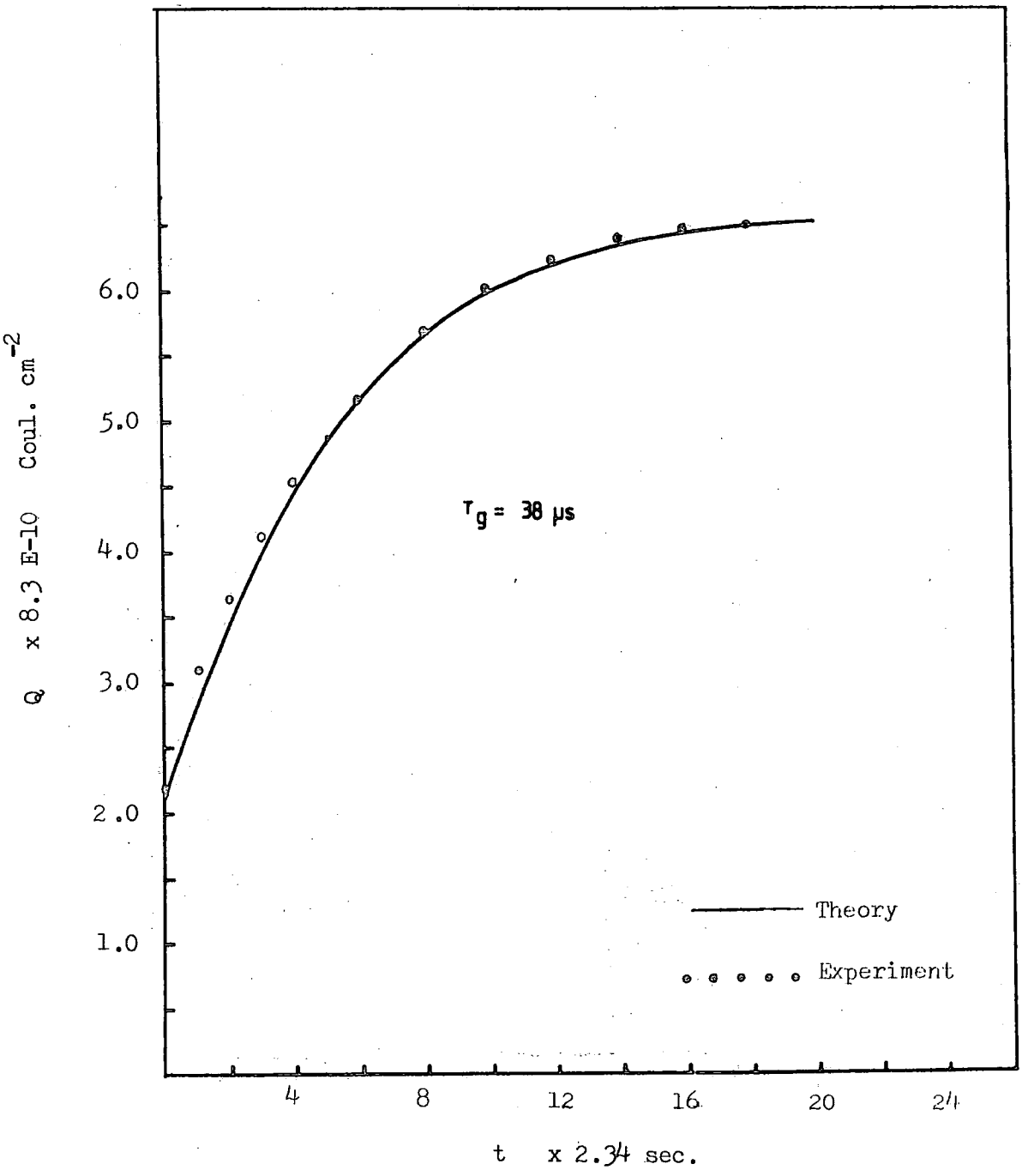

FIG. 8.12(a) The Theoretical and Experimental Plots for ITT135 for ΔV_a = 0.2 V

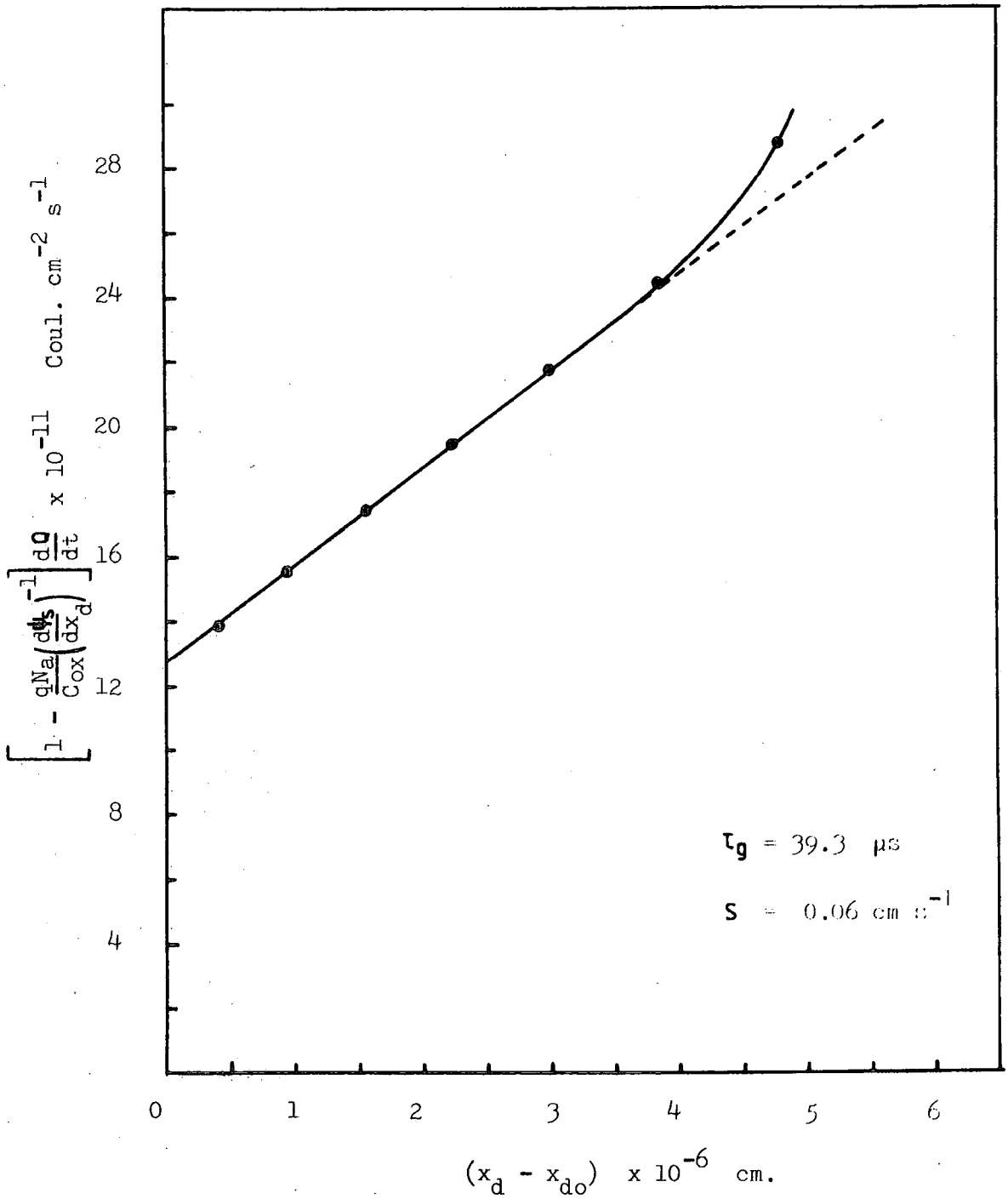

FIG. 8.12(b) The Plot following the Method of Viswanathan and Takino for ITT135 Sample for ΔV_a = 0.2 V

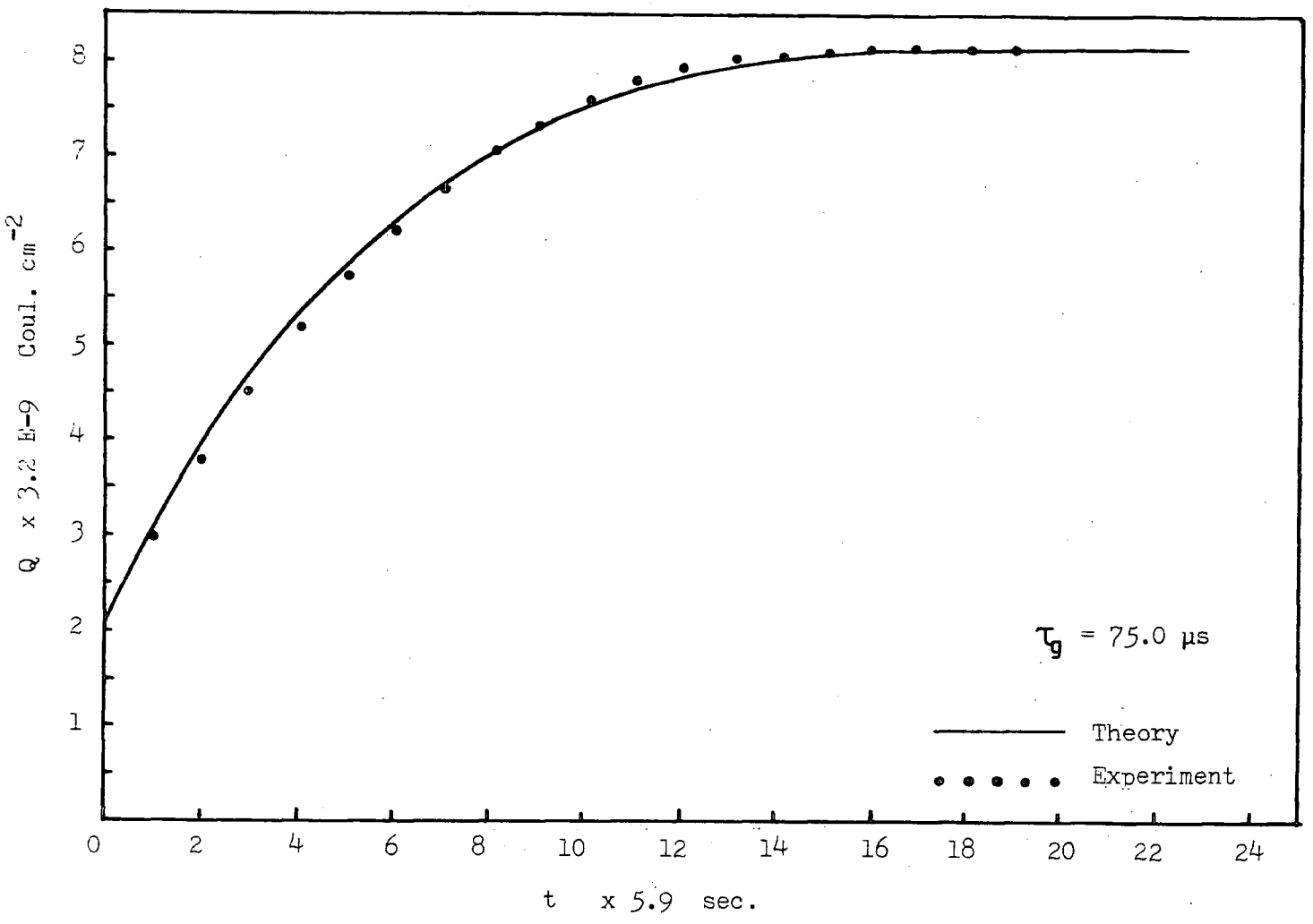

FIG. 8.13(a) THE THEORETICAL AND EXPERIMENTAL PLOTS FOR ITTB4,4

FOR ΔV_a = 1.0 V.

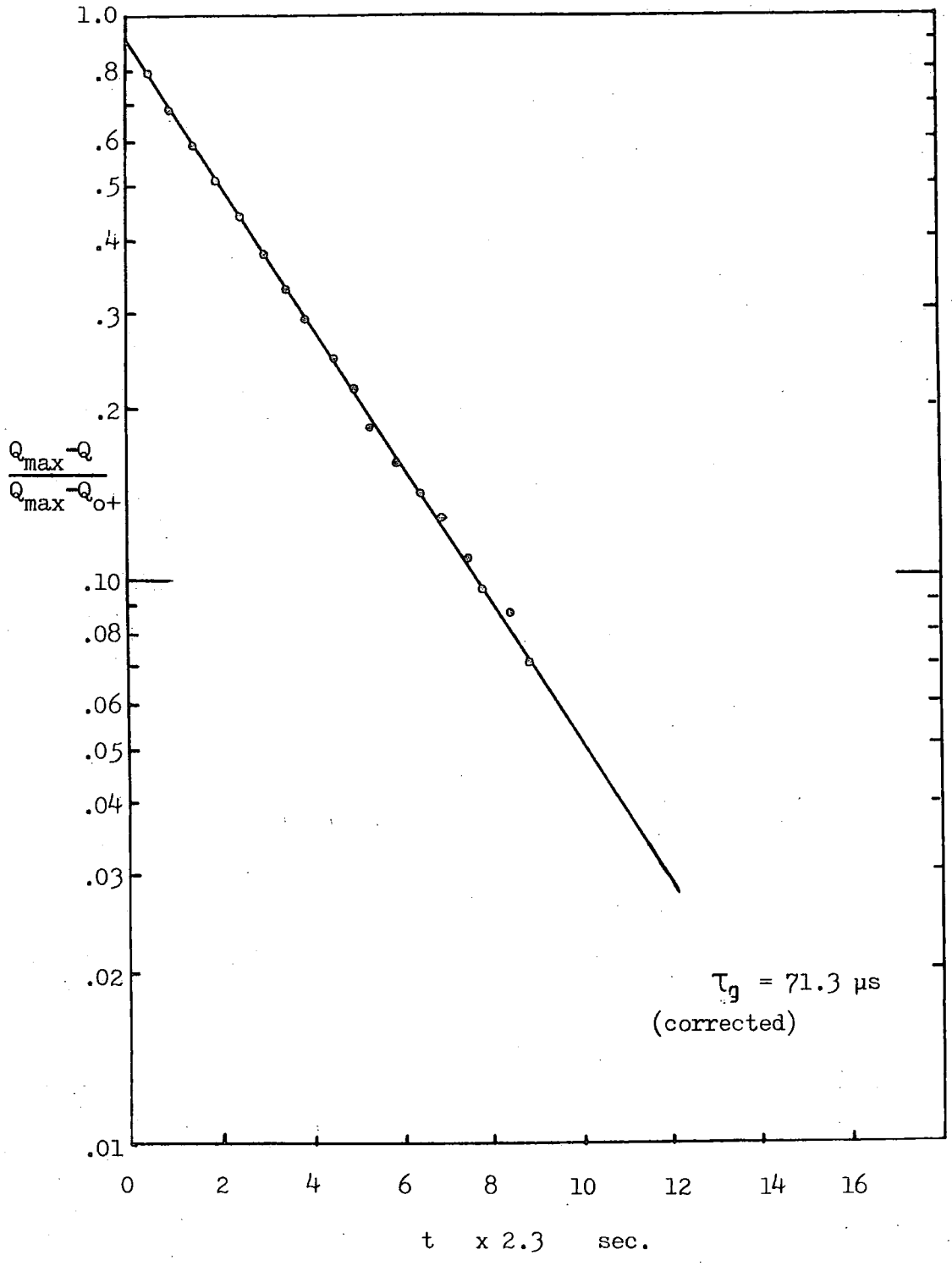

FIG. 8.13(b) LOG. PLOT FOR THE FORWARD TRANSIENT OF ITTB4,4 WITH ΔV_a = 25 mV

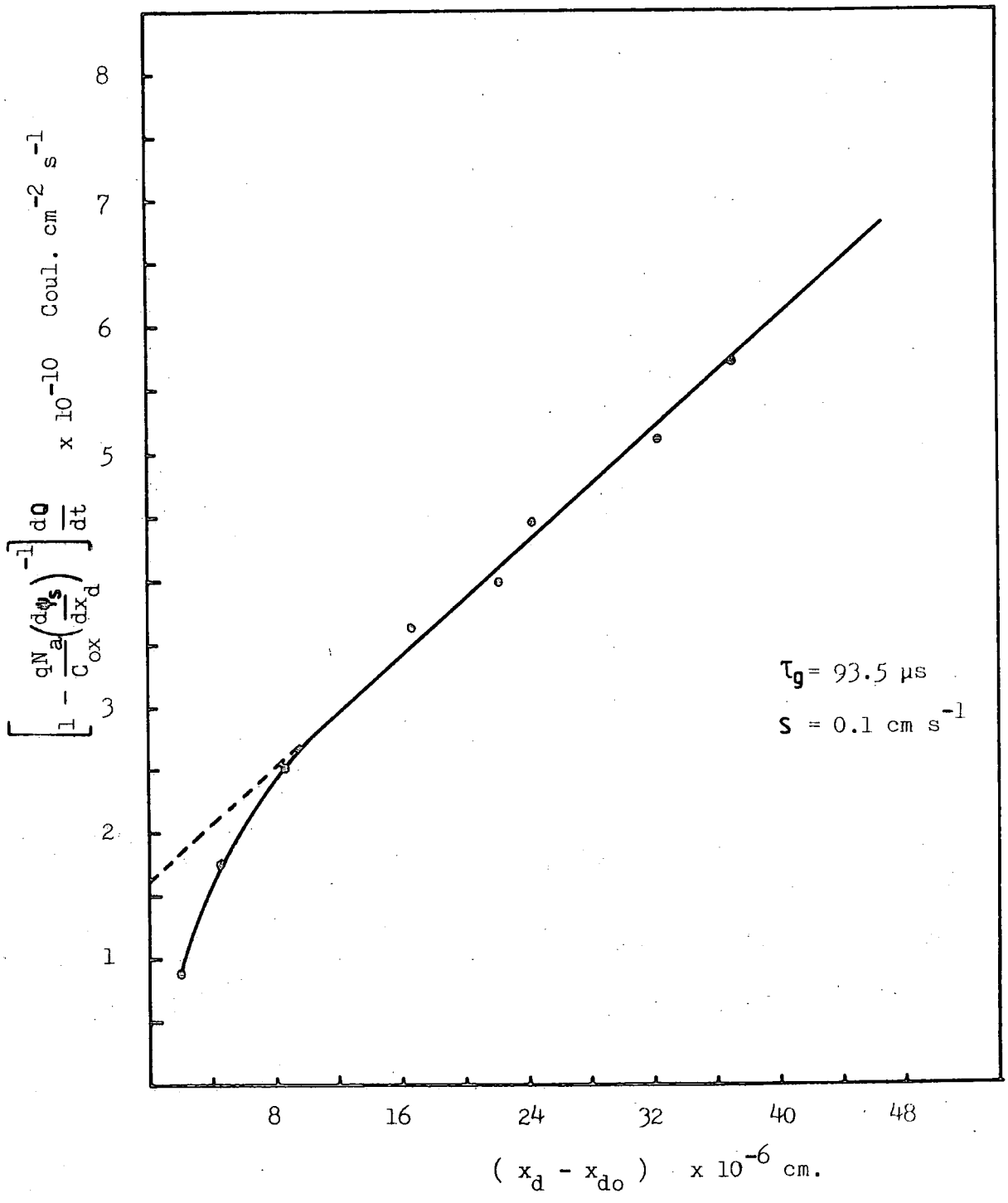

FIG. 8.13(c) The Plot following the Method of Viswanathan and Takino for ITTB4, 4 Sample for ΔV_a = 1.0V

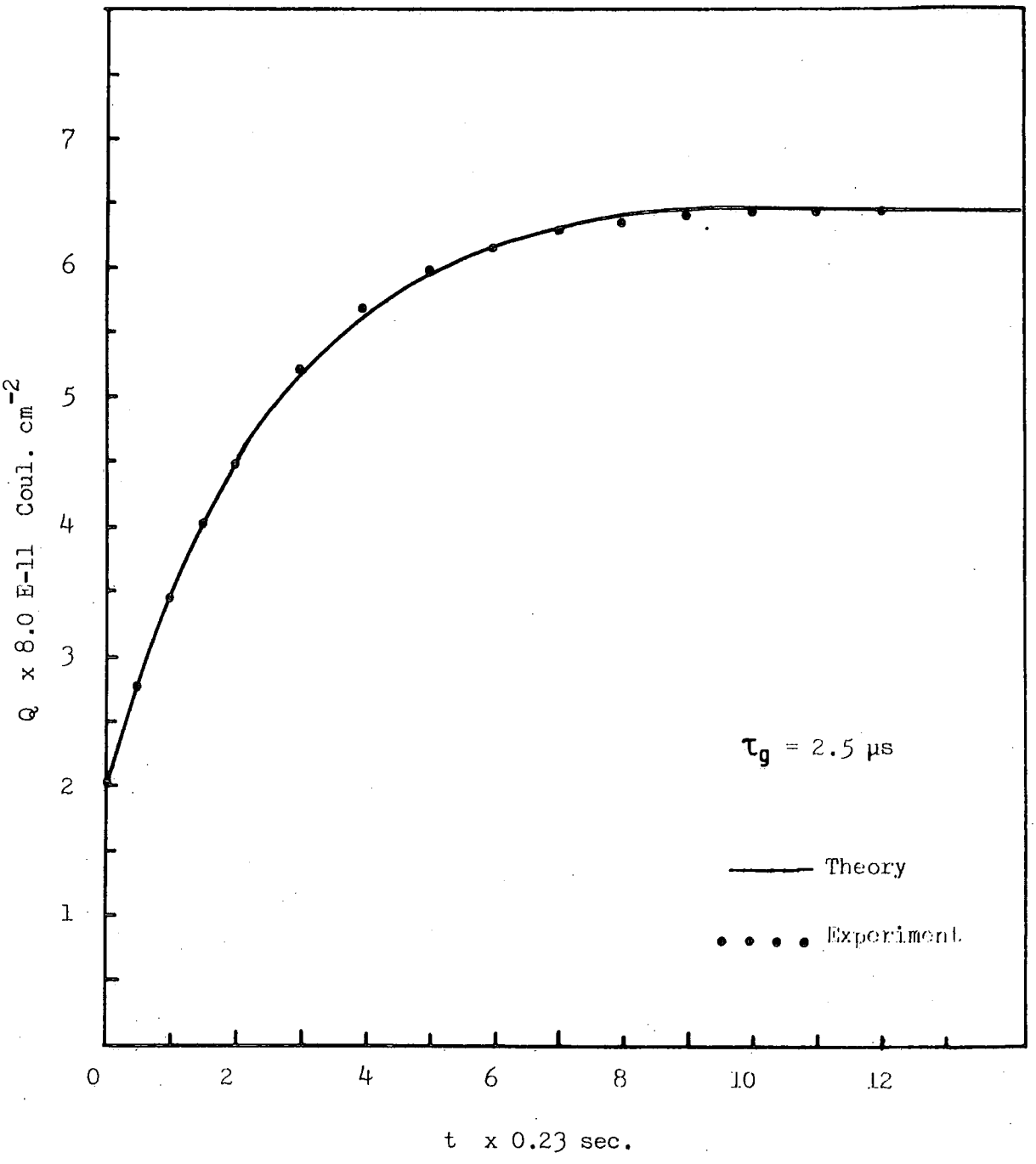

FIG. 8.14(a) The Theoretical and Experimental Plots for ITTAU2, 2 for ΔV_a = 25 mV

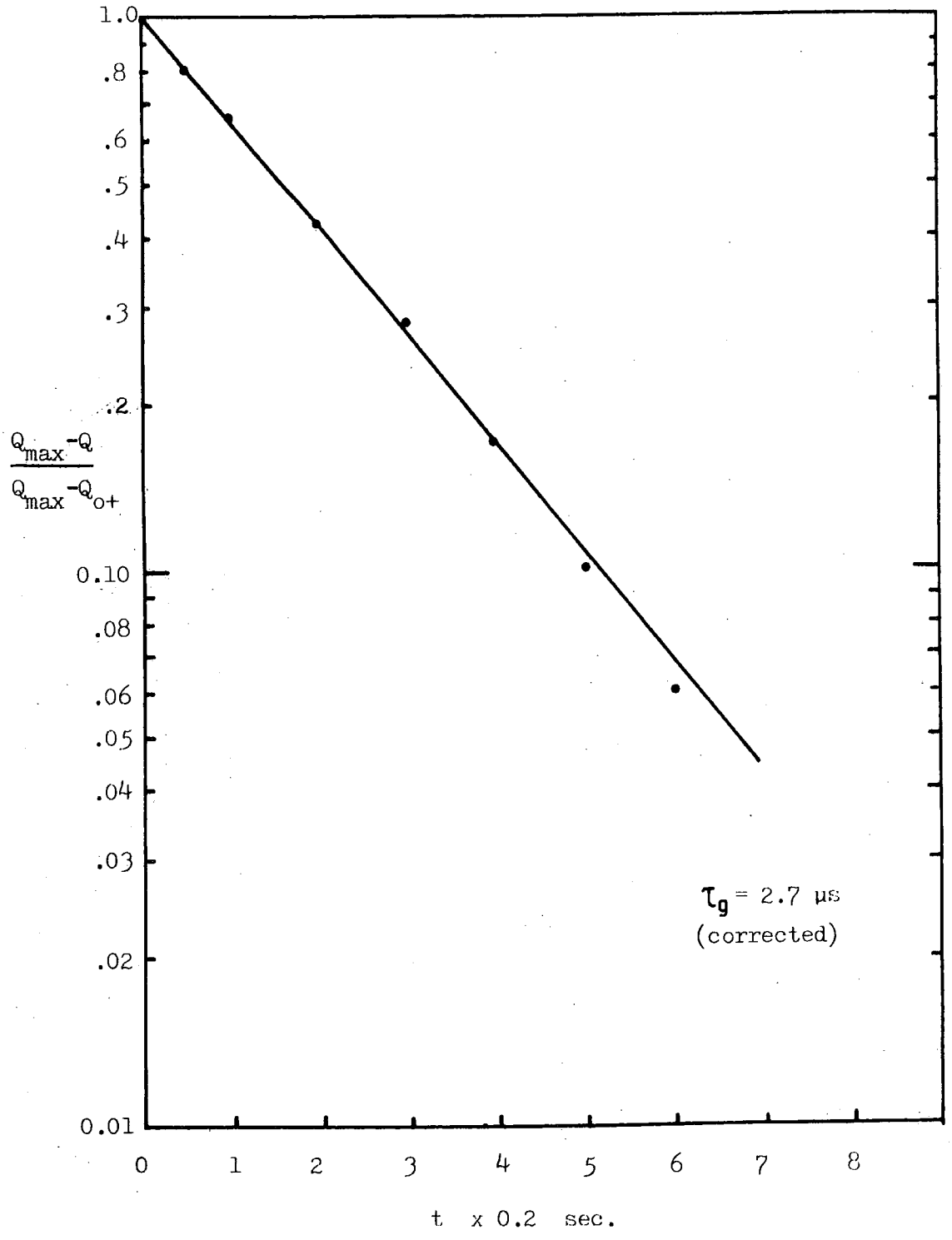

FIG. 8.14(b) LOG. PLOT FOR THE FORWARD TRANSIENT OF ITTAU2,2 WITH ΔV_a = 25 mV

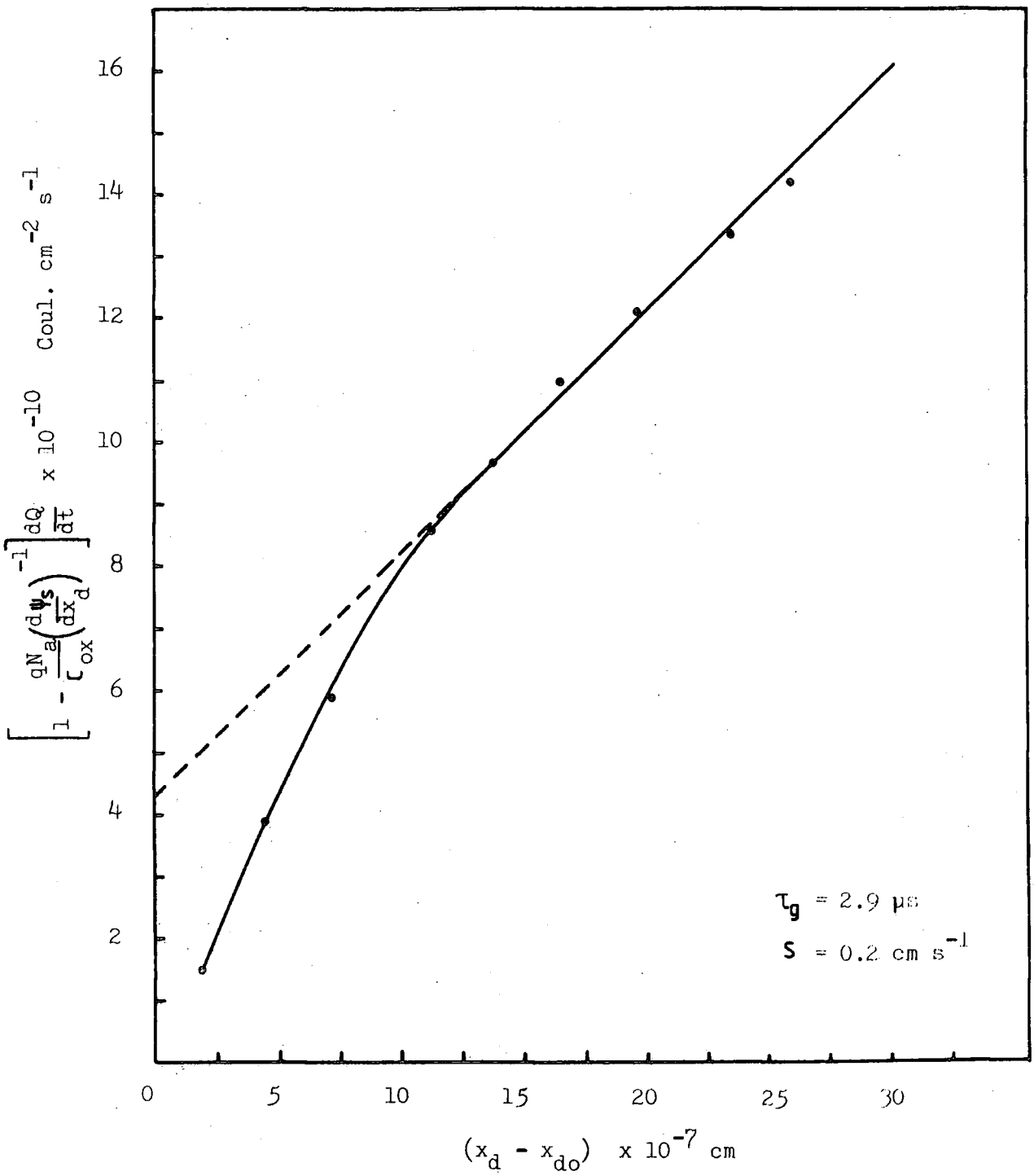

FIG. 8.14(c) The Plot following the Method of Viswanathan and Takino for ITTAU2,2 Sample with ΔV_a = 75 mV

8.3.3 Comparison with the Fast Ramp Results

The values of τ_g obtained by other methods on some common samples were compared. From the Fast Ramp (F-R) method described in Chapter 7, the following comparison was obtained :-

Sample	Hofstein's Mthd. (uncorrected)	Hofstein's Mthd. (corrected)	F-R Method	Present Theory
n-type NI-1	5.9 μs	3.0 μs	6.0μs	2.5 μs
p-type EN-1	5.6 μs	2.8 μs	16.0μs	2.3 μs

and comparison with the present theory is also shown in Figure 8.15. This comparison table is based on F-R results by Abdullah (56) who worked on setting up the F-R technique in this research group. From the results, it is seen that although the agreement between the Hofstein's and F-R values of τ_g was claimed by Abdullah to be good for the NI-1 sample, the Hofstein method used at that time was not corrected for the true generation expression. With this correction, the F-R method does not agree at all well. This difference could possibly be due to the different ways in which the generation process occurs in the two cases and possible reasons for the difference will be given in the discussion in section 8.5. Another possibility is that the evaluation of the fast ramp experiment, being far less direct than Q-t, is less accurate due to hidden assumptions.

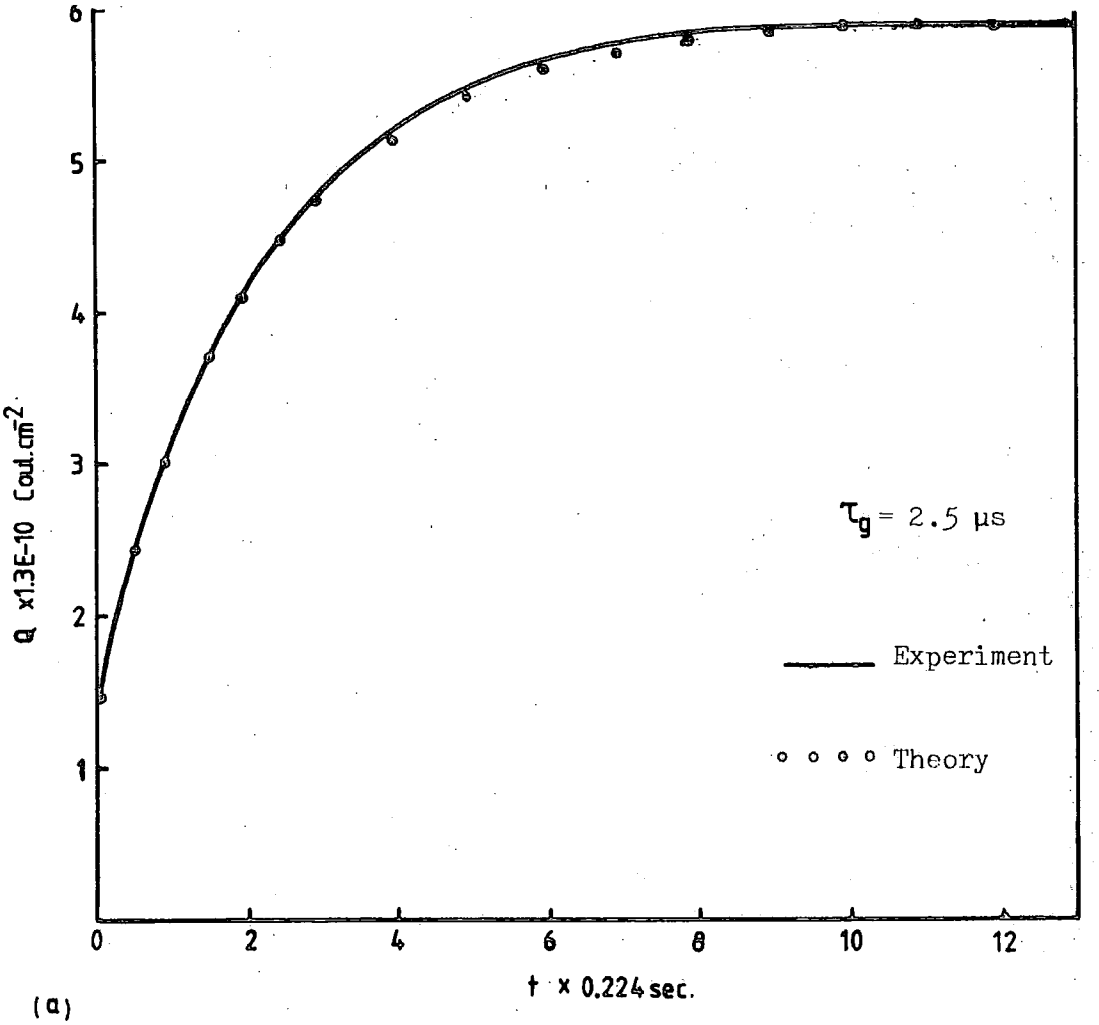

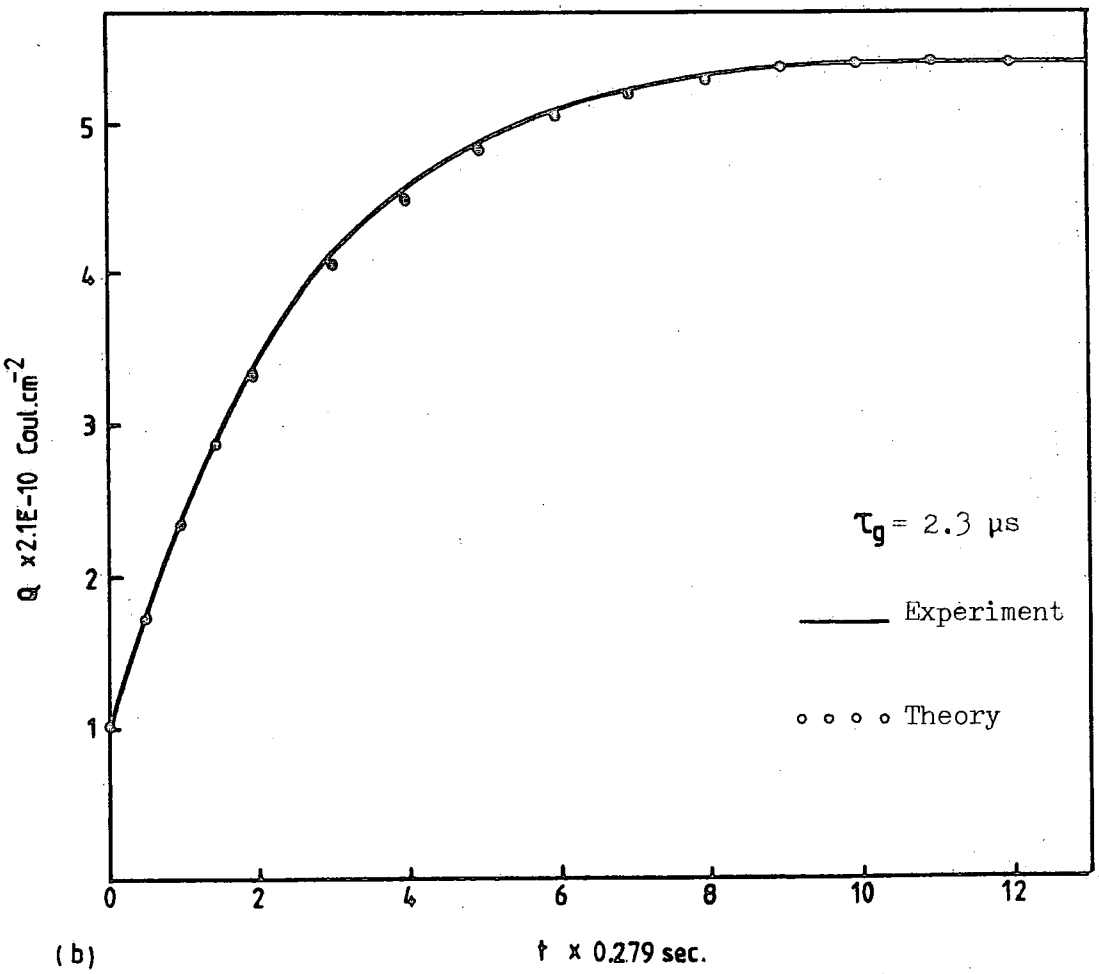

FIG. 8.15 Theoretical and Experimental Q-t Transients for (a) NI-1 and (b) EN-1 Samples

(ΔV_a = 25 mV)

8.3.4 Comparison with the Zerbst C-t Results

The value of the lifetime obtained by the Zerbst C-t method described in Chapter 7 was compared with the Q-t value evaluated by the method of Hofstein and the present theory for the sample ITT135. Since both Zerbst and Hofstein methods use the generation rate expression $\frac{n_i}{\tau_g}$ instead of $\frac{n_i}{2\tau_g}$ as in the present theory, the evaluations were also corrected for both of them. The results obtained are :-

U_g Expression	Hofstein's Method	Zerbst Method	Present Theory
$\frac{n_i}{\tau_g}$	79.5 μs	65.0 μs	-
$\frac{n_i}{2\tau_g}$	39.8 μs	32.5 μs	38.0 μs

The Zerbst method was carried out with a voltage step of 2V, Hofstein's method was with 25 mV, and the present Q-t theory, and experiment, was with 0.2V.

The bigger voltage step needed in the Zerbst and the Viswanathan and Takino methods is necessary because the generation layer expression used in these methods does not include the additional width due to the extra band bending at the surface as in the present theory. The error due to omitting this is large for small voltage step measurements but for larger voltage steps the depletion layer width extends so much that the additional width is only a small fraction of the total generation width, thus making the error small.

It can be seen that the three methods give closely similar results and that the present theory with a 0.2 volt step gives

a lifetime value very similar to that of the small signal Hofstein evaluation.

8.3.5 Comparison of the Taniguchi C-V Results

The C-V method of Taniguchi to determine the minority carrier lifetime was described in Chapter 6. As already mentioned the method showed that the experiemntal points for the ITT14 and ITT134 samples were totally out of the range of the theoretical plots of $| V_{c2} - V_{c1} |$ versus V_{c2}.

Looking at the trend of the theoretical plot for the ITT14 sample, (Figure 6.5(a)), the experimental point would have been within the chart if the theory could have been evaluated for lifetimes lower than 4 μs. This was not possible due to the limitation of the mathematical equations but it is not clear what the physical reason for this might be.

For the ITT134 sample (Figure 6.5(b)), despite the fact that the experimental point was very close to the theoretical chart the theoretical curves seem to be asymptotic at a point short of the experimental result and again it is clear that theory and experiment are not consistent although there is nothing at all peculiar about either the sample or its C-V curves. It has not therefore been possible to explain the failure of the C-V method with these samples.

The experimental point for ITT135 sample did fall within the theoretical chart as seen in Figure 6.5(d), although the lifetime of 265 μs deduced from its position was very large. For this sample the τ_g values obtained by the methods of Zerbst, Viswanathan and Takino, Hofstein, and the present theory are all within 30 and 40 μs, so that the C-V method seems to be erroneous. Since time was not available for further investiga-

tion and that the primary concern of the thesis is not in the C-V technique, this discrepancy was left unresolved. It certainly appears that there is a major error in the theory of the C-V method and this has not been observed previously because of the lack of other comparative measurements.

8.4 Evaluation of the Recombination Lifetime from the Reverse Voltage Step Transient

The reverse transients for the n-type TC3-8D3 sample and the p-type ITTAU2,2 were evaluated by the theory in Chapter 5 first for the rate of recombination R, and then for the recombination lifetime, τ_r. The following are the typical values for the rate of recombination for two of the samples.

Sample	Recombination Rate (R) cm^{-3} s^{-1}
n-type TC3-8D3	4.03×10^{17}
p-type ITTAU2,2	2.07×10^{15}

With these values, and assuming that the recombination rate can be related to the recombination lifetime in the same manner as the generation situation, we then have

$$R = \frac{n_i}{2\tau_r}$$

Thus the recombination lifetimes for the samples TC3-8D3 and ITTAU2,2 were found to be 1.8×10^{-8} s and 3.5×10^{-6} s respectively (Figures 8.16 and 8.17).

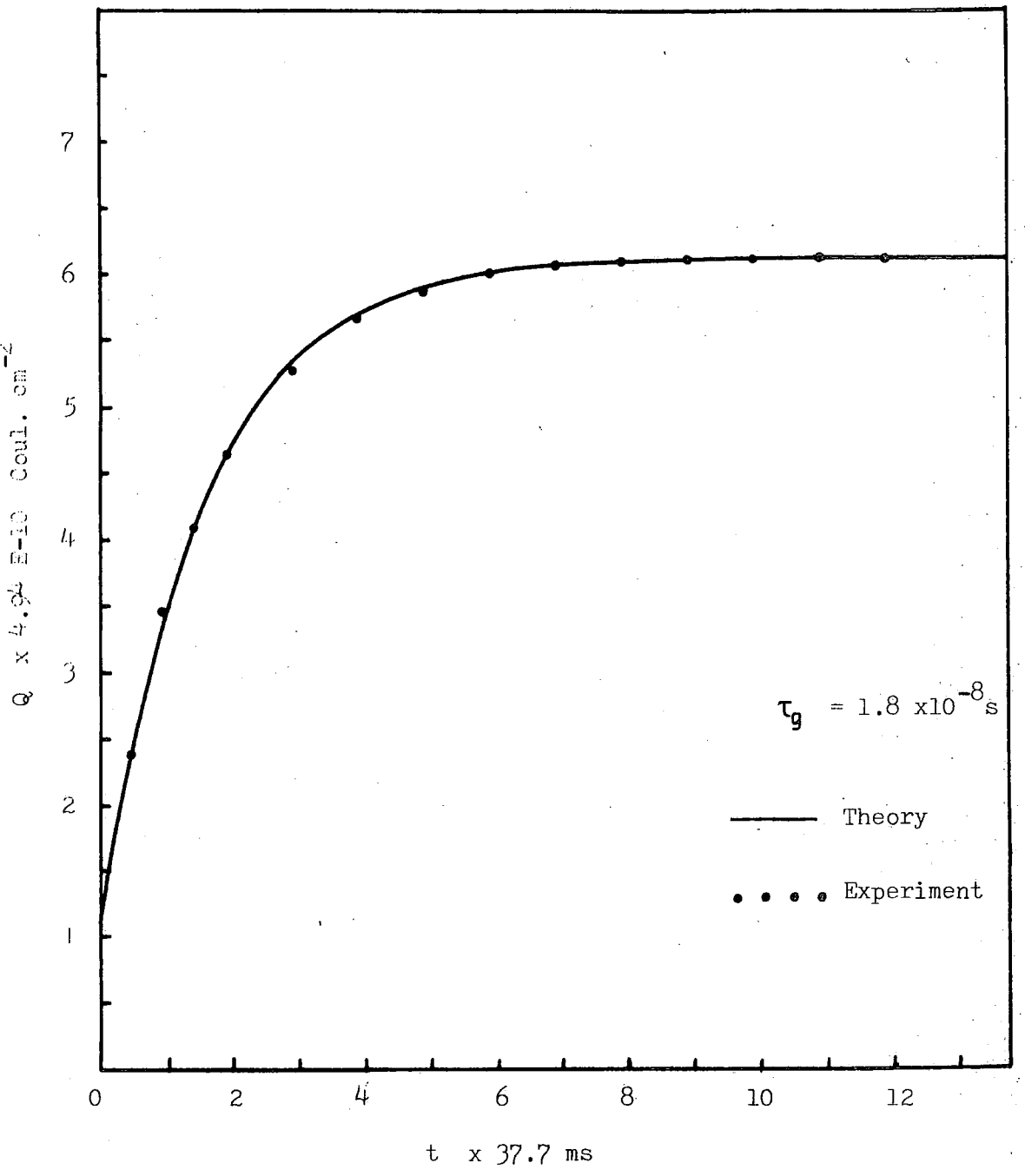

FIG. 8.16 The Reverse Q-t Transient for TC3-8D3 for Voltage Step of 25 mV

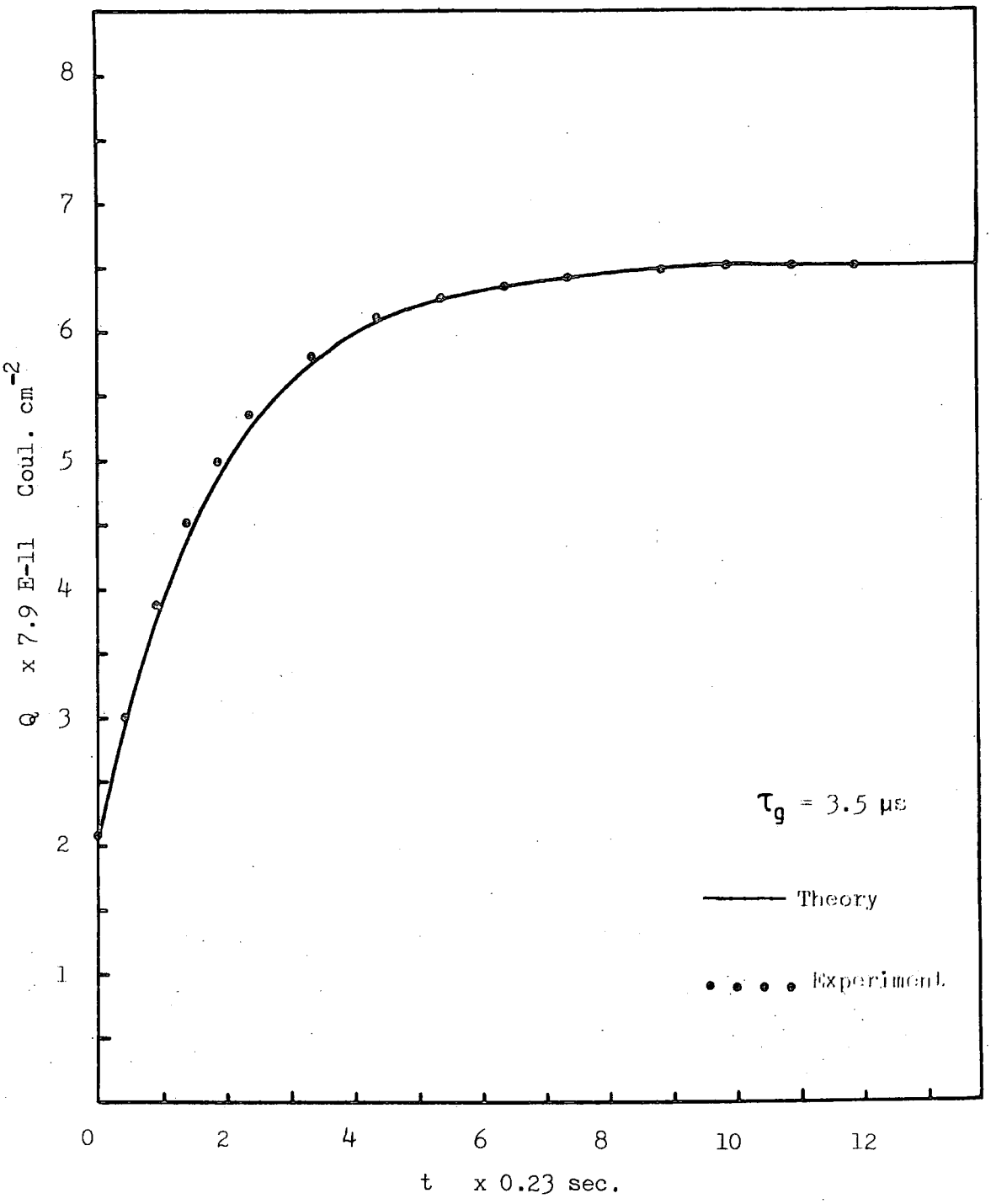

FIG. 8.17 The Reverse Q-t Transient for ITTAU2, 2 for Voltage Step of 25 mV

Comparing these values to the generation lifetime we have the following result :

Sample	τ_r (s)	τ_g (s)
TC3-8D3	1.8×10^{-8}	2.2×10^{-8}
ITTAU2,2	3.5×10^{-6}	2.5×10^{-6}

These values seem to be reasonable since for small voltage steps the transients are quite close to each other. As there are no other published ~~other~~ Q-t methods for the determination of the recombination lifetime, there is no way of telling how accurate this method is.

8.4.1 Effect of the Voltage Step Magnitude on the Reverse Transient

The theoretical reverse transients were calculated for different voltage steps using the theory developed in Chapter 5. Figure 8.18 shows these plots for ΔV_a of 25 mV, 50 mV, 100 mV, 0.5 V, and 0.8 V. Logarithmic plots were then obtained from the theoretical transients as shown in Figure 8.19(a) and were then compared with the experimental results of Figures 8.19(b) and 8.19(c). These experimental plots were obtained from the reverse transient of Figure 4.20 for the TC3-8D3 and ITTAU2,2 samples. It is found that the theoretical plots have the same trend as the experimental ones where on the log plots they are linear for most of the transient for the voltage step of 25 mV but for larger steps, there is a deviation from linearity at the beginning of the transient where the gradient is steeper than for the rest of the curve. However, the main part of the log plot after the non-linear portion has constant

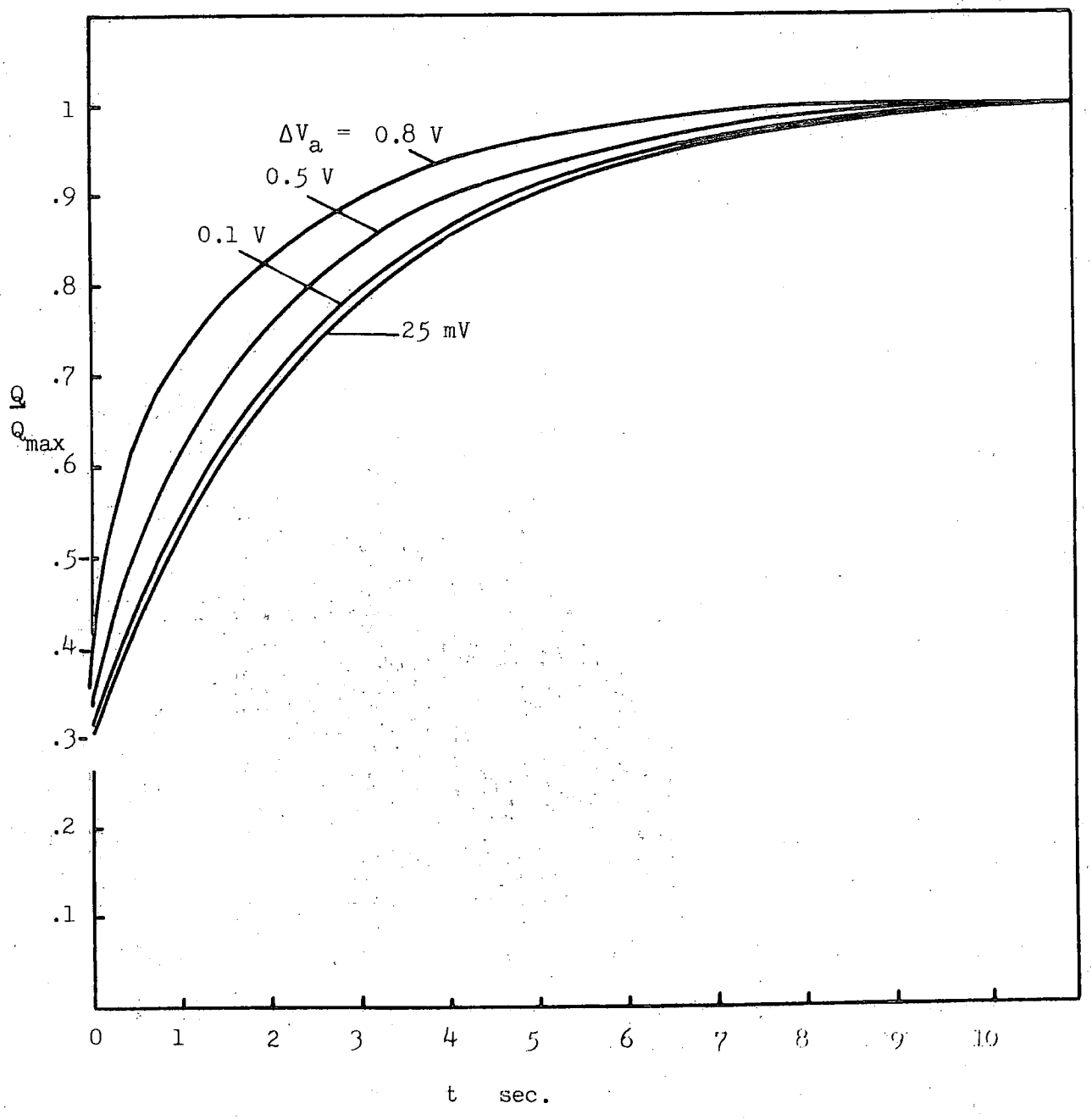

FIG. 8.18 THEORETICAL REVERSE Q-t TRANSIENTS (NORMALISED) FOR DIFFERENT VOLTAGE STEPS FOR τ_g = 20 μs

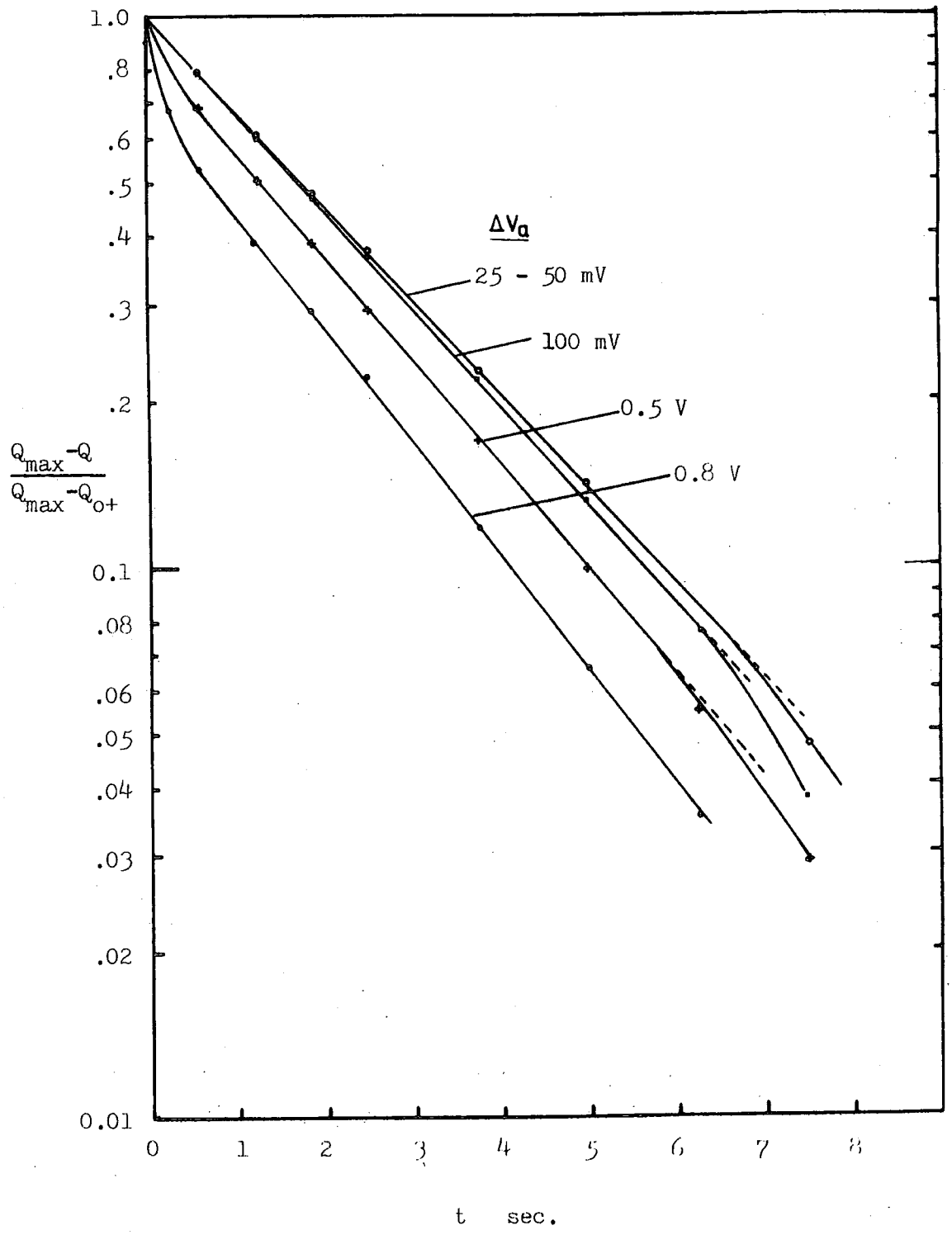

FIG.8.19(a) THEORETICAL REVERSE Q-t LOG. PLOTS FOR DIFFERENT VOLTAGE STEP MAGNITUDES.

(τ_g = 20 μs)

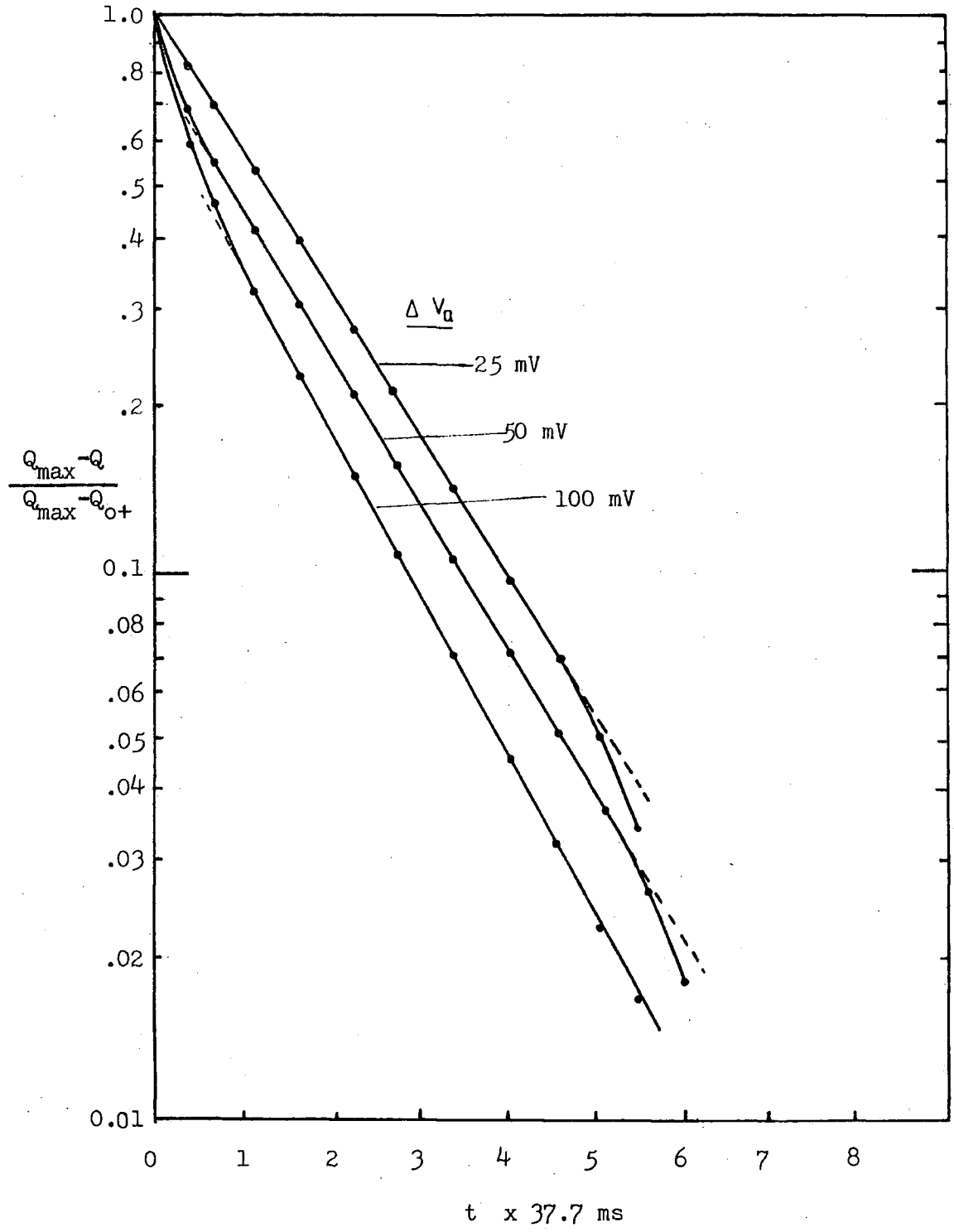

FIG. 8.19(b) LOG. PLOTS FROM THE REVERSE Q-t TRANSIENTS OF TC3-8D3 SAMPLE FOR DIFFERENT VOLTAGE STEP MAGNITUDES (EXPERIMENTAL)

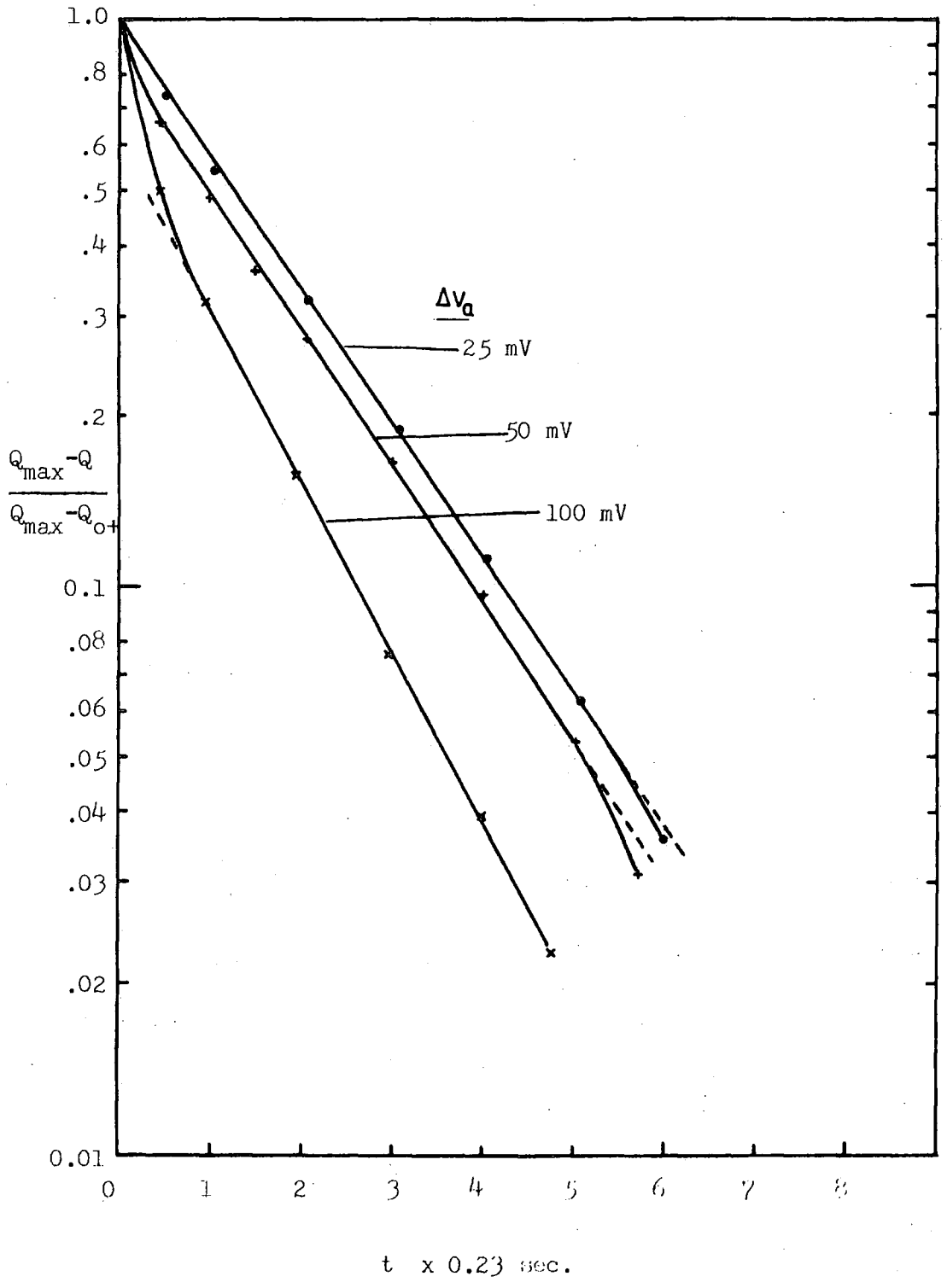

FIG. 8.19(c) LOG. PLOTS FROM THE REVERSE Q-t TRANSIENTS OF ITTAU2,2 SAMPLE FOR DIFFERENT VOLTAGE STEP MAGNITUDES (EXPERIMENTAL)

gradient indicating exponential behaviour. There is also a deviation from the straight line for long times for the smaller voltage steps.

The reason for the first deviation is due to the fact that the initial change of the applied voltage, and hence of the surface potential, causes a sudden rush of minority carriers towards the bulk thus giving rise to a bigger recombination current than the steady state where the gradient is linear.

Towards the end of the transient, the net recombination is reduced as the excess minority carrier concentration falls to the equilibrium value. This causes the recombination current and hence the gradient of the log plot to decrease. This phenomenon is present for all voltage steps. Since this occurs when the energy bands are close to equilibrium, its effect is small compared to the total recombination current for large voltage steps when the results are normalised.

Also from Figure 8.18(a) it was found that the value of Q_{o+} increases with increasing voltage step as seen in Figure 4.21 for ITTB4,4 sample. The reason for this has already been given in Section 4.4.2. To examine this effect more clearly, the values of Q_{o+} were plotted against the voltage step ΔV_a. This is shown in Figure 8.20 for the theoretical transients and Figure 4.23 for the experiment. Both figures show a similar trend with the approximate linear behaviour holding for smaller steps. For larger voltage steps, the value of Q_{o+} eventually becomes more than proportional to ΔV_a in both theory and experiment.

In general the comparisons made between the present theory and experiment for reverse voltage step transients

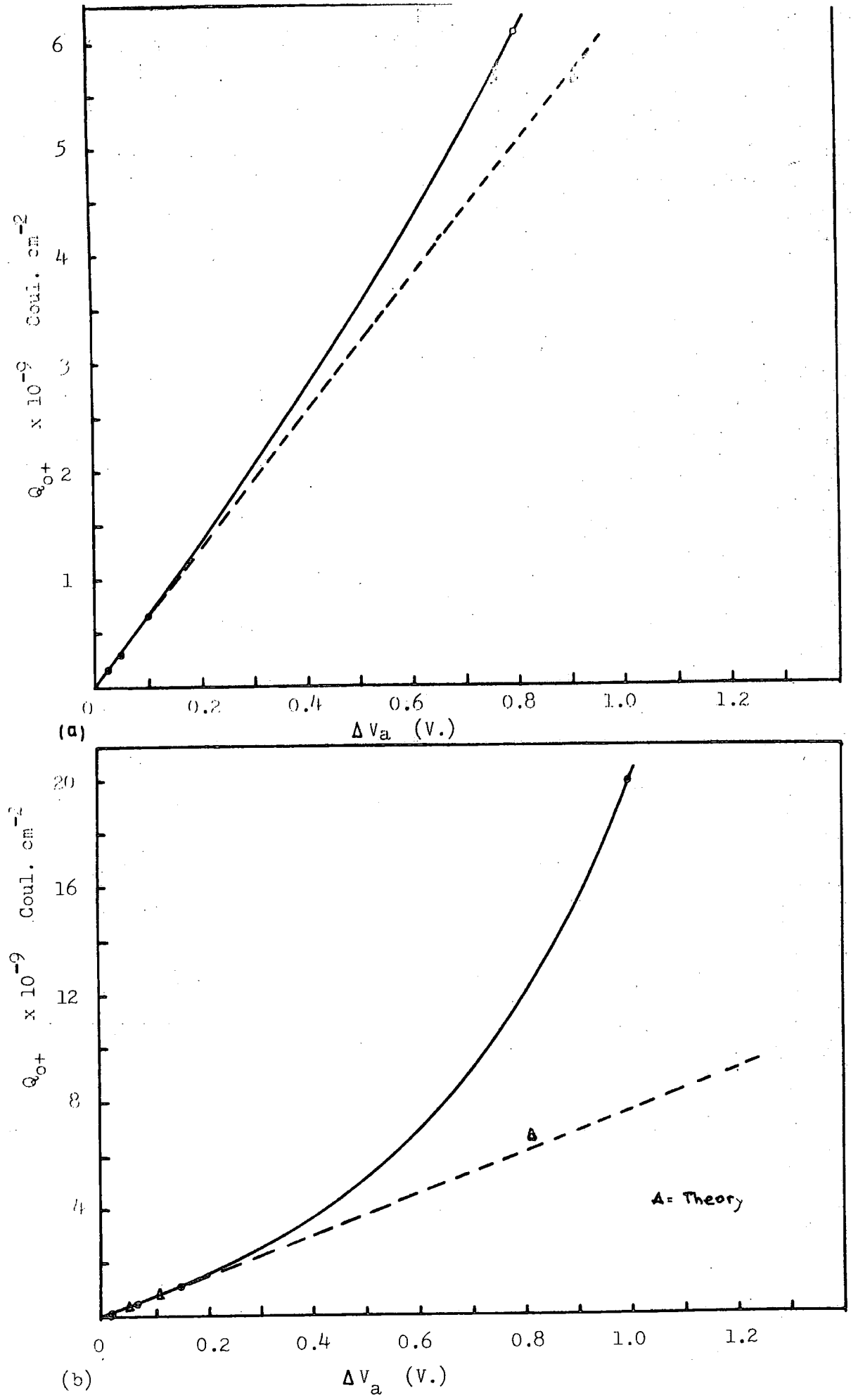

FIG. 8.20 Plots of Q_{o+} versus ΔV_a for Reverse Q-t Transients
(a) From Theory
(b) For ITTB4, 4 Sample

show identical trends although they are not in quantitative agreement. This indicates that the theory developed is on the right lines but it is not exact because it fails to take into account the variation of the minority carrier concentration throughout the depletion layer and as a function of time. For small steps the error is quite small but for larger steps a more accurate theory is required.

8.5 Discussion

It was found in this chapter that the shapes of the Q-t transients obtained from experiments agree well with the theoretical calculations. Some results from Chapter 4 were compared with the theory and was found to be in good agreement both for the small and large forward voltage steps.

Also in this chapter it was seen that the results obtained from Q-t measurements evaluated using the present theory are quite close to those of the theories of Hofstein, Viswanathan and Takino, and of the C-t method as evaluated by Zerbst provided suitable voltage step magnitudes are used in each case and that the necessary correction is made to the Hofstein and Zerbst methods. The choice of the expression for the generation layer width does contribute greatly to the small differences that occur between the present method and the others but it is important for accurate work. Also by dropping the surface generation term, the new method is more tolerant to the voltage step magnitude because as shown earlier, the lifetimes obtained at small and larger voltage steps differ only by a small amount compared to the other methods.

A small difference in the lifetime values obtained by the present method for small and large voltage steps is almost

inevitable because of the way in which the lifetime is obtained. For small voltage steps the lifetime is actually the average over the equilibrium width of the depletion layer, whereas for large voltage steps, the generation region, over which the value of lifetime is averaged may be several times greater. Thus for samples where the concentration of generation centres or traps, N_t, varies with distance into the semiconductor, the values of lifetime might vary with the voltage step magnitude as was observed for the TC3-8D3 sample and rather less so for the ITT135 sample. For ITTAU2,2, the values of τ_g remained the same for voltage steps of 25 mV and 100 mV, indicating constant N_t or τ_g with distance. Generally the values of τ_g obtained for small voltage steps, are less than for larger steps. This agrees with the fact that the trap concentration is often greater nearer the surface and that it decreases into the bulk because it is due to surface contamination and/or the accumulation of recombination centres around crystalline defects caused by surface damage.

The Fast-Ramp and the h.f. C-V methods of measuring τ_g did not give good agreement with the others. This could have been inherent in the nature of the methods. In both of them the applied bias in the form of a triangular wave is always changing. This causes the sample to be out of equilibrium for most of the time so that charges are always moving and the generation width is always changing. The other methods are of the voltage pulse type in which the applied voltage is constant during the transient so that the generation width is determined just by the relaxation process. This could be the reason for not getting a good agreement between

the lifetime values obtained by the two types of experiment.

The new theory extended to the case of the reverse voltage step transient for the first time gave Q-t curves that agreed well with the experimental results (Figure 8.16). The trends in the variation of the reverse transient shape with increasing voltage steps agrees well with the actual experimental result as shown in Section 8.2.3. However, the theoretical forward and reverse Q-t transients for a given voltage step and the same values of τ_g and τ_r, differ more than in the actual experimental results. This could be due to the reverse step theory not allowing sufficiently accurately for the recombination rate as a function of excess minority carrier density. Alternatively it could be due to non-uniform trap concentration in the samples actually used for the recombination measurements. Nevertheless the comparison of the values of τ_g and τ_r in Section 8.4 showed that they are in good agreement for small voltage steps at least.

Recombination in MOS capacitors seems to have been completely neglected in the context of pulse or step relaxation Q-t measurements and the work reported here is the first that has been done both theoretically and experimentally. However, it is only a preliminary investigation and time prevented it being examined in more detail particularly in theory. A full treatment would have to allow more accurately for the rate of recombination as a function of position and of time.

CHAPTER 9

CONCLUSION

9.1 Contributions to the Q-t Method of Determining Minority Carrier Lifetime

The Q-t methods for the determination of minority carrier lifetime available previously were very restricted to particular range of voltage step magnitudes. They were applicable either to small steps or to larger steps only and they fail completely for voltage steps outside their range.

In the case of Hofstein's method, it is necessary to work with small voltage steps of about 25 mV, and the method fails even when the step is increased to only twice this value. This effect was clearly shown in Chapter 4. This limitation on the signal presents a problem for accurate measurements because of noise pick up which can easily be as large as the injected signal. Hence the method necessitates an averaging technique to obtain clean transients. This is very time consuming and complex. Hofstein's method also requires an electrometer capable of measuring very small charges.

The method of Viswanathan and Takino is strictly valid only for large voltage steps and for small voltage steps of below 100 mV the method fails totally giving an erroneously negative intercept with the y-axis, indicating a negative surface recombination velocity ! In Chapter 8 it was also seen that the lifetimes obtained by this method

for the small and large voltage steps differ by about one order of magnitude.

The above problems were resolved by improving the theory as well as the method of evaluation. This led to the development of the present Q-t method of determining the generation lifetime. With this improved theory the Q-t transient is more even accurately calculated by using the improved generation layer width expression originally due to Rabbani and Lamb (12) and by removing the surface generation term which is justified for the reasons given in Chapter 5. This evaluation technique is obviously more involved than the previous ones and the theoretical transients have to be directly compared with the experimental ones for the same sample type. However this removes the need to do graphical differentiation which is the source of gross error in the previous methods. The need to compare curves is not a serious drawback because, by using a microcomputer to aid the process of comparing the Q-t transients, the method is not only more accurate and consistent but it also allows more measurements to be performed in a very short time compared to previous methods. The limit of the accuracy is now the accuracy of the measured transient itself and with the automated equipment developed here this can be very high.

The improvement in the evaluation of lifetime is seen in Chapter 8 where the results obtained for a typical sample, the ITTAU2,2 was the same for small and large voltage steps using the new theory. The differences that occurred for other samples may be due to the non-uniformity of the trap concentration, but the values are still more consistent than those obtained by other methods.

The new theory accurately predicts the variation of Q_{o+} and of the transient shape with voltage step magnitude as shown in Chapter 8. Very good agreement is obtained between theory and experiment for the transient shapes.

From Chapters 4, 5 and 8, the following additional conclusion can be drawn:-

(i) That p-type samples need to have guard rings suitably biased in accumulation before an accurate and consistent measurement can be made by the Q-t technique.

(ii) That for the Q-t method to give consistent results, the sample has to be biased into heavy inversion, and it should remain in inversion both before and after the application of the voltage step.

(iii) That the voltage step magnitude can be either small or large, except that for smaller signal the lifetime is averaged over a smaller depth into the silicon. For samples with non-uniform trap concentrations the method gives the average lifetime for a depth that depends on the voltage step magnitude. The variation of measured lifetime with step height can therefore be used to estimate the non-uniformity.

(iv) That the present theory developed for the reverse Q-t transient is truly applicable only if the voltage step is small enough so that the inversion charge does not contribute significantly to the minority carrier concentration in the recombination region. However, with this limitation it appears to agree well with experiment. The present theory over-estimates the difference between large signal forward and reverse transient because it does not allow accurately for the variation of the recombination rate with position and time.

9.2 Advantages of the Present Method over Other Voltage Step Methods

Although good agreement was obtained between the results from the present method and other experiments that use voltage steps, the Q-t method as analysed here has several advantages over the others for the accurate and easy determination of minority carrier lifetime.

Firstly, the new method is not restricted to small voltage steps as required for Hofstein's analysis thus reducing the difficulty in measuring the charge and improving the accuracy by obtaining a larger signal-to-noise ratio. Secondly, the method being applicable to a wide range of voltage steps, has the advantage of giving some information on the variation of lifetime within a small region of the semiconductor by comparison of transients for small and large voltage steps which allows the lifetime to be averaged over a variable distance.

Compared with the method of Viswanathan and Takino, the generation width expression used here has been improved by considering the generation process in more detail and by removing the surface effect term which is shown to be small in any case. This method, has therefore proved to be more consistent both for small and large voltage steps.

The present method could be further improved by programming the microcomputer to do the automatic comparison of the theoretical and experimental transients by evaluating the time constants of the two transients while scanning through values of τ_g in theory. This can be done with the present method because of the good agreement in the shape of the transient between theory and experiment. With this

improvement, the lifetime could be evaluated almost immediately while doing the measurement itself.

Compared with the Zerbst C-t method,there is no need for the complex capacitance bridge for the Q-t evaluation of lifetime so that the measurement is more direct. Also there is no need to do a laborious graphical differentiation as in the Zerbst method. This allows a fast evaluation of τ_g.

Referring to Equation 5.30, it seems that it should be equally applicable to the measurement of the current transient (34,59-61) instead of the charge transient for the application of a voltage step. However this is less direct than the measurement of charge. Also, the initial, rapid transient, poses problems when measuring current because it gives a very large current surge initially which will appear as a big spike in the current-time transient. This is also undesirable as it can overload the measuring apparatus.

The Q-t and C-t methods give generally similar results as shown in Section 8.3, but it must be concluded that the more indirect fast ramp and C-V methods are not as reliable at the present time.

9.3 Suggestions for Further Work

From the present work it was realised that other investigations relating to the Q-t measurement could be carried out to further establish the method for the characterisation of MOS devices. From these, the following are felt to be the more important ones.

(i) Theoretical work to be carried on the lines of the approach of Collins et al to produce more accurate computer modelling of the Q-t transient of MOS capacitors. This should be able to reproduce the exact behaviour of charges in samples without the need of the approximations used in the present theory.

(ii) Investigation of the Q-t transients by varying the temperature of the sample. This should show the temperature variation of the generation rate, where the latter is mainly

due to thermal generation and so is very temperature dependent, while recombination processes are less so. It should therefore be possible to 'freeze out' generation by lowering the temperature. Also the difference in the generation and recombination rates can be compared at various temperatures. It should be possible to use the exact computer model mentioned above, to predict the exact temperature variation of the Q-t response.

(iii) More work could also be carried out on the effect of trap levels other than the mid-gap traps assumed in this work. The trapping centres could be added intentionally to MOS samples by using gold for instance. It would also be interesting to investigate the effect of having two trap levels from gold recombination centres for example. This behaviour could also be investigated using the present or an improved computer model and experimentally

(iv) In this work, it was assumed that the surface effects are negligible. It would be interesting to investigate the actual dependence of the Q-t transient on the concentration of surface states. By the inclusion of surface generation the Q-t transient could also be measured with a wider bias range instead of being limited only to the heavy inversion bias case as in the present work.

(v) More work should be carried out on improving the theory of the reverse transient. This could be done by considering the basic equations for the generation and recombination rates and the actual charge concentration as a function of the position and time variables.

(vi) The profile of the minority carrier lifetime and hence the trap density can also be obtained by using the Q-t measurement using different voltage steps and some further

experiments on lifetime profiling would be worthwhile. By using the results of (iv) above it should be possible to extend the profile to nearer the surface, when the bias is no longer limited to inversion.

(vii) Finally more work is also needed to investigate the differences in the lifetime values obtained by methods using voltage steps as in Q-t and C-t and those using voltage ramps as in the C-V and Fast Ramp techniques which appear to be in error.

By doing all the work suggested above, the investigation of the Q-t measurement technique will be complete in both theory and experiment. This will then provide a fast and easy means of characterising dynamic processes in MOS capacitors.

REFERENCES

1. M. Zerbst, "Relaxation Effects at Semiconductor Interfaces", Z. Angew.Phys., 22, 30 (1966).
2. J.G.Simmons and L.S.Wei, "Non-Steady-State Bulk-Generation Processes in Pulsed Metal-Insulator-Semiconductor Capacitors", Solid-State Electronics, 19, 153 (1976).
3. T.W.Collins, J.N.Churchill, F.E.Holmstrom and A.Mosdiwitzer, "Modelling of the Transient Response of an MIS Capacitor", Advances in Electronics and Electron Physics, 47, 267 (1978).
4. T.W.Collins, and J.N.Churchill, "Exact Modelling of the Transient Response of an MOS Capacitor", IEEE Trans. on Electron Devices, ED-22, No.3, 90 (1975).
5. C.T.Sah, R.N.Noyce, and W.Shockley, "Carrier-Generation and Recombination in p-n Junctions and p-n Characteristics", Proc.IRE, 45, 1228 (1957).
6. F.P.Heiman, "On the Determination of Minority Carrier Lifetime from the Transient Response of an MOS Capacitor", IEEE Trans.on Electron Devices, ED-14, No.11, 781 (1967).
7. J.S.T.Huang, "Bulk Lifetime Determination using an MOS Capacitor", Proc.IEEE, 1849 (1970).
8. J.Muller and B.Schiek, "Transient Responses of a Pulsed MIS-Capacitor", Solid-State Electronics, 13, 1319 (1970).
9. P.U.Calzolari, S.Graffi, A.M.Mazzone, and C.Morandi, "Bulk Lifetime Determination from Current and Capacitance Transient Response of MOS Capacitors",Alfa Frequenza XLI, No.11 848 (1972.

10. B.J.Baliga and M.S.Adler, "Measurement of Carrier Lifetime Profiles in Diffused Layers of Semiconductors", IEEE Trans. on Electron Devices, ED-25, No.4, 472 (1978).

11. R. Bharat, E.T.Fitzgibbons, and J.E.La Prade, "Temperature Dependence of Transient Capacitance of Al/SiO_2/Si Capacitors", Appl.Phys.Lett. 34(2), 170 (1979).

12. K.S.Rabbani and D.R.Lamb, "On the Analysis of Pulsed MOS Capacitance Measurement", Solid-State Electronics, 21, 1171 (1978).

13. K.S.Rabbani, J.L.Pennock, and D.R.Lamb, "Improved Analysis of Pulsed C-t Measurements on Silicon MOS Capacitors", Solid-State Electronics, 21, 1577 (1978).

14. H. Preier, "Different Mechanisms Affecting the Inversion Layer Transient Response", IEEE Trans. on Electron Devices, ED-15 No.12 990 (1968).

15. C.T.Sah and H.S.Fu, "Current and Capacitance Transient Responses of MOS Capacitor (I)", Phys.Stat.Sol (a) 11, 297 (1972).

16. C.T.Sah and H.S.Fu, "Current and Capacitance Transient Responses of MOS Capacitor (II)", Phys.Stat.Sol (a) 14, 59 (1972).

17. D.K. Schroder and H. .Nathanson, "On the Separation of Bulk and Surface Components of Lifetime using the Pulsed MOS Capacitor", Solid-State Electronics, 13, 577 (1970).

18. P.Tomanek, "Measuring the Lifetime of Minority Carriers in MIS Structures", Solid-State Electronics, 12, 301 (1969).

19. M.W.Hillen and R.B.M.Girisch, "The Influence of Surface States on a Pulsed MOS Capacitor Recombination Lifetime Measurement", Solid-State Electronics, 23, 189 (1980).

20. M.W.Hillen and R.B.M.Girisch, "The Effect of the Incomplete Return of Minority Carriers in a Re-Combination Lifetime Measurement Using a Pulsed MOS Capacitor", Solid-State Electronics, 22, 963 (1979).

21. S.R.Hofstein, "Minority Carrier Lifetime Determination from Inversion Layer Transient Response", IEEE Trans. on Electron Devices, ED-14 No.11, 785 (1967).

22. W.Zechnall and W.M.Werner, "Determination of Generation Lifetime from the Small-Signal Behaviour of MOS Capacitors", Solid-State Electronics, 18, 971 (1975).

23. C.R.Viswanathan and T.Takino, "Minority Carrier Generation Time and Surface Generation Velocity Determination from Q-t Measurements", IEEE Trans.on Electron Devices, ED-25 No.7, 817 (1978).

24. T.Takino, "An Improved Analysis of the Transient Response of an MOS-Capacitor", Ph.D. Dissertation, University of California, Los Angeles (1976).

25. W. Shockley and W.T.Read, "Statistics of the Re-Combinations of Holes and Electrons", Phys.Rev., 87, 835 (1952).

26. R.N.Hall, "Electron-Hole Recombination in Germanium", Phys.Rev., 87, 387 (1952).

27. K.Board and J.G.Simmons, "Non-Equilibrium Response of MOS Devices to a Linear Voltage Ramp - I, Bulk Discrete Traps", Solid-State Electronics, 20, 859 (1977).

28. R.F.Pierret, "A Linear-Sweep MOS-C Technique for Determining Minority Carrier Lifetimes", IEEE Trans on Electron Devices, ED-19 No.7, 869 (1972).

29. R.F.Pierret and D.W.Small, "EFfects of Lateral Surface Generation on the MOS-C Linear-Sweep and C-t Transient Characteristics", IEEE Trans.on Electron Devices, ED-20, 457 (1973).

30. K. Taniguchi, "Graphical Technique to Determine Minority Carrier Lifetime and Surface Generation Velocity using Triangular-Voltage Sweep C-V Method", Solid-State Electronics, 21, 1057 (1978).

31. K.Y. Tsao and D. Leenov, "On Non-Equilibrium C-V Characteristics of MOS Inversion Region", Solid-State Electronics, 19, 27 (1976).

32. A.P.Gorban, V.G.Litovchenko, and D.N. Moskal, "Investigation of the Generation Characteristics of Metal-Insulator-Semiconductor Structures", Solid-State Electronics, 18, 1053 (1975).

33. G.Kaplan, "Determination of Minority Carrier Lifetime and Surface Generation Velocity by Hysteresis Pulsed C-V Method", Solid-State Electronics, 23, 513 (1980).

34. C. Trullermans and F.Van de Wiele, "Bulk Lifetime Determination of MOS Structures by a Voltage Step Response Method", Solid-State Electronics, 21,561,(1978).

35. G. Baccarani, "Majority and Minority-Carrier Lifetime in MOS Structures", Solid-State Electronics,18,1115,(1975)

36. J.Allison, "Electronic Integrated Circuits, Their Technology and Design", McGraw Hill (1975).

37. R.M.Burger and R.P.Donovan, "Fundamentals of Silicon Integrated Device Technology", Prentice Hall (1967).

38. H.F. Wolf , "Silicon Data, A Handbook in Graphs", Pergamon Press (1969).

39. R.A. Colclaser, "Micro-Electronics Processing and Device Design", John-Wiley (1980).

40. N.Hampshire, "The Pet Revealed", Computabits (1979).

41. R.Zaks, "Programming the 6502", Berkeley Sybex (1979).

42. R.Zaks, "6502 Application Book", Berkeley Sybex (1979).

43. R.Zaks and A.Lesea, "Microprocessor Interfacing Techniques", Berkeley Sybex (1977).

44. Commodore MOS "MCS 6522 Versatile Interface Adaptor - Preliminary Data Sheet".

45. E.H.Nicollian and J.R.Brews, "MOS Physics and Technology", Wiley, New York 1982.

46. R.S.C.Cobbold, "Theory and Applications of Field-Effect Transistors", John Wiley (1970).

47. A.S. Grove, "Physics and Technology of Semiconductor Devices", John Wijley (1967).

48. D.V. Morgan and M.J.Howes, "Charge-Coupled Devices and Systems", John Wiley (1979).

49. S.M.Sze, "Physics of Semiconductor Devices", John Wiley (1981).

50. M. Kuhn, "A Quasistatic Technique for MOS C-V and Surface State Measurements", Solid-State Electronics 13, 873 (1970).

51. C.Jund and R.Poirier, "Carrier Concentration and Minority Carrier Lifetime Measurement in Semi-Conductor Epitaxial Layers by the MOS-Capacitance Method", Solid State Electronics, 9, 315 (1966).

52. P. Kuper and C.A.Grimbergen, "Determination of Generation Lifetime from Non-Equilibrium Linear-Sweep Current and Capacitance Measurements on an MOS Capacitor", Solid-State Electronics 21, 549 (1978).

53. K.Board, J.G.Simmons and P.G.C.Allman, "Experimental Response of MOS Devices to a Fast Linear Voltage Ramp", Solid-State Electronics 21, 1157 (1978).

54. K.Board, J.G.Simmons, and P.G.C.Allman,"Equilibrium and Non-Equilibrium Response of an MOS System containing Interface Traps to a Linear Voltage Ramp", Solid-State and Electron Devices 3, No.1, 11 (1979).

55. P.G.C.Allman and K.Board, "Non-Equilibrium Response of MOS Devices to a Linear Voltage Ramp in the presence of Illumination", Solid-State and Electron Devices 3, No.5, 117 (1979).

56. M.J.Abdullah, "Non-Equilibrium Generation Lifetime Measurements on MOS Devices", M.Sc.Thesis, Durham University (1982).

57. M.I.Rahman, "A Study of the Non-Equilibrium Response of an MOS Device Subjected to a Triangular Voltage Waveform" M.Sc.Thesis, University of Durham (1983).

58. P.G.C.Allman, private communication.

59. P.U.Calzolari and S.Graffi, "Effects of Surface States on Relaxation Phenomena in MOS Capacitors", Solid-State Electronics 19, 325 (1976).

60. B. Lubberts and C.R.Viswanathan, "Generation and External Current in MOS Capacitors", Solid-State Electronics 23, 507 (1980).

61. E.Arnold and M.Poleshuk, "Carrier Generation at the Si-SiO_2 Interface under Pulsed Conditions", J.of Appl. Phys. 46, 3016 (1975).

APPENDIX 1

BASIC Program Listing for the Experiment Control

```
10 REM:-----------------------------------------------------:
11 REM:                                                     :
12 REM:    ***         The Q-t Response Measurement         ***    :
13 REM:                                                     :
14 REM:-----------------------------------------------------:
20 PRINT "DEVICE TYPE :-  'P' OR 'N' "
25 CLR
30 D=254:J=0:Z=0:SS=2:G=0:S=0:DA=0:BF=50
35 B$=CHR$(3)
40 GET TY$
45 IF TY$="" THEN 40
50 PRINT TY$
55 GOSUB 500                          :REM  Fetch Constants
65 DIM A(D),AA(D),B(D),BB(D)
70 POKE 52,0: POKE 53,60              :REM Set Top of RAM
75 GOSUB 4000                         :REM Load M/C Code Program
80 PRINT "Type :- 'A' for Expt. Data"
85 PRINT "        'B' for Taped Data"
90 GET D$
100 IF D$="" THEN 90
105 IF D$="B"THEN GOSUB 3000: GOTO 400
110 PRINT "Sample Parameters :-"
115 PRINT "Ox. Cap.     =";CO
120 PRINT "Gate Area    =";AG
125 PRINT "Dopant Conc.=";N
130 INPUT "O.K. ?";A$
135 IF LEFT$(A$,1)="Y" THEN 160
140 PRINT "Enter :-"
145 INPUT "Ox. Cap.";CO
150 INPUT "Gate Area    =";AG
155 INPUT "Dopant Conc.=";N
160 REM-------------------------------          ( Test Run )
165 OPEN 6,6
170 PRINT "Test Run"
175 PRINT "Press Any Key to Proceed"
180 PRINT#6, CHR$(XO);: T=TI
185 IF TI<T+360 THEN 185
190 GET A$
195 IF A$="" THEN 180
197 CLOSE 6
200 REM-------------------------------- ( Check Expt'al Set-up )
205 PRINT "Check Expt. Set-up"
210 PRINT "Electro meter / Amplifier Gain =";A
215 PRINT "Feed-back Cap. =";CF
220 INPUT "O.K. ?";A$
225 IF LEFT$(A$,1)="Y" THEN 245
230 PRINT "Enter :-"
235 INPUT "New Gain =";A
240 INPUT "New Feed-back Cap.=";CF
```

```
245 HI=PEEK(864): LO=PEEK(859)     :REM Delay Factor
250 TF=((HI-1)*256+(LO-1))*0.0155
255 PRINT "Delay Factor =";TF,"(";HI;LO;")"
260 INPUT "O.K ?";A$
265 IF A$<>"NO" THEN 300
270 INPUT "Enter :- HI ;LO";HI,LO
275 POKE 864,HI: POKE 859,LO
280 GOTO 250
300 REM--------------------------------      ( Check Input Data )
305 POKE 59468,192: POKE 59468,224
310 DO=PEEK(59457)                  :REM I/P Initial Value
315 PRINT J,DO
320 IF DO<3 THEN PRINT "I/P Too Small": STOP
325 IF DO>252 THEN PRINT "I/P Too Large": STOP
330 IF Z=1 THEN 360
335 OPEN 6,6
340 PRINT#6, CHR$(XO);
345 CLOSE 6
350 GOTO 370
360 GOSUB 1000
365 IF Z=1 THEN 9030
370 FOR I=0 TO D
375 A(I)=AA(I)
380 B(I)=BB(I)
385 NEXT
400 PRINT "Please Type In :-"
405 PRINT "'0' For I/P Reading"
410 PRINT "'1' For Averaging"
415 PRINT "'2' For Recording Data"
420 PRINT "'3' For Q-t Plot"
425 PRINT "'4' For New Data I/P"
430 INPUT G
435 ON G GOSUB 9000,5000,6000
440 IF G=0 GOTO 300
445 IF G=4 GOTO 80
450 GOTO 400
500 REM--------------------------------     ( Table of Constant )
505 ES=1.036E-12
510 NI=1.45E10
515 Q =1.62E-19
520 KT=0.0259*Q
525 AD=0.01
550 REM---------------------------------
555 IF TY$="N" THEN XO=01:YO=05:GOTO 585
580 XO=05: YO=01
585 VA=0.025
590 N =1.5E15
595 AG=9.013E-3
600 CO=2.08E-10
610 A =33.33
615 CF=1E-10
620 RETURN
1000 REM-------------------------------- ( O/P TO IEEE PORT +/- )
1005 OPEN 5,6
1010 PRINT#5,CHR$(XO);
1015 T=TI
1020 IF TI<T+60 THEN 1020
1025 POKE 59468,192: POKE 59468,224
1030 D1=PEEK(59457)
1035 PRINT#5,CHR$(YO);
1040 SYS (826)
```

```
1035 PRINT#5,CHR$(YO);
1040 SYS (826)
1045 FOR I=1 TO D
1050 AA(I)=PEEK(15873+D-I)
1055 NEXT I
1060 POKE 59468,192: POKE 59468,224
1065 D2=AA(D)
1070 PRINT#5,CHR$(XO);
1075 SYS (826)
1080 FOR I=1 TO D
1085 BB(I)=PEEK(15873+D-I)
1090 NEXT I
1095 CLOSE 5
3000 REM-------------------------------- ( Data Input from Tape )
3005 INPUT "File Name :-";p$
3010 OPEN 1,1,0,P$
3015 INPUT#1,TF
3020 INPUT#1,D1
3025 INPUT#1,D2
3030 INPUT#1,A
3035 INPUT#1,CF
3040 INPUT#1,CO
3045 INPUT#1,BF
3050 FOR I=0 TO D
3055 INPUT#1,A(I)
3060 NEXT I
3065 INPUT "Need -ve Part of Trace ?";A$
3070 IF LEFT$(A$,1)<>"Y" THEN 3090
3075 FOR I=0 TO D
3080 INPUT#1,B(I)
3085 NEXT I
3090 CLOSE 1
3095 RETURN
4000 REM-------------------------------( Load in M/C Code Prog. )
4005 RESTORE
4010 FOR I=1 TO 84
4015 READ H
4020 POKE 825+I,H
4025 NEXT I
4030 DATA 169,58,141,19,232,169,224,141,76,232,169,0,141,75,232
4035 DATA 169,0,141,67,232
4040 DATA 162,255,169,192,141,76,232,169,224
4045 DATA 141,76,232
4050 REM------- Delay Loop Start ------
4055 DATA
169,200,141,1,61,169,6,141,2,61,206,2,61,206,1,61,169,0,205,1,61
4060 DATA 208,246,169,0,205,2,61,208,236
4065 REM------- Delay Loop End --------
4070 DATA 173,77,232,41,2,240,249
4075 DATA 173,65,232,157,0,62
4080 DATA 202,208,200,169,61,141,19,232,96
4085 RETURN
5000 REM--------------------------------     ( Dump Data to Tape )
5005 INPUT "File Name :-";P$
5010 OPEN 1,1,2,P$
5015 PRINT#1,TF
5020 PRINT#1,D1
5025 PRINT#1,D2
5030 PRINT#1,A
```

```
5035 PRINT#1,CF
5040 PRINT#1,CO
5045 PRINT#1,BF
5050 FOR I=0 TO D
5055 PRINT#1,A(I)
5060 NEXT I
5065 FOR I=0 TO D
5070 PRINT#1,B(I)
5075 NEXT I
5080 RETURN
6000 REM------------------------------                ( Q-t Plot )
6005 OPEN 2,5
6010 BV=245: BW=850
6015 PRINT "Last Scale....BF=",BF
6020 INPUT "Scale O.K. ?";D$
6025 IF LEFT$(D$,1)="Y" THEN 6035
6030 INPUT "Enter New Scale";BF
6035 INPUT "'+' OR '-' Trace ?";A$
6040 IF A$="-" THEN 6065
6045 FOR I=0 TO D
6050 BB(I)=A(I)-D1
6055 NEXT I
6060 GOTO 6080
6065 FOR I=0 TO D
6070 BB(I)=B(I)-D2
6075 NEXT I
6080 PRINT#2, "SC-100,2400,-500,8500"
6085 FOR I=0 TO 250
6090 PRINT#2, "PA",I*10,",",(ABS(BB(I)))*BF,";PD;PU"
6095 NEXT I
6100 PRINT "Delay Factor....TF=";TF, "(";HI;LO;")"
6105 INPUT "O.K. ?";A$
6110 IF A$="NO" THEN CLOSE 2: GOTO 270
6115 INPUT "Another Plot ?";A$
6120 IF LEFT$(A$,1)="Y" THEN 6020
6125 IF LEFT$(A$,1)="S" THEN CLOSE 2: RETURN
6130 PRINT#2, "VS6"
6135 FOR I=0 TO 24
6140 PRINT#2, "PA"I*100",0;XT;PD"
6145 NEXT I
6150 PRINT#2, "PD;PA 2500,0,2500,8500,0,8500"
6155 FOR I=1 TO 17
6160 PRINT#2, "PR0,-500;YT"
6165 NEXT I
6170 PRINT#2, "PU"
6180 FOR I=0 TO 240 STEP 20
6185 PRINT#2, "SI.15,.18;PA"I*10",0; CP-2,-1;LB";I;B$
6190 NEXT I
6195 PRINT#2, "PA 800,-500;LB VALUES OF TIME-T (X";TF;"MILLISEC.)",B$
6200 FOR I=1 TO 8
6205 PRINT#2, "PA 0,"I*1000";"CP-4.5,-.3;LB";I;B$
6210 NEXT I
6215 PRINT#2, "DI0,1;PU;PA-120,3500"
6220 PRINT#2, "LBQ-VALUES (X";1000*(1/BF)*CF*AD/A; ")",B$
6225 PRINT#2, "SI;DI1,0;PU;PA900,8500;CP 0,-1"
6230 PRINT#2, "LB PLOT OF Q VS. TIME",B$,"VS"
6235 CLOSE 2
6240 RETURN
```

```
9000 REM--------------------------------     ( Averaging Routine )
9000 INPUT "Enter Sample Size";SS
9005 Z=1
9010 FOR J=1 TO SS
9015 GOTO 300
9020 FOR I=0 TO D
9025 A(I)=(A(I)*(J-1)+AA(I))/J
9030 B(I)=(B(I)*(J-1)+BB(I))/J
9035 NEXT I
9040 DA=(DA*(J-1)+D1)/J
9045 DB=(DB*(J-1)+D2)/J
9050 NEXT J
9055 Z=0: D1=INT(DA): D2=INT(DB)
9060 FOR I=0 TO D
9065 A(I)=INT(A(I))
9070 B(I)=INT(B(I))
9075 NEXT I
```

APPENDIX 2

BASIC Program Listing for the Present Q-t Theory

```
 20 REM:-----------------------------------------------------:
 21 REM:                                                     :
 22 REM:                  Q-t THEORY ( +ve Transient )       :
 23 REM:                                                     :
 24 REM:-----------------------------------------------------:
 30 OPEN1,5
 37 INPUT"ENTER Tg";TG
 35 B$=CHR$(3)
 40 GOSUB 1000
 80 PRINT'''"   Q - T   THEORY  &  PLOT "
 90 PRINTL$
 95 REM-----------------------------------( Display Initial Values )
100 PRINT" At Vg= ";VG;" Volts :-"
110 GOSUB2000
112 QE=QP
114 QS=QT
116 PS=SP
118 XF(0)=XD(0)
120 XD(1)=XD(2)
135 PQ=Q*ND/(2*ES)*XD(1)^2
140 PRINT" Qs at Eqm.";VG;" V.    =";Q
170 PRINT" Xdo  =";XF(0)
190 VG=VG+VD
200 PRINTL$
210 PRINT" At Vg=";VG" Volts :-"
220 GOSUB2000
222 PRINT" Xdo+ =";XD(1)
224 PRINT" Inc. in Qs.        =";QD
230 PRINT" Qs at Eqm.";VG" V.    =";QP
235 PRINT" Tot. Qs at to+     =";QT
245 XF(1)=XD(0)
250 PRINT" Xfo  =";XF(1)
255 PRINTL$
257 REM ( Wait for Keyboard I/P )
260 PRINT"Type 'P' for Q-t Plot"
265 PRINT"Type 'S' for SP-t Plot"
270 GET A$
275 IF A$="P" THEN P=1
280 IF A$="S" THEN S=1
285 IF A$="" THEN 270
295 REM ( Num. Calc. )
290 T1=0
300 QG=QS
310 A=(ES*Q*ND/2)^0.5
315 B=UG/ND^0.5*(2*Q*ES)^0.5
330 E=2*ES/(Q*ND)*(VG-QG)/CX)-XF(0)^2/2
340 T1=T2
360 C=(VG-(QG-QE)/CX+Q*ND*XF(0)^2/(2*EA))^0.5
370 DX=SQR(2*ES/(Q*ND))*C
380 D1=Q*UG*(SQR(E1)-XF(0)/2^.5)
390 D2=1+A/(CX*C)
```

```
395 REM     ( DT=dQ/dt )
400 DT=D1/D2
405 PT=PS+(PQ-PS)+(QS-QE)/CX-(QG-QE)/CX
410 IF P=1 OR S=1 THEN GOTO 500
415 IF S=1 THEN PRINT T1;TAB(6);PT :GOTO 425
420 PRINT T1;TAB(9);QG-QE;TAB(25);DX
425 IFDX-XF(1)<=0THEN 510
430 T2=T1+0.100
435 Q1=DT*(T2-T1)
440 QG=QG+Q1
450 GOTO 330
500 REM-----------------------------------------( Plot Routine )
502 YF=1E-12 :TF=20 :FY=300
504 PRINT#1,"SC-100,2400,-50,850"
505 IF S=1 THEN 507
506 GOTO 508
507 PRINT#1,"PA",INT(T1*TF),",",INT(PT*FY),";PD;PU" :GOTO 509
508 PRINT#1,"PA",INT(T1*TF),",",INT((QG-QE)*YF),";PD;PU"
509 GET A$ :IF A$="" THEN 340
510 REM    ( Graph Scale )
511 PRINT#1,"VS6;TL0.5,0"
512 FOR I=0 TO 25
514 PRINT#1,"PA"I*100",0;XT;PD"
516 NEXT
518 PRINT#1,"PA2500,0,2500,850,0,850;LT"
520 FOR I=1 TO 17
522 PRINT#1,"PR0,-50;YT"
524 NEXT
526 PRINT#1,"PU"
527 FOR I=0 TO 2400 STEP 200
535 PRINT#1,"SI0.15,0.18;PA"I",0;CP-2,-1;LB";I/100;B$ :NEXT
550 PRINT#1,"PA800,-50;LB VALUES OF TIME X" 1/TF*100" SEC.",B$
560 FOR I=1 TO 8
563 PRINT#1,"SI0.15,0.18;PA0,"I*100";CP-2.5,-0.2;LB";I;B$ :NEXT
565 IF S=1 THEN 567
566 GOTO 570
567 PRINT#1,"DI0,1;PA-100,300;LB SURF. POTL. X" 1/FY*100" VOLT",B$
568 GOTO 580
570 PRINT#1,"DI0,1;PA-100,300;LB VALUES OF Q X" 1/YF*100" C.",B$
580 PRINT#1,"DI"
600 CLOSE1
700 END
1000 REM-------------------------------------------( Constants )
1010 Q=1.6E-19
1020 K=1.38E-23
1030 T=300
1040 NI=1.45E10
1050 VG=5
1060 ES=1.036E-12
1070 ND=1.5E15
1080 UG=2.4E14
1100 X0=(2*ES/(Q*ND)*0.299)^0.5
1110 TX=1000E-8
1120 EX=3.46E-13
1140 CX=EX/TX
1150 VD=1
1160 TF=50
1170 YF=1.5E10
1172 I1=0:T2=0:PR=0:S=0
1180 FORI=1TO39:L$=L$+"_":NEXT
1190 RETURN
```

```
2000 REM-----------------------------------( Surf. Potl. Routine )
2010 X=0.1
2020 SP=1.0
2030 GOSUB5000
2032 V2=V1
2034 DV(1)=V2-VG
2036 SP=SP+X
2038 GOSUB5000
2040 V3=V1
2050 DV(2)=V3-VG
2060 IF SGN(DV(1))=SGN(DV(2))THEN 2140
2090 REM  ( Increment Sens. )
2100 SP=SP-X
2110 X=X/10
2120 GOTO2036
2130 REM
2140 IF ABS(DV(2))<0.0005THEN2220
2150 IF DV(1)>DV(2) THEN 2036
2170 REM ( SP Inc./Dec. )
2180 X=-X
2190 SP=SP+X
2200 GOTO 2036
2220 V3=SGN(V3)*(INT(ABS(V3*1000+0.5)))/1000
2230 PRINT" SP= "; SP
2235 PRINT
2240 VG=V3
2250 REM ( Xd & Qo Calc. )
2270 XD(0)=(2*ES/(Q*ND)*SP)^0.5
2280 XD(2)=-ES/CX+SQR(ES^2/CX^2+XD(0)^2+2*ES*XD(0)/CX+2*ES*VD/(Q*ND))
2290 QD=Q*ND*(XD(2)-XD(0))
2300 QT=QP+QD
2310 RETURN
5000 REM   ( Va & Eqm Qd  Calc. )
5010 QS(1)=EXP(-SP*Q/(K*T))+SP*Q/(K*T)-1
5020 QS(2)=NI^2/ND^2*(EXP(SP*Q/(K*T))-SP*Q/(K*T)-1)
5030 QP=((2*ND*ES*K*T)*(QS(1)+QS(2)))^0.5
5040 V1=QP/CX+SP
5050 RETURN
```

FOR THE REVERSE TRANSIENT THE FOLLOWING CHANGES ARE REQUIRED:-

```
 190 VG=VG-VD
 330 E=Q*UG*XF(0)
 360 C=(-VD+(QE-QG)/CX+Q*ND*XF(0)^2/(2*ES))^.5
 380 D1=B*C-E
 390 D2=1-A/(CX*C)
 405 PT=PS+(PQ-PS)+(QE-QS)/CX-(QE-QG)/CX
 420 PRINT T1; TAB(9); QE-QG; TAB(25); DX
 425 IFXF(1)-DX<=0THEN 510
 508 PRINT#1,"PA",INT(T1*TF),",",INT((QE-QG)*YF),"; PD; PU"
2290 QD=Q*ND(XD(2)-XD(0))
2300 QT=QP+QD
```

APPENDIX 3

BASIC program Listing for the C-V Method

```
 10 REM:-------------------------------------------------:
 15 REM:                                                 :
 20 REM:                  C-V  Tg DETERMINATION          :
 25 REM:                                                 :
 30 REM:-------------------------------------------------:
100 DIMV1(50),V2(50),T1(50),T2(50),S(50),VC(50),X(50),Y(50)
110 GOSUB 500
120 FOR S=.5 TO 0 STEP -.1
130 FOR K=1 TO 2
140 CF=CF(K)/AG
150 VT=VT(K)
160 FOR TA=TD TO TN STEP -10
170 TB=TA*1E-6
180 GOSUB 9000
300 REM-----------------------------------------( -ve AL )
305 X=CF/CX
310 XF=CF/CX
315 AL=-AL(K)
320 XM=CM/CX
325 A=NI/(2*TB*NA)
330 B=CX*(AL-Q*NI*S/CX)*CF/(ES*Q*NA)
335 IF A+B>=0 THEN PRINT"A>=B":TA=TD:GOTO 400
340 AS=A*CF/(CX*(A+B))
345 REM    AR=-A/AL*(V-VM)
350 AR=(1/X-1/XM)-(1/AS+1)*(LOG(X/(X-AS))-LOG(XM/(XM-AS)))
355 VO=-AR*AL/A+VM
360 VC=VO-VT : J=J+1
365 IF K=2 THEN 385
370 REM
375 REM
380 V1(J)=VC :T1(J)=TB :S(S)=S :GOTO 390
385 V2(J)=VC :T2(J)=TB :S(S)=S
390 IF J>=200 THEN TA=TD :GOTO 400
395 NEXT TA
400 D(K)=J :J=0 :NEXT K
405 D=D(1) :IF D(1)>D(2) THEN D=D(2)
410 IF C=1 THEN P=3 :GOTO 455
415 PRINT"TYPE :-"
420 PRINT"' 0 '- Proceed"
425 PRINT"' 1 '- Printout Result"
430 PRINT"' 2 '- Plot Result"
435 PRINT"' 3 '- Continuous"
440 PRINT"' 4 '- Read Data From Tape"
445 PRINT"' 5 '- Scale Graph"
450 INPUT P
455 ON PGOSUB1000,3000,4000,5000,6000
460 IF P=0 THEN 470
465 GOTO 410
470 NEXT S:C=0
475 GOTO 415
```

```
 500 REM----------------------------------( Table of Constants )
 512 OPEN2,5
 514 Q=1.6E-19
 515 NI=1.45E10
 516 ES=1.036E-12
 517 NA=1.5E15
 520 AG=9.013E-3     :GATE AREA
 530 VM=8.30
 545 CX=210E-12/AG
 550 CF(1)=64.4E-12   :CF(2)=67.4E-12
 555 VT(1)=-0.20      :VT(2)=-0.20
 565 AL(1)=0.061      :AL(2)=0.338
 585 TD=400           :TN=20
 590 XA=3000          :YA=1000
 595 XO=0             :YO=0
 600 MX=8             :MY=6
 650 A$="" :FOR L=1TO39 :A$=A$+"-" :NEXT
 699 RETURN
3000 REM----------------------------------------( Plot Routine )
3005 HO=(MX-XO)*XA :VE=(MY-YO)*YA
3010 PRINT#2,"SC-"HO/20","HO",-"VE/20","VE""
3020 B$=CHR$(3)
3030 PRINT"XA,YA: -";XA,YA
3040 INPUT"SCALE O.K.";A$
3050 IF LEFT$(A$,1)="Y" THEN 3070
3060 INPUT"ENTER: -XA,YA";XA,YA
3070 FOR I=1 TO D
3090 VC(I)=ABS(V2(I)-V1(I))
3100 NEXT
3105 IF C=1 THEN 3200
3110 PRINT"'ORIGIN' XO,YO: -";XO,YO
3130 INPUT"O.K.";A$
3140 IF LEFT$(A$,1)="Y" THEN 3200
3150 INPUT"ENTER OFFSET (XO,YO)";XO,YO
3200 REM----------------------------------( Plotter Commands )
3230 FOR I=DTO-1 STEP -1
3231 PRINT"Tg=";T1(I)
3235 Y(I)=INT((VC(I)-YO)*YA)
3236 X(I)=INT((V2(I)-XO)*XA)
3250 PRINT#2,"PA",X(I),",",Y(I),";PD;PU"
3260 NEXT
3265 IF C=1 THEN GOTO 3300
3270 INPUT"ANOTHER PLOT";A$
3280 IF LEFT$(A$,1)="N" THEN 3300
3290 GOTO 3030
3310 RETURN
4000 REM-----------------------------------( Continuous Cond. )
4005 C=1
4020 GOSUB 3070
4030 P=0
4040 RETURN
```

```
6000 REM----------------------------------------( Graph Scale )
6005 OPEN2,5
6010 PRINT#2,"VS6"
6015 RX=INT((MX-XO)*XA)
6016 RY=INT((MY-YO)*YA)
6018 V=INT(RX/40)
6020 FOR I=0 TO 40
6030 PRINT#2,"PA"I*V",0;TL0.5,0;XT;PD"
6040 NEXT
6045 PRINT#2,"PU"
6055 W=INT(RY/30)
6060 FOR I=0 TO 30
6070 PRINT#2,"PA0,"I*W";TL0.5,0;YT;PD"
6080 NEXT
6085 PRINT#2,"PU"
6090 PRINT#2,"SI0.15,0.18"
6100 FOR I=(MX-XO)/24 TO (MX-XO) STEP (MX-XO)/12
6110 PRINT#2,"PA"I",0"
6120 PRINT#2,"CP-2,-1"
6130 PRINT#2,"LB";I;B$
6140 NEXT
6150 PRINT#2,"PA80,-50"
6160 PRINT#2,"LB VALUES OF VC(2) (X";FX;"VOLT)",B$
6170 FOR I=MY/16 TO MY STEP MY/8
6180 PRINT#2,"PA0,"I""
6190 PRINT#2,"CP-4.5,-0.3"
6200 PRINT#2,"LB";I;B$
6210 NEXT
6220 PRINT#2,"DI0,1"
6230 PRINT#2,"PA-12,350"
6240 PRINT#2,"LBVC(2)-VC(1) (X";FY;"VOLT)",B$
6250 CLOSE2
6260 RETURN
9000 REM-----------------------------------( CM Calculation )
9030 DC=0.20
9032 AL=AL(K)
9035 W=8.00
9037 CD=W*10^-9
9040 GA=0
9042 GOSUB 9200
9045 IF GA=1 THEN W=W+DC :GOTO9040
9050 V1=VO
9053 VK=VM-V1
9056 IF V1<0 THEN W=W-DC :GOTO9040
9060 GA=0
9062 W=W-DC
9065 GOSUB 9200
9070 IF GA=1 THEN W=W+DC :DC=DC/2 :GOTO9060
9075 V2=VO
9080 VL=VM-V2
9085 IF VK<VL THEN PRINT"WRONG DIRN." :STOP
9090 IF VL<0.001 AND VL>=0 THEN CM=CD :RETURN
```

```
9095 REM-------------------------------------( Increment Sens. )
9105 IF SGN(VL)=SGN(VK) THEN 9060
9110 W=W+DC
9115 DC=DC/2
9120 GOTO 9060
9200 REM-----------------------------------------------( +ve AL )
9240 CD=W*1E-9
9260 X=CD/CX
9270 XF=CF/CX
9280 A=NI/(2*TB*NA)
9300 B=CX*(AL-Q*NI*S/CX)*CF/(ES*Q*NA)
9320 AS=A*CF/(CX*(A+B))
9340 IF X<=AS THEN PRINT" CD TOO LOW" :GA=1 :RETURN
9400 AR=(1/X-1/XF)-(1/AS+1)*(LOG(X/(X-AS))-LOG(XF/(XF-AS)))
9420 VO=-AR*AL/A+VT
9440 RETURN
```

APPENDIX 4

Theory of the Zerbst Method of Analysis of the C-t Transient

The voltage equation of an MOS capacitor is :

$$V_a = V_{ox} + \psi_s \qquad (A4.1)$$

where $\psi_s = \frac{qN_a}{2\varepsilon_s} x_d^2$

and $V_{ox} = \frac{Q_m}{C_{ox}}$

$$= - \frac{\left(Q_{inv} - q\ N_a x_d \right)}{C_{ox}}$$

Substituting these, A4.1 becomes

$$V_a = - \frac{\left(Q_{inv} - q\ N_a x_d \right)}{C_{ox}} + \frac{q\ N_a x_d^2}{2\ \varepsilon_s} \qquad (A4.2)$$

Since V_a is constant during the transient, $\frac{dV_a}{dt} = 0$

On differentiating (A4.2)

$$\frac{dV_a}{dt} = - \frac{1}{C_{ox}} \frac{dQ_{inv}}{dt} + \frac{qN_a}{C_{ox}} \frac{dx_d}{dt} + \frac{q\ N_a x_d}{\varepsilon_s} \frac{dx_d}{dt} \qquad (A4.3)$$

$$= 0$$

Rearranging (A4.3):-

$$\frac{d\ Q_{inv}}{dt} = q\ N_a C_{ox} \left(\frac{1}{C_{ox}} + \frac{x_d}{\varepsilon_s} \right) \frac{dx_d}{dt} \qquad (A4.4)$$

From the relation for series capacitors

$$\frac{1}{C} = \frac{1}{C_{ox}} + \frac{1}{C_d}$$

$$= \frac{1}{C_{ox}} + \frac{x_d}{\varepsilon_s} \qquad \text{(A4.5)}$$

Differentiating (A4.5) and rearranging

$$\frac{1}{\varepsilon_s} \frac{dx_d}{dt} = \frac{d}{dt} \left(\frac{1}{C}\right) \qquad \text{(A4.6)}$$

Substituting (A4.5) and (A4.6) into equation (A4.4):

$$\frac{d\, Q_{inv}}{dt} = q\, N_a\, C_{ox}\, \varepsilon_s\, \frac{1}{C} \frac{d}{dt} \left(\frac{1}{C}\right) \qquad \text{(A4.7)}$$

Equation (A 4.7) can be written as :-

$$\frac{d\, Q_{inv}}{dt} = \frac{q\, N_a \varepsilon_s\, C_{ox}}{2} \frac{d}{dt} \left(\frac{1}{C}\right)^2 \qquad \text{(A4.8)}$$

The rate of increase of the inversion charge Q_{inv}, has contributions from the thermal generation of carriers due to the increase in the depletion width and the surface generation.

That is

$$\frac{d\, Q_{inv}}{dt} = - q\, U_g\, (x_d - x_f) - q\, n_i S \qquad \text{(A4.9)}$$

Replacing x_d and x_f with the corresponding capacitance and $U_g = \frac{n_i}{\tau_{ge}}$ in (A4.9)

$$\frac{d\, Q_{inv}}{dt} = - \frac{q\, n_i\, \varepsilon_s}{\tau_{ge}} \left(\frac{1}{C} - \frac{1}{C_f}\right) - q\, n_i S \qquad \text{(A4.10)}$$

Equating (A4.8) and (A4.10) gives the equation for the Zerbst plot :

$$-\frac{d}{dt}\left(\frac{1}{C}\right)^2 = \frac{2\,n_i}{N_a C_{ox} \tau_{ge}}\left(\frac{1}{C} - \frac{1}{C_f}\right) + \frac{2\,n_i S}{N_a \epsilon_s C_{ox}} \qquad \text{(A4.11)}$$

The plot of $\frac{d}{dt}\left(\frac{1}{C}\right)^2$ against $\left(\frac{1}{C} - \frac{1}{C_f}\right)$ should therefore be a straight line with an intercept proportional to S.

APPENDIX 5

Theory of Non-Equilibrium Fast Ramp I-V Technique

The total gate charge Q_m on an MOS capacitor is given by:

$$Q_m = Q_{ox} + Q_d + Q_{inv} \qquad (A5.1)$$

where Q_{ox} is the fixed oxide charge

Q_d is the depletion charge

Q_{inv} is the inversion charge

On differentiating equation (A5.1) and noting that

$$Q_i = q\, U_g \int_o^t (x_d - x_o)\,dt$$

because generation will predominate in positions where the generation centres are below the Fermi level.

$$I_g = q\, U_g\, (x_d - x_o) + q\, N_d \frac{d\, x_d}{dt} \qquad (A5.2)$$

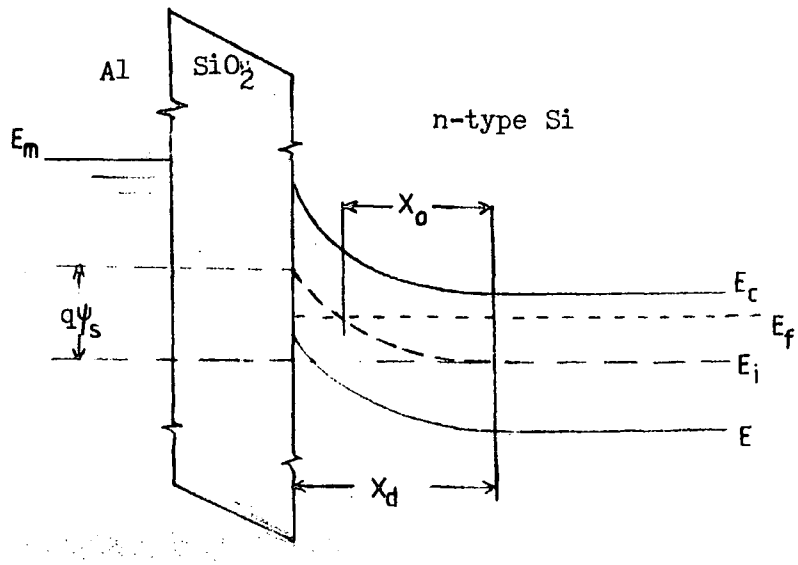

From the voltage equation

$$V_a = V_{ox} + {}_s + V_{FB}$$

$$= - \frac{Q_m}{C_{ox}} + \frac{q\ N_d x_d^{\ 2}}{2\ \varepsilon_s} + V_{FB} \qquad \text{(A5.3)}$$

For the forward voltage sweep (i.e. from accumulation to depletion), $\frac{dv_a}{dt} = -d$

On differentiating (A4.3)

$$- \frac{dv_a}{dt} = \alpha = \frac{I_g}{C_{ox}} + \frac{q\ N_d x_d}{\varepsilon_s} \frac{dx_d}{dt} \qquad \text{(A5.4)}$$

Substituting for the value of I_g into (A5.2) gives :

$$\left(1 + \frac{C_{ox}\ x_d}{\varepsilon_s}\right)\frac{dx_d}{dt} = \frac{U_g}{N_d} (L_e + x_o - x_d) \qquad \text{(A5.5)}$$

where $L_e = \frac{\alpha C_{ox}}{q\ U_g}$

Solving (A5.5) with the boundary condition $x_d \simeq x_o$ at $t = 0$

$$\left[1 + \frac{C_{ox}(x_o + L_e)}{\varepsilon_s}\right] \ell n(1-z) + \frac{L_E C_{ox}\ z}{\varepsilon_s} = - \frac{C_{ox}\ V}{q\ N_d L_e} \qquad \text{(A5.6)}$$

where $z = \frac{(x_d - x_o)}{L_e}$

Differentiating (A5.6) with respect to z yields :-

$$\frac{dz}{dv} = \frac{C_{ox}(1 - z)}{q\ N_d L_e \left[1 + \frac{C_{ox}}{\varepsilon_s} (x_o + z\ L_e)\right]} \qquad \text{(A5.7)}$$

Equation (A5.2) can be written as

$$I_g = \alpha C_{ox} z + q N_d L_e \alpha \frac{dz}{dv} \qquad (A5.8)$$

Substituting (A5.7) into (A5.8)

$$I_g = \alpha C_{ox} \left[z + \frac{1 - z}{1 + \frac{C_{ox}}{\varepsilon_s} (x_o + z L_e)} \right] \qquad (A5.9)$$

This equation gives the value of the gate current during the forward voltage sweep.

For the reverse sweep $\left(\frac{dv_a}{dt} = \alpha \right)$ the same procedure can be used to show that

$$I_g = \alpha C_{ox} \left[z - \frac{1 + z}{1 + \frac{C_{ox}}{\varepsilon_s} (x_o + z L_E)} \right] \qquad (A5.10)$$